October 2019

ENGINEERING NANOMATERIALS FOR IMAGING AND THERAPY OF BACTERIA AND BIOFILM-ASSOCIATED INFECTIONS

Akash Gupta

ENGINEERING NANOMATERIALS FOR IMAGING AND THERAPY OF BACTERIA AND BIOFILM-ASSOCIATED INFECTIONS

A Dissertation Presented

By

AKASH GUPTA

Submitted to the Graduate School of the
University of Massachusetts Amherst in partial fulfillment
of the requirements for the degree of

DOCTOR OF PHILOSOPHY

September 2019

Chemistry

ENGINEERING NANOMATERIALS FOR IMAGING AND THERAPY OF BACTERIA AND BIOFILM-ASSOCIATED INFECTIONS

A Dissertation Presented

By

AKASH GUPTA

Approved as to style and content by:

Vincent M. Rotello, Chair

Michael J. Maroney, Member

Margaret Riley, Member

Ashish A. Kulkarni, Member

Richard W. Vachet, Department Head

Department of Chemistry

DEDICATION

This work is dedicated to my father

ACKNOWLEDGMENTS

As I reach this final milestone in my journey towards a PhD. degree, I would like to express my thanks to those who have helped this work come to fruition.

I begin by thanking my advisor Vincent Rotello, for his generous support and guidance in being a mentor and a role model. This research has greatly benefited from his scientific expertise "the sword", and his vision towards a big picture "the beautiful land". I deeply appreciate the freedom and encouragement he provided me to pursue the scientific challenges that I thought were interesting. I hold you with utmost respect and greatly cherish the confidence you have bestowed in me.

I would like to thank my dissertation committee Professors Mike Maroney, Peg Riley, Sam Nugen and Ashish Kulkarni. I truly appreciate your critical insights and interest in my research over the years. I am grateful for your support as I continue to the next stage of my career.

I was fortunate to work in a research group filled with enthusiastic researchers who made the lab a great place to come in every day. I am thankful to all the past and present rotello group members for their immense support, countless brainstorming sessions and fruitful collaborations. My special thanks are due to Ryan Landis whose passion to make new molecules allowed us to collaborate and design polymer-based materials mentioned in Chapter 5-8. I am grateful to Riddha for being my "go-to" collaborator, her dedication and expertise helped me tremendously in completion of Chapter 4 and 5. I would also like to thank Xiaoning and Brad for being excellent mentors in the early days of my graduate school. It would like to acknowledge the contributions that Jessa, Ian, Bill, Lucy, Martin, Staci, Neveen, AP and Alex made to the work in this thesis. There are many other colleagues at UMass whom I am indebted for the countless favors they have done for me.

I deeply appreciate the advice and help from our collaborators at Riley lab (Peg, Sandy) and Mayo Clinic (Robin, Suzy). Their expertise has greatly helped me in exploring new scientific avenues and making this research more impactful.

I acknowledge the moral support of my friends, both near and far. You have always appreciated my interest towards studies. Through visits, calls or emails, you have been generous in lending support. I would especially like to thank Riddha for being a spirited friend, her "out of the box" thinking will continue to inspire me in the years to come.

Finally, I would not be here without the love and support of my parents – Sanjay and Sunita Gupta. They let their son go places 15 years ago and have been very encouraging as I continue on the path to explore my dreams. I would especially like to acknowledge my father for teaching me how to notice things and understanding them for what they really are. He taught me the importance of the 'process' with the ability to look beyond the results. His teachings have motivated me in sciences and this work is dedicated to him.

ABSTRACT

ENGINEERING NANOMATERIALS FOR IMAGING AND THERAPY OF BACTERIA AND BIOFILM-ASSOCIATED INFECTIONS

SEPTEMBER 2019

AKASH GUPTA

B.S., IIT (ISM) DHANBAD

INTEGRATED M.SC., IIT (ISM) DHANBAD

Ph.D., UNIVERSITY OF MASSACHUSETTS AMHERST

Directed by: Professor Vincent M. Rotello

Infections caused by multidrug-resistant (MDR) bacteria pose a serious global burden of mortality, causing thousands of deaths each year. The "superbug" risk is further exacerbated by chronic infections generated from antibiotic-resistant biofilms that are highly resistant to available treatments. Synthetic macromolecules such as polymers and nanoparticles have emerged as promising antimicrobials. Moreover, ability to modulate nanomaterial interaction with bacterial cellular systems plays a pivotal role in improving the efficacy of the strategy.

In the initial studies on engineering nanoparticle surface chemistry, I investigated the role played by surface ligands in determining the antimicrobial activity of the nanoparticles. In further study, I determined that surface monolayer of hydrophobic ligands facilitated the nanoparticles to block bacterial efflux pumps, yielding reduction in antibiotic dosage to treat pathogenic bacteria including methicillin-resistant *S. aureus* (MRSA). Moreover, functionalization of nanoparticle surface with pH-responsive ligand was used to develop a general strategy to target and image bacterial biofilms for a broad-range of species. In a subsequent study, I have utilized a unique approach of integrating synthetic nanomaterials on the surface of natural super carrier-Red Blood Cells for selective delivery of nanoparticles to the site of bacterial infection for antimicrobial therapy. This strategy shows potential to combat bacterial infections without harming the ecology

of human microbiome, as well as circumvent the issues associated with non-specific uptake of nanoparticles by the reticuloendothelial system.

In another study, systematic investigation of antimicrobial activity of oxanorbornene-polymer derivatives generated polymer nanoparticles with unprecedented therapeutic selectivity towards MDR bacteria. Additionally, polymeric nanoparticles prevented onset of resistance development in bacteria for ~1300 generations and eradicate biofilms on infected mammalian cells, a feat unachieved by previous antimicrobial polymers. Amphiphilic polymer derivates increased the influx of antibiotics in Gram-negative bacteria and biofilms, resulting in synergistic antimicrobial therapy. Subsequently, we utilized engineered polymers to generate nanosponges through self-assembly of polymers around essential-oil based cores for topical treatment of wound biofilms. Overall, our results show strong potential as an infectious disease therapeutic while simultaneously provide a rational approach to design novel antimicrobials for sustainably combating bacterial infections.

TABLE OF CONTENTS

Page

LIST OF TABLES

LIST OF FIGURES

Figure Page

CHAPTER 1

INTRODUCTION

1.1 Emergence of multi-drug resistant bacteria

Over the past-century, antibiotics have been used to combat bacterial infections with high potency and cost-effectiveness. However, in the last few decades, widespread overuse of antibiotics has resulted in the emergence of multi-drug resistant (MDR) bacteria that are resistant to multiple antibiotics simultaneously.[1] The rise of "superbugs" resistant to antibiotics, constitutes one of the dominant challenges in human health. Antibiotic-resistant bacteria cause more than 2 million cases of infections every year with more than 23,000 annual deaths in US alone.[2] Number of annual deaths caused by MDR infections world-wide increases to 700,000 every year. Recent projections by World Health Organization (WHO) indicate that bacterial infections will cause more than 10 million deaths each year by 2050, more than that caused by cancer presently.[3] In recent years, numerous strains such as New Delhi metallo *β-lactamase*-producing *Enterobacteriaceae* strains have been found to be resistant to almost all antibiotics except tigecycline and colistin.[4] Furthermore, there have been multiple reports of other "superbug" outbreaks where the infection causing strains were resistant to all the clinically available antibiotics.

Most-cases of MDR-infections require prolonged antibiotic therapy with tissue debridement (*i.e.* surgical removal) in some cases, resulting in low-patient compliance and excessive healthcare-costs.[5] Notably, widespread antibiotic resistance poses an economic burden of more than $55 billion per year towards excess healthcare and societal costs in the US.[6] Moreover, conventional treatment strategies utilizing antibiotics further contributes to increased resistance in the surviving bacterial cells. For example, 40% of the *S. aureus* strains isolated from hospitals are resistant to methicillin (methicillin-resistant *S. aureus,* MRSA) and some even

resistant to last-resort antibiotic-vancomycin (vancomycin-resistant *S. aureus*, VRSA) and carbapenems.[7,8]

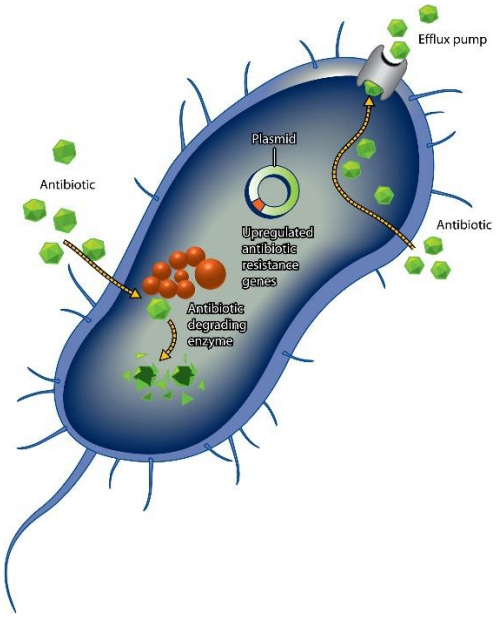

Figure 1.1. Three of the main antibiotic resistance strategies used by bacteria. Reproduced by permission from Reference 10.

Antibiotics execute their antibacterial effect by specifically targeting essential surviving mechanisms in bacteria, such as inhibiting synthesis of cell wall and interfering in production of DNA, RNA and vital proteins.[9,10] However, with billions of years of evolutionary progress, bacteria have developed an intrinsic ability to overcome the threats posed by these traditional antibacterials through mutations and transfer of DNA (horizontal gene transfer).[11] Single bacterial strain can acquire multiple drug-resistance genes from different microbes, resulting in generation of multi-drug resistant (MDR) "superbugs".[12] Antibiotic resistance in bacteria will increase and the situation will become more dire as the number of MDR strains continues to grow. This rapidly escalating threat has contributed to an urgent need to discover novel antibacterials and new treatment strategies to combat these highly resistant bacteria.

1.2 Bacterial biofilms

Bacterial cells often adhere to damaged tissues, medical implants or indwelling devices to cause persistent infections by forming biofilms as shown in Figure 1.2.[13] Biofilms are three-dimensional microcolonies of bacteria that are embedded inside a slimy matrix of extracellular polymeric substance (EPS).[14] The EPS matrix possesses complex composition of extracellular polysaccharides, proteins, nucleic acids and lipids that plays a significant role in protecting the biofilm residing microbes.[15,16] Importantly, EPS matrix acts as a barrier that prevents penetration of antimicrobials, rendering them ineffective against these refractory infections.[17,18]

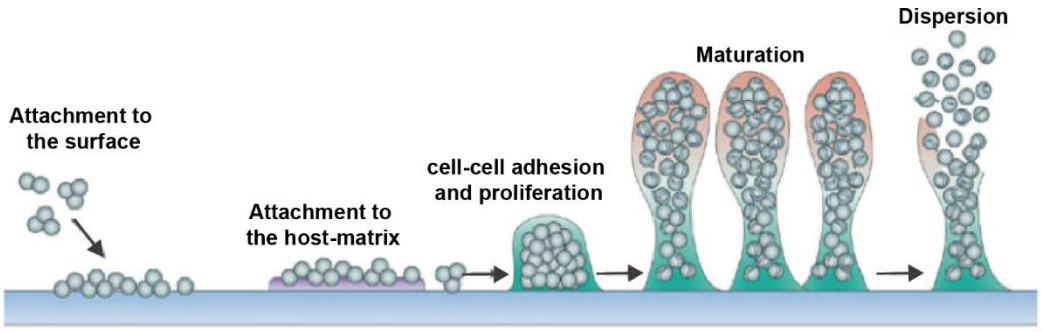

Figure 1.2. Schematic showing the cycle of biofilm formation, starting from planktonic bacterial cells to eventual dispersal of microbes from the matrix. Adapted with permission from Reference 50.

Approximately ~80% of human bacterial infections involve the formation of biofilm on the living tissue.[19] Multiple nosocomial infections are caused due to adherence of biofilms onto the biomaterial surface such as those associated with the use of urinary catheters, central venous catheters, orthopedic devices, arthro-prostheses and dental implants.[20,21] Biofilm formation on diseased or damaged tissues is associated with cystic fibrosis, endocarditis and chronic wounds.[22] Biofilm infections are highly refractory to conventional antibiotics and can evade host immune response.[23] Moreover, biofilm infections can frequently result in chronic inflammation of surrounding tissue due to invasion of neutrophils and other immune complexes.[24,25]

The main mechanisms for resistance in bacterial biofilms can include limited penetration of antibiotics inside the biofilm matrix due to physiochemical characteristics of the EPS as shown in Figure 1.1.[23,26] In some cases, enzymatic degradation of antibiotics inside the matrix can also retard antibiotic penetration.[27] Secondly, biofilms have an altered chemical microenvironment that plays a crucial role in its resistance against biofilms. For example, biofilms have a very low pH due to accumulation of acidic waste products that can antagonize antibiotics such as vancomycin.[28] Similarly, deep layers of biofilms can have anaerobic microenvironment that can also compromise the activity of antibiotics such aminoglycosides.[26] Finally, ~1% of biofilm microbes phenotypically mutate into persister cells that can continue to survive even after exposure to antibiotics.[19]

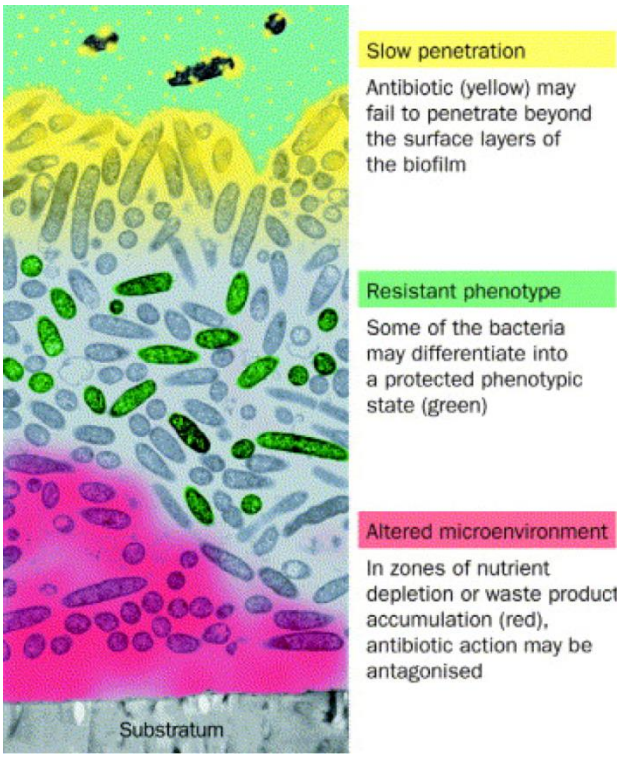

Figure 1.3. Schematic representation showing mechanism of resistance in biofilms caused by limited penetration of antibiotics, resistant phenotypes and altered microenvironment of EPS. Adapted with permission from Reference 23.

1.3 Current Strategies to combat bacterial infections

Discovery of antibiotics in mid-20th century revolutionized the treatment of infectious diseases facilitating treatment of potentially life-threatening conditions and greatly reducing the burden of mortality caused by bacterial infections. Most of the antibiotics discovered in the early years of invention were predominantly obtained from screening natural products produced during the process of microbial fermentation.[29] Recently, researchers have identified antibiotics from different ecological systems that exhibit novel mechanisms of actions. Alternatively, medicinal chemists have focused on modifying the chemical structures of the existing classes of antibiotics to generate new antibacterials. For instance, fourth generation cephalosphorins and β-lactam antibiotics exhibit extended spectrum activity against Gram-positive and Gram-negative bacteria.[30,31] Another actively pursued strategy in the clinic to combat MDR infections involves use of antibiotic cocktails that can target multiple pathways to kill bacteria.[32,33] These strategies have shown improved efficacy; however they involve increased risks of developing antibiotic resistance in the patients.[34] Moreover, rapid and continuous spread of antibiotic resistance in bacteria has contributed to the urgent need of developing alternative antimicrobial therapies.

Majority of "non-antibiotic" approaches for the treatment of bacterial infections involves targeting virulence factors of bacterial pathogens rather than actively killing the microbes.[35,36] Most bacterial pathogens produce virulence factors to evade host-immune response, proliferate inside and cause damage to the host cells.[37,38] Antivirulence compounds can block the activity of these virulence factors, making pathogens susceptible to the host-immune response or adjunct antibiotics. For example, monoclonal antibodies and small molecules binding with bacterial toxins have shown to be effective in treatment of bacterial infections, with some studies even being pursued in clinical trials.[39,40] Similarly, therapeutics that target quorum-sensing pathways

(bacterial cell communication) have demonstrated ability to prevent infections caused by formation of biofilms.[41,42] Some of the other actively pursued antibacterial strategies utilize engineering bacteriophages (virus eating bacteria) and manipulating the microbiome, however they are still in their preliminary stages.[43,44]

Antimicrobial peptides (AMPs) have emerged as promising therapeutics that actively target and kill bacterial cells. AMPs are host-defense molecules that demonstrate broad-spectrum activity and reduced resistance acquisition.[45,46] These favorable characteristics can be attributed to the unique amphiphilic topology of peptides, featuring polycationic headgroups, enabling them to disrupt microbial membranes.[47] AMPs exhibit low hemolytic activity and minimal toxicity to mammalian cells, rendering them highly effective in antimicrobial therapies. However, AMPs are susceptible to proteolytic degradation compromising their antimicrobial efficacy in physiological environment.[48,49]

Building on the structural advantages of both antibiotics and AMPs, nanomaterials provide another potential solution for antimicrobial therapies. For example, nanomaterials can simultaneously disrupt the bacterial membrane and target intracellular components to impede proper functioning of the cellular machinery.[50,51,52] The distinct physio-chemical traits of nanomaterials make them promising candidates to achieve enhanced therapeutic efficacy against resilient MDR infections.[53,54] Nanomaterials can execute multiple bactericidal pathways, making it difficult for bacteria to adapt against these therapeutics.[55] These pathways are dependent upon the inherent core material, shape, size and surface chemistry of nanomaterial scaffolds.[56,57,58] Moreover, high therapeutic loading coupled with the enhanced ability to penetrate biological membranes make nanomaterials excellent candidates for the transport of drugs at the site of infection.[59,60,61] Finally, the ability to modulate nanomaterial interaction with bacterial cellular systems plays a pivotal role in improving the therapeutic efficacy of the treatment.[62]

1.4 Interaction of nanomaterials with bacteria

Nanomaterial-bacteria interactions depend upon multiple factors such as electrostatic attraction, hydrophobic and receptor–ligand interaction and van der Waals forces.[50] A fundamental study of the interactions between nanomaterials and bacteria provides crucial insight for designing novel antimicrobial agents.

Bacteria are mainly classified into Gram-negative and Gram-positive depending upon the structure of their cell wall (Fig. 1a).[63] The cell wall of Gram-positive bacteria has a thick peptidoglycan layer (15–100 nm) with polymeric techoic acids and a cytoplasmic membrane underneath.[52] The phosphates present in the techoic acid polymeric chains are responsible for the bacterial negative charge and serve as binding sites for the divalent cations in the solution. On the other hand, Gram-negative bacteria consists of a cytoplasmic membrane followed by a thin peptidoglycan layer (20–50 nm), which is further protected by a hydrophobic lipid bilayer consisting of lipopolysaccharides. This additional lipid layer greatly reduces the penetration ability of numerous hydrophobic antibacterial agents such as detergents.[63]

The bacterial membrane is negatively charged primarily due to the presence of phosphates and carboxylates as components of lipopolysaccharides present on Gram-negative bacteria. The structure of the bacterial cell wall plays a crucial role in determining the interaction of NPs with the microbes. In early studies of nanoparticle–microbe interactions, Murphy and coworkers have demonstrated that CTAB coated gold nanorods or nanospheres were homogenously distributed on Gram-positive *B. cereus*. This phenomenon was attributed to the electrostatic interaction between the positively charged nanomaterial and the negatively charged techoic acid moieties on the bacteria.[64] Alternatively, mannose substituted gold nanoparticles bind with the pili on Gram-negative *E. coli*. Pili are hair like structures emanating from bacterial surfaces that are rich in lectin (sugar-binding proteins) and hence preferentially binding to the mannose coated NPs.[65] Building on these observations, Rotello and coworkers demonstrated that cationic NPs exhibited toxicity against bacteria.[66] In subsequent studies, the subtle interplay

between NP coverage and membrane structure indicated that the positively charged hydrophobic AuNPs formed spatial aggregates on the bacterial membrane. Gold nanoparticles (AuNP) of 2 nm core diameter exhibited low toxicity against *E. coli* (Gram-negative) but rapidly lysed *B. subtilis* (Gram-positive) bacteria.[67] The interaction between the specific NP functionality and membrane structure can result in blebbing, tubule formation or other membrane defects.

As we have previously studied in section 1.2, the complex architecture, dynamics, and composition of extracellular polymeric substances (EPS) in the matrix are profoundly responsible for the low penetration of therapeutic agents. Diffusion of therapeutics inside the biofilm can be affected by several genetic and physiological heterogeneities such as the hydrophobicity of bacterial cell walls.[68] Hence, fundamentally understanding the interactions between NPs and complex biofilm matrices is crucial in designing materials for biofilm treatment.

The penetration and deposition of NPs within the biofilms are key components for the design of biofilm therapeutics. Peulen and Wilkinson reported that the penetration ability of NPs decreased inversely to their size due to small pore sizes within biofilms.[69] Furthermore, NP deposition inside the biofilms is largely dependent upon the electrostatic interaction as well as the homogeneity of the charges across the biofilm surface. In a related study, Rotello and co-workers provided further insight on the penetration ability of the NPs inside the biofilms. They demonstrated that the neutral and anionic quantum dots (QDs) did not show any penetration inside the biofilms, while cationic QDs were widely distributed throughout the biofilm. Furthermore, cationic QDs with hydrophobic terminal groups were found inside the bacterial cells, whereas their hydrophilic counterparts remained in the EPS matrix of the biofilm (Figure 2).[70]

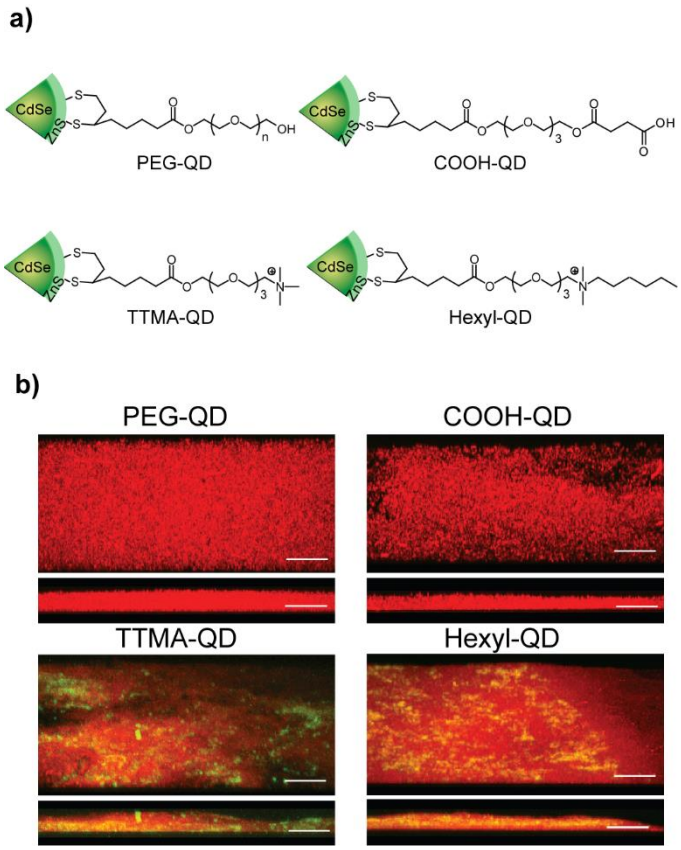

Figure 1.4. Surface design controls penetration ability of nanoparticles. **a**. Quantum dots used in study. **b.** Micrographs of microtomed slices of the biofilm showing no penetration by anionic and neutral particles and efficient infiltration by cationic quantum dots. Adapted from reference 70.

1.5 Antimicrobial mechanism of NPs

The therapeutic activity of many antibiotics originates from their ability to inhibit cell wall synthesis, interfering with the expression of essential proteins and disrupting the DNA replication machinery. However, bacteria have developed the ability to resist each of these mechanisms of action. One fundamental mechanism of bacterial resistance is the alteration of the target of the antibiotic.[71] For example, modification of cell wall components confers resistance to vancomycin, whereas altered structures of ribosomes resist tetracycline.[72] Similarly, bacteria can overexpress enzymes such as β-lactamases and aminoglycosides to degrade antibiotics. Additionally, overexpression of efflux pumps enables bacteria to evade multiple antibiotics simultaneously. Finally, many pathogens such as Chlamydophila pneumonia reside inside the

cellular compartments of the host cells to escape from the antibiotics that are mostly confined to extracellular space.[73]

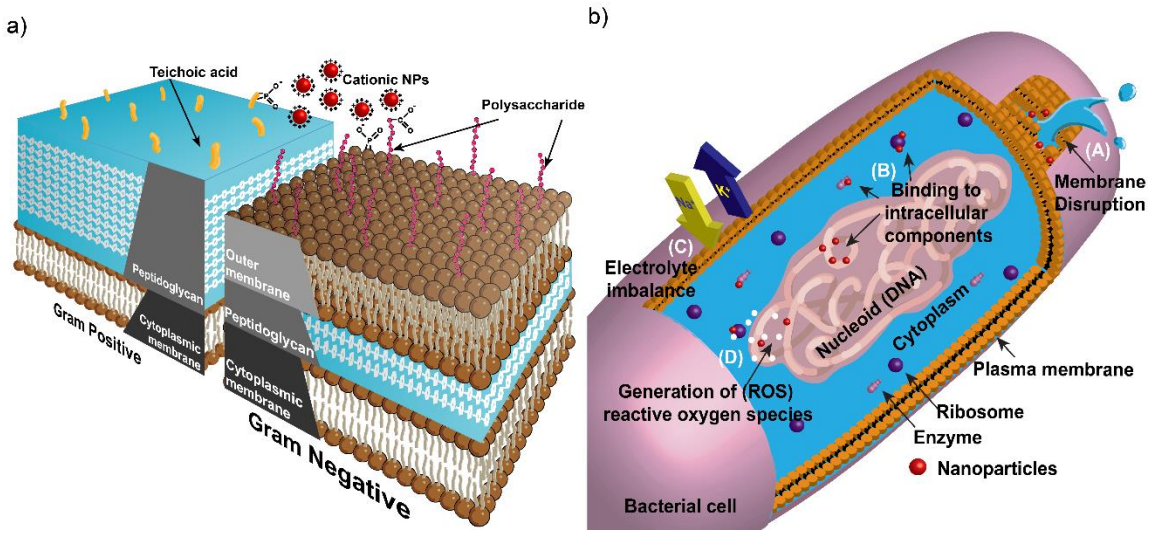

Figure 1.5. Schematic diagram showing **a.** cell wall structures of Gram-positive and Gram-negative bacteria and **b.** antimicrobial mechanism of NPs: (A) disruption of cell membrane resulting in cytoplasmic leakage; (B) binding and disruption of intracellular components; (C) disruption of electron transport causing electrolyte imbalance and (D) generation of reactive oxygen species (ROS).

Nanomaterials can overcome the antibiotic-resistance mechanisms owing to their unique physio-chemical properties, enabling nanomaterials to execute multiple novel bactericidal pathways to achieve antimicrobial activity. Nanomaterials can bind and disrupt bacterial membranes, causing leakage of cytoplasmic components.[54] Upon membrane permeation, nanomaterials can also bind to intracellular components such as DNA, ribosomes and enzymes to disrupt the normal cellular machinery (Fig. 1.5b). Disruption in the cellular machinery can lead to oxidative stress, electrolyte imbalance and enzyme inhibition, resulting in cell death.[52] The bactericidal pathways followed by nanomaterials are inherently dependent upon their core material, shape, size and surface functionalization. In early studies on nanomaterial-based antimicrobials, researchers varied the inherent core materials to generate nanomaterials with different mechanisms of action. For example, silver nanoparticle-based antimicrobials utilize free

Ag^+ ions as active agents. The silver ions disrupt the bacterial membrane and electron transport while simultaneously causing DNA damage.[74] Similarly, free Cu^{2+} ions from copper NPs can generate reactive oxygen species (ROS) that disrupt amino acid synthesis and DNA in bacterial cells. On the other hand, ZnO and TiO_2 based nanomaterials cause cell membrane damage and generate ROS to kill bacteria.[75,76] Different nanomaterial cores can offer a range of antibacterial mechanisms to combat drug-resistant superbugs. However, these non-functionalized nanomaterials often exhibit narrow-spectrum activity against bacterial species. Moreover, they display low therapeutic indices (i.e. selectivity) against healthy mammalian cells, limiting their widespread use in biomedical applications. The surface chemistry of nanomaterials is critical to modulate their interaction with bacteria, improving their broad-spectrum activity while simultaneously reducing their toxicity against mammalian cells.

Nanomaterials based antimicrobials have demonstrated their efficacy against both planktonic (free floating bacteria) and biofilm (bacterial community) infections. In the following sections, we have briefly discussed some of the nanomaterial-based strategies for combating MDR bacterial and biofilm infections.

1.6 Nanomaterials as self-therapeutic antimicrobial agents

NPs provide multiple attributes that facilitate the development of unique antimicrobial strategies.[77,78] NPs can interact with and penetrate bacterial cells with unique bacteriostatic and bactericidal mechanisms.[79] For example, possessing slightly larger diameters than drug efflux pumps, NPs can potentially reduce efflux-mediated extrusion.[80,81] Exploiting these characteristic properties, several NP-based systems have been employed for antimicrobial applications.

Xu and co-workers demonstrated enhanced *in vitro* antibacterial activities of vancomycin-capped AuNPs (Au-Van) against vancomycin-resistant *enterococci* and *E. coli* strains (Figure 1.6).[82] Similarly, Feldheim and co-workers demonstrated that antimicrobial activity of NPs functionalized with non-antibiotic molecules depended upon their composition on

the surface.[83] These studies indicate that modulating NP surfaces exhibits great potential for antimicrobial therapy. However, further studies on how NP surface functionality modulates antimicrobial activity can provide valuable information for future NP-based antimicrobial agents.

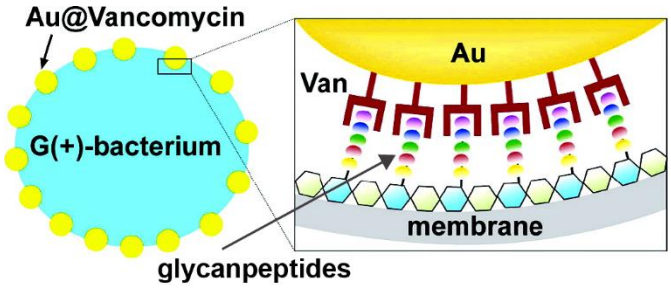

Figure 1.6. Schematic diagram showing the binding of vancomycin capped gold nanoparticles with vancomycin-resistant enterococci. Adapted from reference 82.

The antibacterial activity of silver has been well established. High surface area and concomitant increase in dissolution rate are key to its use in silver-based antimicrobials, where free Ag^{+} ions are the active agents.[84] However, they face certain shortcomings, such as high toxicity to mammalian cells and limited penetration in biofilm matrices.[85,86] Recent studies have focused on countering these issues by using inherent NP properties and surface functionalization as their toolkit. For example, Mahmoudi and co-workers developed silver ring-coated superparamagnetic iron oxide NPs (SPIONS) with ligand gaps that demonstrated high antimicrobial activity and remarkable compatibility with healthy cells. Additionally, these NPs exhibited enhanced activity against biofilm infections due to deeper penetration under an external magnetic field.[87]

Graphene NPs,[88] AuNPs,[89] and carbon nanotubes[90] possess photothermal properties that can be utilized to design therapeutic agents. These nanomaterials absorb light (700–1100 nm) and release heat. Ling and co-workers designed graphene-based photothermal NPs that captured and killed *Staphylococcus aureus* and *E. coli* bacteria upon near-infrared (NIR) laser irradiation. In this approach, graphene oxide was reduced and functionalized with magnetic NPs (MRGO). These NPs were functionalized with glutaraldehyde (GA) to induce excellent crosslinking

properties with Gram-positive and Gram-negative bacteria (Figure 1.7). Rapid and effective killing of 99% of both bacterial species was achieved upon NIR irradiation.[91]

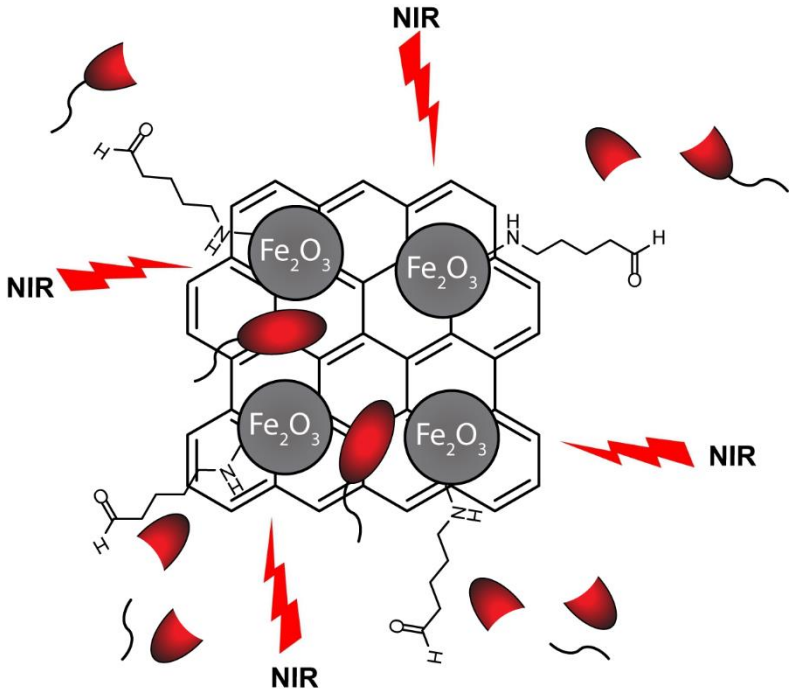

Figure 1.7. Schematic representation of antibacterial photothermal treatment by mildly reduced graphene oxide functionalized with glutaraldehyde.

1.7 Nanomaterials as delivery vehicles for antimicrobial therapy

The antimicrobial efficacy of therapeutics can be increased by using delivery vehicles to successfully transport them to the infection site.[59,60] Nanoparticle-based drug delivery systems can provide increased drug retention time in blood and reduced nonspecific distribution and targeted delivery of drugs at the site of infection. The surface chemistry of the NP plays a crucial role in ensuring the solubility of the NP in the blood stream and in providing a ‘‘stealth’’ invisibility against the body’s natural defense system. The mononuclear phagocytic system can eliminate these nanovehicles from the blood stream unless the vehicles are engineered to escape recognition.[92,93] Another important biological barrier to nanoparticle-based drug delivery is the process of opsonization. Opsonin proteins in blood rapidly adhere to nanoparticles, allowing the macrophages from the mononuclear phagocytic system (MPS) to bind and remove NPs from

circulation.[94,95] Numerous strategies have been used to hide nanoparticles from the MPS to address these limitations.[96] Of these methods, the most preferred is the adsorption or grafting of hydrophilic polymers such as PEG[97] on the surface of nanoparticles. These coatings create a 'cloud' of uncharged hydrophilic moieties on the particle's surface that repel plasma proteins and increase the circulation and retention time in the circulatory system of the body.

Bacterial infections are able to evade antibiotic treatment through reduced bactericidal concentration or reduced antimicrobial activity of therapeutic agents at the site of infection.[98] Localized delivery of the drugs/antimicrobials can increase their therapeutic efficacy. Therefore, NPs can serve as promising drug delivery vehicles owing to their tunable surface functionality, biocompatibility, and high drug loading capacity.[99]

NPs such as mesoporous silica possess a uniquely large surface area and tunable pore size that make them promising candidates for designing drug delivery vehicles.[100] For example, Schoenfisch and co-workers designed amine-functionalized silica NPs that were able to readily penetrate and eradicate pathogenic biofilms through rapid nitric oxide release.[101] Similarly, silica NPs have been fabricated as scaffolds for silver NP (AgNP) release.[102] Using NPs for controlled antimicrobial release can markedly improve their biocompatibility with mammalian cells and mitigate their hazardous environmental impact.[103,104,105] In one such study, biodegradable lignin-core NPs (EbNPs) infused with silver ions were proposed as greener alternatives to AgNPs. EbNPs were coated with cationic polyelectrolytes and loaded with Ag^+ ions. These NPs exhibited broad-spectrum biocidal action against Gram-positive and Gram-negative bacteria at lower Ag^+ ion concentrations than conventional AgNPs.[106] Therapeutic selectivity is critical when designing effective drug delivery vehicles. Triggered release of antimicrobials from these nanocarriers can be an alternative strategy to diminish their undesirable side effects. In one particular study, Langer and co-workers designed PLGA-PLH-PEG NPs as a carrier to deliver vancomycin to bacterial cells, exploiting their localized acidity. PLGA-PLH-PEG NPs demonstrated high binding affinity to bacterial cells at pH 6.0 as compared to 7.4. Vancomycin-encapsulated NPs

exhibited a 1.3-fold increase in the MIC against *S. aureus* as compared to 2.0-fold and 2.3-fold for free and PLGA-PEG encapsulated vancomycin, respectively.[107] In a similar study, pH-responsive NPs were used to deliver hydrophobic drugs to biofilm moieties. Polymeric NPs used in this study consisted of a cationic outer shell to bind with the EPS matrix and a pH-responsive hydrophobic inner shell to release encapsulated farnesol molecules on demand. These scaffolds resulted in a 2-fold increase in efficacy in the treatment of biofilms as compared to the drug alone.[108]

Apart from acidic microenvironments, NPs can be designed to trigger antibiotic release upon exposure to bacterial toxins. For example, Zhang and co-workers designed AuNP-stabilized phospholipid liposomes (AuChi-liposomes) that respond to bacterial toxins. Chitosan-functionalized AuNPs were adsorbed on the liposomal surfaces to provide stability and prevent undesirable antibiotic leakage. In the presence of α-toxin-secreting *S. aureus* bacteria, AuChi-liposomes released vancomycin that effectively inhibited their growth.[109]

Cationic NPs exhibit excellent penetration ability in biofilms. Moreover, they can self-assemble at the oil-water interfaces to generate nanocapsules.[110] Combining these two characteristic features, Rotello and co-workers generated a highly effective therapeutic system for the treatment of bacterial biofilm infections. Peppermint oil and cinnamaldehyde were chosen as the therapeutic oil template, owing to their inherent antimicrobial nature, in combination with amine-functionalized cationic silica NPs that stabilized the oil-water interface to generate nanocapsules (CP-caps) (Figure 1.8). These capsules were further stabilized by the formation of hydrophobic Schiff bases upon reacting with cinnamaldehyde. The cationic NPs enabled the capsules to readily penetrate the biofilms and release the antimicrobial oils to eradicate the biofilm infections. Moreover, the therapeutic selectivity of CP-caps was tested on a biofilm-fibroblast cell co-culture model. These studies showed effective biofilm infection eradication with simultaneous growth enhancement of fibroblast cells.[111]

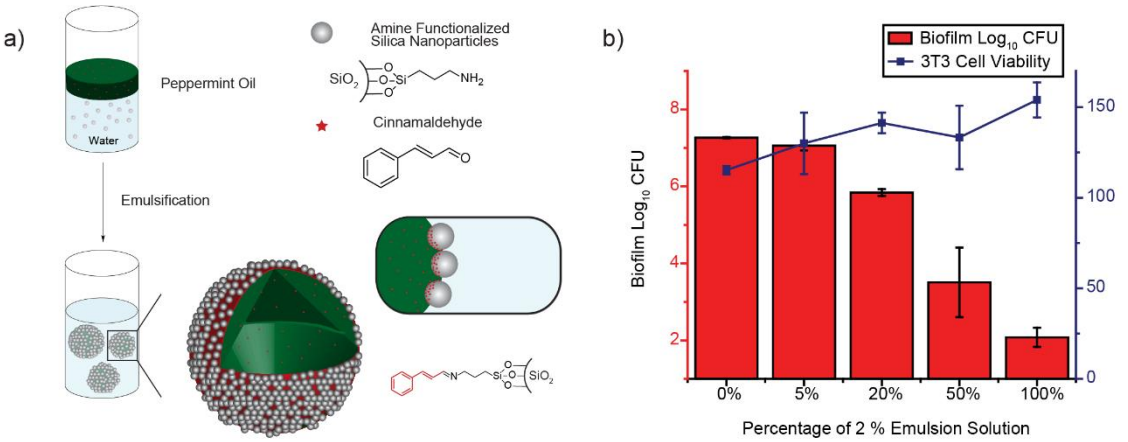

Figure 1.8. Nanoparticle-stabilized capsules for treatment of biofilm infections. **a.** Fabrication of capsules. **b.** Toxicity of CP-Cap against *Escherichia coli* cells while enhancing fibroblast viability.

1.8 Dissertation overview

Nanomaterials have emerged as new tools that can be used to combat deadly bacterial infections and overcome the barriers faced by traditional antimicrobials such antibiotic resistance. The surface engineering of nanomaterials dictates their interaction with bacterial cellular system and plays a pivotal role in determining the ability of nanoparticles to combat bacterial infections. In this thesis, we have focused on tuning the surface chemistry of nanomaterials for imaging and therapy of bacterial infections. We have demonstrated that tailoring of surface functionalities can enable unique mechanism of actions to combat multi-drug resistant bacteria as well as increase the selectivity of the therapy while showing minimal toxicity to the host cells.

In the Chapter 2 of this thesis, I have investigated the structure-activity relationship between the surface chemistry and the antimicrobial activity of the gold nanoparticles. This study demonstrates high potential of engineered gold nanoparticles as antimicrobials as well as provides a basis for developing novel nanoparticle-based antimicrobials. Building on these studies, In Chapter 3 I further explored the ability of these engineered nanoparticles in combination with existing antibiotics to treat MDR bacteria. These nanoparticles showed unique mechanisms of action to combat resistant bacteria, suggesting their potential as next-generation therapeutics.

In Chapter 4, I have fabricated nanoparticles with pH-responsive ligands for selectively targeting acidic microenvironment of the biofilms. Further these engineered nanoparticles were embedded with transition metal catalysts for bioorthogonal imaging of biofilms. This study illustrates an example for increasing the selectivity of nanomaterials by tailoring nanomaterial surface chemistry. In Chapter 5, I have used an alternative strategy to improve the selectivity of the bioorthogonal nanoparticles (nanozymes) to target bacterial biofilms. These nanozymes were electrostatically adsorbed on carrier Red Blood Cells, enabling them to selectively accumulate at the site of bacterial infection while avoiding non-specific uptake in macrophages. This study shows that interactions at nano-bio interface can play a crucial role in integration of synthetic materials with naturally occurring systems, resulting in novel antimicrobial therapies.

Synthetic polymers show structural conformations reminiscent of host-defense antimicrobial peptides. In Chapter 6, I have explored the structure-activity relationship by varying the polymer structure and screening their antimicrobial and hemolytic activity. These studies provide a deeper insight about tuning the polymer structures to generate polymer nanoparticles with high therapeutic indices against MDR bacteria. In the subsequent Chapter 7, I have utilized engineered polymer nanoparticles for synergistic antimicrobial therapy showing novel mechanisms to address bacterial and biofilm infections. These studies further corroborate the importance of surface chemistry in antimicrobial therapies. In Chapter 8, we have utilized functionalized polymers to fabricate nanosponges through self-assembly of polymers around essential-oil based cores for topical treatment of wound biofilms.

1.9 References

1. C. Willyard, *Nature* **2017**, *543*, 15.

2. A. Prüss, D. Kay, L. Fewtrell, J. Bartram, *Environ. Health Perspect.* **2002**, *110*, 537.

3. *FY15 Detect and Protect Against Antibiotic Resistance Budget Initiative*, Centers for Disease Control and Prevention, **2003**.

4. R. Laxminarayan, A. Duse, C. Wattal, A. K. M. Zaidi, H. F. L. Wertheim, N. Sumpradit, E. Vlieghe, G. L. Hara, I. M. Gould, H. Goossens, C. Greko, A. D. So, M. Bigdeli, G. Tomson, W. Woodhouse, E. Ombaka, A. Q. Peralta, F. N. Qamar, F. Mir, S. Kariuki, Z. A. Bhutta, A. Coates, R. Bergstrom, G. D. Wright, E. D. Brown, O. Cars, *Lancet Infect. Dis.* **2013**, *13*, 1057.

5. A. S. Lynch, G. T. Robertson, *Annu. Rev. Med.* **2008**, *59*, 415.

6. F. Prestinaci, P. Pezzotti, A. Pantosti, *Pathog. Glob. Health* **2015**, *109*, 309.

7. C. L. Ventola, *P T A peer-reviewed J. Formul. Manag.* **2015**, *40*, 277.

8. G. Meletis, *Ther. Adv. Infect. Dis.* **2016**, *3*, 15.

9. H. C. Neu, *Science (80-.).* **1992**, *257*, 1064.

10. B. D. Brooks, A. E. Brooks, *Adv. Drug Deliv. Rev.* **2014**, *78*, 14.

11. H. Ochman, J. G. Lawrence, E. A. Groisman, *Nature* **2000**, *405*, 299.

12. P. Nordmann, T. Naas, N. Fortineau, L. Poirel, *Curr. Opin. Microbiol.* **2007**, *10*, 436.

13. Debeer, D.; Stoodley, P.; Lewandowski, Z. *Biotechnol. Bioeng.* **1994**, *44*, 636-641.

14. J. W. Costerton, K. J. Cheng, G. G. Geesey, T. I. Ladd, J. C. Nickel, M. Dasgupta, T. J. Marrie, *Annu. Rev. Microbiol.* **1987**, *41*, 435.

15. Kumon, H.; Tomochika, K.; Matunaga, T.; Ogawa, M.; Ohmori, H. *Microbiol. Immunol.* **1994**, *38*, 615-619.

16. Shigeta, M.; Tanaka, G.; Komatsuzawa, H.; Sugai, M.; Suginaka, H.; Usui, T. *Chemotherapy* **1997**, *43*, 340-345.

17. Gordon, C. A.; Hodges, N. A.; Marriott, C. *J. Antimicrob. Chemother.* **1988**, *22*, 667-674.

18. Nichols, W. W.; Dorrington, S. M.; Slack, M. P. E.; Walmsley, H. L. *Antimicrob. Agents Chemother.* **1988**, *32*, 518-523.

19. Kim Lewis, *Nat. Rev. Microbiol.* **2007**, *5*, 48.

20. R. M. Donlan, *Emerg. Infect. Dis.* **2001**, *7*, 277.

21. Donlan, R. M.; Costerton, J. W. *Clin. Microbiol. Rev.* **2002**, *15*, 167-193.

22. J. W. Costerton, P. S. Stewart, E. P. Greenberg, *Science (80-.).* **1999**, *284*, 1318.

23. Stewart, P. S.; Costerton, J. W. *Lancet* **2001**, *358*, 135-138.

24. J. D. Bryers, *Biotechnol. Bioeng.* **2008**, *100*, 1.

25. Romling, U.; Balsalobre, C. *J. Intern. Med.* **2012**, *272*, 541-561.

26. Shigeta, M.; Tanaka, G.; Komatsuzawa, H.; Sugai, M.; Suginaka, H.; Usui, T. *Chemotherapy* **1997**, *43*, 340-345.

27. Gordon, C. A.; Hodges, N. A.; Marriott, C. *J. Antimicrob. Chemother.* **1988**, *22*, 667-674.

28. H. Wu, C. Moser, H.-Z. Wang, N. Høiby, Z.-J. Song, *Int. J. Oral Sci.* **2014**, *7*, 1.

29. P. Fernandes, *Nat Biotech* **2006**, *24*, 1497.

30. J.-M. Ghuysen, *Trends Microbiol.* **1994**, *2*, 372.

31. G. E. Stein, L. B. Johnson, *Clin. Infect. Dis.* **2011**, *52*, 1156.

32. G. Cottarel, J. Wierzbowski, *Trends Biotechnol.* **2007**, *25*, 547.

33. M. a. Fischbach, *Curr. Opin. Microbiol.* **2011**, *14*, 519.

34. E. D. Brown, G. D. Wright, *Nature* **2016**, *529*, 336.

35. E. Pierson, D. T. Hung, A. E. Clatworthy, *Nat. Chem. Biol.* **2007**, *3*, 541.

36. D. A. Rasko, V. Sperandio, *Nat. Rev. Drug Discov.* **2010**, *9*, 117.

37. F. C. O. Los, T. M. Randis, R. V Aroian, A. J. Ratner, *Microbiol. Mol. Biol. Rev.* **2013**, *77*, 173.

38. L. G. Rahme, E. J. Stevens, S. F. Wolfort, J. Shao, R. G. Tompkins, F. M. Ausubel, *Science (80-.).* **1995**, *268*, 1899.

39. L. Hua, T. S. Cohen, Y. Shi, V. Datta, J. J. Hilliard, C. Tkaczyk, J. Suzich, C. K. Stover, B. R. Sellman, *Antimicrob. Agents Chemother.* **2015**, *59*, 4526.

40. M. H. Wilcox, D. N. Gerding, I. R. Poxton, C. Kelly, R. Nathan, T. Birch, O. A. Cornely, G. Rahav, E. Bouza, C. Lee, G. Jenkin, W. Jensen, Y.-S. Kim, J. Yoshida, L. Gabryelski, A. Pedley, K. Eves, R. Tipping, D. Guris, N. Kartsonis, M.-B. Dorr, *N. Engl. J. Med.* **2017**, *376*, 305.

41. G. Rampioni, L. Leoni, P. Williams, *Bioorg. Chem.* **2014**, *55*, 60.

42. M. Hentzer, H. Wu, J. B. Andersen, K. Riedel, T. B. Rasmussen, N. Bagge, N. Kumar, M. A. Schembri, Z. Song, P. Kristoffersen, M. Manefield, J. W. Costerton, S. Molin, L. Eberl, P. Steinberg, S. Kjelleberg, N. Hoiby, M. Givskov, *EMBO J.* **2003**, *22*, 3803.

43. B. M. Knoll, E. Mylonakis, *Clin. Infect. Dis.* **2014**, *58*, 528.

44. D. P. Pires, D. Vilas Boas, S. Sillankorva, J. Azeredo, *J. Virol.* **2015**, *89*, 7449.

45. Zasloff, M. *Nature* **2002**, *415*, 389-395.

46. Falagas, M. E.; Grammatikos, A. P.; Michalopoulos, A. *Expert Rev. Anti. Infect. Ther.* **2008**, *6*, 593-600.

47. R. E. W. Hancock, H. G. Sahl, *Nat Biotech* **2006**, *24*, 1551.

48. Giuliani, A.; Rinaldi, A. C. *Cell. Mol. Life Sci.* **2011**, *68*, 2255-2266.

49. Rotem, S.; Mor, A. *Biochim. Biophys. Acta Biomembr.* **2009**, *1788*, 1582-1592.

50. L. Wang, C. Hu, L. Shao, *Int. J. Nanomedicine* **2017**, *12*, 1227.

51. A. J. Huh, Y. J. Kwon, *J. Control. Release* **2011**, *156*, 128.

52. M. J. Hajipour, K. M. Fromm, A. Akbar Ashkarran, D. Jimenez de Aberasturi, I. R. de Larramendi, T. Rojo, V. Serpooshan, W. J. Parak, M. Mahmoudi, *Trends Biotechnol.* **2012**, *30*, 499.

53. M. De, P. S. Ghosh, V. M. Rotello, *Adv. Mater.* **2008**, *20*, 4225.

54. A. Gupta, S. Mumtaz, C.-H. Li, I. Hussain, V. M. Rotello, *Chem. Soc. Rev.* **2018**, *48*, 415.

55. A. Gupta, R. F. Landis, V. M. Rotello, *F1000Research* **2016**, *5*, 364.

56. S. M. Dizaj, F. Lotfipour, M. Barzegar-Jalali, M. H. Zarrintan, K. Adibkia, *Mater. Sci. Eng. C* **2014**, *44*, 278.

57. S. Prabhu, E. K. Poulose, *Int. Nano Lett.* **2012**, *2*, 32.

58. G. Ren, D. Hu, E. W. C. Cheng, M. A. Vargas-Reus, P. Reip, R. P. Allaker, *Int. J. Antimicrob. Agents* **2009**, *33*, 587.

59. L. Zhang, D. Pornpattananangku, C.-M. J. Hu, C.-M. Huang, *Curr. Med. Chem.* **2010**, *17*, 585.

60. W. Gao, Y. Chen, Y. Zhang, Q. Zhang, L. Zhang, *Adv. Drug Deliv. Rev.* **2018**, *127*, 46.

61. K. Forier, K. Raemdonck, S. C. De Smedt, J. Demeester, T. Coenye, K. Braeckmans, *J. Control. Release* **2014**, *190*, 607.

62. L.-S. Wang, A. Gupta, V. M. Rotello, *ACS Infect. Dis.* **2016**, *2*, 3.

63. T. J. Silhavy, D. Kahne, S. Walker, *Cold Spring Harb. Perspect. Biol.* **2010**, *2*, a000414.

64. V. Berry, A. Gole, S. Kundu, C. J. Murphy, R. F. Saraf, *J. Am. Chem. Soc.* **2005**, *127*, 17600.

65. C. C. Lin, Y. C. Yeh, C. Y. Yang, C. L. Chen, G. F. Chen, C. C. Chen, Y. C. Wu, *J. Am. Chem. Soc.* **2002**, *124*, 3508.

66. C. M. Goodman, C. D. McCusker, T. Yilmaz, V. M. Rotello, *Bioconjug. Chem.* **2004**, *15*, 897.

67. S. C. Hayden, G. Zhao, K. Saha, R. L. Phillips, X. Li, O. R. Miranda, V. M. Rotello, M. A. El-Sayed, I. Schmidt-Krey, U. H. F. Bunz, *J. Am. Chem. Soc.* **2012**, *134*, 6920.

68. O. Habimana, K. Steenkeste, M.-P. Fontaine-Aupart, M.-N. Bellon-Fontaine, S. Kulakauskas, R. Briandet, *Appl. Environ. Microbiol.* **2011**, *77*, 367.

69. T. O. Peulen, K. J. Wilkinson, *Environ. Sci. Technol.* **2011**, *45*, 3367.

70. X. Li, Y. C. Yeh, K. Giri, R. Mout, R. F. Landis, Y. S. Prakash, V. M. Rotello, *Chem. Commun.* **2015**, *51*, 282.

71. P. A. Lambert, *Adv. Drug Deliv. Rev.* **2005**, *57*, 1471.

72. G. D. Wright, *Adv. Drug Deliv. Rev.* **2005**, *57*, 1451.

73. K. Rajalingam, H. Al-Younes, A. Müller, T. F. Meyer, A. J. Szczepek, T. Rudel, *Infect. Immun.* **2001**, *69*, 7880.

74. J. S. Kim, E. Kuk, K. N. Yu, J.-H. Kim, S. J. Park, H. J. Lee, S. H. Kim, Y. K. Park, Y. H. Park, C.-Y. Hwang, Y.-K. Kim, Y.-S. Lee, D. H. Jeong, M.-H. Cho, *Nanomedicine Nanotechnology, Biol. Med.* **2007**, *3*, 95.

75. K. R. Raghupathi, R. T. Koodali, A. C. Manna, *Langmuir* **2011**, *27*, 4020.

76. A. Kubacka, M. S. Diez, D. Rojo, R. Bargiela, S. Ciordia, I. Zapico, J. P. Albar, C. Barbas, V. A. P. Martins dos Santos, M. Fernández-García, M. Ferrer, *Sci. Rep.* **2014**, *4*, 4134.

77. D. Peer, J. M. Karp, S. Hong, O. C. Farokhzad, R. Margalit, R. Langer, *Nat. Nanotechnol.* **2007**, *2*, 751.

78. R. Mout, D. F. Moyano, S. Rana, V. M. Rotello, *Chem. Soc. Rev.* **2012**, *41*, 2539.

79. J. T. Seil, T. J. Webster, *Int. J. Nanomedicine* **2012**, *7*, 2767.

80. J. Bresee, C. M. Bond, R. J. Worthington, C. a. Smith, J. C. Gifford, C. a. Simpson, C. J. Carter, G. Wang, J. Hartman, N. a. Osbaugh, R. K. Shoemaker, C. Melander, D. L. Feldheim, *J. Am. Chem. Soc.* **2014**, *136*, 5295.

81. M. K. Higgins, E. Bokma, E. Koronakis, C. Hughes, V. Koronakis, *Proc. Natl. Acad. Sci. United States Am.* **2004**, *101*, 9994.

82. H. Gu, P. L. Ho, E. Tong, L. Wang, B. Xu, *Nano Lett.* **2003**, *3*, 1261.

83. J. Bresee, K. E. Maier, A. E. Boncella, C. Melander, D. L. Feldheim, *Small* **2011**, *7*, 2027.

84. V. K. Sharma, R. A. Yngard, Y. Lin, *Adv. Colloid Interface Sci.* **2009**, *145*, 83.

85. S. M. Hussain, K. L. Hess, J. M. Gearhart, K. T. Geiss, J. J. Schlager, *Toxicol. In Vitro* **2005**, *19*, 975.

86. J. Fabrega, J. C. Renshaw, J. R. Lead, *Environ. Sci. Technol.* **2009**, *43*, 9004.

87. M. Mahmoudi, V. Serpooshan, *ACS Nano* **2012**, *6*, 2656.

88. S. P. Sherlock, S. M. Tabakman, L. Xie, H. Dai, *ACS Nano* **2011**, *5*, 1505.

89. V. P. Zharov, K. E. Mercer, E. N. Galitovskaya, M. S. Smeltzer, *Biophys. J.* **2006**, *90*, 619.

90. J.-W. Kim, E. V Shashkov, E. I. Galanzha, N. Kotagiri, V. P. Zharov, *Lasers Surg. Med.* **2007**, *39*, 622.

91. M.-C. Wu, A. R. Deokar, J.-H. Liao, P.-Y. Shih, Y.-C. Ling, *ACS Nano* **2013**, *7*, 1281.

92. H. H. Gustafson, D. Holt-Casper, D. W. Grainger, H. Ghandehari, *Nano Today* **2015**, *10*, 487.

93. E. Blanco, H. Shen, M. Ferrari, *Nat. Biotechnol.* **2015**, *33*, 941.

94. D. E. Owens, N. A. Peppas, *Int. J. Pharm.* **2006**, *307*, 93.

95. J.-W. Yoo, E. Chambers, S. Mitragotri, *Curr. Pharm. Des.* **2010**, *16*, 2298.

96. V. P. Torchilin, *Nat. Rev. Drug Discov.* **2014**, *13*, 813.

97. B. Seijo, E. Fattal, L. Roblot-Treupel, P. Couvreur, *Int. J. Pharm.* **1990**, *62*, 1.

98. M. A. Kohanski, M. A. DePristo, J. J. Collins, *Mol. Cell* **2010**, *37*, 311.

99. B. Duncan, C. Kim, V. M. Rotello, *J. Control. Release* **2010**, *148*, 122.

100. C. T. Kresge, M. E. Leonowicz, W. J. Roth, J. C. Vartuli, J. S. Beck, *Nature* **1992**, *359*, 710.

101 E. M. Hetrick, J. H. Shin, H. S. Paul, M. H. Schoenfisch, *Biomaterials* **2009**, *30*, 2782.

102. Y. Tian, J. Qi, W. Zhang, Q. Cai, X. Jiang, *ACS Appl. Mater. Interfaces* **2014**, *6*, 12038.

103. M. Ahamed, M. S. AlSalhi, M. K. J. Siddiqui, *Clin. Chim. Acta* **2010**, *411*, 1841.

104. J. Fabrega, S. N. Luoma, C. R. Tyler, T. S. Galloway, J. R. Lead, *Environ. Int.* **2011**, *37*, 517.

105. P. Anastas, N. Eghbali, *Chem. Soc. Rev.* **2010**, *39*, 301.

106. A. P. Richter, J. S. Brown, B. Bharti, A. Wang, S. Gangwal, K. Houck, E. A. Cohen Hubal, V. N. Paunov, S. D. Stoyanov, O. D. Velev, *Nat Nano* **2015**, *10*, 817.

107. A. F. Radovic-Moreno, T. K. Lu, V. A. Puscasu, C. J. Yoon, R. Langer, O. C. Farokhzad, *ACS Nano* **2012**, *6*, 4279.

108. B. Horev, M. I. Klein, G. Hwang, Y. Li, D. Kim, H. Koo, D. S. W. Benoit, *ACS Nano* **2015**, *9*, 2390.

109. D. Pornpattananangkul, L. Zhang, S. Olson, S. Aryal, M. Obonyo, K. Vecchio, C. M. Huang, L. Zhang, *J. Am. Chem. Soc.* **2011**, *133*, 4132.

110. X.-C. Yang, B. Samanta, S. S. Agasti, Y. Jeong, Z.-J. Zhu, S. Rana, O. R. Miranda, V. M. Rotello, *Angew. Chemie Int. Ed.* **2011**, *50*, 477.

111. B. Duncan, X. Li, R. F. Landis, S. T. Kim, A. Gupta, L. S. Wang, R. Ramanathan, R. Tang, J. A. Boerth, V. M. Rotello, *ACS Nano* **2015**, *9*, 7775.

CHAPTER 2

ENGINEERING SURFACE FUNCTIONALITY OF GOLD NANOPARTICLES TO COMBAT MULTI-DRUG RESISTANT BACTERIA

2.1 Introduction

The emergence of multi-drug resistant (MDR) bacteria has become a severe threat to public health.[1] According to a report published by the U.S. Centers for Disease Control and Prevention, antibiotic resistant bacteria cause millions of infections and thousands of deaths every year in the U.S.[2] Additionally, the significant and continuous decrease in the number of approved antibiotics in the past decade has contributed to the increasingly threatening situation[3] that has resulted in an urgent need for the discovery of novel antibacterials and treatment strategies.[4] There are a number of actively pursued strategies, including searching for new antimicrobials from natural products, modification of existing antibiotic classes, and the development of antimicrobial peptides.[5]

Nanoparticles (NPs) provide versatile platforms for therapeutic applications based on their physical properties.[6,7,8] For example, NP size range is commensurate with biomolecular and bacterial cellular systems, providing additional interactions to small molecule antibiotics.[9,10] The high surface to volume ratio allows incorporation of abundant functional ligands, enabling multivalency on NP surface to enhance interactions to target bacteria. Utilizing these characteristic features, NPs have been conjugated with known antibiotics to combat MDR bacteria. The antibiotic molecules can be infused with NPs via noncovalent interactions[11,12] or incorporated on NPs via covalent bonds.[13,14] Both methods have been reported for enhanced activity against bacteria, showing decreased minimum inhibitory concentration (MIC) in comparison with use of free antibiotics.[15,16,17] The improved performance is proposed to result from polyvalent effect of concentrated antibiotics on the NP surface as well as enhanced

internalization of antibiotics by NPs.[18] Yet the dependence on existing antibiotics in these approaches may not be able to delay the onset of acquired resistance.

The functional ligands on NP surface can provide direct multivalent interactions to biological molecules, allowing NPs to be exploited as self-therapeutic agents.[19,20,21] This strategy can circumvent the employment and the potential limitation of existing antibiotics in nanocarrier systems.[22] For assembly of such self-therapeutic NPs, the essentially inert and nontoxic nature of gold makes it an attractive core material.[23] To this end, we synthesized a series of self-therapeutic gold nanoparticles (AuNPs) as an antimicrobial agent. The structure-activity relationship of the functional ligands on 2 nm core AuNP revealed that AuNP antimicrobial properties can be tailored through surface hydrophobicity, providing a new aspect to design antimicrobial nanomaterials.

On the basis of these studies, we focused on the most potent AuNP candidate and tested this particle with clinically isolated uropathogens. The result showed inhibited growth of multiple strains of uropathogens, including many MDR strains and methicillin-resistant Staphylococcus aureus (MRSA). Significantly, this AuNP did not induce bacterial resistance even after 20 generations. These particles are also compatible with mammalian cells: the maximum hemolytic index of this AuNP is >50, and at the MIC against MRSA, the C10-AuNP treated mammalian cells maintained >80% viability.

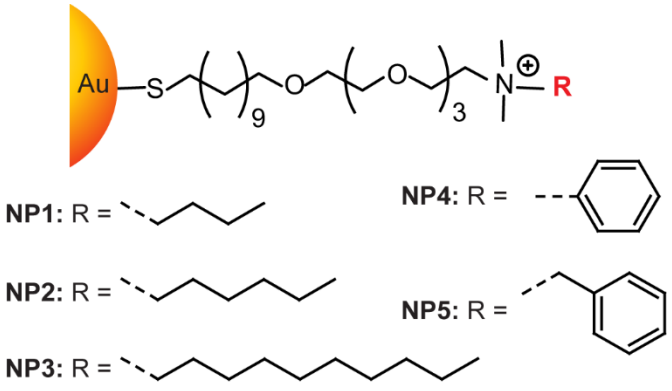

Figure 2.1. Molecular structures of functional ligands on AuNPs.

2.2 Results and Discussions

We recently reported that 2 nm core cationic monolayer-protected AuNPs can interact with cell membrane of Gram-positive and Gram-negative bacteria, resulting in formation of distinct aggregation patterns and lysis of bacterial cell.[24] Similarly, Jiang and co-workers also demonstrated that blebbing caused by cationic AuNPs induced bacterial membrane damage.20 These results suggested that 2 nm AuNPs with cationic surface properties could be used as antimicrobial agents. To systematically investigate the role of surface chemistry in NP antimicrobial efficacy, AuNPs were synthesized with a range of different cationic functionalities featuring different chain length, nonaromatic, and aromatic characteristics (Figure 2.1). All AuNPs were highly soluble in water; including NP 3 with the most hydrophobic end group (stock solution concentration was 56 μM).

We first evaluated the functional AuNP antimicrobial activities on a laboratory strain (*Escherichia coli* DH5α), using broth dilution methods to determine the minimal inhibitory concentrations (MICs).[25] AuNPs were incubated with 5 $\times 10^5$ cfu/mL of *E. coli* overnight. All AuNPs were able to completely inhibit the proliferation of *E. coli* at nanomolar concentrations; the MICs of different AuNPs, however, varied by the R group. To correlate antimicrobial activity with AuNP surface functionality, we plotted the MICs against the calculated AuNP end group log P values that quantitatively represent the relative NP surface hydrophobicity (Figure 2.2).[26] A marked structure-activity relationship was observed, with hydrophobic NPs being more effective against *E. coli* growth. The most hydrophobic AuNP tested, NP 3 that carried an n-decane end group was capable of inhibiting *E. coli* proliferation at only 32 nM.

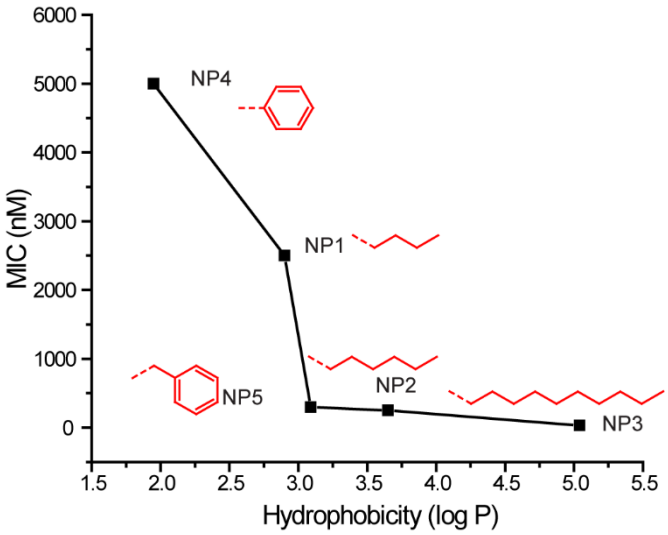

Figure 2.2. MIC values (nM) of AuNPs bearing different hydrophobic surface ligands against *E. coli* DH5α. Log P represents the calculated hydrophobic values of the end groups.

We next tested the antimicrobial activities of the most potent antimicrobial (NP 3) on uropathogenic *E. coli* clinical isolates (Table 2.1). Five isolates with differing resistance to clinically used antibiotics. (resistant to 1-17 drugs, depending on strain) were used for this study. NP 3 suppressed the growth of all five uropathogenic strains of *E. coli*, including three MDR at a concentration of 16 nM, lower [27] or similar to[20] reported antibiotic capped AuNPs. The comparable MIC values of MDR and laboratory strains suggest that C10-AuNP could potentially address the common mechanisms of bacterial resistance.

Next, NP 3 was further tested with more species/ strains of uropathogenic clinical isolates, including Gram-negative *Enterobacter cloacae* complex and *Pseudomonas aeruginosa* and Gram-positive *S. aureus* and methicillin-resistant *S. aureus* (MRSA) (Table 2.1). Among these isolates, *P. aeruginosa* has intrinsic resistance to a variety of antibiotics due to their exceptionally low outer-membrane permeability and multidrug efflux pumps.[28] Likewise, *S. aureus* has been a stumbling block for antimicrobial treatment, overcoming most of the therapeutic chemo-agents developed in the past five decades.[29] Particularly, MRSA has emerged as “superbug”, resistant to most antibiotics commonly used for the staph infections.[30] NP 3 was effective in treating each of these pathogens, with MICs of 8-64 nM.

Table 2.1. MIC values of C10-AuNP against uropathogenic clinical isolates.

Strain	Species	MIC (nM)	# of resistant drugs	MDR
CD-2	*E. coli*	16	1	No
CD-496	*E. coli*	16	2	Yes
CD-3	*E. coli*	16	3	Yes
CD-19	*E. coli*	16	4	Yes
CD-549	*E. coli*	16	17	Yes
CD-866	*E. cloacae complex*	16	2	Yes
CD-1412	*E. cloacae complex*	8	4	Yes
CD-1545	*E. cloacae complex*	16	7	Yes
CD-1006	*P. aeruginosa*	16	1	No
CD-23	*P. aeruginosa*	32	13	Yes
CD-1578	*S. aureus*	64	4	Yes
CD-489	*S. aureus - MRSA*	32	10	Yes

On the basis of the enhanced toxicity of NP 3, we hypothesized that the cationic hydrophobic AuNPs are particularly effective at compromising the integrity of bacterial membrane, causing toxicity to bacterial cells.[24] To support this hypothesis, we employed a propidium iodide (PI) staining assay. PI can only penetrate bacterial cells with compromised membrane and binds nucleic acids, with a concomitant enhancement of red fluorescence.[31,32] Uropathogens, *E. coli* CD-2 and *S. aureus* CD-489, were chosen as representative Gram-negative and Gram-positive strains. Bacteria (1×10^8 cfu/mL) were incubated with NP 3 at a final concentration of 500 nM for 3 h at 37 °C and then stained with PI before imaging. Confocal laser scanning microscopy (CLSM) images in Figure 2.3 showed NP induced membrane damage in both bacteria.

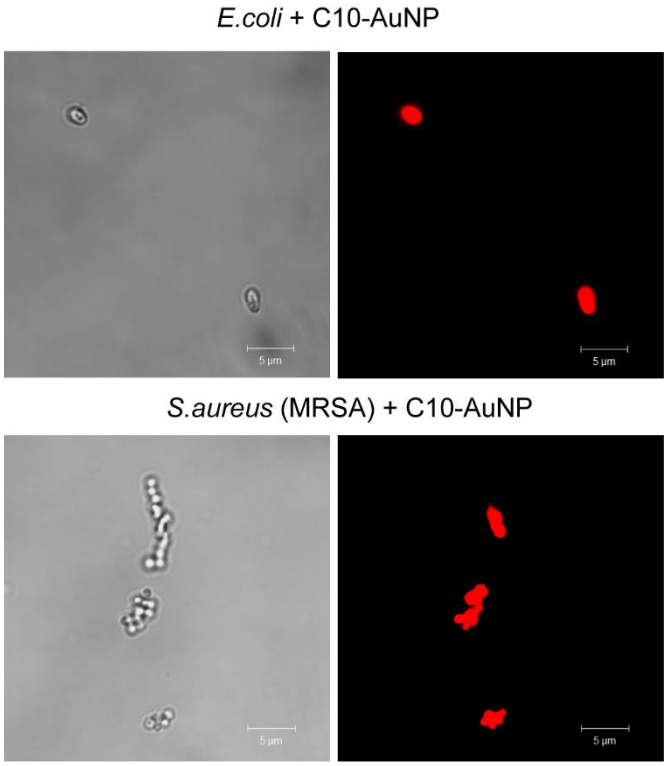

Figure 2.3. PI staining showing NP 3 (C10-AuNP)-induced bacterial cell membrane damage. Scale bar is 5 µm.

To study the development of bacterial resistance to NP 3, *E. coli* CD-2 was exposed to sub-MIC (66% of MIC) of NP 3, with the obtained bacterial cell population defined as the first generation. After harvesting the first generation, the MIC was tested, and a second generation was generated by exposing the first generation at its sub-MIC (66%). After 20 generations, *E. coli* remained susceptible to the original MIC of 16 nM. Compared to literature reported rate at which *E. coli* acquires resistance to conventional antibiotics,[20] NP 3 significantly delayed evolution of resistance. This lack of bacterial adaptation provides a means of potentially controlling and preventing the drug resistance.[33,34]

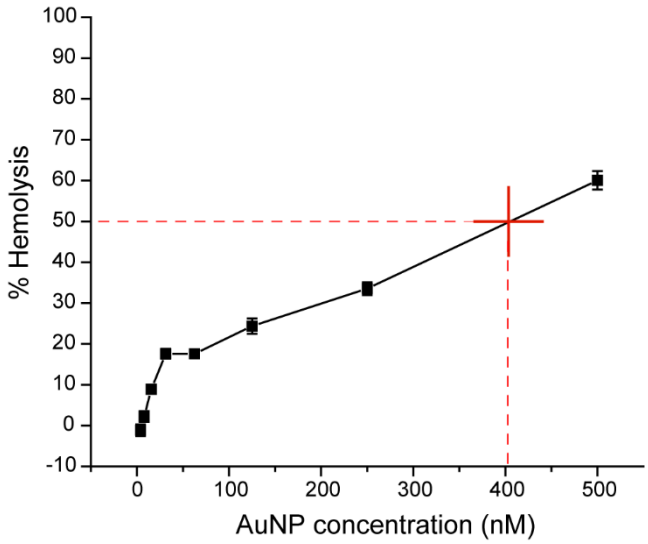

Figure 2.4. Hemolytic activity of NP 3 at different concentrations. HC_{50} was estimated to be ~400 nM (as denoted by the red cross in figure).

To assess the biocompatibility of our antimicrobial NP 3, we performed hemolysis assay on human red blood cells as well as viability assays on mammalian cells. At all the MIC concentrations tested (in the range of 4 nM to 128 nM), NP 3 showed modest hemolytic activity as shown in Figure 2.4. HC_{50}, which is the concentration to lyse 50% of human red blood cells,[35] was ~400 nM for NP 3. The hemolytic index (HC_{50}/MIC) was used to assess NP 3 selectivity against eukaryotic cells; therefore, the maximum hemolytic index of NP 3 was 50 (400 nM/8 nM). The observed AuNP cell selectivity could be explained by the fact that the surface of bacterial cells are more negatively charged than mammalian cells,[36] therefore accounting for the better affinity toward multi cations in bacteria. Also, the presence of cholesterol in mammalian cell membranes helps to stabilize the membranes, making them less sensitive to destruction by antimicrobial AuNPs.[37] It should be noted that the mammalian cell culture model used in this study may not fully reflect the in vivo toxicity profile.

2.3 Conclusions

We report here an antimicrobial strategy using self-therapeutic AuNPs to combat MDR bacteria. Cationic and hydrophobic functionalized AuNPs effectively suppressed growth of 11 clinical MDR isolates, including both Gram-negative and Gram-positive bacteria. The NP ligand structure-activity relationship revealed that surface chemistry played an important role in AuNP antimicrobial properties, providing a design element for prediction and rational design of new antibiotic NPs. Considering the efficient antimicrobial effect on MDR bacteria, the high biocompatibility, and the slow development of resistance, cationic hydrophobic nanoparticles such as NP 3 offer a promising strategy for the long-term combating of (MDR) bacteria, a key issue in healthcare.

2.4 Experimental methods

2.4.1 Synthesis of AuNPs

2 nm diameter gold nanoparticles were synthetized by the Brust-Schiffrin two-phase methodology1 using pentanethiol as the stabilizer; these clusters were purified with successive extractions with ethanol and acetone. A Murray place exchange reaction2 was carried out in dry DCM to functionalize the nanoparticles with each ligand.[38, 39] The monolayer-protected nanoparticles were redispersed in water and the excesses of ligand/pentanethiol were removed by dialysis using a 10,000 MWCO snake-skin membrane. The final concentration was measured by UV spectroscopy on a Molecular Devices SpectraMax M2 at 506nm according to the reported methodology.

2.4.2 Determination of antimicrobial activities of cationic gold nanoparticles

Bacteria were cultured in LB medium at 37 °C and 275 rpm until stationary phase. The cultures were then harvested by centrifugation and washed with 0.85% sodium chloride solution for three times. Concentrations of resuspended bacterial solution were determined by optical density

measured at 600 nm. M9 medium was used to make dilutions of bacterial solution to a concentration of 1×10^6 cfu/mL. A volume of 50 μL of these solutions was added into a 96-well plate and mixed with 50 μL of NP solutions in M9, giving a final bacterial concentration of 5×10^5 cfu/mL. NPs concentration varied in half fold according to a standard protocol, ranging from 125 to 3.9 nM. A growth control group without NPs and a sterile control group with only growth medium were carried out at the same time. Cultures were performed in triplicates, and at least two independent experiments were repeated on different days. The MIC is defined as the lowest concentration of AuNP that inhibits visible growth as observed with the unaided eye.

2.4.3 Propidium Iodide staining assay

E. coli CD-2 and MRSA CD-489 (1×10^8 cfu/mL) were incubated with 500 nM C10-AuNP in M9 at 37 °C and 275 rpm for 3 h. The bacteria solutions were then mixed with PI (2 μM) and incubated for 30 min in dark. Five microliters of the samples were placed on a glass slide with a glass coverslip and observed with a confocal laser scanning microscopy, Zeiss 510 (Carl Zeiss, Jena, Germany) using a 543 nm excitation wavelength.

2.4.4 Resistance development

E. coli CD-2 was inoculated in M9 medium with 10.4 nM (2/3 of 15.6 nM, MIC) at 37 °C and 275 rpm for 16 h. The culture was then harvested and tested for MIC as describe above. *E. coli* CD-2 was cultured without NP as well every time as a control for comparison of MICs.

Hemolysis assay. Hemolysis assay was performed on human red blood cells as we described in a previous study.[40] Briefly, citrate stabilized human whole blood (pooled, mixed gender) was purchased from Bioreclamation LLC, Westbury, NY. The red blood cells were purified and resuspended in 10 mL of phosphate buffered saline as soon as received. A total of 0.1 mL of RBC solution was added to 0.4 mL of NP solution in PBS in 1.5 mL centrifuge tube the mixture was incubated at 37 °C, 150 rpm for 30 min followed by centrifugation at 4000 rpm for 5 min. The absorbance value of the supernatant was measured at 570 nm with absorbance at 655 nm as a

reference. RBCs incubated with PBS as well as water were used as negative and positive control, respectively. All samples were prepared in triplicate.

2.4.5 Mammalian cell viability assay

A total of 20 000 NIH 3T3 (ATCC CRL-1658) cells were cultured in Dulbecco's modified Eagle medium (DMEM; ATCC 30-2002) with 10% bovine calf serum and 1% antibiotics at 37 °C in a humidified atmosphere of 5% CO_2 for 48 h. Old media was removed and cells were washed one time with phosphate-buffered saline (PBS) before addition of NPs in the prewarmed 10% serum containing media. Cells were incubated for 24 h at 37 °C under a humidified atmosphere of 5% CO_2. Cell viability was determined using Alamar blue assay according to the manufacturer's protocol (Invitrogen Biosource). After a wash step with PBS three times, cells were treated with 220 μL of 10% alamar blue in serum containing media and incubated at 37 °C under a humidified atmosphere of 5% CO_2 for 3 h. After incubation, 200 μL of solution from each well was transferred in a 96-well black microplate. Red fluorescence, resulting from the reduction of Alamar blue solution, was quantified (excitation/emission: 560 nm/590 nm) on a SpectroMax M5 microplate reader (Molecular Device) to determine the cellular viability. Cells without any NPs were considered as 100% viable. Each experiment was performed in triplicate.

2.5 References

1. H. C. Neu, *Science* **1992**, *257*, 1064–1073.

2. *FY15 Detect and Protect Against Antibiotic Resistance Budget Initiative*, Centers for Disease Control and Prevention, **2003**.

3. Spellberg, B.; Powers, J. H.; Brass, E. P.; Miller, L. G.; Edwards, J. E. *Clin. Infect. Dis.* **2004**, *38*, 1279-1286.

4. Alanis, A. J. *Arch. Med. Res.* **2005,** *36*, 697-705

5. O'Connell, K. M. G.; Hodgkinson, J. T.; Sore, H. F.; Welch, M.; Salmond, G. P. C.; Spring, D. R. *Angew. Chemie Int. Ed.* **2013**, *52*, 10706.

6. Davis, M. E.; Chen, Z.; Shin, D. M. *Nat. Rev. Drug Discov.* **2008,** *7*, 771-782.

7. Peer, D.; Karp, J. M.; Hong, S.; Farokhzad, O. C.; Margalit, R.; Langer, R. *Nat. Nanotech.* **2007,** *2*, 751-760.

8. De, M.; Ghosh, P. S.; Rotello, V. M. *Adv. Mater.* **2008,** *20*, 4225-4241.

9. Redl, F. X.; Black, C. T.; Papaefthymiou, G. C.; Sandstrom, R. L.; Yin, M.; Zeng, H.; Murray, C. B.; O'Brien, S. P. *J. Am. Chem. Soc.* **2004,** *126*, 14583-14599.

10. Daniel, M. C.; Astruc, D. *Chem. Rev.* **2004,** *104*, 293-346.

11. Grace, A. N.; Pandian, K. *Colloids Surf., A* **2007,** *297*, 63-70.

12. Ahangari, A.; Salouti, M.; Heidari, Z.; Kazemizadeh, A. R.; Safari, A. A. *Drug Deliv.* **2013,** *20*, 34-39.

13. Gu, H. W.; Ho, P. L.; Tong, E.; Wang, L.; Xu, B. *Nano Lett.* **2003,** *3*, 1261-1263.

14. Rai, A.; Prabhune, A.; Perry, C. C. *J. Mater. Chem.* **2010,** *20*, 6789-6798.

15. Brown, A. N.; Smith, K.; Samuels, T. A.; Lu, J. R.; Obare, S. O.; Scott, M. E. *Appl. Environ. Microbiol.* **2012,** *78*, 2768-2774.

16. Fayaz, A. M.; Girilal, M.; Mandy, S. A.; Somsundar, S. S.; Venkatesan, R.; Kalaichelvan, P. T. *Process Biochem.* **2011,** *46*, 636-641.

17. Alekshun, M. N.; Levy, S. B. *Cell* **2007,** *128*, 1037-1050.

18. Zhao, Y. Y.; Jiang, X. Y. *Nanoscale* **2013,** *5*, 8340-8350.

19. Arvizo, R. R.; Saha, S.; Wang, E. F.; Robertson, J. D.; Bhattacharya, R.; Mukherjee, P. *Proc. Natl. Acad. Sci. U.S.A.* **2013,** *110*, 6700-6705.

20. Zhao, Y. Y.; Tian, Y.; Cui, Y.; Liu, W. W.; Ma, W. S.; Jiang, X. Y. *J. Am. Chem. Soc.* **2010,** *132*, 12349-12356.

21. Bresee, J.; Maier, K. E.; Boncella, A. E.; Melander, C.; Feldheim, D. L. *Small* **2011,** *7*, 2027-2031.

22. L. B. Capeletti, L. F. De Oliveira, K. D. A. Gonçalves, J. F. A. De Oliveira, Â. Saito, J. Kobarg, J. H. Z. Dos Santos, M. B. Cardoso, *Langmuir* **2014**, *30*, 7456.

23. Connor, E. E.; Mwamuka, J.; Gole, A.; Murphy, C. J.; Wyatt, M. D. *Small* **2005**, *1*, 325-327.

24. Hayden, S. C.; Zhao, G. X.; Saha, K.; Phillips, R. L.; Li, X. N.; Miranda, O. R.; Rotello, V. M.; El-Sayed, M. A.; Schmidt-Krey, I.; Bunz, U. H. F. *J. Am. Chem. Soc.* **2012**, *134*, 6920-6923.

25. Wiegand, I.; Hilpert, K.; Hancock, R. E. W. *Nat. Protoc.* **2008**, *3*, 163-175.

26. Moyano, D. F.; Goldsmith, M.; Solfiell, D. J.; Landesman-Milo, D.; Miranda, O. R.; Peer, D.; Rotello, V. M. *J. Am. Chem. Soc.* **2012**, *134*, 3965-3967.

27. J. Bresee, K. E. Maier, C. Melander, D. L. Feldheim, *Chem. Commun. (Camb).* **2010**, *46*, 7516.

28. Nikaido, H. *J. Bacteriol.* **1996**, *178*, 5853-5859.

29. Hiramatsu, K.; Cui, L.; Kuroda, M.; Ito, T. *Trends. Microbiol.* **2001**, *9*, 486-493.

30. Klevens, R. M.; Morrison, M. A.; Nadle, J.; Petit, S.; Gershman, K.; Ray, S.; Harrison, L. H.; Lynfield, R.; Dumyati, G.; Townes, J. M.; Craig, A. S.; Zell, E. R.; Fosheim, G. E.; McDougal, L. K.; Carey, R. B.; Fridkin, S. K.; Investigators, A. B. M. *JAMA* **2007**, *298*, 1763-1771.

31. Boulos, L.; Prevost, M.; Barbeau, B.; Coallier, J.; Desjardins, R. *J. Microbiol. Methods* **1999**, *37*, 77-86.

32. Cox, S. D.; Mann, C. M.; Markham, J. L.; Bell, H. C.; Gustafson, J. E.; Warmington, J. R.; Wyllie, S. G. *J. Appl. Microbiol.* **2000**, *88*, 170-175.

33. Levy, S. B.; Marshall, B. *Nat. Med.* **2004**, *10*, S122-S129.

34. Davies, J.; Davies, D. *Microbiol. Mol. Biol. Rev.* **2010**, *74*, 417-433.

35. Eren, T.; Som, A.; Rennie, J. R.; Nelson, C. F.; Urgina, Y.; Nusslein, K.; Coughlin, E. B.; Tew, G. N. *Macromol. Chem. Phys.* **2008**, *209*, 516-524.

36. Miranda, O. R.; Chen, H. T.; You, C. C.; Mortenson, D. E.; Yang, X. C.; Bunz, U. H. F.; Rotello, V. M. *J. Am. Chem. Soc.* **2010**, *132*, 5285-5289.

37. K. Matsuzaki, K. I. Sugishita, N. Fujii, K. Miyajima, *Biochemistry* **1995**, *34*, 3423.

38. M. Brust, M. Walker, D. Bethell, D. J. Schiffrin, R. Whyman, *J. Chem. Soc. Chem. Commun.* **1994**, 801.

39. M. J. Hostetler, A. C. Templeton, R. W. Murray, *Langmuir* **1999**, *15*, 3782.

40. Saha, K. M., D. F.; Rotello, V. M. *Mater. Horiz.* **2014**, *1*, 102-105.

CHAPTER 3

SYNERGISTIC ANTIMICROBIAL THERAPY USING ENGINEERED NANOPARTICLES FOR THE TREATMENT OF MULTI-DRUG RESISTANT BACTERIAL INFECTIONS

3.1 Introduction

Increasing antibiotic resistance in bacterial strains is a serious and growing threat to human health,[1,2] as multi-drug resistant (MDR) bacteria cause millions of infections each year. For instance, more than 40% of *Staphylococcus aureus* strains collected from hospitals are resistant to methicillin (methicillin-resistant *S. aureus*, MRSA) and in some cases even resistant to broad-spectrum antibiotics such as carbapenems and vancomycin.[3,4,5] Most cases of MDR infections require prolonged antibiotic treatment that are associated with extensive health-care costs and further contribute to increase in antibiotic tolerance in surviving bacterial cells.[6] Recent projections suggest that annual global deaths caused by MDR infections will reach 10 million by 2050.[7] Immunity to traditional antibiotics will continue to increase, and the situation will become more dire as the number of strains of MDR bacteria increases.[8,9]

There have been considerable efforts to develop new antimicrobials by screening natural products, modifying existing antibiotics, and synthesizing antimicrobial peptides.[10] Synthetic macromolecules such as polymers that mimic host-defense peptides are frequently used as biocidal agents.[11,12] More recently, nanoparticles (NPs) have emerged as promising weapons in our antimicrobial arsenal. Their antimicrobial efficacy is attributable to their large surface area enabling high synergy arising from multivalent interactions.[13,14] For example, NPs functionalized with small molecule ligands exhibit broad-spectrum activity against bacteria.[15,16] Additionally, NPs can address common antibiotic resistance mechanisms such as efflux pump mediated expulsion.[17,18] Recently, Feldheim and coworkers showed that appropriate surface functionalization of AuNPs with small molecule ligands can regulate the expression of genes responsible for multiple antibiotic resistance in bacteria.16

One strategy to enhance the efficacy of NPs against bacterial cells is to functionalize them with antibiotics. For example, NPs “capped” with vancomycin and aminoglycoside exhibit enhanced antibacterial activities against resistant strains as compared to antibiotics and NPs alone.[19,20] However, an alternative strategy is to use NPs in combination with existing antibiotics to combat MDR bacterial infections.[21,22] We hypothesized that fine-tuning of NP surface chemistry could exhibit synergistic effect with antibiotics in combating MDR bacteria. We investigated the role of the surface chemistry of NPs in combination therapy by screening NPs with different functional groups in combination with antibiotics against resistant bacteria. Assessment of the structure activity relationship revealed that hydrophobic functionalized C10 and C12-AuNPs lowered the minimum inhibitory concentration (MIC) of fluoroquinolone antibiotics against MDR bacteria by 8 to 16 times. The synergy of this combination therapy was attributed to the ability of functionalized NPs to act as efflux pump inhibitors,22 confirmed by accumulation of ethidium bromide (EtBr) inside bacterial cells upon incubation with NPs. We also investigated the outer-membrane proteins (OMPs) of bacterial cells, which serve as their first line of defense.33 Combination of NPs with antibiotics provides a complementary approach to target MDR bacteria while helping to avoid the regulatory issues associated with other bioconjugate systems, further improving current therapeutic strategies.

3.2 Results and discussion

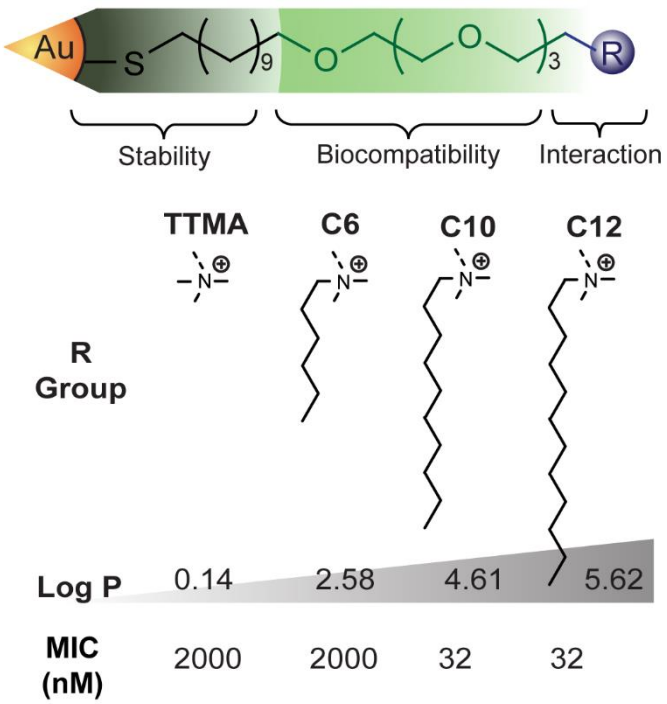

Figure 3.1. Molecular structures of functional ligands on AuNPs. Log P represents the calculated hydrophobic values of the end groups. Minimum inhibitory concentrations (MICs) of the NPs against *E. coli* (CD-549) are shown.

We have previously reported that positively charged 2 nm AuNPs bind to the surface of bacterial membranes, forming distinct aggregation patterns and causing cellular lysis.[23] Further modification of the NP surface monolayer with hydrophobic ligands elicited broad-spectrum activity against clinical MDR isolates.[24] These studies suggest that tuning NP surface chemistry can regulate their interactions with bacteria, in-turn affecting their efficacy in antimicrobial combination therapies. We screened a library of NPs with varying hydrophobicity of ligands to evaluate their efficacy in combination with antibiotics (levofloxacin and ciprofloxacin) using a checkerboard titration method.

Table 3.1. Table showing lowest FICI (fractional inhibitory concentration index) indices obtained for the combination of NPs and antibiotics.

Combination	FICI	Effect	Fold increase in Antibiotic efficacy
TTMA – levofloxacin	0.56	Additive	2
TTMA –ciprofloxacin	1	Additive	2
C6 – levofloxacin	0.625	Additive	8
C6 – ciprofloxacin	0.75	Additive	2
C10 – levofloxacin	**0.25**	**Synergistic**	**8**
C10 – ciprofloxacin	**0.25**	**Synergistic**	**8**
C12 – levofloxacin	**0.375**	**Synergistic**	**8**
C12 – ciprofloxacin	**0.375**	**Synergistic**	**8**

We first evaluated the antimicrobial activity of different functional NPs by determining their minimum inhibitory concentration (MIC) against uropathogenic *E. coli* (*Escherichia coli*, CD-549) as a model strain. MIC was determined using broth dilution method where 5×10^5 cfu/ml of bacterial cells were incubated with different concentration of AuNPs overnight.[25] The MIC for different NPs are listed in Figure 3.1. The MIC of antibiotics (levofloxacin and ciprofloxacin) against *E. coli* (CD-549) was determined to be 512 mg/ L.

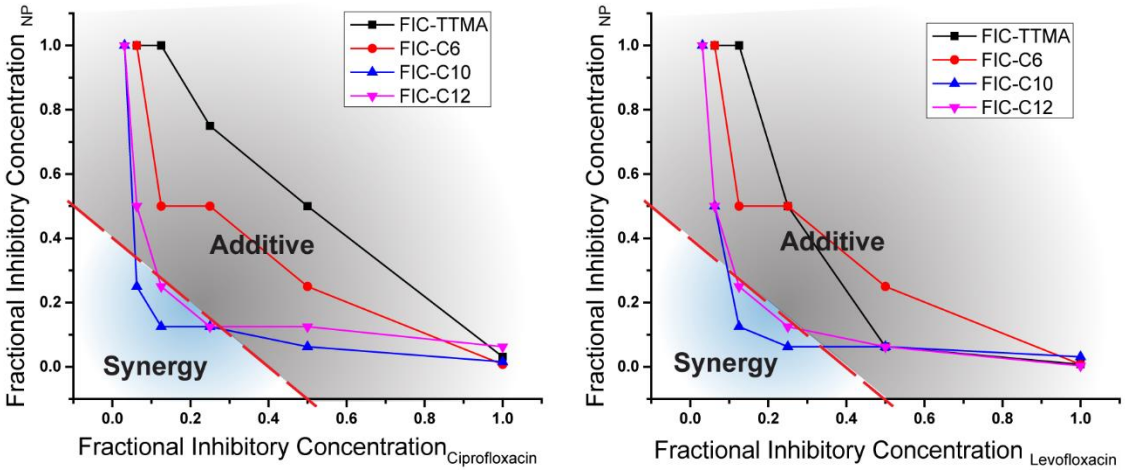

Figure 3.2. Graphs showing synergistic and additive interactions between nanoparticles and antibiotics (ciprofloxacin and levofloxacin) tested in pairs. Data are the fractional inhibitory concentrations (FICs) of the two factors in combination. TTMA and C6 shows additive interactions with antibiotics; C10 and C12 NPs show synergistic response (concave curve).

To determine the potency of the combination of AuNPs and antibiotics, we performed checkerboard titration and calculated the fractional inhibitory concentration index (FICI) for both NPs and antibiotics (Table 3.1).[26,27] The FICI values corresponding to TTMA and C6-AuNPs (≥ 0.5 and <4.0) indicate an additive response, whereas the FICI values for C10 and C12-AuNPs indicate a synergistic response (< 0.5) with the antibiotics. Additionally, the concave curve obtained with microdilution checkerboard method in case of C10 and C12 AuNPs indicate synergistic response (Figure 3.2).[28] The MIC of antibiotics was decreased 8-fold (64 mg/L) in presence of C-10 and C-12 AuNPs at sub-MIC NP dosages (4 nM, 8 nM respectively).

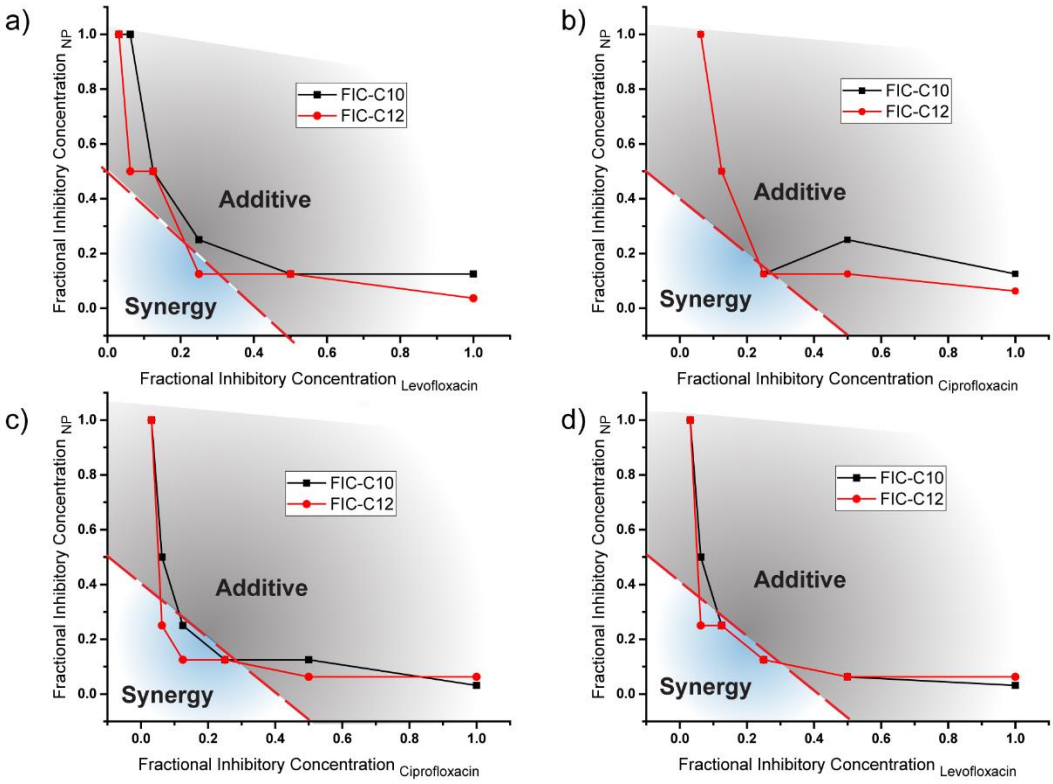

Figure 3.3. Graphs showing synergistic and additive interactions between C10 and C12 nanoparticles and antibiotics (ciprofloxacin and levofloxacin) tested in pairs against **a.** and **b.** methicillin resistant *S. aureus* and **c.** and **d.** uropathogenic *P. aeruginosa*.

After determining the most effective NPs for combination therapy, NP-antibiotic cocktails were further tested against uropathogenic clinical isolates of *Pseudomonas aeruginosa* (CD-23) and methicillin-resistant *Staphylococcus aureus* (MRSA, CD-489). C10 and C12 AuNPs showed synergistic effect in combination with fluoroquinolone antibiotics resulting in upto 16-fold reduction in the MIC of antibiotics (Figure 3.3). These results indicate the ability of functionalized NPs to antibiotic efficacy against both Gram positive (*S. aureus*) and Gram negative (*E. coli*, *P. aeruginosa*) strains. More information regarding the checkerboard combinations is provided in the Table 3.2, 3.3.

Table 3.2. FIC indexes of NP-antibiotic combinations against CD-489 (MRSA)

Combination	NP Conc. (nM)	Antibiotic Conc. (mg/L)	FICI = FIC_{NP} + FIC_{Ab}	Effect	Fold increase in Antibiotic efficacy
C10 – levofloxacin	8	16	0.5 = 0.25 + 0.25	Additive	4
C10 – ciprofloxacin	8	8	0.375 = 0.25 + 0.125	**Synergistic**	**8**
C12 – levofloxacin	8	8	0.375 = 0.25 + 0.125	**Synergistic**	**8**
C12 – ciprofloxacin	8	8	0.375 = 0.25 + 0.125	**Synergistic**	**8**

Table 3.3. FIC indexes of NP-antibiotic combinations against CD-23 (*P. aeruginosa*)

Combination	NP Conc. (nM)	Antibiotic Conc. (mg/L)	FICI = FIC_{NP} + FIC_{Ab}	Effect	Fold increase in Antibiotic efficacy
C10 – levofloxacin	8	64	0.375 = 0.25 + 0.125	**Synergistic**	**8**
C10 – ciprofloxacin	8	64	0.375 = 0.25 + 0.125	**Synergistic**	**8**
C12 – levofloxacin	4	32	0.313 = 0.25 + 0.062	**Synergistic**	**16**
C12 – ciprofloxacin	4	32	0.313 = 0.25 + 0.062	**Synergistic**	**16**

After establishing synergy obtained from the combination of NPs and antibiotics, we probed the effect of different AuNPs on MDR bacteria that could be relevant in establishing synergy with antibiotics. We investigated the ability of NPs to act as efflux pump inhibitors, as expulsion of antibiotics via efflux pumps is a major contributor to drug resistance in bacteria.[29,30] We used ethidium bromide (EtBr), which is widely used as a substrate for efflux pumps in cells, to determine the ability of NPs to act as efflux pump inhibitors.[31] We first conducted kinetics study using Carbonyl cyanide m-chlorophenyl hydrazine (CCCP) to determine influx and efflux of EtBr in bacteria. We observed that at sub-MIC dosages (0.5 × MIC) of CCCP (efflux pump inhibitor), accumulation of EtBr inside bacterial cells was significantly increased, as shown by the increase in fluorescence in Figure 3.4 a. Subsequently, ability of NPs to accumulate EtBr inside cells the bacterial cells was also tested. NPs at sub-MIC concentrations (0.5 × MIC) were added to bacterial cells followed by addition of EtBr (4 µg/mL) and the fluorescence kinetics (Ex: 530 nm and Em: 585 nm) was studied after 30 minutes' incubation. Carbonyl cyanide m-chlorophenyl hydrazine (CCCP), a widely-used efflux pump inhibitor, was used as a positive control, and untreated cells were used as negative control.[32] We observed that hydrophobic NPs (C10 and C12) enhanced accumulation of EtBr inside cells similar to that of CCCP (Figure 3.4 b, c, d). Whereas, untreated cells showed high efflux of EtBr corresponding to their low fluorescence. Notably, less hydrophobic TTMA NPs also showed accumulation of EtBr inside cells but it was comparatively lesser than CCCP. Importantly, synergistic interaction of hydrophobic NPs as compared to additive interaction of TTMA NPs can be explained due to higher ability of hydrophobic NPs to inhibit efflux mediated exclusion in bacterial cells.

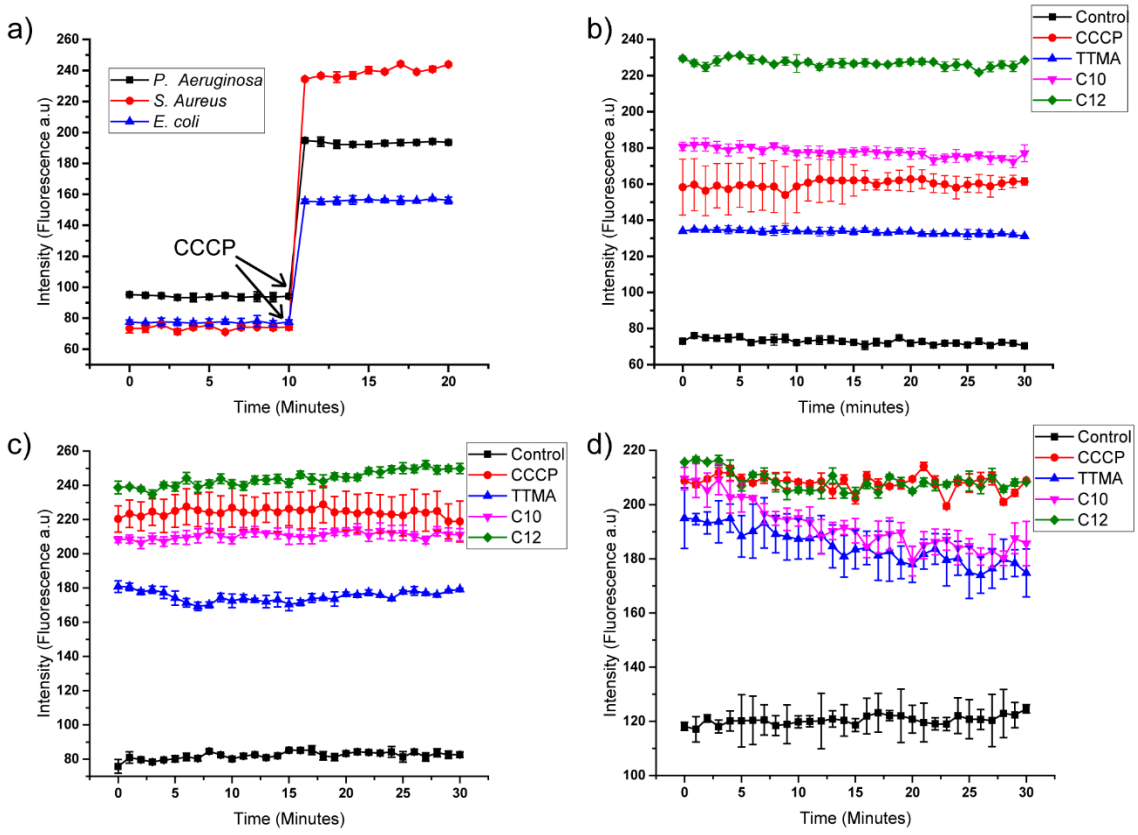

Figure 3.4. a. Fluorescence kinetics showing influx and efflux of EtBr before and after the addition of CCCP (efflux pump inhibitor) in bacteria. Fluorometric kinetics of bacterial cells after addition of NPs and CCCP showing increase in fluorescence due to accumulation of ethidium bromide inside the cells upon addition of NPs in **b.** *E. coli* **c.** methicillin-resistant *S. aureus* and **d.** *P. aeruginosa*. Only bacterial cells are used as negative controls.

We next investigated the proteomic profiles of the bacterial membrane to further understand the effect of NPs on bacteria, since the bacterial membrane acts as the first line of defense against foreign attack.[33] We used *E. coli* as model strain for our proteomic studies, due to their high relevance in clinical studies. We extracted bacterial membrane protein from untreated bacterial cells and cells treated with C-10 and C-12 AuNPs using sarkosyl method, and further analyzed them by mass spectrometry.[34,35]

We identified two distinct mechanisms underlying the synergy achieved by the addition of engineered NPs – (i) deregulation of major efflux pump protein and (ii) downregulation of proteins responsible for regulating important cellular processes. The Tolc-AcrAB efflux pumps

are major contributors to antibiotic resistance in *E. coli* species.[36] Upon incubation with hydrophobic AuNPs, the expression of tolC is downregulated indicating suppression of efflux pumps. Furthermore bamA, bamD, and bamE proteins, crucial for assembly of tolC at bacterial outer membrane proteins are strongly deregulated, compromising the detoxification of the cell.[37]

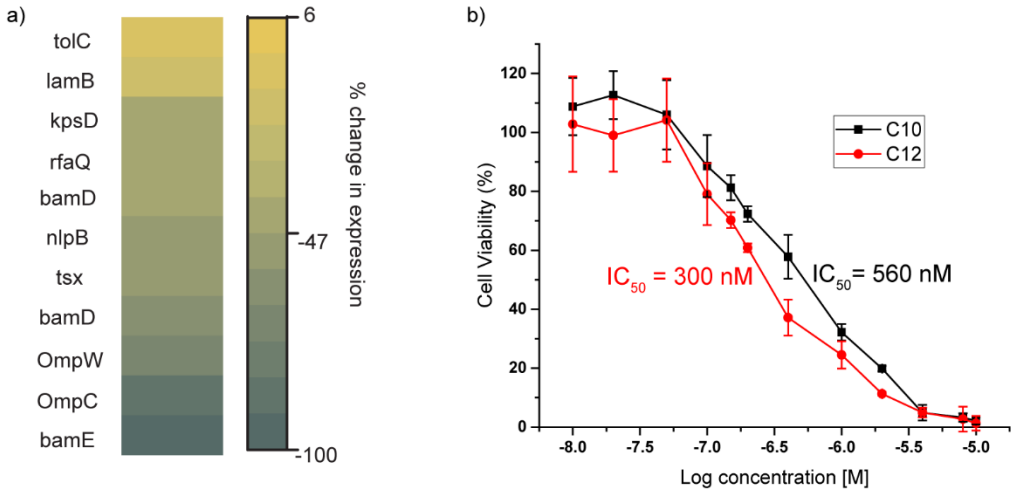

Figure 3.5. a. Proteomic profiles of outer membrane protein expression after treatment with C12 AuNPs. **b.** Cell viability of 3T3 fibroblast cells after treatment with C10 and C12 NPs.

Secondly, we concluded that hydrophobic NPs also interact with multiple proteins to disrupt crucial cell-survival processes that can also contribute to enhancing the efficacy of antibiotics. For example, proteins such as kpsD and rfaQ, responsible for export of polysaccharides through the outer membrane and biosynthesis of lipopolysaccharides (respectively) were downregulated (Figure 3.5 a).[38,39] Additionally, Lam B, transporter of carbohydrates into cells was downregulated along with Tsx, a nucleoside transporter protein.[40] Furthermore, downregulated proteins such as LamB, OmpC, Tsx, OmpW, and NlpB were previously confirmed to contribute to antibiotic resistance in *E. coli* species.[41]

We next investigated the biocompatibility of hydrophobic NPs by performing viability assays on mammalian cells. NIH-3T3 fibroblast cells were cultured and treated with AuNPs using

previously reported protocols.24 C10 AuNPs showed an IC_{50} of 560 nM, while more hydrophobic C12 AuNP had an IC_{50} of 300 nM. Additionally, after treatment with 100 nM of AuNPs (C10 and C12), NIH-3T3 fibroblast cells showed 80% (for C12) and 90% (for C10) cell viability, indicating the low toxicity of these NPs against mammalian cells. The observed specificity of NPs for bacterial cells can be attributed to more negatively charged bacterial membrane as compared to mammalian cells. Moreover, the cholesterol present on mammalian cells helps stabilize the membrane and prevents toxicity from cationic AuNPs.24

3.3 Conclusions

We have reported a strategy to use nanoparticles in combination with current antibiotics to combat MDR bacteria. We concluded that NP surface chemistry plays a vital role in regulating the nature of the interactions possessed by NP-antibiotic combinations for treatment of these pathogens. Combining NPs with antibiotics is a new modular approach to the existing therapeutics, which could assist in "recycling" currently ineffective antibiotics while circumventing the regulatory issues associated with other bioconjugate systems. Additionally, further studies by fine-tuning NP surface chemistry and using their combinations with "no more effective" antibiotics can unveil to us, novel pathways that have been unexplored in the fight against these resistant microbes.

3.4 Experimental methods

3.4.1 Ligand synthesis

Previous synthesis of our thiol-terminated ligands (TTMA, C6 and C10) can be found here.[42] Synthesis of the C-12 quaternary ammonium ligands starts with Trit-C11-Teg-OMs. The procedure is the following.

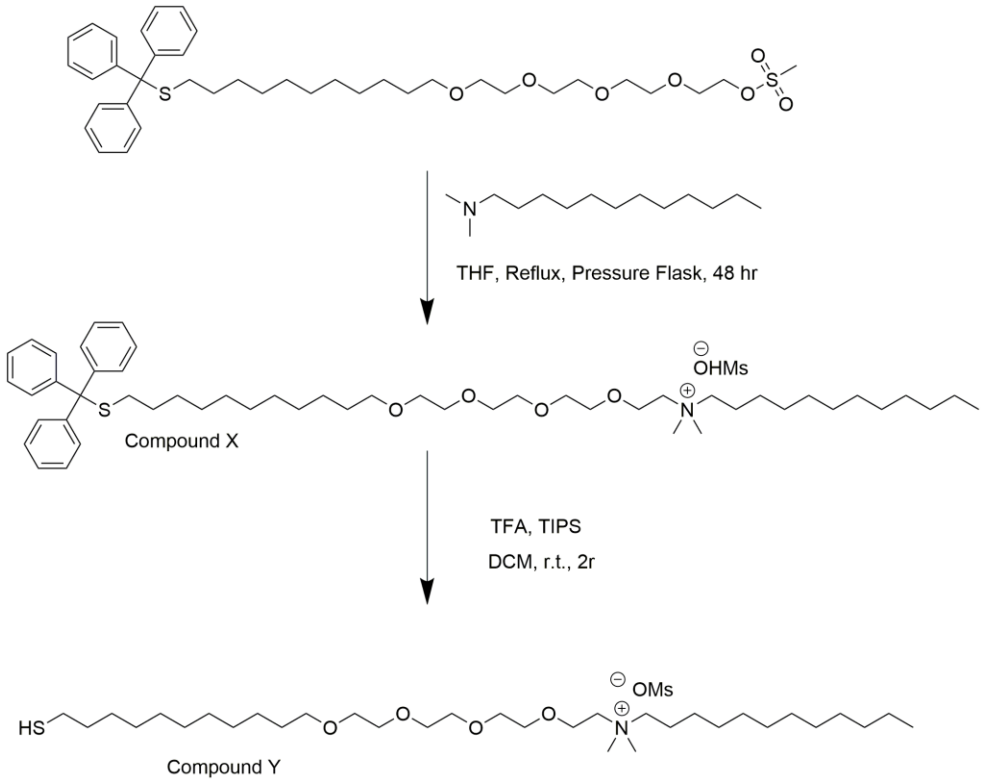

Compound X: To a round bottom flask equipped with a stirbar and capable of being pressurized, Trit-C11-Teg-OMs (0.6 g, 0.86 mmol) and N, N-dimethyldodecylamine (1.0 g, 4.68 mmol, 5.4 eq) were dissolved in tetrahydrofuran (THF, 5 mL) and stirred at reflux . Crude product was checked by TLC and THF was evaporated at reduced pressure. The residue was purified by successive hexane (4 times) and diethylether:hexane (1:1, 4 times) washings with support of sonication and then dried in a high vacuum system. The product formation was quantified, and their structure was confirmed by NMR.

Compound Y: To a round bottom flask equipped with a stirbar, Compound X (0.4 g, 0.44 mmol) was dissolved in dry dichloromethane (DCM, 5 mL) and an excess of trifluoroacetic acid (TFA, 20 equivalents, 1.0 g, 0.67 mL, 8.8 mmol) was added. The color of the solution was turned to yellow upon addition of TFA. Then, triisopropylsilane (TIPS, 0.105 g, 0.14 mL, 0.66 mmol, 1.5 eq) was added to the reaction mixture. The reaction mixture was stirred for 2 hours under N_2 at room temperature. The solvent and most of the TFA/TIPS were evaporated under reduced

pressure. The residue was purified by hexane washings (5 times) and dried in a high vacuum system. The product formation was quantitative, and their structure was confirmed by NMR.

3.4.2 Nanoparticles synthesis

2 nm diameter gold nanoparticles were synthetized by the Brust-Schiffrin two-phase methodology[43] using pentanethiol as the stabilizer; these clusters were purified with successive extractions with ethanol and acetone. A Murray place exchange reaction[44] was carried out in dry DCM to functionalize the nanoparticles with each ligand.[45,46] The monolayer-protected nanoparticles were redispersed in water and the excesses of ligand/pentanethiol were removed by dialysis using a 10,000 MWCO snake-skin membrane. The final concentration was measured by UV spectroscopy on a Molecular Devices SpectraMax M2 at 506 nm according to the reported methodology.[47]

3.4.3 Determination of minimum inhibitory concentrations

MIC is the minimum concentration of an antimicrobial agent that inhibits visible growth of bacteria overnight. The MIC of fluoroquinolone antibiotics (ciprofloxacin and levofloxacin), CCCP (EPI), and AuNPs for MDR *E. coli* was determined using a broth microdilution method as recommended by the Clinical and Laboratory Standards Institute. *E. coli* CD-549 was cultured in lysogeny broth (LB) medium at 37°C and 275 rpm to stationary phase. The cultured bacteria were then harvested by washing and centrifuging cycles with 0.85% sodium chloride solution three times. The concentration of bacteria was determined by measuring the optical density at 600 nm. Bacterial solution (100 µl) was mixed with 100 µl serially diluted concentrations of antimicrobial agent (antibiotics or NPs) in a 96-well plate, yielding a final bacterial concentration of 5×10^5 cfu/ml. The bacterial solution without antimicrobial agent was used as a growth control, whereas medium alone was used as a sterile control. All the assays were performed in triplicate, and at least two independent experiments were repeated on different days.

3.4.4 Checkerboard titrations for synergy testing

To assess possible synergy between antibiotics and NPs, we performed two-dimensional checkerboard titrations using a micro-dilution method. In 96-well plates, 2-fold dilutions of antibiotics against a range of 2-fold dilutions of NPs were used to determine the MIC of the combinations. Antibiotic-NP interaction was determined by calculating the fractional inhibitory concentration of antibiotics (FIC $_{Ab}$) and NPs (FIC $_{NP}$):

$$FIC_{Ab} = (MIC\ of\ antibiotic\ and\ NP\ combination) \div (MIC\ of\ antibiotic\ alone)$$

$$FIC_{NP} = (MIC\ of\ antibiotic\ and\ NP\ combination) \div (MIC\ of\ NP\ alone)$$

$$FICI_{combination} = FIC_{Ab} + FIC_{NP}$$

FIC_{Ab} was plotted against FIC_{NP}. A concave curve indicates synergy, whereas a convex curve indicates antagonism. Synergy was defined as FICI values ≤0.5, antagonism by FICI values >4.0, and additive interaction by FICI values between >0.5 and 4.0.

3.4.5 Ethidium bromide accumulation assay

To determine the ability of NPs to act as efflux pump inhibitors, we used a previously reported procedure. The *E. coli* CD-549 strain was grown in LB medium until mid-log phase (OD_{600} = 0.6). Next, bacteria were centrifuged at 16,000 g for 5 min and washed with PBS. OD_{600} of bacteria was adjusted to 0.3. Subsequently, EtBr was added to the final sample at a concentration of 4 µg/ml followed by addition of CCCP/NPs at ½ MIC concentrations and incubated for 30 minutes. Kinetics study of fluorescence obtained was measured using UV/Vis spectrophotometer at excitation and emission wavelength of 530 nm and 585 nm (respectively) at 25 °C for 30 minutes. Extraction of bacterial outer-membrane proteins. *E. coli* was grown with ½ MIC of engineered NPs in M9 medium for 18 h at 37 ºC. Outer membrane proteins of MDR *E. coli* were extracted following previously reported protocols.34 Briefly, overnight bacterial cultures were centrifuged at 10,000 g at 4 º C for 15 min. The bacterial pellet was suspended in 20 ml ice-cold 30 mM Tris HCl (pH 7.2) and the suspension was again centrifuged at 10,000 g at 4 º C for 15 min. The pellet

was resuspended again in 10 ml ice-cold 30 mM Tris HCl (pH 7.2). The suspended cells were disrupted by sonication in ice using a Soniprep sonicator (Misonix S-4000, USA) for 45 seconds with intermittent cooling every 45 seconds for a total of 2.5 min. The lysate was centrifuged for 15 min at 10,000 g at 4 ºC. The membranes were collected by ultracentrifuge (OptimaTM L-100XP, Beckman, USA) at 50,000 g for 1h at 4 ºC. The obtained OM pellet was suspended in a small amount of 30 mM Tris HCl (pH 7.2) and stored at -20 ºC. The concentration of OMPs was determined by BCA assay.

3.4.6. Tryptic digestion and 1D LC-MS/MS analysis

30 µg of total proteins in 150 µl of 8M urea in 50 mM ammonium bicarbonate were reduced and alkylated by adding 2 µl of 0.5M Tris(2-carboxyethyl) phosphine (TCEP) and incubating at 30 °C for 60 min. The reaction was cooled to room temperature before alkylation by adding 4 µl of 0.5M iodoacetamide at room temperature in the dark for 30 min. To dilute the 8M urea to 1M before digestion, 430 µl of 50 mM Ammonium Bicarbonate was added. Mass spectrometry-grade LysC/Trypsin (Promega) was added (1:20 ratio) for overnight digestion at 30 °C using an Eppendorf Thermomixer at 700 rpm. Formic acid was added to the peptide solution (2%), followed by desalting by C18 TopTip (Item# TT200C18.96, PolyLC) and finally drying on a SpeedVac. Tryptic peptides were re-suspended in 150 µl of 2% Acetonitrile in % 0.1 formic acid to bring the concentration to [0.2 µg/µl]. 10 µl of total tryptic peptides (2 µg total) was utilized for 1D LC-MSMS analysis in triplicate runs by on-line analysis of peptides by high-resolution, high-accuracy LC-MS/MS, consisting of an EASY-nLC 1000 HPLC Acclaim PepMap peptide trap, a 50 cm- 2µm Easy-Spray C18 column, Easy Spray Source, and a Q Exactive Plus mass spectrometer (all from Thermo Fisher Scientific). A 230-min gradient consisting of 5–16%B (100% acetonitrile) in 140 min, 16-28% in 70 min, 28-38% in 10 min, and 38-85% in 10 min was used to separate the peptides. The total LC time was 250 min. The Q Exactive Plus is set to scan

precursors at 70,000 resolution followed by data-dependent MS/MS at 17,500 resolution of the top 12 precursors.

3.4.7. 2D LC-MS/MS analysis

Twenty µg total desalted protein digests were reconstituted in 1.5% acetonitrile in 100 mM ammonium formate pH ~10. A total of 2.5 µg was then loaded onto a first-dimension column, XBridge BEH130 C18 NanoEase (300 µm x 50 mm, 5 µm), using a 2D nanoACQUITY Ultra Performance Liquid Chromatography (UPLC) system (Waters corp., Milford, MA) equilibrated with solvent A (20 mM ammonium formate pH 10, first dimension pump) at 2 µL/min. The first fraction was eluted from the first-dimension column at 17.5% of solvent B (100% acetonitrile) for 4 min and transferred to the second-dimension Symmetry C18 trap column 0.180 x 20 mm (Waters corp., Milford, MA) using a 1:10 dilution with 99.9% second-dimensional pump solvent A (0.1% formic acid in water) at 20 µL/min. Peptides were then eluted from the trap column and resolved on the analytical C18 BEH130 PicoChip column 0.075 x 100 mm, 1.7 µm particles (NewObjective, MA) at low pH by increasing the composition of solvent B (100% acetonitrile) from 1 to 6% in 2 min, then to 16% in 80 min, to 26% in 12 min, and finally to 38% in 2 min, all at 400 nL/min. Subsequent fractions were carried with increasing concentrations of solvent B. The following four first-dimension fractions were eluted at 20, 23, 27, and 60% solvent B. The analytical column outlet was directly coupled to an Orbitrap Velos Pro mass spectrometer (Thermo Fisher Scientific) operated in positive data-dependent acquisition mode. MS1 spectra were measured with a resolution of 60,000, an AGC target of 1e6, and a mass range from 350 to 1400 m/z. Up to 5 MS2 spectra per duty cycle were triggered, fragmented by collision-induced dissociation, and acquired in the ion trap with an AGC target of 1e4, an isolation window of 2.0 m/z, and a normalized collision energy of 35. Dynamic exclusion was enabled with duration of 20 sec.

3.4.8. Protein Identification and data analysis

The LC-MSMS raw data were submitted to Integrated Proteomics Pipelines (IP2) Version IP2 v.3 (Integrated Proteomics Applications, Inc.) with ProLucid algorithm as the search program[48] for peptide/protein identification. ProLucid search parameters were set up to search the UniProt ECOLI.CFT073.ATCC700928.UPEC (vs. October 2015) protein fasta database including reversed protein sequences using trypsin for enzyme with the allowance of up to two missed cleavages, Semi Tryptic search with fixed modification of 57 Da for cysteines to account for carboxyamidomethylation and precursor mass tolerance of 50 ppm. Differential search includes 16 Da for-methionine oxidation. The search results were viewed, sorted, filtered, and statically analyzed using DTASelect for proteins with protein FDR rates ≤2.5.[49] Differential label-free proteomics data analysis was performed using IP2-Census, Protein Identification STAT COMPARE[50] with 1D LC-MS/MS in three technical replicates and one technical replicate of 2D LC-MS/MS dataset to discover lower-abundance proteins. The result was a label-free quantification analysis, with t-test and DAVID Bioinformatics Resources Functional Annotation 6.7.[51]

3.5 References

1. S. B. Levy and M. Bonnie, *Nat. Med.*, **2004**, *10*, S122–S129.

2. H. C. Neu, *Science* **1992**, *257*, 1064–1073.

3. M. L. Cohen, *Nature*, **2000**, *406*, 762–7.

4. W. Weerakoon, S. Atukorala, D. Gamage and M. Wijeratne, *Ceylon Med. J.*, **2011**, *48*, 58.

5. Hong, T.; Smith Moland, E.; Abdalhamid, B.; Hanson, N. D.; Wang, J.; Sloan, C.; Fabian, D.; Farajallah, A.; Levine, J.; Thomson, K. S. *Clin. Infect. Dis.* **2005**, *40*, e84–e86.

6. K. Bush, P. Courvalin, G. Dantas, J. Davies, B. Eisenstein, P. Huovinen, G. A. Jacoby, R. Kishony, B. N. Kreiswirth, E. Kutter, S. A. Lerner, S. Levy, K. Lewis, O. Lomovskaya, J. H. Miller, S. Mobashery, L. J. V. Piddock, S. Projan, C. M. Thomas, A. Tomasz, P. M. Tulkens, T. R. Walsh, J. D. Watson, J. Witkowski, W. Witte, G. Wright, P. Yeh and H. I. Zgurskaya, *Nat. Rev. Microbiol.*, **2011**, *9*, 894–896.

7. F. Walsh, *BBC News*, **2014**, 1–14.

8. B. Spellberg, J. H. Powers, E. P. Brass, L. G. Miller and J. E. Edwards, *Clin. Infect. Dis.*, **2004**, *38*, 1279–1286.

9. H. W. Boucher, G. H. Talbot, J. S. Bradley, J. E. Edwards, D. Gilbert, L. B. Rice, M. Scheld, B. Spellberg and J. Bartlett, *Clin. Infect. Dis.*, **2009**, *48*, 1–12.

10. K. M. G. O'Connell, J. T. Hodgkinson, H. F. Sore, M. Welch, G. P. C. Salmond and D. R. Spring, *Angew. Chemie Int. Ed.*, **2013**, *52*, 10706–10733.

11. M. F. Ilker, K. Nüsslein, G. N. Tew and E. B. Coughlin, *J. Am. Chem. Soc.*, **2004**, *126*, 15870–15875.

12. R. W. Scott, W. F. DeGrado and G. N. Tew, *Curr. Opin. Biotechnol.*, **2008**, *19*, 620–627.

13. A. J. Huh and Y. J. Kwon, *J. Control. Release*, **2011**, *156*, 128–145.

14. M. J. Hajipour, K. M. Fromm, A. Akbar Ashkarran, D. Jimenez de Aberasturi, I. R. de Larramendi, T. Rojo, V. Serpooshan, W. J. Parak and M. Mahmoudi, *Trends Biotechnol.*, **2012**, *30*, 499–511.

15. Y. Zhao, Y. Tian, Y. Cui, W. Liu, W. Ma and X. Jiang, *J. Am. Chem. Soc.*, **2010**, *132*, 12349–12356.

16. J. Bresee, C. M. Bond, R. J. Worthington, C. A. Smith, J. C. Gifford, C. A. Simpson, C. J. Carter, G. Wang, J. Hartman, N. A. Osbaugh, R. K. Shoemaker, C. Melander and D. L. Feldheim, *J. Am. Chem. Soc.*, **2014**, *136*, 5295–5300.

17. A. Gupta, R. F. Landis and V. M. Rotello, *F1000Research*, **2016**, *5*, 364.

18. M. E. Davis, Z. Chen and D. M. Shin, *Nat. Rev. Drug Discov.*, **2008**, *7*, 771–782.

19. H. Gu, P. L. Ho, E. Tong, L. Wang and B. Xu, *Nano Lett.*, **2003**, *3*, 1261–1263.

20. A. Nirmala Grace and K. Pandian *Colloids Surfaces A Physicochem. Eng. Asp.*, **2007**, *297*, 63–70.

21. A. M. Allahverdiyev, K. V. Kon, E. S. Abamor, M. Bagirova and M. Rafailovich, *Expert Rev. Anti. Infect. Ther.*, **2011**, *9*, 1035–1052.

22. L. R. Christena, V. Mangalagowri, P. Pradheeba, K. B. A. Ahmed, B. I. S. Shalini, M. Vidyalakshmi, V. Anbazhagan and N. S. Subramanian, *RSC Adv.*, **2015**, *5*, 12899–12909.

23. S. C. Hayden, G. Zhao, K. Saha, R. L. Phillips, X. Li, O. R. Miranda, V. M. Rotello, M. A. El-Sayed, I. Schmidt-Krey and U. H. F. Bunz, *J. Am. Chem. Soc.*, **2012**, *134*, 6920–6923.

24. X. Li, S. M. Robinson, A. Gupta, K. Saha, Z. Jiang, D. F. Moyano, A. Sahar, M. A. Riley and V. M. Rotello, *ACS Nano*, **2014**, *8*, 10682–10686.

25. I. Wiegand, K. Hilpert and R. E. W. Hancock, *Nat. Protoc.*, **2008**, *3*, 163–175.

26. R. L. White, D. S. Burgess, M. Manduru and J. A. Bosso, *Antimicrob. Agents Chemother.*, **1996**, *40*, 1914–1918.

27. F. C. Odds, *J. Antimicrob. Chemother.*, **2003**, *52*, 1–1.

28. P. K. Singh, B. F. Tack, P. B. McCray and M. J. Welsh, *Am. J. Physiol. Lung Cell. Mol. Physiol.*, **2000**, *279*, L799–L805.

29. X.-Z. Li and H. Nikaido, *Drugs*, **2004**, *64*, 159–204.

30. H. Nikaido, *Science*, **1994**, *264*, 382–388.

31. L. Paixão, L. Rodrigues, I. Couto, M. Martins, P. Fernandes, C. C. C. R. de Carvalho, G. A. Monteiro, F. Sansonetty, L. Amaral and M. Viveiros, *J. Biol. Eng.*, **2009**, *3*, 18.

32. M. Malléa, J. Chevalier, A. Eyraud and J.-M. Pagès, *Biochem. Biophys. Res. Commun.*, **2002**, *293*, 1370–1373.

33. T. J. Silhavy, D. Kahne and S. Walker, *Cold Spring Harb. Perspect. Biol.*, **2010**, *2*, a000414.

34. A. Gauthier, J. L. Puente and B. B. Finlay, *Infect. Immun.*, **2003**, *71*, 3310–3319.

35. M. Shah, D. Su, J. S. Scheliga, T. Pluskal, S. Boronat, K. Motamedchaboki, A. R. Campos, F. Qi, E. Hidalgo, M. Yanagida and D. A. Wolf, *Cell Rep.*, **2016**, *16*, 1891–1902.

36. H. Nikaido, *Clin. Infect. Dis.*, **1998**, *27 Suppl 1*, S32-41.

37. H. I. Zgurskaya, G. Krishnamoorthy, A. Ntreh and S. Lu, *Front. Microbiol.*, **2011**, *2*, 189.

38. C. McNulty, J. Thompson, B. Barrett, L. Lord, C. Andersen and I. S. Roberts, *Mol. Microbiol.*, **2006**, *59*, 907–922.

39. C. T. Parker, E. Pradel and C. A. Schnaitman, *J. Bacteriol.*, **1992**, *174*, 930–934.

40. A. Death, L. Notley and T. Ferenci, *J. Bacteriol.*, **1993**, *175*, 1475–1483.

41. C. Xu, X. Lin, H. Ren, Y. Zhang, S. Wang and X. Peng, *Proteomics*, **2006**, *6*, 462–473.

42 . C.-C. You, O. R. Miranda, B. Gider, P. S. Ghosh, I.-B. Kim, B. Erdogan, S. A. Krovi, U. H. F. Bunz and V. M. Rotello, *Nat. Nanotechnol.*, **2007**, *2*, 318–323.

43. M. Brust, M. Walker, D. Bethell, D. J. Schiffrin and R. Whyman, *J. Chem. Soc. Chem. Commun.*, **1994**, 801–802.

44. A. C. Templeton, W. P. Wuelfing and R. W. Murray, *Acc. Chem. Res.*, **2000**, 33, 27–36.

45. O. R. Miranda, H. T. Chen, C. C. You, D. E. Mortenson, X. C. Yang, U. H. F. Bunz and V. M. Rotello, *J. Am. Chem. Soc.*, **2010**, *132*, 5285–5289.

46. M. De, S. Rana, H. Akpinar, O. R. Miranda, R. R. Arvizo, U. H. F. Bunz and V. M. Rotello, *Nat. Chem.*, **2009**, *1*, 461–465.

47. X. Liu, M. Atwater, J. Wang and Q. Huo, *Colloids Surfaces B Biointerfaces*, **2007**, *58*, 3–7.

48. Xu T, Venable JD, Park SK, Cociorva D, Lu B, Liao L, Wohlschlegel J, Hewel J, 3rd Yates, *Mol. Cell Proteomics.*, **2006**, *5*: S174.

49. D. L. Tabb, W. H. McDonald and J. R. 3rd Yates, *J. Proteome Res.*, **2002**, *1*, 21–26.

50. S. K. Park, J. D. Venable, T. Xu and J. R. Yates, *Nat. Methods*, **2008**, *5*, 319–322.

51. D. W. Huang, B. T. Sherman and R. A. Lempicki, *Nucleic Acids Res.*, **2009**, *37*, 1–13.

CHAPTER 4

CHARGE-SWITCHABLE NANOZYMES FOR BIOORTHOGONAL IMAGING OF BIOFILM-ASSOCIATED INFECTIONS

4.1 Introduction

Bacterial infections are serious threat to public health, causing > 2 million cases of illnesses and >23,000 deaths each year in U.S.[1] The majority of human bacterial infections (~80%) are associated with biofilm formation on living tissues.[2] Biofilms are three-dimensional bacterial communities where microbes reside in an extracellular polymeric substance (EPS) matrix, and are highly protected from exogenous agents. Biofilm-associated infections are responsible for a range of chronic diseases including endocarditis, osteomyelitis and implant dysfunction, and are key co-morbity threats for other diseases such as cystic fibrosis.[3,4] Currently, biofilm infections are typically diagnosed only after they have become systemic or have caused significant anatomical damage,[5,6] highlighting the need for effective imaging tools.

Current techniques for imaging bacteria use probes such as autologous white blood cells[7], maltodextrin[8] and dipicolylamine zinc (II).[9] Although these systems are effective for imaging planktonic (dispersed) bacterial infections, only limited studies have been conducted on imaging of biofilm-associated infections.[10,11,12] Other imaging modalities such as ^{67}Ga-citrate and radiolabeled autologous white blood cells lack the spatial resolution required for surgical procedures such as debridement of infected tissue.[6,13] Most high resolution optical imaging approaches rely on fluorescent dyes conjugated to a biorecognition element, generating highly specific imaging probes that are susceptible to false responses due to phenotypic mutations of biofilm residing microbes.[14,15] Moreover, physical heterogeneity and complex biofilm architecture further complicates imaging of these highly refractory infections.[16] In particular, the dense and amphiphilic nature of EPS matrix prevents the penetration of imaging agents.[17,18] Synthetic macromolecules such as nanoparticles (NPs) have shown potential to penetrate

biofilms [19], however they currently lack the ability to intrinsically target these resilient infections.[20,21]

Biofilms have inherently acidic microenvironments (pH 4.5-6.5) as a by-product of sugar fermentation caused by bacteria.[22] For instance, pH in human dental biofilms often reaches below 4.5 causing acidic dissolution of tooth enamel.[23] Similarly, cystic fibrosis (CF) pulmonary infections are associated with acidification of airways in CF patients.[24] We hypothesized that pH-responsive sulfonamide-functionalized gold nanoparticles (AuNPs)[25] could be used to target this acidic environment. In this system, targeting of the biofilm is achieved through charge-switchable NPs that transition from zwitterionic (non-adhesive) to cationic (adhesive) at the pH values typically found in biofilms, providing a broad-spectrum recognition platform for bacteria with selectivity towards biofilms compared to healthy mammalian cells. Imaging of the biofilms is achieved by the embedded transition metal catalysts (TMCs) that activate the pro-fluorophores *in situ* inside the biofilms. These bioorthogonal 'nanozymes' provide an effective imaging system that selectively targets bacterial biofilms and provides amplified fluorescence signal output using bioorthogonal catalysis. This nanozyme platform was used to effectively image biofilms of different bacterial species with complete EPS matrix penetration, and to image biofilms in a complex mammalian cell - biofilm co-culture model.

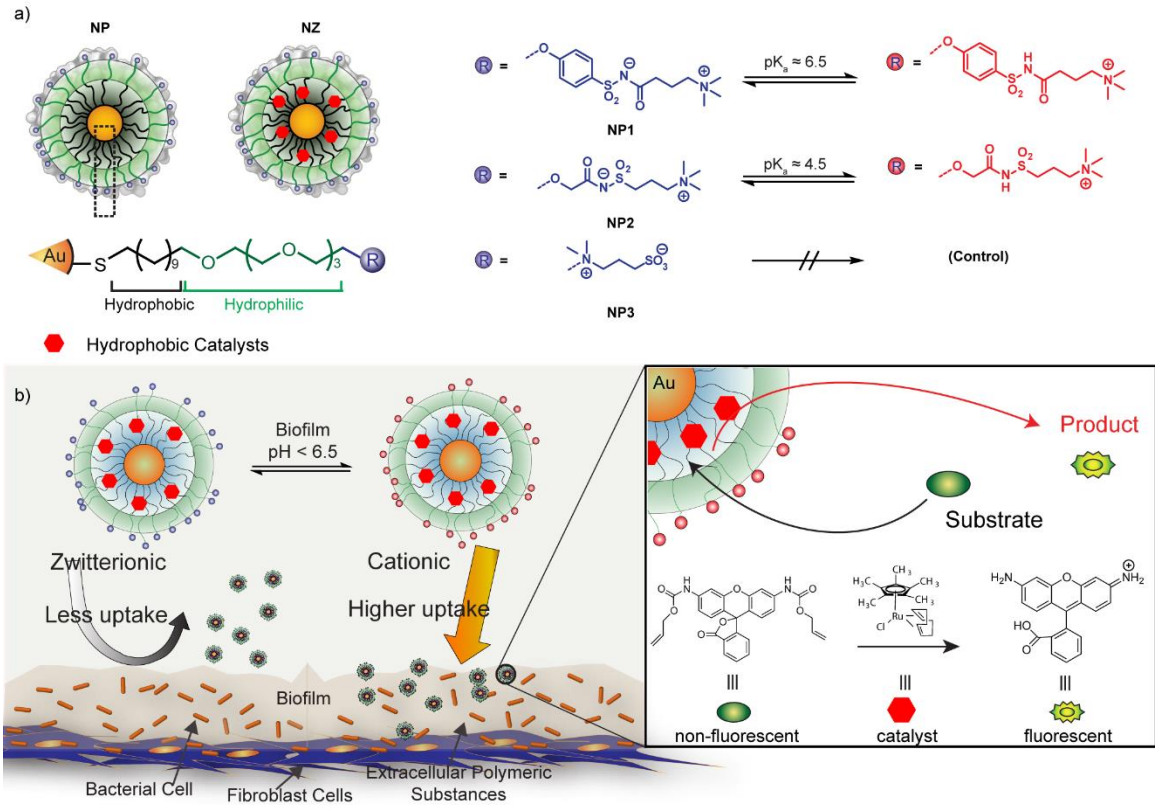

Figure 4.1. a. Molecular structures of pH-switchable and control ligands on gold nanoparticles (AuNPs). **b.** Schematic representation showing selective targeting of biofilm infections using pH-responsive nanoparticles and intrabiofilm fluorogenesis of profluorophores by transition metal catalysts (TMCs) embedded in the nanoparticle monolayers.

4.2 Results and discussion

Sensing was performed with 2nm AuNPs featuring terminal groups with distinct pK_a values to selectively target the acidic microenvironment of biofilms.[25] Alkoxyphenyl acylsulfonamide-functionalized NP1 features groups that are protonated under weakly acidic conditions (pK_a ~ 6.5), consistent with normal biofilm pH. Acylsulfonamide-functionalized NP2 has slightly lower pK_a (~4.5) than its aryl analog, providing a tool for measuring the lower extremes of biofilm pH.**Error! Bookmark not defined.** Finally, NP3 features a sulfobetaine t ermini, providing a stable zwitterionic control for our studies (pKa < 1) (Figure 4.1 a).[26,27] These particles were synthesized from pentane-thiol capped 2nm core AuNPs using a place exchange reaction.

The nanozymes were generated through encapsulation of a ruthenium-based catalyst-[Cp*Ru(cod)Cl] (Cp* = pentamethylcyclopentadienyl, cod = 1,5-cyclooctadiene) into the ligand monolayer of NP1-3 to generate the respective nanozymes (NZ1-3).[28] Transmission electron microscopy (TEM) images and dynamic light scattering data of NPs before and after encapsulation of catalysts show no signs of aggregation. Further size distribution studies for NZs were conducted at a range of pH (3.5-7.4) using DLS, demonstrating their stability even in the acidic conditions (Figure 4.5, Figure 4.6). The quantification of catalysts encapsulated was done using inductively coupled plasma mass spectrometry (ICP-MS), indicating that 24 ± 2 catalyst molecules were encapsulated per AuNP for NZ1-3. The catalysts encapsulated per AuNP were similar at different pH ranges (3.5-7.4), as validated using ICP-MS (Figure 4.7).

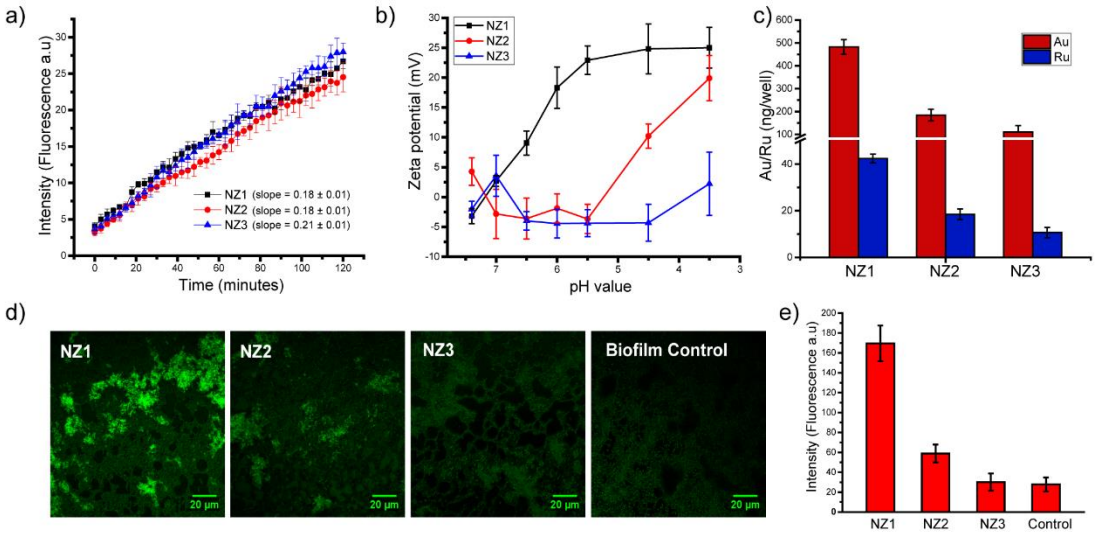

Figure 4.2. a. Catalysis of nanozymes with different chemical headgroups in neutral pH for 2 h at 37 °C. **b.** ζ-Potential of NZ1−3 (1 μM) measured in the pH range of 3.5−7.4 is plotted against different pH values. Error bars represent standard deviations based on three independent measurements per pH value. **c.** Nanoparticle and catalyst diffusion into P. aeruginosa (CD-1006) biofilms after incubation for 1 hr in pH 7.4 media with NZ1−3 (400 nM), as measured by ICP-MS. **d.** Confocal images of biofilm incubated with nanozymes (1 h, 400 nM) followed by incubation with alloc-Rho (1 h, 100 μM); biofilm control is the negative control in the absence of nanozyme. **e.** Quantitative analysis of fluorescence intensity generated upon addition of different nanozymes.

The catalytic activities of NZ1-3 were assessed in solution by deallylation of bis-N, N'-allyloxycarbonyl rhodamine 110 (alloc-Rho, Figure 4.1) at pH = 7.4.[29] The rate of increase in

fluorescence was similar (Figure 4.2a) for the NZ1-3 complexes, indicating similar catalytic activity for all NZs at physiological pH. Further, we tested the catalytic activity of NZ1 with varying pH (3.5-7.4), indicating no significant difference in the catalysis rate for the nanozyme (Figure 4.8).

After establishing their catalytic activity in solution, we determined the pH dependence of the NZ's surface charge by measuring their zeta potential. The surface charge of all three NZs (1-3) were close to neutral at physiological pH (7.4), consistent with their zwitterionic structures. NZ (1-2) exhibited a sharp transition from neutral to overall positive charge at pH 6.5 and pH 4.5 respectively, consistent with their respective pKa's. As expected, NZ3 possessed near neutral charge even at highly acidic pH values as seen in Figure 4.2b and Figure 4.6. Next, we performed NZ diffusion studies in biofilms using ICP-MS to investigate their ability to penetrate and accumulate inside biofilms. We observed that switchable NZ1 showed the highest diffusion into biofilms based on Au, with lesser amounts observed with NZ2 and NZ3 respectively (Figure 4.2c). This trend is mirrored in the Ru signal from the catalyst. This overall change to cationic surface charge of the pH-responsive NZs can play a crucial role in their ability to intrinsically target biofilms over the mammalian cells (Figure 4.9).

We then investigated the ability of NZs to image biofilms using confocal microscopy. We chose uropathogenic clinical isolate of *P. aeruginosa* (CD-1006) as a model strain for imaging studies due to their high prevalence in clinical biofilms.[30,31] Imaging studies of biofilms were based on generation of fluorophore (Rhodamine 110) through deallylation of a non-fluorescent precursor as shown in Figure 4.1b. Catalytic activity of the NZs was probed inside the biofilms by incubating the NZs with biofilms for 1 h, followed by multiple washings to remove absorbed particles. Fresh media containing substrate was added following 1 h incubation and subsequent washings. Confocal images of biofilms treated with switchable NZ1 exhibited bright fluorescence, with only localized fluorescence observed with NZ2, and little or no fluorescence beyond auto fluorescence observed with NZ3, results mirrored in the quantified intensities (Figure 4.2 d, e).

These results suggest that pH responsive zwitterionic nanozyme NZ1 can be used to target the biofilms for imaging applications.

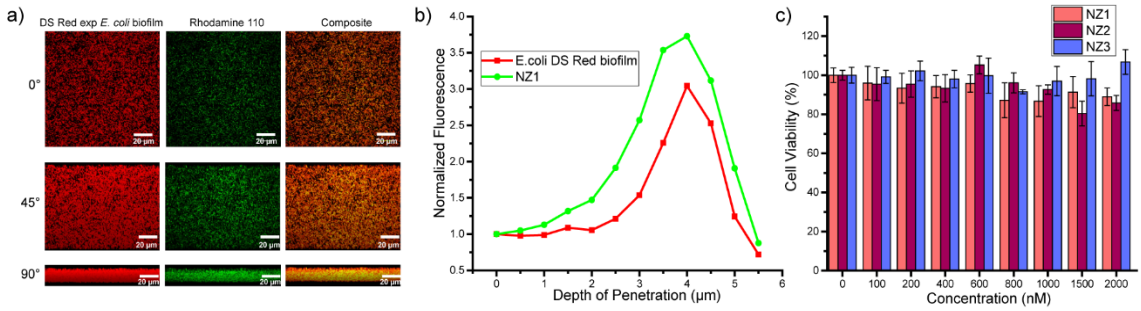

Figure 4.3. a. Confocal microscopy images of DS Red exp E. coli and activated Rhodamine 110 fluorophore in the presence of NZ1. Composite images show homogeneous colocalization of biofilm and activated fluorophores. The panels are projections at 0, 45, and 90° angle turning along the Y-axis. The scale bars are 20 μm. **b.** Integrated intensity of Rhodamine 110 and DS Red biofilm after 1 h incubation with NZ1. The x-axis is the depth of penetration of biofilms, where 0 μm represents the top layer and ~5.6 μm the bottom layer. The y-axis, normalized fluorescence, is normalized intensity of red and green channels at the top layer to compare their localization. **c.** Cell viability of 3T3 fibroblast cells after 24 h incubation with NZ1−3 (0.1−2 μM). The data are average of triplicates, and the error bars indicate standard deviations.

Z-stack confocal imaging was used to determine the localization of activated fluorophores inside DS Red (red fluorescent protein) expressing *E. coli* biofilms (Figure 4.3a). The penetration profile of NZ1 was quantified by using NIS element analysis software.[32] The intensity of green and red channel represents the intensity of Rhodamine-110 and biofilms respectively. The integrated intensities were normalized at the top layer of biofilm to compare their co-localization with varying biofilm depth (0-5.6 μm). As shown in Figure 4.3b, the activated fluorophore (Rhodamine 110) was distributed throughout the biofilm. Biofilms incubated without NZ1 were used as negative control. The ability of switchable NZ1 to image bacterial biofilms was further validated against three bacterial strains of clinical isolates - *Enterobacter cloacae* (CD-1412), methicillin-resistant *Staphylococcus aureus* (CD-489) and *Escherichia coli* (CD-2), demonstrating effective imaging of biofilms formed by both Gram positive (*S. aureus*) and Gram negative (*E. coli, P. aeruginosa, E. cloacae*) (Figure 4.10) species. Further, we tested the cytotoxicity of these NZs against NIH 3T3 Fibroblast-cells that maintain

high cell viability at 2 μM NZ incubation (Figure 4.3c). These studies indicate the biocompatibility of our zwitterionic nanozymes with mammalian cells.

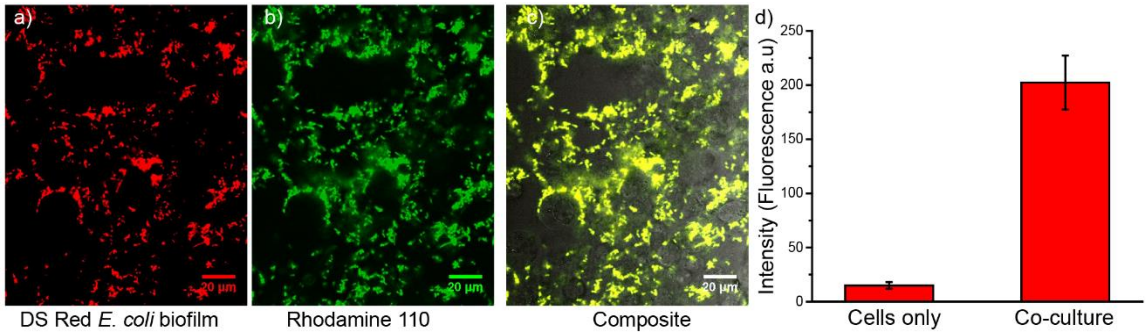

Figure 4.4. Confocal images of a fibroblast-DS Red E. coli biofilm coculture model incubated with switchable nanozyme NZ1 (400 nM) and alloc-rhodamine (nonfluorescent, 100 μM) for 1 h. **a.** DS Red, **b.** Rhodamine 110, and **c.** merged channels. **d.** Quantitative analysis of fluorescence intensity observed in the images of noninfected cells (cells only) and cells infected with biofilm (coculture). Scale bar is 20 μm.

Imaging of biofilms on biomedical surfaces such as medical implants and indwelling devices is a critical capability. However, tracking biofilm-associated infections on human tissues and organs is even more challenging and relevant for medical applications. In most cases of bacterial infections, microbes are embedded in human tissues inside resilient biofilms comprised of EPS.[33] Having established that pH responsive NZ1 exhibits the highest selectivity towards biofilms and are non-toxic to fibroblast cells, we next investigated their ability to track biofilms, using fibroblast-biofilm co-culture as a model. We chose DS Red (red fluorescent protein) expressing *E. coli* as representative strain to generate co-culture model using previously established protocols.[34,35,36] Co-cultures were then incubated with NZ1 for 1 hour, followed by multiple washings to remove non-adhering NZs. Subsequently, substrate alloc-Rho was added in fresh media for 1 hour, followed by multiple washing to remove excess substrate. The co-culture models were examined using confocal microscopy, exhibiting strong co-localization of Rhodamine and DS Red (from biofilm) and minimal fluorescence around mammalian cells (Figure 4.4, procedure to analyze image intensity is described in section 4.5, Figure 4.11). The co-cultures incubated with alloc-Rho in absence of NZ1 was used as negative control. This high

level of selectivity demonstrates the potential of switchable NZs to image bacterial biofilms in physiologically relevant conditions. Their ability to selectively target the biofilms can be attributed to the overall change in their surface charge (from neutral to cationic) at acidic conditions. The positively charged NZ1 shows high accumulation inside the biofilm, whereas the neutral charged NZ1 exhibits minimal uptake in fibroblast cells. Hence, the pro-fluorophore gets selectively activated in the biofilm, already inhabited by the charge switchable nanozyme.

4.3 Conclusions

In conclusion, we have developed a strategy for rapid and effective imaging of biofilms that was effective in a complex co-culture model. The pH-responsive NPs penetrate and accumulate inside the acidic microenvironment of biofilms, with bioorthogonal catalysis providing a sensitive readout mechanism. This bioorthogonal activation of imaging agents is a promising approach to detect biofilm-associated infections, and to locate infected sites during critical debridement surgeries. These pH responsive nanozymes offer a broad-spectrum strategy for imaging biofilms arising from different and/or mixed bacteria species, circumventing the need for designing microbe-specific probes. Considering their enhanced ability to penetrate the biofilm matrix, nanozymes hold a strong advantage against currently used imaging probes. In a broader context, this study demonstrates the utility of bioorthogonal catalysis for bioimaging.

4.4 Experimental methods

4.4.1 Synthesis of gold nanoparticles

Ligands were synthesized using previously reported procedure.[25,37] AuNPs was prepared through place-exchange reaction of 1-pentanethiolprotected 2 nm gold nanoparticle (Au-C5) according to previously reported procedure.[38] Briefly, to the solution of Au-C5 (10 mg) in CH_2Cl_2 (1 mL) was added the solution of ligand 1 (30 mg) in CH_2Cl_2: MeOH (4:1, 3 mL). After being stirred at rt for

24 h, the solvent was evaporated *in vacuo*. After nanoparticle residue was washed with EtOAc (10 mL × 3), the nanoparticle was immediately dissolved in MilliQ water and the aqueous solution of the nanoparticle was purified by dialysis with distilled water using SnakeSkin™ Dialysis Tubing (Thermo Scientific, 10,000 MWCO).

4.4.2 Catalyst encapsulation in AuNP monolayer

The catalyst, [Cp*Ru(cod)Cl] (3.0 mg) was dissolved in 1 ml acetone and the AuNP (20 μM, 0.5 mL) were diluted to a final concentration of 5 μM with DI water (1 ml). Then, the catalyst and the AuNP solutions were mixed together and acetone was slowly removed by evaporation. During the evaporation, hydrophobic catalyst was encapsulated in the particle monolayer to yield to NP_Ru. Excess catalysts which precipitated in water were removed by filtration (Millex-GP filter; 25 mm PES, pore Size: 0.22 μm) and dialysis (Snake Skin® dialysis tubing, 10K) against water (5 L) for 24 h. Further purifications were followed by multiple filtrations (five times, Amicon® ultra 4, 10K) to remove free catalysts. The amount of encapsulated catalysts was measured by ICP-MS by tracking ^{101}Ru relative to ^{197}Au for NP_Ru.

4.4.3 Nanozyme kinetics in solution

Allylcarbamate protected Rhodamine 110 (alloc-Rho) was used as a substrate to test the catalytic activity of the nanozymes. A solution containing 100 nM nanozyme and 1 μM substrate was prepared in a 96-well plate. 400 nM nanozyme solution and 100 nM substrate solutions alone were used as negative controls. The kinetic study was done by tracking the fluorescence intensity (Ex: 488 nm, Em: 521 nm, Cutoff: 515 nm) using a Molecular Devices SpectraMax M2 microplate reader.

4.4.4 Biofilm culture

Bacteria were inoculated in LB broth at 37°C until stationary phase. The cultures were then harvested by centrifugation and washed with 0.85% sodium chloride solution three times. Concentrations of resuspended bacterial solution were determined by optical density measured at

600 nm. Seeding solutions were then made in minimal media, M9 broth to reach OD_{600} of 0.1. 500 µL of the seeding solutions were added to each well of the 24-well microplate. M9 medium without bacteria was used as a negative control. The plates were covered and incubated at room temperature under static conditions for a desired period of 24 hours. Planktonic bacteria were removed by washing with PB saline three times.

4.4.5 Diffusion of nanozymes inside biofilms

After plating bacterial cells in a 24-well plate. On the following day, planktonic bacteria were removed by washing with PBS three times. and incubated with NZ 1, NZ 2 and NZ 3 (400 nM each) in minimal M-9 media (pH 7.4) for 3 h at 37 °C. After incubation, biofilms were washed three times with PBS and lysis buffer was added to each well. All lysed samples were then further processed for ICP-MS analysis (*vide infra*) to determine the intracellular amount of gold and ruthenium. Diffusion experiments were performed independently at least two times and each experiment was comprised of three replicates.

4.4.6 Confocal imaging of biofilms

10^8 bacterial cells/ml were seeded (2 ml in M9 media) in a confocal dish and were allowed to grow, old media was replaced every 24 hours. After 3 days media was replaced by 400 nM of the NZ 1, NZ 2 and NZ 3 and biofilms were incubated for 1 h, biofilm samples incubated with only M9 media were used as control. After 1 h, biofilms were washed with PBS three times and were incubated with 100 µM of the substrates for 1 h. The cells were then washed with PBS three times. Confocal microscopy images were obtained on a Zeiss LSM 510 Meta microscope by using a 60× objective. The settings of the confocal microscope were as follows: green channel: λ_{ex}=488 nm and λ_{em}=BP 505-530 nm; red channel: λ_{ex}=543 nm and λ_{em}=LP 650 nm. Emission filters: BP=band pass, LP=high pass.

4.4.7 Mammalian cell viability studies

These experiments were done using previously reported protocol.[39] Briefly, 20,000 NIH 3T3 fibroblast cells (ATCC CRL-1658) were cultured in DMEM medium in presence of 10% bovine calf serum and 1% antibiotic solution. The cells were cultured at 37 °C in a humidified atmosphere of 5% CO_2 for 48 h. Next, the cells were washed with phosphate-buffered saline (PBS) and different concentration of NZs (1-3) in 10% serum containing media were incubated with the cells for 3 h at 37 °C. After the incubation period, cells were washed with PBS (3 times) and cell viability was then determined using Alamar blue assays according to manufacturer's protocol (Invitrogen Biosource). Washed cells were incubated with 220 µl of 10% Alamar Blue solution in 10% serum containing media. The solution was incubated at 37 °C under a humidified atmosphere of 5% CO_2 for 3 h. Subsequently, 200 µl solution from the wells was transferred in a 96-well black-microplate. The fluorescence reading was measured using a UV/vis spectrophotometer with excitation and emission at 560 and 590 nm respectively. Cell incubated without NPs were treated as 100% viable cells and the cell viability was calculated accordingly. These experiments were performed in triplicates.

4.4.8 Imaging of co-culture models

Fibroblast-3T3 co-culture was performed using a previously reported protocol.[36] A total of 20,000 NIH 3T3 (ATCC CRL-1658) cells were cultured in Dulbecco's modified Eagle medium (DMEM; ATCC 30-2002) with 10% bovine calf serum and 1% antibiotics at 37°C in a humidified atmosphere of 5% CO_2. Cells were kept for 24 hours to reach a confluent monolayer in a confocal dish. Bacteria (*P. aeruginosa*) were inoculated and harvested as mentioned above. Afterwards, seeding solutions 10^8 cells/ml were inoculated in buffered DMEM supplemented with glucose. Old media was removed from 3T3 cells followed by addition of 2 mL of seeding solution. The co-cultures were then stored in a box humidified with damp paper towels at 37°C overnight without shaking. The co-cultures were treated with NZs and substrates using similar procedure used for biofilm models.

4.5 Supplementary information

4.5.1. Stability of NZs at different pH values

Hydrodynamic diameter of the NZs at different pH were measured by dynamic light scattering (DLS) in 5mM Phosphate buffer (pH 5.5-7.4) and 5mM Citrate buffer (pH 3.5-4.5) using a Malvern Zetasizer Nano ZS instrument. The NZs (1 µM) were incubated in the respective buffers for 3 hours before each measurement. No significant changes in the NZ size were observed. The size distribution by number are presented in the Figure 4.5.

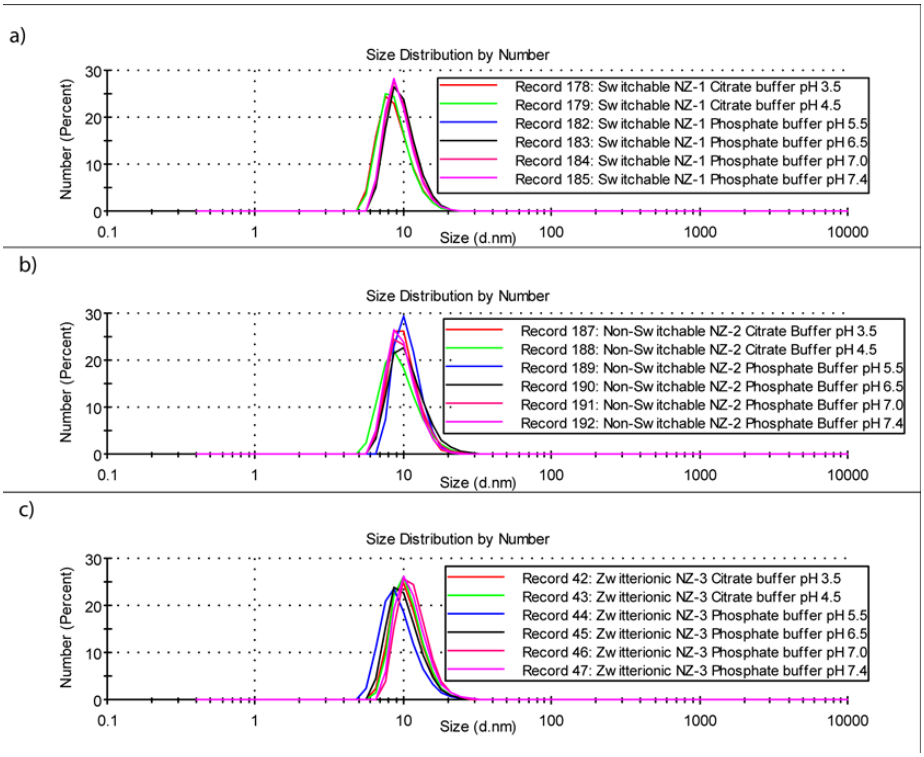

Figure 4.5. DLS measurements of NZs after 3-hour incubation in buffers with varying pH (3.5-7.4) indicate that NZ size remains same even at acidic conditions.

4.5.2. Zeta potential of NZs at different pH values

Zeta potential of the NZs at different pH were measured by dynamic light scattering (DLS) in 5mM Phosphate buffer (pH 5.5-7.4) and 5mM Citrate buffer (pH 3.5-4.5) using a Malvern Zetasizer Nano ZS instrument. The NZs (1 µM) were incubated in the respective buffers for 3

hours before each measurement. The zeta potential measured at different pH are presented below in the Figure 4.6.

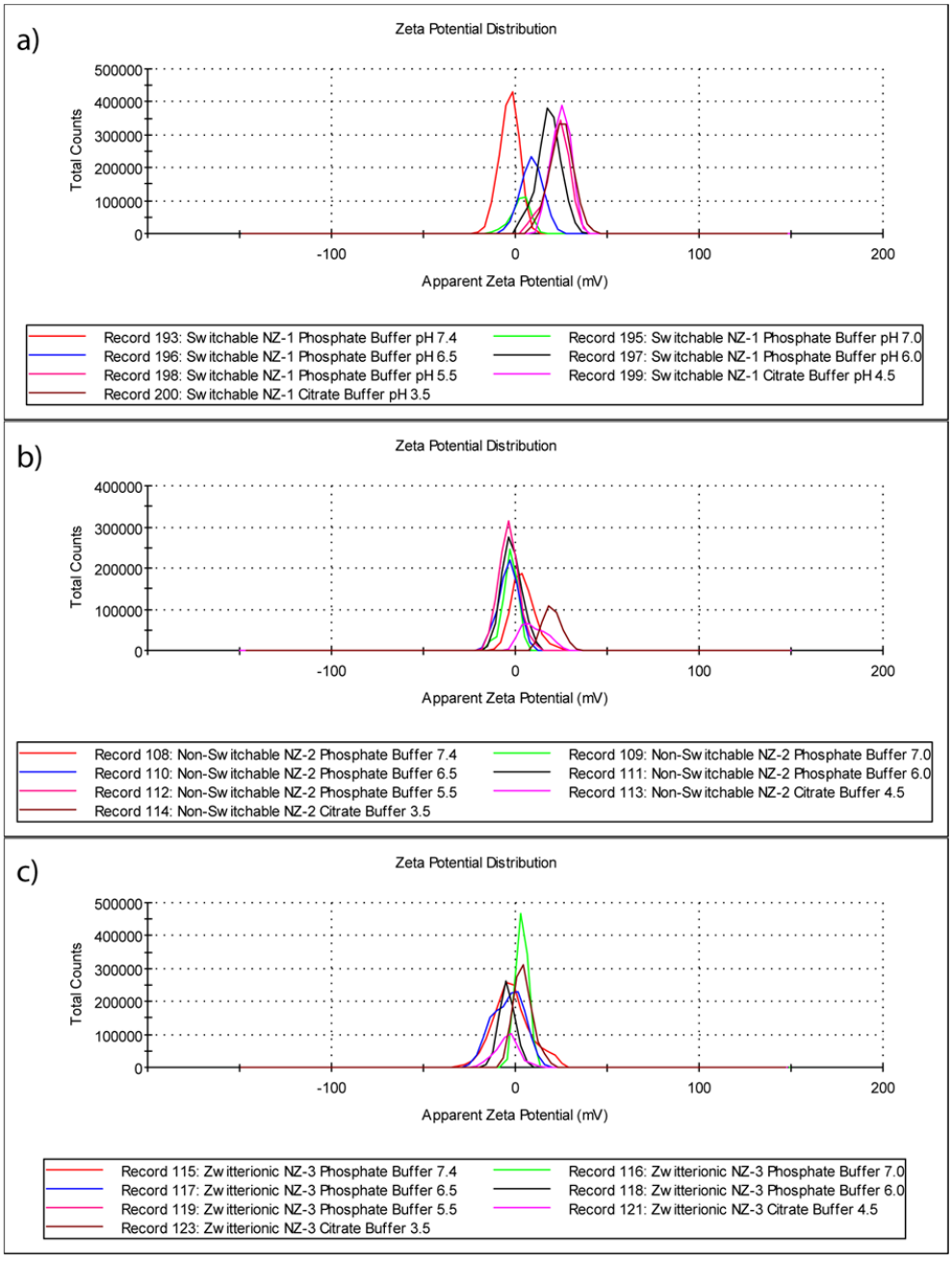

Figure 4.6. Zeta potential of NZs at different pH values, indicating overall change in surface charge of NZ1 and NZ2 at pH 6.5 and 4.5 respectively. NZ3 remains neutral in charge throughout the pH range.

4.5.3. Quantification of Au and Ru using ICP-MS characterization

ICP-MS analyses were performed on a Perkin-Elmer NexION 300X ICP mass spectrometer to quanify ^{197}Au and ^{101}Ru. Operating conditions are listed as below: nebulizer flow rate: 0.95 L/min; rf power: 1600 W; plasma Ar flow rate: 18 L/min; dwell time: 50 ms. A series of solutions with gold and ruthenium (concentration: 0, 0.2, 0.5, 1, 2, 5, 10, and 20 ppb) were prepared for calibration. Nanozyme solutions were diluted in water to 200 nM. 10 µL sample solution was transferred to 15 mL centrifuge tubes. 0.5 mL of fresh *aqua regia* was added to each sample including the standard samples and was diluted to 10 mL with de-ionized water.

Sample Preparation: was added to the 10 µL sample solution and then the sample was diluted to 10 mL with de-ionized water.

	Au (ng)	Ru (ng)	Ru(ng)/ AuNP (pmol)	Ru/AuNp
NZ 1	238.367	11.380	2.257	
	239.175	11.442	2.408	
	234.014	11.946	2.565	23.850
NZ 2	235.474	10.918	2.187	
	242.668	12.273	2.531	
	239.170	11.290	2.450	23.644
NZ 3	229.469	10.845	2.193	
	231.307	11.718	2.466	
	231.790	12.253	2.687	24.230

Figure 4.7. Ruthenium amount in the nanozymes using ICP-MS measurement. The Catalyst/NP represents number of Ruthenium catalysts encapsulated per gold nanoparticle.

4.5.4. Nanozyme catalysis in solution at different pH

Allylcarbamate protected Rhodamine 110 (alloc-Rho) was used as a substrate to test the catalytic activity of the nanozymes. A solution containing 400 nM nanozyme and 100 µM substrate was prepared in a 96-well plate using buffers with varying pH (3.5-7.4). 400 nM nanozyme solution and 100 µM substrate solutions alone were used as negative controls. The kinetic study was done

by tracking the fluorescence intensity (Ex: 488 nm, Em: 521 nm, Cutoff: 515 nm) using a Molecular Devices SpectraMax M2 microplate reader as shown in Figure 4.8. 5 mM Phosphate buffer were used for pH range (5.5-7.5) and 5mM Citrate buffer for pH range (3.5-4.5).

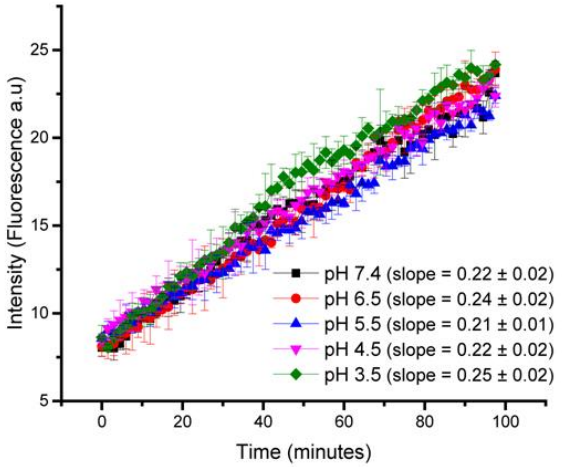

Figure 4.8. Catalysis of NZ1 at different pH for 2 hours at 37 ºC.

4.5.5. Cellular uptake of NZs in 3T3 Fibroblast cells

The cellular uptake experiments were done using previously approved protocols. 30K Fibrobast cell/well were plated in a 24-well plate prior to the experiment. Next day, the cells were washed with PBS and incubated with NZ1 (1 μM) in 10% serum-containing media for 3h at 37 °C. Subsequently, the cells were washed with PBS (3 times) and then subjected to lysis buffer. The lysed cells were then further processed for ICP-MS analysis as shown in Figure 4.9. These experiments were performed independently two times and each experiment was comprised of 3 replicates.

4.5.6. Sample preparation for ICP-MS and ICP-MS instrumentation

Samples were prepared using previously reported protocols. The cells were lysed by a lysis buffer and were transferred to 15 mL centrifuge tubes. A series of standard solutions of gold and ruthenium (0, 0.2, 0.5, 1, 2, 5, 10, and 20 ppb) were prepared for calibration. 0.5 mL of fresh *aqua regia* were added to each sample including the standard samples and were diluted to 10 mL

with de-ionized water. ^{197}Au and ^{101}Ru quantification were done on a Perkin-Elmer NexION 300X ICP mass spectrometer under standard mode. Operating conditions are listed as below: nebulizer flow rate: 0.95-1 L/min; rf power: 1600 W; plasma Ar flow rate: 18 L/min; dwell time: 50 ms.

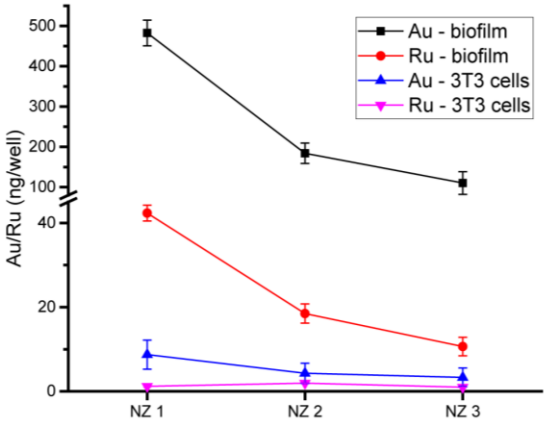

Figure 4.9. Nanoparticle and catalyst uptake in P. aeruginosa (CD-1006) biofilms and NIH-3T3 Fibroblast cells after incubation for 1 hour in pH 7.4 (cell culture media with 10% serum) with NZ1 (400 nM), as measured by ICP-MS.

4.5.7. Confocal imaging of 4 different strains

We used the same procedure for imaging biofilms as described in the materials and methods section of the manuscript in Figure 4.10.

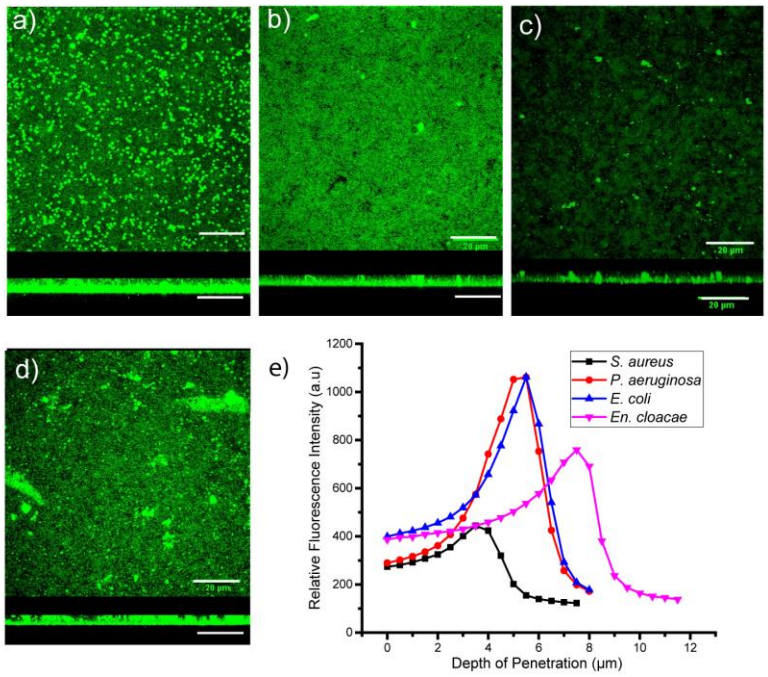

Figure 4.10. Confocal microscopy images of **a.** CD-489 (*S. aureus*, a methicillin resistant strain), **b.** CD-1006 (*P. aeruginosa*), **c.** CD-2 (*E. coli*) and **d.** CD-1412 (*En. cloacae*) treated with nanozymes (NZ1) and pro-rhodamine. The panels are projections at 0º and 90º angle turning along Y-axis. The scale bars are 20 μm. e) Integrated intensity of Rhodamine 110 after 1-hour incubation with NZ1. The x-axis is the depth of penetration of biofilms, where 0 μm represents the top layer. The y-axis is the integrated intensity of the fluorescence resulted from the deprotection of Alloc-Rho.

4.5.8. Data analysis of confocal images

The data analysis of the confocal images was done using the previously reported procedure.[40,41] Briefly, confocal images obtained were analyzed using ImageJ software. After opening the file in ImageJ, the site of interest was selected using drawing selection tool (rectangle). Next, from the analyze menu, "set measurements" was selected for determining Area, Integrated density and mean grey value. To obtain final cell/biofilm fluorescence, the following formula was used -:

CTCF = Integrated Density – (Area of selected location × Mean fluorescence of background readings)

An example for the data points obtained for image analysis can be explained using Figure S7. Box 1 represents the background, box 2 represents the site for cells only and box 3 represents biofilm-mammalian cell coculture in Figure 4.11. The fluorescence calculated for cells only and

biofilms was done by selecting 50 similar data points and averaging the results obtained for all them.

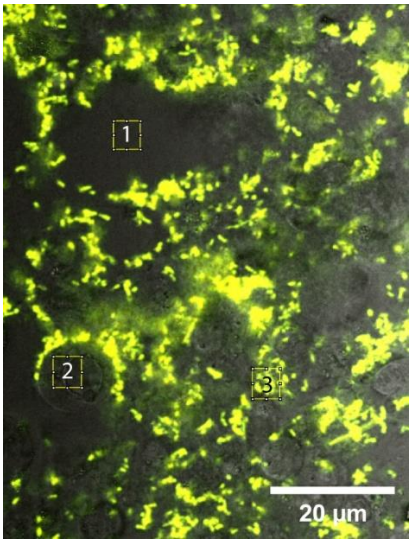

Figure 4.11. Image showing an example of sites used for image analysis of biofilm-mammalian cell co-culture models. Box 1, 2, 3 represents background, cells only and biofilm-cells respectively.

4.6 References

1. *FY15 Detect and Protect Against Antibiotic Resistance Budget Initiative*, Centers for Disease Control and Prevention, **2003**.

2. Kim Lewis, *Nat. Rev. Microbiol.* **2007**, *5*, 48.

3. L. Hall-Stoodley, J. W. Costerton, P. Stoodley, *Nat. Rev. Microbiol.* **2004**, *2*, 95.

4. T. Bjarnsholt, *Apmis* **2013**, *121*, 1.

5. J. W. Costerton, J. C. Post, G. D. Ehrlich, F. Z. Hu, R. Kreft, L. Nistico, S. Kathju, P. Stoodley, L. Hall-Stoodley, G. Maale, G. James, N. Sotereanos, P. DeMeo, *FEMS Immunol. Med. Microbiol.* **2011**, *61*, 133.

6. M. Van Oosten, T. Schäfer, J. A. C. Gazendam, K. Ohlsen, E. Tsompanidou, M. C. De Goffau, H. J. M. Harmsen, L. M. A. Crane, E. Lim, K. P. Francis, L. Cheung, M. Olive, V. Ntziachristos, J. M. Van Dijl, G. M. Van Dam, *Nat. Commun.* **2013**, *4*, 2584.

7. C. Love, M. B. Tomas, G. G. Tronco, C. J. Palestro, *RadioGraphics* **2005**, *25*, 1357.

8. X. Ning, S. Lee, Z. Wang, D. Kim, B. Stubblefield, E. Gilbert, N. Murthy, *Nat Mater* **2011**, *10*, 602.

9. W. M. Leevy, S. T. Gammon, H. Jiang, J. R. Johnson, D. J. Maxwell, E. N. Jackson, M. Marquez, D. Piwnica-Worms, B. D. Smith, *J. Am. Chem. Soc.* **2006**, *128*, 16476.

10. L. Hall-Stoodley, P. Stoodley, S. Kathju, N. Høiby, C. Moser, J. William Costerton, A. Moter, T. Bjarnsholt, *FEMS Immunol. Med. Microbiol.* **2012**, *65*, 127.

11. K. Sauer, A. K. Camper, G. D. Ehrlich, J. W. Costerton, D. G. Davies, *J. Bacteriol.* **2002**, *184*, 1140.

12. L. Hall-Stoodley, F. Z. Hu, A. Gieseke, L. Nistico, D. Nguyen, J. Hayes, M. Forbes, D. P. Greenberg, B. Dice, A. Burrows, P. A. Wackym, P. Stoodley, J. C. Post, G. D. Ehrlich, J. E. Kerschner, *J. Am. Med. Assoc.* **2006**, *296*, 202.

13. T. A. Sasser, A. E. Van Avermaete, A. White, S. Chapman, J. R. Johnson, T. Van Avermaete, S. T. Gammon, W. M. Leevy, *Curr. Top. Med. Chem.* **2013**, *13*, 479.

14. T. R. Neu, G. D. W. Swerhone, J. R. Lawrence, *Microbiology* **2001**, *147*, 299.

15. Bjarnsholt, T.; Alhede, M.; Alhede, M.; Eickhardt-Sørensen, S. R.; Moser, C.; Kühl, M.; Jensen, P. Ø.; Høiby, N. The *in vivo* Biofilm. *Trends Microbiol*. **2013**, *21*, 466–474.

16. C. A. Fux, P. Stoodley, L. Hall-Stoodley, J. W. Costerton, *Expert Rev. Anti. Infect. Ther.* **2003**, *1*, 667.

17. J. N. Anderl, M. J. Franklin, P. S. Stewart, *Antimicrob. Agents Chemother.* **2000**, *44*, 1818.

18. P. S. Stewart, J. W. Costerton, *Lancet (London, England)* **2001**, *358*, 135.

19. X. Li, Y. C. Yeh, K. Giri, R. Mout, R. F. Landis, Y. S. Prakash, V. M. Rotello, *Chem. Commun.* **2015**, *51*, 282.

20. T. O. Peulen, K. J. Wilkinson, *Environ. Sci. Technol.* **2011**, *45*, 3367.

21. A. Gupta, R. F. Landis, V. M. Rotello, *F1000Research* **2016**, *5*, 364.

22. D. S. W. Benoit, H. Koo, *Nanomedicine* **2016**, *11*, 873.

23. B. Horev, M. I. Klein, G. Hwang, Y. Li, D. Kim, H. Koo, D. S. W. Benoit, *ACS Nano* **2015**, *9*, 2390.

24. T. F. Moriarty, J. S. Elborn, M. M. Tunney, *Br. J. Biomed. Sci.* **2007**, *64*, 101.

25. T. Mizuhara, K. Saha, D. F. Moyano, C. S. Kim, B. Yan, Y. K. Kim, V. M. Rotello, *Angew. Chemie - Int. Ed.* **2015**, *54*, 6567.

26. M. Das, N. Sanson, E. Kumacheva, *Chem. Mater.* **2008**, *20*, 7157.

27. J. D. Madura, J. B. Lombardini, J. M. Briggs, D. L. Minor, A. Wierzbicki, *Amino Acids* **1997**, *13*, 131.

28. G. Y. Tonga, Y. Jeong, B. Duncan, T. Mizuhara, R. Mout, R. Das, S. T. Kim, Y. C. Yeh, B. Yan, S. Hou, V. M. Rotello, *Nat. Chem.* **2015**, *7*, 597.

29. R. M. Yusop, A. Unciti-Broceta, E. M. V. Johansson, R. M. Sánchez-Martín, M. Bradley, *Nat. Chem.* **2011**, *3*, 239.

30. A. Oliver, R. Cantón, P. Campo, F. Baquero, J. Blázquez, *Science* **2000**, *288*, 1251.

31. J. C. Nickel, I. Ruseska, J. B. Wright, J. W. Costerton, *Antimicrob. Agents Chemother.* **1985**, *27*, 619.

32. S.-W. Yun, C. Leong, D. Zhai, Y. L. Tan, L. Lim, X. Bi, J.-J. Lee, H. J. Kim, N.-Y. Kang, S. H. Ng, L. W. Stanton, Y.-T. Chang, *Proc. Natl. Acad. Sci.* **2012**, *109*, 10214.

33. W. Costerton, R. Veeh, M. Shirtliff, M. Pasmore, C. Post, G. Ehrlich, *J. Clin. Invest.* **2003**, *112*, 1466.

34. G. G. Anderson, S. Moreau-Marquis, B. A. Stanton, G. A. O'Toole, *Infect. Immun.* **2008**, *76*, 1423.

35. G. G. Anderson, T. F. Kenney, D. L. Macleod, N. R. Henig, G. A. O'Toole, *Pathog. Dis.* **2013**, *67*, 39.

36. R. F. Landis, A. Gupta, Y. W. Lee, L. S. Wang, B. Golba, B. Couillaud, R. Ridolfo, R. Das, V. M. Rotello, *ACS Nano* **2017**, *11*, 946.

37. S. Huo, Y. Jiang, A. Gupta, Z. Jiang, R. F. Landis, S. Hou, X. J. Liang, V. M. Rotello, *ACS Nano* **2016**, *10*, 8732.

38. C. C. You, O. R. Miranda, B. Gider, P. S. Ghosh, I. B. Kim, B. Erdogan, S. A. Krovi, U. H. F. Bunz, V. M. Rotello, *Nat. Nanotechnol.* **2007**, *2*, 318.

39. A. Gupta, N. M. Saleh, R. Das, R. F. Landis, A. Bigdeli, K. Motamedchaboki, A. R. Campos, K. Pomeroy, M. Mahmoudi, V. M. Rotello, *Nano Futur.* **2017**, *1*, 015004.

40. A. Burgess, S. Vigneron, E. Brioudes, J.-C. Labbé, T. Lorca, A. Castro, *Proc. Natl. Acad. Sci.* **2010**, *107*, 12564.

41. R. A. McCloy, S. Rogers, C. E. Caldon, T. Lorca, A. Castro, A. Burgess, *Cell Cycle* **2014**, *13*, 1400.

CHAPTER 5

RBC-MEDIATED DELIVERY OF BIOORTHOGONAL NANOZYMES FOR SELECTIVE TARGETING OF BACTERIAL INFECTIONS

5.1 Introduction

Bioorthogonal catalysis offers a strategy for chemical transformations complementary to bioprocesses and has proven to be a powerful tool in biochemistry and medical sciences.[1,2] Nanoparticles embedded with transition metal catalysts (nanozymes) have demonstrated excellent ability to catalyze reactions beyond the capabilities of biological systems.[3,4] Nanozymes can implement bioorthogonal approach to chemically transform a biologically inert substrate to its active form at the site of interest.[5] Localization of bio-orthogonal nanozymes at targeted biological site is central in maximizing the efficacy of the strategy.[6,7] For example, selective activation of pro-antimicrobials at the infected tissue can kill disease-causing pathogens while causing minimal harm to the beneficial human microbiome.

One approach to control spatiotemporal localization of biorthogonal catalysts utilizes tuning the size of carrier.[8,9] Alternatively, biorthogonal catalysts can be functionalized with different ligands, peptides or biomolecules to target the diseased physiological site.[10,11,12] However, these synthetic carrier-based approaches are susceptible to non-specific uptake and potential degradation of vehicles in macrophages, compromising the efficacy of therapy.[13]

Red blood cells (RBCs) have been used as cell-based drug delivery systems owing to their biocompatibility, long circulation time and low immunogenicity.[14,15] RBCs are significantly hemolyzed by bacterial toxins, providing these RBC carriers with intrinsic targeting ability towards pathogenic bacteria.[16,17] Moreover, high surface to volume ratio of RBCs provides an ideal surface for hitchhiking of nanoparticles through supramolecular interactions with RBC cell surface.[18] Recent studies have demonstrated that RBC-hitchhiking of NPs enhanced the

delivery efficacy to the target organs with minimal non-specific uptake by the reticuloendothelial system.[19,20]

Notably, maintaining the stability of RBC membranes is critical in retaining the biocompatibility and immune-evading ability of NP-hitchhiked RBCs.[21] Surface functionality of NPs dictates their interaction with RBCs and is key to generate RBC "super-carriers" as effective drug delivery systems.[22] For example, cationic NPs can bind to the anionic glycocalyx on RBC cell surface. Whereas, NPs can also bind to hydrophobic domains present on RBC's plasma membranes irrespective of NP surface charge.[23] Moreover, tuning hydrophilic and hydrophobic moieties on NP-surface can significantly impact the hemolysis caused by NPs.

We hypothesized that integration of "super-carrier" RBCs with bioorthogonal nanozymes would offer a novel route to combat bacterial infections while minimizing the possible off-target effects. Here, we have designed a series of nanozymes that feature diverse functional groups with different binding ability to RBCs. The structure-activity studies revealed that hydrophilic cationic NZs can effectively hitchhike onto RBC surface without compromising the stability of RBC plasma membrane. Subsequently, these NZs can detach from RBCs upon hemolysis by bacterial toxins and accumulate at the site of bacterial infection. These NZs could activate protected-antibiotic molecules and effectively eradicate biofilms formed by uropathogenic bacteria, whereas minimal toxicity was observed against non-virulent bacterial strains. Moreover, RBC-NZs showed minimal uptake in macrophage cells as opposed to free nanozymes, suggesting that nanozyme hitchhiking does not compromise the immune-evading ability of RBCs. Overall, we have generated RBC-hitchhiked nanozymes illustrating the ability of passively targeting bacterial infections triggered by bacterial toxins while minimizing non-selective killing of bacteria. This strategy can be further explored to activate multiple therapeutic molecules at the targeted site to combat complex infections and promote healing of the surrounding tissue simultaneously.

5.2 Results and discussion

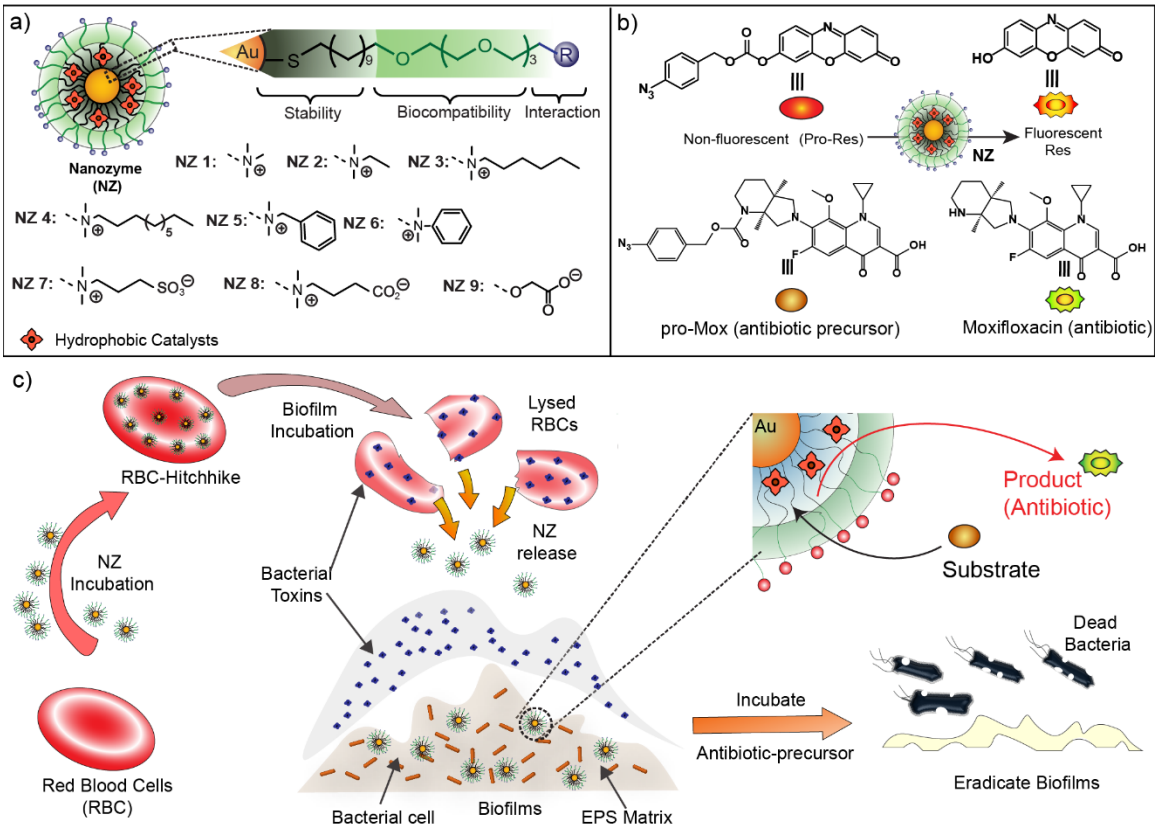

Figure 5.1. a. Molecular structures of the ligand structures used on nanozymes used in the RBC-adsorption study. **b.** Structures of the substrates Resorufin and moxicillin derivative (Pro-Res, Pro-Mox) and products (Resorufin, Moxifloxacin) after cleavage by TMC **c.** Schematic representation showing hitchhiking of NZs on Red Blood Cells, selective targeting of biofilms infections due to lysis of RBCs in presence of bacterial toxins and intrabiofilm generation of antibiotics by transition metal catalysts (TMCs) embedded in the nanoparticle monolayers.

AuNPs with ~ 2 nm core diameter were functionalized with ligands featuring three main components: (1) a hydrophobic alkyl chain interior enabling encapsulation of hydrophobic catalysts, (2) tetra ethylene glycol spacer providing biocompatibility and (3) terminal groups dictating NP-binding with Red Blood Cells.[3,22] Nanozymes (NZs) were generated by encapsulation of iron (III) tetraphenyl porphyrin (FeTPP) catalyst in the surface monolayer of AuNPs. The chemical functionality of NZ-surface ligands plays a critical role in determining their compatibility with RBCs, in-turn dictating ability of NZs to hitchhike on RBC surface.[23] We synthesized a family of NZs with varying surface charge, hydrophobicity and aromatic properties

and studied their compatibility and binding with RBCs. NPs (1-9) were synthesized by ligand place exchange reactions with pentanethiol-capped 2 nm Au core. Next, these NPs were encapsulated with FeTTP catalysts to generate NZ (1-9) (Figure 5.1).

Our initial focus was to adsorb NZs on RBCs without compromising the stability of cell membrane, hence we screened the library of NZs for hemolytic activity against RBCs. NZs (1-9) were incubated with RBCs for 30 minutes and the absorbance of released hemoglobin was measured at 570 nm.[24] We observed that cationic hydrophilic NZs (NZ 1-2) showed minimal hemolysis as compared to their hydrophobic counterparts. Similarly, anionic and zwitterionic NZs (NZ 7-9) showed minimal hemolysis of RBCs (Figure 5.2 a), consistent with previously reported studies. Next, we studied the adsorption of non-hemolytic NZs (NZ1-2, NZ7-9) on RBCs to determine their suitability for RBC-hitchhiking. NZs were incubated with RBCs for 30 minutes and washed to remove excess NZs. The harvested RBCs were then analyzed using inductively coupled mass spectrometry (ICP-MS) to quantify gold content on the cells. Cationic NZs showed significant adsorption on RBCs as compared to the anionic and zwitterionic NZs (Figure 5.2 b), attributing to electrostatic interaction between NZs and RBCs.

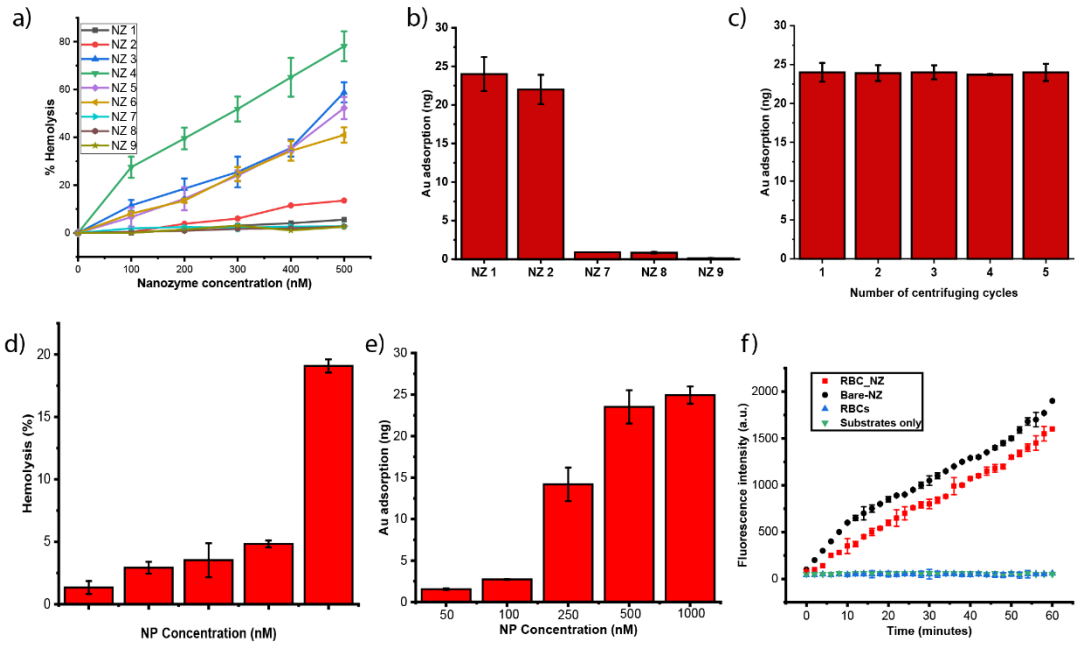

Figure 5.2. a. Dose-dependent hemolytic activity of NZ 1–NZ 9 in the absence of plasma proteins. % hemolysis was calculated using water as the positive control. Error bars represent standard deviations (n = 3). Amount of NZ adsorption on Red Blood Cells after **b.** incubation for 30 minutes **c.** after multiple cycles of centrifugation, at a concentration of 500 nM, as measured using ICP-MS. Dose dependent **d.** hemolytic activity of NZ 1 for 10^7 Red Blood Cell/mL, **e.** NZ adsorption for NZ 1 for 10^7 Red Blood Cell/mL. **f.** Catalysis of free nanozymes and RBC-NZs in PBS for 1 h at 37 °C.

Nanoparticles can frequently detach from RBCs due to shear force and are subsequently recognized by the reticuloendothelial system.[18] Hence, we further investigated the stability of NZs hitchhiked on RBCs (RBC-NZ) by subjecting these RBC-NZs to multiple washing and centrifuging cycles. No significant difference in Au content was observed even after 5 centrifuging cycles, indicating that NZs remain attached to RBCs (Figure 5.2c). Hemolysis and adsorption studies of TTMA with RBCs were further studied at reduced incubation time of 30 minutes (Figure 5.2 d,e).

The catalytic activity of RBC-NZs was assessed by fluorometric measurement of resorufin molecule fragmented from the non-fluorescent pro-Res (Figure 5.1 b) due to azide reduction by FeTTP catalyst. Linear increase in the fluorescence indicate that NZs retain their catalytic activity even after adsorption on RBCs (Figure 5.2 f). However, the rate of fluorescence increase was higher for free NZs as compared to RBC-NZs that can be attributed to conformational restrictions of NZs adsorbed on RBCs.

Infections caused by bacteria often involve secretion of pore-forming toxins (PFTs) as a virulence mechanism.[25] These toxins disrupt the host-cell membrane for pathogenesis, in particular causing high hemolysis of RBCs.[26] Next, we investigated the hemolysis of RBCs caused by uropathogenic clinical isolates (*E. coli*, methicillin-resistant *S. aureus* (MRSA)) and non-pathogenic laboratory strains (*P. aeruginosa*, *B. sub*). We observed that uropathogenic strains caused complete hemolysis of the RBCs within 30 minutes of incubation with RBCs, whereas the non-pathogenic strains caused minimal hemolysis of RBCs even after incubation (Figure 5.3a). Having established that cationic hydrophilic NZs can hitchhike onto RBCs and

these RBCs were hemolyzed in presence of bacterial infections. We set out to determine whether hemolysis of RBCs could result in detachment of NZs from RBC-surface and enhance the accumulation of NZs at the site of bacterial infection.[27] We evaluated the amount of Au on the surface of hemolyzed RBCs and non-hemolyzed RBCs using ICP-MS. It was determined that NZs were subsequently released into the solution upon hemolysis of RBCs, whereas NZs remained attached to cell-surface in case of non-hemolyzed RBCs (Figure 5.3 b). This phenomenon could be attributed to compromised electrostatic interaction between NZs and RBCs upon lysis of cells. Next, we tested the accumulation of NZs using ICP-MS in uropathogenic and non-pathogenic biofilms. We observed that RBC-NZs showed high accumulation in toxin-secreting uropathogenic bacterial biofilms based on Au, whereas minimal amount of Au was observed in non-virulent bacterial biofilms (Figure 5.3 c). Similarly, only NZs (bare-NZ) showed high uptake in macrophages whereas RBC-NZs showed minimal uptake as quantified by ICP-MS. These results indicate that hitchhiking of RBCs can play a crucial role in selectively targeting pathogenic infections over docile bacteria as well avoid non-specific uptake in macrophages.

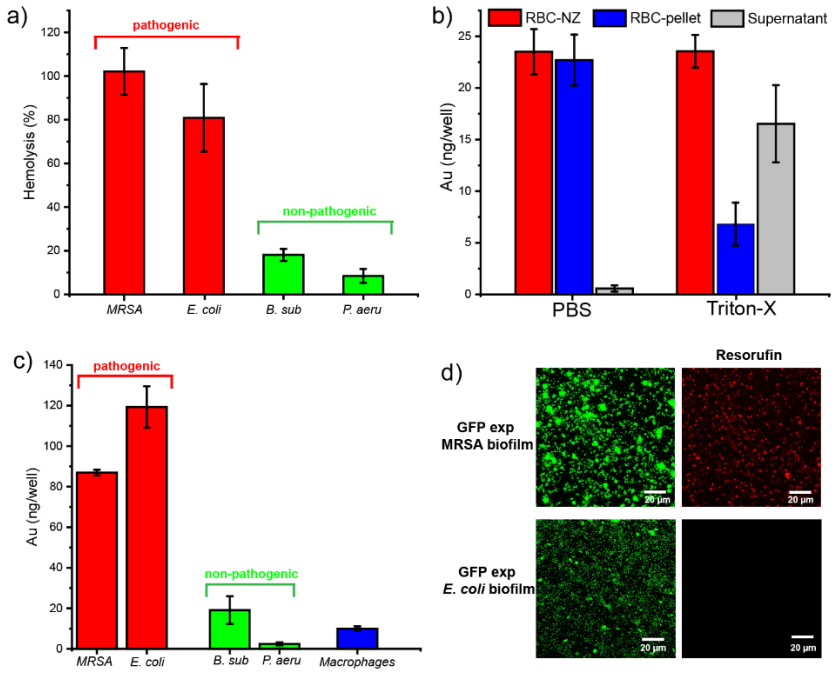

Figure 5.3. a. Hemolysis of Red Blood Cells by bacterial biofilms. **b.** Quantification of Au (ng/well) on RBCs-nanozymes incubated in PBS and Triton-X. **c.** Nanozyme diffusion of Au (ng/well) in different bacterial biofilms including pathogenic (methicillin-resistant *S. aureus*, MRSA and *E. coli*) and non-virulent (*P. aeruginosa* ATCC 17660, *B. Sub* FD6b) biofilms after incubation for 1 day with RBC-NZ (10^7 cell/mL, 100 nM NZ), as measured by ICP-MS. Cellular uptake of Au (ng/well) in macrophage (RAW 264.7) (20,000 cells/well) after incubation for 1 day with RBC-NZ (10^7 cell/mL, 100 nM NZ), as measured by ICP-MS. **d.** Confocal images of biofilms incubated with RBC-NZs (1 h) followed by incubation with Pro-Res (1 h, 10 μM).

We further corroborated the selectivity of RBC-NZs towards virulent biofilms through imaging studies using confocal microscopy. Studied for imaging biofilms were based on generation of fluorophore (Resorufin) through aryl-reduction of non-fluorescent precursor (Pro-Res) as shown in Figure 5.1 b. RBC-NZs were incubated with toxin-secreting uropathogenic (*E. coli*, MRSA) and non-virulent (*B. sub*, *P. aeruginosa*) bacterial biofilms for 24 hours. Biofilms were then washed multiple times, followed by 1-hour incubation with substrate and subsequent washings. Uropathogenic biofilms showed bright red fluorescence when observed under confocal, with minimal fluorescence observed in non-pathogenic biofilms (Figure 5.3 d). Additionally, macrophages incubated with RBC-NZs exhibited minimal fluorescence after 24 hours incubation. These results further suggest that RBC-hitchhiking can be used to selectively target pathogenic biofilms while avoiding non-specific uptake by macrophages.

Conventional antibiotic-based strategies to combat bacterial infections often disrupt the ecology of human microbiome by killing helpful bacteria species inhabiting the host.[28,29] After establishing the localization of NZs at the site of pathogenic bacteria, we investigated their ability to selectively activate antibiotic-precursor to eradicate virulent bacterial biofilms. For this study, aryl azide protected moxifloxacin (pro-Mox) was chosen as a model pro-antibiotic due to the high clinical relevance of moxifloxacin in the treatment of MDR infections.[30] The synthetic protection of secondary amine group on moxifloxacin inhibits them to bind with target bacterial enzymes, inhibiting their antimicrobial activity prior to activation. Alamar Blue assays were performed on biofilms treated with RBC-NZs and pro-Mox determine biofilm viability.

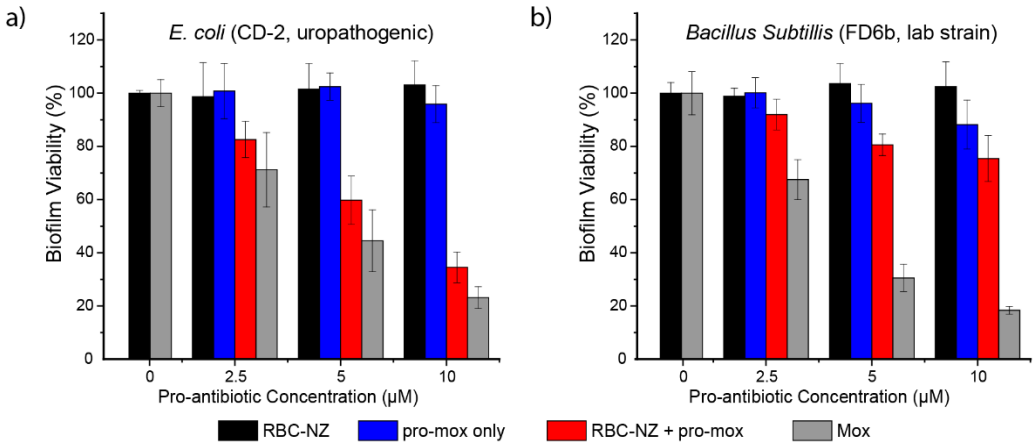

Figure 5.4. Deprotection of antimicrobials in biofilms using RBC-hitchhiked nanozymes. RBC-NZ was used for selective activation of antibiotic prodrugs that decrease biofilms viability. a. *E. coli* (toxin producing) biofilms and **b.** *B. sub* (non-virulent) biofilms treated with pro-Mox and RBC-NZ (red bars) at 37 ºC. Biofilms treated only with pro-Mox (blue bars) or with Mox (grey bars) were used in all experiments as negative and positive controls, respectively. Each experiment was replicated five times. Error bars represent standard deviations of these measurements.

For biofilm viability studies, virulent uropathogenic (*E. coli*, MRSA) and non-pathogenic bacterial strains (*B. sub*) were incubated with RBC-NZs (10^7 cells/ml, 500 nM-NZ) for 24 hours, washed and subsequently incubated with different concentrations of pro-Mox for 24 hours. Cells incubated with only pro-Mox and Moxifloxacin antibiotics were used as negative and positive controls respectively. It was observed that pro-Mox did not reduce biofilm viability against both pathogenic and non-pathogenic biofilms. However, pro-Mox incubated with RBC-NZs showed reduced biofilm viability of pathogenic biofilms while no significant antimicrobial activity was observed against non-pathogenic biofilms. These results indicate that selective accumulation of NZs in pathogenic biofilms enabled catalytic activation of pro-antibiotics thereby increasing the specificity of the therapy. Moreover, moxifloxacin reduced bacterial viability of both pathogenic and non-pathogenic species, indicating the non-selective bacteria killing caused by antibiotic treatment.

5.3 Conclusions

In this chapter, I have investigated a strategy utilizing hitchhiking of functionalized bioorthogonal nanozymes on Red Blood Cells. These RBCs are hemolyzed in presence of toxins secreted by pathogenic bacteria resulting in selective accumulation of nanozymes at the site of bacterial infection. These accumulated nanozymes can subsequently activate antibiotics at the site and eradicate pre-formed biofilms, without harming non-virulent bacterial species. Moreover, RBC-hitchhiked nanozymes show minimal uptake in macrophages. This strategy can be utilized to increase the specificity of nanomaterial-based strategies while minimizing the off target effects of the current antimicrobial therapies.

5.4 Experimental methods

5.4.1. NP synthesis

2nm diameter gold nanoparticles were synthetized by the Brust-Schiffrin two-phase methodology using pentanethiol as the stabilizer; these clusters were purified with successive extractions with ethanol and acetone. A Murray place exchange reaction was carried out in dry DCM to functionalize the nanoparticles with each ligand.[31,32] The monolayer-protected nanoparticles were redispersed in water and the excesses of ligand/pentanethiol were removed by dialysis using a 10,000 MWCO snake-skin membrane. The final concentration was measured by UV spectroscopy on a Molecular Devices SpectraMax M2 at 506 nm according to the reported methodology.[33]

5.4.2. Hemolysis assay

Hemolysis assay was performed on human red blood cells as we described in previous study.[34] Briefly, citrate-stabilized human whole blood (pooled, mixed gender) was purchased from Bioreclamation LLC, NY. The red blood cells were purified and re-suspended in 10 mL

phosphate buffered saline as soon as received. 0.1 mL of RBC solution was added to 0.4 mL of NP solution in PBS in 1.5 mL centrifuge tube.

The mixture was incubated at 37 ˚C, 150 rpm for 30 minutes followed by centrifugation at 4000 rpm for 5 minutes. The absorbance value of the supernatant was measured at 570 nm with absorbance at 655 nm as a reference. RBCs incubated with PBS as well as water were used as negative and positive control, respectively. All samples were prepared in triplicate. The percent hemolysis was calculated using the following formula:

% Hemolysis = ((sample absorbance-negative control absorbance)) / ((positive control absorbance-negative control absorbance)) × 100.

5.4.3. Biofilm culture

Bacteria were inoculated in LB broth at 37 °C until stationary phase. The cultures were then harvested by centrifugation and washed with 0.85% sodium chloride solution three times. Concentrations of resuspended bacterial solution were determined by optical density measured at 600 nm. Seeding solutions were then made in minimal media, M9 broth to reach OD600 of 0.1. Then, 500 μL of the seeding solutions was added to each well of the 24-well microplate. M9 medium without bacteria was used as a negative control. The plates were covered and incubated at room temperature under static conditions for a desired period of 24 h. Planktonic bacteria were removed by washing with phosphate-buffered saline (PBS) three times.

5.4.4. Nanozyme accumulation in biofilms

After plating bacterial cells in a 24-well plate. On the following day, planktonic bacteria were removed by washing with PBS three times and incubated with RBC-NZ, Bare-NZ (10^7 RBC/ml, 500 nM respectively) in minimal M-9 media (pH 7.4) for 1 h at 37 °C. After incubation, biofilms were washed three times with PBS, and lysis buffer was added to each well. All lysed samples were then further processed for ICP-MS analysis (vide inf ra) to determine the intracellular

amount of gold and ruthenium. Diffusion experiments were performed independently at least two times, and each experiment comprised three replicates.

5.4.5. Confocal Imaging of Bacteria

A total of 10^8 bacterial cells/mL was seeded (2 mL in M9 media) in a confocal dish and allowed to grow; old medium was replaced every 24 h. After 3 days, medium was replaced by RBC-NZ and biofilms were incubated for 1 h; biofilm samples incubated with only M9 media were used as the control. After 1 h, biofilms were washed with PBS three times and were incubated with 10 μM of the substrates for 1 h. The cells were then washed with PBS three times. Confocal microscopy images were obtained on a Zeiss LSM 510 Meta microscope by using a 60× objective. The settings of the confocal microscope were as follows: green channel, λex = 488 nm and λem = BP 505−530 nm; red channel, λex = 543 nm and λem = LP 650 nm. Emission filters: BP =band pass, LP = high pass.

5.4.6. Prodrug activation

Biofilms were cultured as mentioned in the above section. Biofilms were washed off and incubated with RBC-NZ (500 nM) in minimal M9 media. After 24 h, biofilms were washed with PBS buffer three times and treated with pro-Mox at a concentration of 2.5, 5, 10 μM for 24 h. The cells were then completely washed off and 10% alamar blue in minimal media was added to each well (220 μl) and incubated further at 37°C for 2 h. Biofilm viability was then determined by measuring the fluorescence intensity at 570 nm using a SpectraMax M5 microplate spectrophotometer.

5.5 References

1. J. T. Ngo, S. R. Adams, T. J. Deerinck, D. Boassa, F. Rodriguez-Rivera, S. F. Palida, C. R. Bertozzi, M. H. Ellisman, R. Y. Tsien, *Nat. Chem. Biol.* **2016**, *12*, 459.

2. C. R. Bertozzi, *Acc. Chem. Res.* **2011**, *44*, 651.

3 . G. Y. Tonga, Y. Jeong, B. Duncan, T. Mizuhara, R. Mout, R. Das, S. T. Kim, Y. C. Yeh, B. Yan, S. Hou, V. M. Rotello, *Nat. Chem.* **2015**, *7*, 597.

4. Y. Zhou, B. Liu, R. Yang, J. Liu, *Bioconjug. Chem.* **2017**, *28*, 2903.

5. X. Zhang, R. Huang, S. Gopalakrishnan, R. Cao-Milán, V. M. Rotello, *Trends Chem.* **2019**, *1*, 90.

6. H. K. Han, G. L. Amidon, *AAPS PharmSci* **2000**, *2*, E6.

7. R. Das, R. F. Landis, G. Y. Tonga, R. Cao-Milán, D. C. Luther, V. M. Rotello, *ACS Nano* **2019**, *13*, 229.

8. R. M. Yusop, A. Unciti-Broceta, E. M. V. Johansson, R. M. Sánchez-Martín, M. Bradley, *Nat. Chem.* **2011**, *3*, 239.

9. Y. Okamoto, R. Kojima, F. Schwizer, E. Bartolami, T. Heinisch, S. Matile, M. Fussenegger, T. R. Ward, *Nat. Commun.* **2018**, *9*, 1943.

10. L. Du, H. Qin, T. Ma, T. Zhang, D. Xing, *ACS Nano* **2017**, *11*, 8930.

11. W. R. Algar, D. E. Prasuhn, M. H. Stewart, T. L. Jennings, J. B. Blanco-Canosa, P. E. Dawson, I. L. Medintz, *Bioconjug. Chem.* **2011**, *22*, 825.

12. Y. Bai, J. Chen, S. C. Zimmerman, *Chem. Soc. Rev.* **2018**, *47*, 1811.

13. H. H. Gustafson, D. Holt-Casper, D. W. Grainger, H. Ghandehari, *Nano Today* **2015**, *10*, 487.

14. V. R. Muzykantov, *Expert Opin. Drug Deliv.* **2010**, *7*, 403.

15. X. Han, C. Wang, Z. Liu, *Bioconjug. Chem.* **2018**, *29*, 852.

16. S. Bhakdi, J. Tranum-Jensen, *Microbiol. Rev.* **1991**, *55*, 733 LP.

17. K. Orf, A. J. Cunnington, *Front. Microbiol.* **2015**, *6*, 666.

18. E. Chambers, S. Mitragotri, *Exp. Biol. Med. (Maywood).* **2007**, *232*, 958.

19. J. S. Brenner, D. C. Pan, J. W. Myerson, O. A. Marcos-Contreras, C. H. Villa, P. Patel, H. Hekierski, S. Chatterjee, J.-Q. Tao, H. Parhiz, K. Bhamidipati, T. G. Uhler, E. D. Hood, R. Y. Kiseleva, V. S. Shuvaev, T. Shuvaeva, M. Khoshnejad, I. Johnston, J. V Gregory, J. Lahann, T. Wang, E. Cantu, W. M. Armstead, S. Mitragotri, V. Muzykantov, *Nat. Commun.* **2018**, *9*, 2684.

20. C. Wang, X. Sun, L. Cheng, S. Yin, G. Yang, Y. Li, Z. Liu, *Adv. Mater.* **2014**, *26*, 4794.

21. I. V Zelepukin, A. V Yaremenko, V. O. Shipunova, A. V Babenyshev, I. V Balalaeva, P. I. Nikitin, S. M. Deyev, M. P. Nikitin, *Nanoscale* **2019**, *11*, 1636.

22. K. Saha, D. F. Moyano, V. M. Rotello, *Mater. Horizons* **2014**, *1*, 102.

23. C. H. Villa, A. C. Anselmo, S. Mitragotri, V. Muzykantov, *Adv. Drug Deliv. Rev.* **2016**, *106*, 88.

24. S. Huo, Y. Jiang, A. Gupta, Z. Jiang, R. F. Landis, S. Hou, X. J. Liang, V. M. Rotello, *ACS Nano* **2016**, *10*, 8732.

25. L. Pirofski, A. Casadevall, *Infect. Immun.* **1999**, *67*, 3703.

26. C.-M. J. Hu, R. H. Fang, J. Copp, B. T. Luk, L. Zhang, *Nat. Nanotechnol.* **2013**, *8*, 336.

27. A. Gupta, R. Das, G. Yesilbag Tonga, T. Mizuhara, V. M. Rotello, *ACS Nano* **2018**, *12*, 89.

28. A. Langdon, N. Crook, G. Dantas, *Genome Med.* **2016**, *8*, 39.

29. C. Jernberg, S. Lofmark, C. Edlund, J. K. Jansson, *Microbiology* **2010**, *156*, 3216.

30. P. M. Tulkens, P. Arvis, F. Kruesmann, *Drugs R. D.* **2012**, *12*, 71.

31. Miranda, O. R.; Chen, H. T.; You, C. C.; Mortenson, D. E.; Yang, X. C.; Bunz, U. H. F.; Rotello, V. M. *J. Am. Chem. Soc.* **2010**, *132*, 5285-5289.

32. De, M.; Rana, S.; Akpinar, H.; Miranda, O. R.; Arvizo, R. R.; Bunz, U. H. F.; Rotello, V. M. *Nat. Chem.* **2009**, *1*, 461-465.

33. Liu, X. O.; Atwater, M.; Wang, J. H.; Huo, Q. *Colloid. Surface. B* **2007**, *58*, 3-7.

34. Saha, K. M., D. F.; Rotello, V. M. *Mater. Horiz.* **2014**, *1*, 102-105.

CHAPTER 6

ENGINEERED POLYMERIC NANOPARTICLES WITH UNPRECEDENTED ANTIMICROBIAL EFFICACY AND THERAPEUTIC INDICES AGAINST MULTI-DRUG RESISTANT BACTERIA AND BIOFILMS

6.1 Introduction

Indiscriminate use of antibiotics in agricultural[1] and medical fields[2] has created multi-drug resistant (MDR) "superbugs" such as methicillin-resistant *Staphylococcus aureus* (MRSA) along with particularly refractory Gram-negative species that pose a serious threat to global health. Planktonic bacteria cause acute infections resulting in sepsis, with the threat further intensified by chronic infections from biofilms.[3,4] Biofilm-associated infections frequently occur on medical implants and indwelling devices such as catheters, prosthesis and dental implants.[5] Biofilm infections can also occur on or around dead tissues leading to endocarditis and chronic wound infections.[6] These intractable infections are challenging due to the high resistance of these infections towards both host immune response and traditional antimicrobial therapies.[7] Current biofilm treatment techniques require aggressive antibiotic therapy coupled with debridement of infected tissue.[8] However, this standard regimen incurs high treatment costs and low patient compliance due to the invasive nature of the treatment.[9] The therapeutic challenge is exacerbated by the increasing number of antibiotic-resistant bacterial strains, further impairing the therapeutic effectiveness of existing antibiotics.[10]

Antimicrobial peptides (AMPs) have emerged as an alternative to conventional antibiotic therapy, exhibiting broad spectrum activity against antibiotic-resistant bacteria.[11,12] AMPs have demonstrated high therapeutic indices (TI, selectivity towards bacterial cells calculated as HC_{50} (Hemolytic activity)/MIC) of ~900 and ~3,300[13] against planktonic bacteria, however these α-helical peptides are susceptible to proteolytic degradation, reducing their efficacy.[14,15] Host-defense peptide mimicking synthetic polymers have recently been developed, demonstrating broad spectrum activity against microbes.[16-20] However, high toxicity towards

mammalian cells and red blood cells, resulting in low therapeutic indices (ranging from ~1-10)[16,18-20] have impaired their practical applications in clinical settings. Low toxicity to mammalian cells, in particular red blood cells is critical for effective application of antimicrobials in or on patients.[29,36] Limited studies have demonstrated synthetic polymers with improved therapeutic indices (~150-550)[21-24], exhibiting their ability to kill bacteria while causing minimal hemolysis of red blood cells. However, these polymers have focused on the treatment of planktonic microbes, overlooking the more drug-resistant biofilm counterparts. To the best of our knowledge, synthetic polymers exhibiting high biofilm efficacy while maintaining low toxicity towards mammalian cells have not been reported.

We report here engineered polymers that effectively eradicate pre-formed biofilms while maintaining high therapeutic indices (>1000) against red blood cells (RBCs). In the design of these materials we hypothesized that the therapeutic window of cationic polymers could be regulated by varying hydrophobic moieties, similar to the hydrophobic residues present in the active sites of antimicrobial peptides.[25] To this end we synthesized a library of quaternary ammonium poly(oxanorborneneimides) possessing different degrees of hydrophobicity (Figure 6.1) and screened their antimicrobial and hemolytic activities. These polymers form 10-15 nm nanoparticles in aqueous solution, increasing their overall cationic charge and molecular mass. We observed that longer hydrophobic alkyl chains that bridge the cationic head group and polymer backbone greatly enhances toxicity against planktonic bacteria while maintaining low hemolytic activity towards RBCs (TI 1250-2500). These nanoparticles readily penetrate biofilms and eradicate pre-formed biofilms while still maintaining high TI (60-165). Polymeric NPs (PNPs) demonstrated a 6-fold log reduction in bacterial colonies with no mammalian cell toxicity when tested in a biofilm-mammalian cell coculture model. Notably, we observed that bacteria did not develop any resistance against PNPs even after 20 serial passages, in stark contrast to conventional antibiotics. Overall, our engineered polymeric nanoparticle platform shows strong

potential as an infectious disease therapeutic and simultaneously provides a rational approach to design novel antimicrobials for sustainably combating bacterial infections.

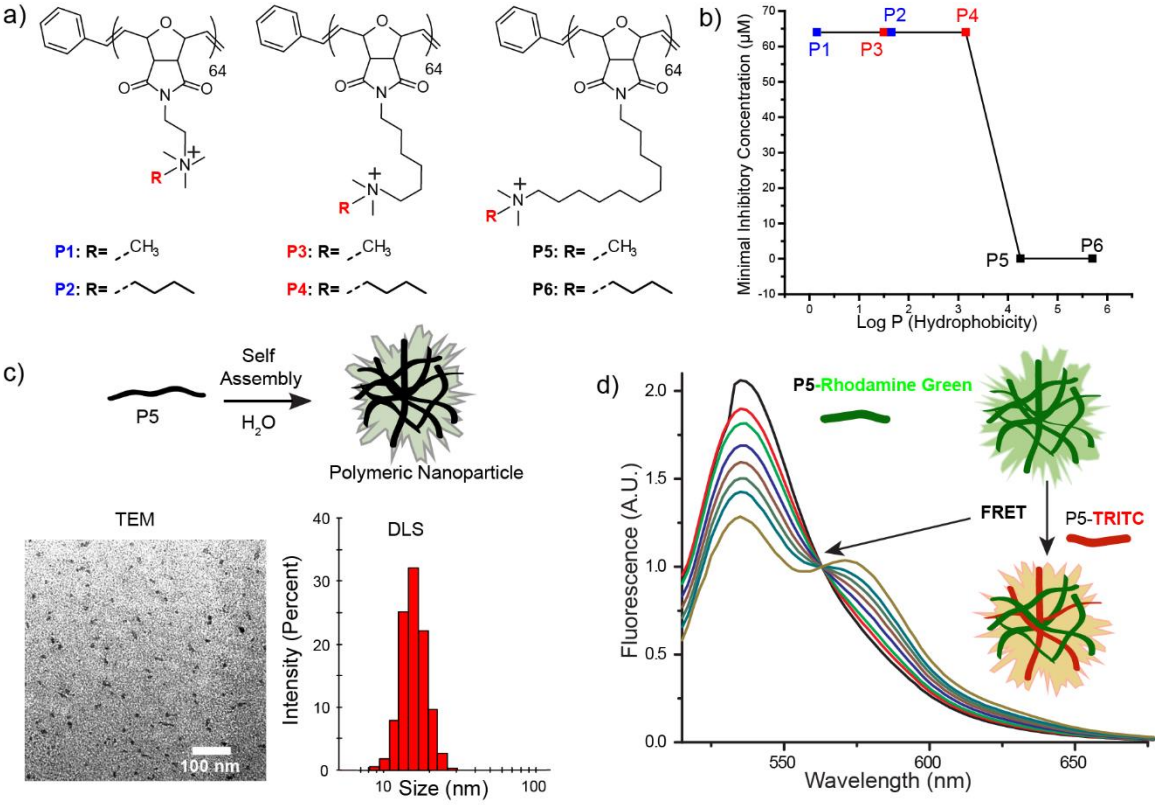

Figure 6.1. Molecular structures of **a.** oxanorbornene polymer derivatives. **b.** MIC values of polymer derivatives with different hydrophobic chain lengths. Log *P* represents the calculated hydrophobic values of each monomer **c.** Schematic representation depicting self-assembly of P5-homopolymers. Characterization of P5 PNPs using TEM imaging and DLS measurement. **d.** Graph for FRET experiments between P5-Rhodamine Green and P5-TRITC indicating formation of polymeric NPs.

6.2 Results and discussion

Norbornene/oxanorbornene-based polymers feature conformational restrictions reminiscent of peptides, and amphiphilic cationic polymers with this backbone have shown promising antimicrobial properties.[24,26] Additionally, the synthetic scalability provides a key advantage over antimicrobial peptides.[27,28] The distribution of hydrophobic moieties on antimicrobial macromolecules plays a pivotal role in determining their bactericidal activity.[25,29] In particular, careful consideration of "Amphiphilic balance", i.e. distribution of cationic charge

and hydrophobic moieties on the polymer are critical to ensure antimicrobial selectivity towards bacteria over mammalian cells.[30] We explored this design space through a library of oxanorbornene polymers (Figure 6.1 a, 6.2 a) with varying unbranched alkyl chains both bridging the cationic head group and the polymer backbone itself, allowing systematic determination of structure-antimicrobial efficacy relationships. We found that polymers containing a bridged C_{11} alkyl chain spontaneously self-assemble into cationic PNPs (~13 nm) in aqueous solutions as confirmed by transmission electron microscopy (TEM, Figure 6.1 c), dynamic light scattering (DLS, Figure 6.1 c) and Förster resonance energy transfer (FRET) experiments (Figure 6.1 d, Structural details of dye-tagged polymer are in experimental methods section 6.4). These micellar structures formed at low polymer concentrations: dilution experiments of encapsulated Nile Red within P5 PNPs indicated a critical micelle concentration of < 2.5 μM (Figure 6.6, Section 6.5).[31]

The PNP library was screened for antimicrobial activity against an uropathogenic strain of *Escherichia coli* (CD-2), using broth dilution methods to evaluate their minimal inhibitory concentrations (MICs).[32] We observed a 1000-fold increase in the antimicrobial activity of polymeric nanoparticles upon increasing the hydrophobicity of the alkyl chain bridging the backbone and cationic headgroup (Figure 6.1 b). Polymers with shorter internal alkyl chains (P1-P4) displayed MICs of 64 μM, while analogs with more hydrophobic C_{11} chains (P5, P6) inhibited bacteria growth at 0.064 μM. We further extended the hydrophobicity on the cationic headgroup of the polymers and monitored the change in antimicrobial activity. We determined that the MICs of PNPs did not change significantly upon increasing the hydrophobicity at the cationic headgroup (Figure 6.2 a). This result indicates that careful placement of local hydrophobic domains on polymer structure plays a crucial role in determining the antimicrobial activity of the polymer. Similar behavior has also been reported in antimicrobial peptides where the location of hydrophobic residues determines antimicrobial activity.[33,34]

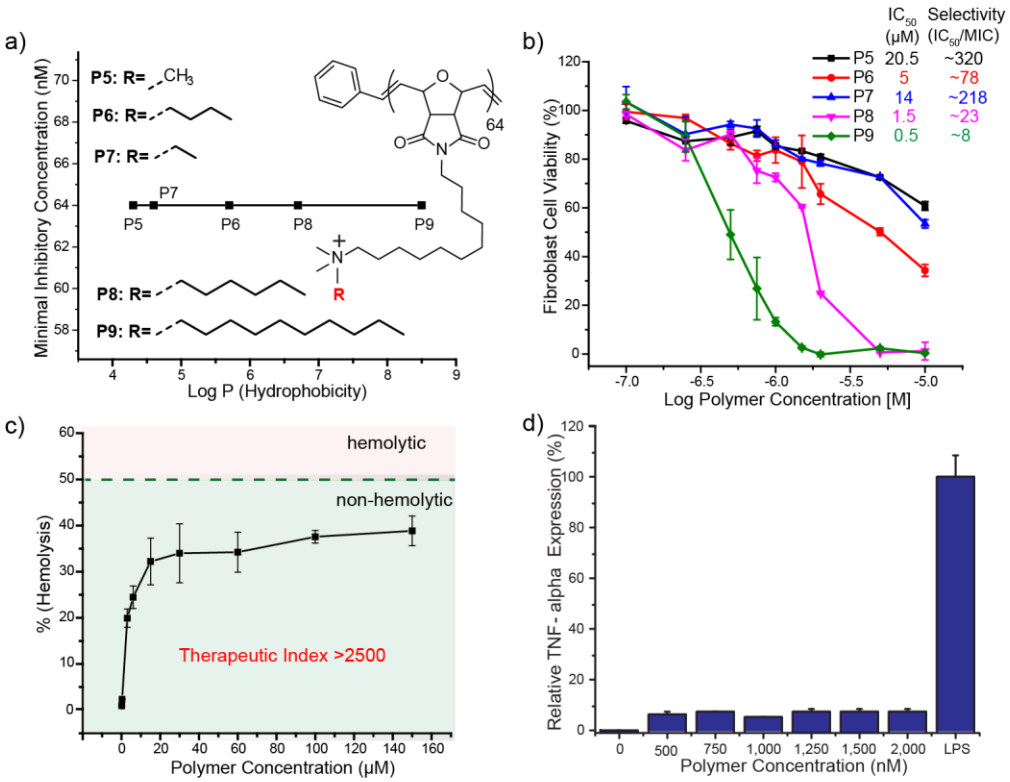

Figure 6.2. a. Graph showing minimum inhibitory concentrations (MIC) and structure details of oxanorbornene derivatives with different hydrophobicity of the cationic headgroups. Log *P* represents the calculated hydrophobic values of each monomer. **b.** Graph showing toxicity of P5-P9 polymers against 3T3 Fibroblast cells indicating increase in cytotoxicity with increased hydrophobicity of the cationic headgroup. Selectivity towards bacteria as compared to mammalian cells is calculated as (IC_{50}/MIC). **c.** Hemolytic activity of PNPs at different concentrations indicates their non-hemolytic behavior at relevant therapeutic concentrations. **d.** TNF-α secretion of Raw 264.7 cells in the presence of PNPs. Lipopolysaccharide (LPS) was used as a positive control.

After establishing antimicrobial efficacy, we performed cell toxicity assays on human fibroblast cell lines to determine the IC_{50} (half-maximal inhibitory concentration) of the most hydrophobic polymers (P5-P9) and evaluate their therapeutic selectivity.[35] Therapeutic selectivity is defined as IC_{50}/MIC that determines the ability of polymers to kill bacteria while causing minimal toxicity to mammalian cells. It was observed that polymer cytotoxicity towards fibroblasts increased with increasing hydrophobicity of the alkyl chain at cationic headgroup (Figure 6.2 b). Least hydrophobic P5 showed IC_{50} of 20.5 μM, yielding therapeutic selectivity of ~320. On the contrary, its most hydrophobic counterparts (P6, P8 and P9) showed therapeutic

selectivity as low as 78, 23 and 8 respectively. These results further indicate that careful placement of hydrophobic domains on polymer can regulate their toxicity towards mammalian cells. Similar study has previously reported that co-localization of the charge and hydrophobic domains reduced the antibacterial effect, however dramatically reduced the chance of red blood cell hemolysis, thereby improving the overall selectivity of the system.30 Hence, we concluded that P5 polymer with internally hydrophobic alkyl chains demonstrated highest antimicrobial activity with least cytotoxicity.

Next, we performed hemolysis assays on human RBCs with our most potent polymer P5 and calculated their HC_{50} (concentration that causes 50% lysis of RBCs) to determine their biocompatibility.[36,37] MIC and HC_{50} values were used to calculate a therapeutic index (TI = HC_{50}/MIC) of PNPs against planktonic bacteria. PNPs P5 with undecyl-bridging alkyl chains showed minimal hemolytic character (Figure 6.2 c). The highest antimicrobial efficiency was observed with P5 PNPs, with an MIC of 64 nM (1.8 $\mu g.ml^{-1}$) against *E. coli*. P5 PNPs showed little hemolytic character (HC_{50} >160 µM, 4700 $\mu g.ml^{-1}$) providing an unprecedented therapeutic index of > 2500, 5-fold higher than previous polymer-based antimicrobials. Having established P5 PNPs are non-acutely toxic, we next investigated their chronic effects in relation to inflammatory cytokine responses from macrophage RAW 264.7 cells (Figure 6.7). P5 PNP concentrations up to 2 µM showed no significant toxicity or tumor necrosis factor alpha (TNF-α) cytokine expression (Figure 6.2 d), suggesting *in vitro* immunocompatibility with mammalian immune cells.[38]

We next tested P5 PNPs against multiple uropathogenic clinical isolates (Table 6.1) to establish their broad-spectrum activity. P5 PNPs suppressed bacterial proliferation at concentrations ranging from 64-128 nM (1.8 $\mu g.ml^{-1}$ – 3.6 $\mu g.ml^{-1}$), once again similar or lower to previously reported antimicrobial polymers. These polymers showed similar antimicrobial activity against 5 clinical isolates of *E. coli* with different susceptibilities to clinical antibiotics (resistant to 1-17 drugs), indicating their ability to evade common mechanisms of bacterial

resistance. Notably, engineered polymers were effective against clinical isolates of Gram-negative *P. aeruginosa* and *E. cloacae* complex. Similarly, Gram-positive strains of *S. aureus* were susceptible to P5 PNPs including the highly virulent strain of methicillin-resistant *S. aureus* (MRSA).

Table 6.1. Minimum inhibitory concentrations and therapeutic indices of P5 PNPs against multiple uropathogenic clinical isolate bacterial strains.

Strain	Species	MIC (nM)	TI (HC_{50}/MIC)
CD-23	*P. aeruginosa*	64	~2500
CD-1006	*P. aeruginosa*	128	~1250
CD-489	*S. aureus- MRSA*	64	~2500
CD-2	*E. coli*	128	~2500
CD-3	*E. coli*	64	~2500
CD-19	*E. coli*	64	~2500
CD-549	*E. coli*	128	~1250
CD-496	*E. coli*	128	~1250
CD-866	*E. cloacae complex*	128	~1250
CD-1412	*E. cloacae complex*	128	~1250
CD-1545	*E. cloacae complex*	128	~1250

Due to the highly cationic and hydrophobic nature of our PNPs, we hypothesized their activity arose from the disruption of bacterial cell membranes.[39,40] This expectation was supported through staining with membrane-impermeable propidium iodide (PI) where only cells with compromised membranes generate red fluorescence.[41,42] Pathogenic *E. coli* (CD-2), *S. aureus* (CD-489) and non-pathogenic *P. aeruginosa* (ATCC 19660) were treated with 1 μM of P5 PNPs for 3 hours at 37 °C and subsequently stained with PI before imaging. The confocal images (Figure 6.3 b) clearly show that the PNPs generate substantial bacterial membrane disruption in all three species, regardless of membrane composition or pathogenicity.

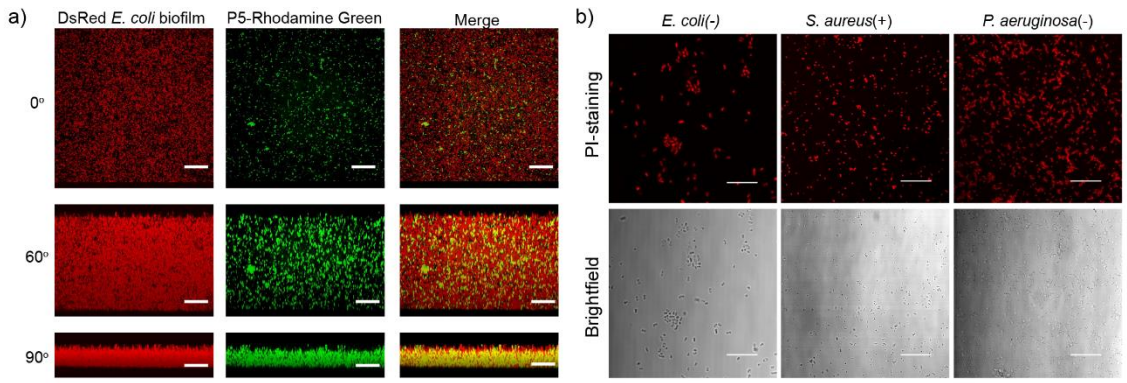

Figure 6.3. a. Representative 3D projection of confocal image stacks of E2-Crimson (Red Fluorescent Protein) expressing *E. coli* DH5α biofilm after 1 h treatment with P5-Rhodamine Green at 1 μM concentration. The panels are projection at 0°, 60° and 90° angle turning along X axis. Scale bars are 30 μm. **b.** Confocal images of *E. coli* (CD-2), *S. aureus* (MRSA, CD-489) and *P. aeruginosa* (ATCC 19660) stained with Propidium Iodide (PI) after treatment with PNPs. Scale bars are 30 μm.

After establishing the efficacy of our NPs against bacterial "superbugs", we tested their efficacy against the even more refractory bacterial biofilms. Bacteria in biofilms produce extracellular polymeric substance that provides a potent barrier against therapeutics.[8] Penetration and accumulation of therapeutics inside biofilms is crucial for effective therapy of these infections,[43,44] so the ability of PNPs to penetrate biofilms was determined using confocal microscopy. We treated biofilms formed by *E. coli* expressing E2-Crimson (a red fluorescent protein) with P5 PNPs functionalized with Rhodamine-Green fluorescent dyes. As shown in Figure 6.3a, fluorescently labeled nanoparticles readily penetrated and dispersed throughout the biofilms (Figure 6.8), suggesting their ability to be an effective anti-biofilm agent.

Having established biofilm penetration, the therapeutic ability of P5 PNPs against pre-formed bacterial biofilms was quantified. We chose a laboratory strain of *P. aeruginosa* (ATCC 19660) and 3 uropathogenic clinical isolates, *P. aeruginosa* (CD-1006), *En. cloacae* complex (CD-1412) and *S. aureus* (CD-489, a methicillin-resistant strain). As shown in Figure 6.4, P5 PNPs demonstrate minimum concentrations to eradicate 90% of biofilms ($MBEC_{90}$) ranging from 1-3 μM, providing unprecedented therapeutic indices ranging from 60-165 for biofilms (TI =

HC_{50}/$MBEC_{90,}$ Figure 6.9). Nanoparticles could treat both Gram-negative (*P. aeruginosa*, and *En. cloacae* complex) and Gram-positive (*S. aureus*) bacterial strains, further highlighting their broad-spectrum activity against biofilms. Notably, P5 PNPs demonstrated similar efficacy in treating MDR (CD-489, CD-1412) and non-resistant strains (CD-1006, ATCC 19660), suggesting their value as a therapeutic alternative to traditional antibiotics.

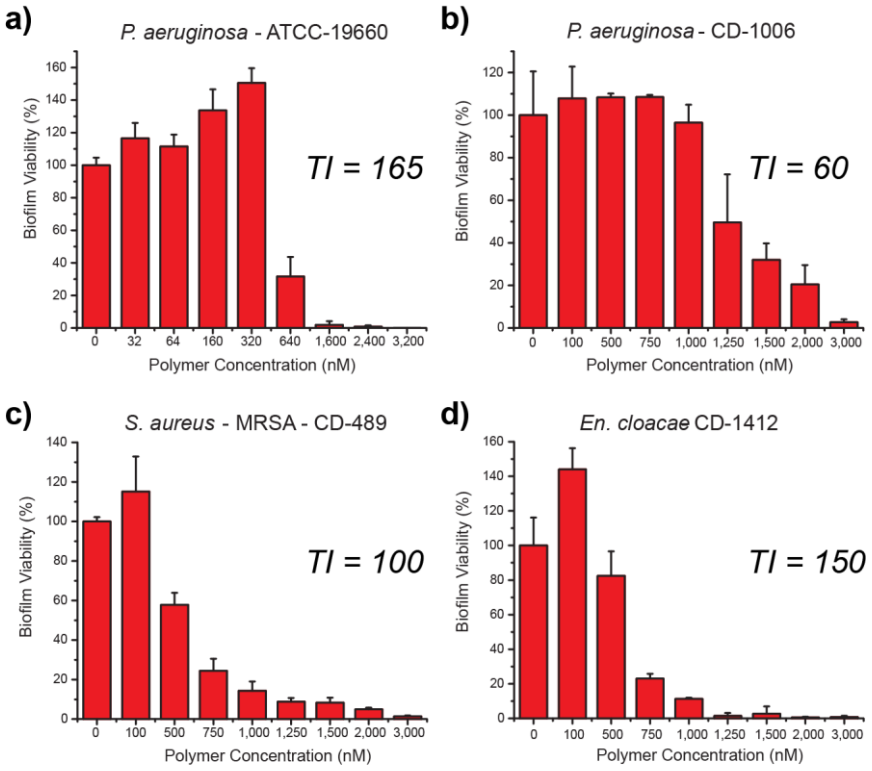

Figure 6.4. Viability of 1-day-old **a.** *P. aeruginosa* (ATCC-19660), **b.** *P. aeruginosa* (CD-1006), **c.** *S. aureus* (CD-489), and d. *En. cloacae* complex (CD-1412) biofilms after 3 h treatment with P5 PNPs. The data are average of triplicates, and the error bars indicate the standard deviations. TI is the therapeutic index relative to $MBEC_{90}$ and hemolysis against red blood cells (HC_{50}).

The ability to eradicate biofilms on biomedical surfaces such as medical implants and indwelling devices is a critical capability. However, treating biofilm infections on human tissues or organs is more challenging and relevant to medical settings.[45] Biofilm infections on wounds significantly impair the healing process regulated by fibroblast skin cells.[46]

First, we investigated P5 PNPs compatibility with mammalian NIH 3T3 fibroblast cells at concentrations used to eradicate pre-formed biofilms, with no significant toxicity observed

(Figure 6.7). We next used an *in vitro* coculture model comprised of mammalian fibroblast cells with bacterial biofilm overgrowth.[47,48] In practice, *P. aeruginosa* bacteria were seeded on a confluent monolayer of NIH 3T3-fibroblast cells overnight to generate biofilms prior to treatment. The cocultures were treated with P5 PNPs for 3 hours, washed, and the viabilities of both bacteria and fibroblasts were determined. As shown in Figure 6.5a, a 4-6-fold log reduction (99.5%-99.99%) in bacterial colonies occurred at concentrations ranging from 7.5-15 μM, while no substantial loss of fibroblast viability was observed in this concentration range.

Bacteria rapidly acquire resistance towards antibiotics and other antimicrobials, limiting their long-term efficacy. Given the membrane disruption mechanism used by the PNPs, development of resistance in bacteria would require dramatic changes in the bacterial phenotype.[43,45] The ability of PNPs to evade resistance was tested by subjection of uropathogenic *E. coli* (CD-2) to multiple serial passages of sub-MIC (66% of MIC) concentrations of P5 PNPs. The resulting bacterial population was harvested, and its MIC was evaluated. As shown in Figure 6.5 b, even at the 20th serial passage (~1,300 bacterial generations) of CD-2, there was no change in MIC. Similar experiments were conducted on ciprofloxacin (quinolone), ceftazidime (*β*-lactam) and tetracycline, clinically relevant antibiotics. Respectively, there was a 33,000, 4,200 and 256-fold increase in the MICs of antibiotics against CD-2 *E. coli* after only a few passages. Our polymeric nanoparticles evade resistance towards bacteria longer than previously reported polymer-based nanomaterials [49] (~600 generations – *A. baumannii* FADDI-AB156) and comparable to a recently discovered novel antibiotic, teixobactin (~1,300 generations – *S. aureus* ATCC 29213).[50]

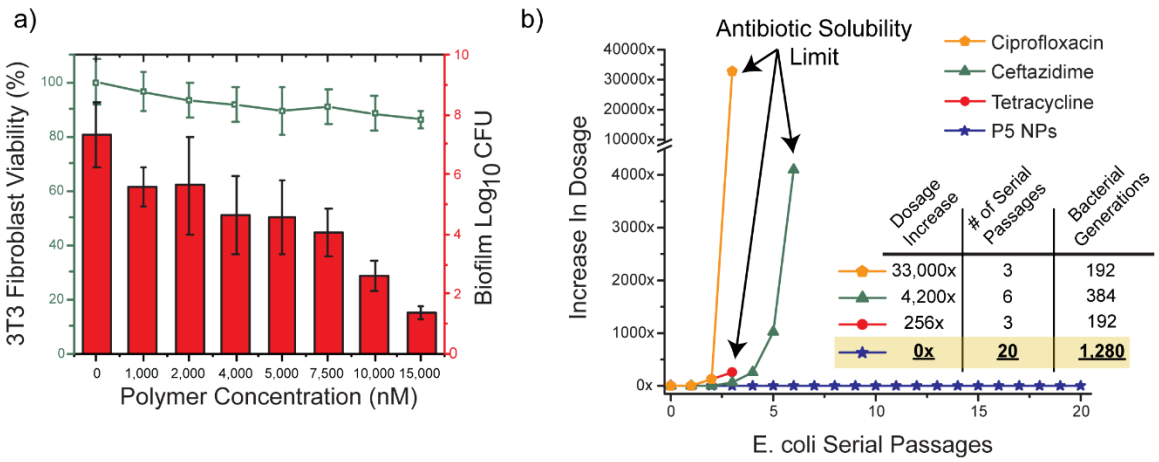

Figure 6.5. a. Viability of 3T3 fibroblast cells and *E. coli* biofilms in the co-culture model after 3 h treatment with P5 PNPs. Scatters and lines represent 3T3 fibroblast cell viability. Bars represent $\log_{10}$ of colony forming units in biofilms. The data are average of triplicates and the error bars indicate the standard deviations. **b.** Resistance development during serial passaging in the presence of sub-MIC levels of antimicrobials. The y axis is the highest concentration the cells grew in during passaging. The figure is representative of 3 independent experiments.

6.3 Conclusions

We have designed and fabricated an effective polymer nanoparticle-based therapeutic platform to combat MDR bacterial and biofilm infections. Our research demonstrates the ability of these PNPs to modulate antimicrobial activity and therapeutic efficacy by structure-specific incorporation of hydrophobic and cationic moieties. These amphiphilic cationic PNPs demonstrate excellent efficiency in combating planktonic superbugs as well as their more drug-resistant biofilm counterparts. Their ability to penetrate and eradicate biofilms provides the foundation for a therapeutic strategy against biofilm infections that does not require debridement and extensive antimicrobial regimens. These PNPs function through a membrane disruption mechanism that strongly attenuates generation of tolerance or resistance. Taken together, PNP-based antimicrobial therapy has the potential to provide an effective platform to combat bacterial infections while circumventing standard antibiotic resistance pathways.

6.4 Experimental methods

6.4.1. Polymer synthesis

Generation of C2 and C6-bridged polyoxanorbornene polymers can be successfully made using the same procedures used to generate C11-bridged polymers however replacing 11-bromoundecanol with bromoethanol or 6-bromohexanol, respectively.

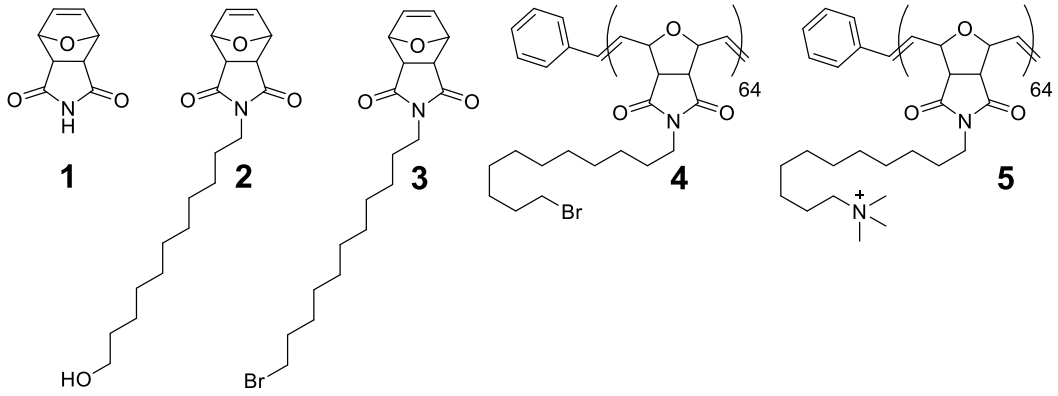

Synthesis of 1. In a pressure tube, furan (4.5ml, 61.7mmol, 1.5eq) and maleimide (4.0g, 41.1mmol, 1.0eq) were added in addition to 5ml of diethyl ether. The tube was sealed and heated at 100 °C overnight. Afterwards, the pressure tube was cooled to r.t. and the formed solid was removed, filtered, and washed with copious amounts of diethyl ether to isolate 1 as a white solid (95% yield) and was used without further purification. ^{1}H NMR (400MHz, MeOD) 11.14 (s, 1H), 6.52 (s, 2H), 5.12 (s, 2H), 2.85 (s, 2H).

Synthesis of 2. To a 250 ml round bottom flask equipped with a stir bar was added 60 ml of DMF. Next, 1 (3.76g, 22.7mmol, 1.0eq) was added along with potassium carbonate (12.59g, 91.1mmol, 4.0eq). The reaction mixture was heated at 50 °C for five minutes. Finally, potassium iodide (0.68g, 4.5mmol, 0.2eq) and 11-bromoundecanol (6.00g, 23.90mmol, 1.05eq) were added and stirred at 50 °C overnight. Afterwards, the reaction mixture was cooled to room temperature, diluted to 150 ml with ethyl acetate and washed with water (7x, 50ml) and brine (1x, 50ml). The organic layer was dried with sodium sulfate, filtered, and rotovaped to yield 2.2 was purified by sonication of the rotovaped solid in hexanes and filtered (82% yield). ^{1}H NMR (400MHz, $CDCl_3$)

6.44 (s, 2H), 5.19 (s, 2H), 3.55, (t, 2H), 3.49 (t, 2H), 2.79 (s, 2H), 1.9 (s, 1H), 1.39 (m, 4H), 1.2 (m, 14H).

Synthesis of 3. To a 250ml round bottom flask equipped with a stir bar was added 2 (2.64g, 7.87mmol, 1.0eq). Next, DCM (100ml) was added along with tetrabromomethane (3.13g, 9.44mmol, 1.2eq). The reaction was cooled to 0 °C using an ice bath. Finally, triphenylphosphine was added in portions (2.47g, 9.44mmol, 1.2eq) and allowed to stir for three hours. Afterwards, the reaction mixture was rotovaped and ethyl ether was added (200 ml) and placed in the freezer for 2 hours to precipitate out triphenylphosphine oxide. The reaction mixture was filtered, and the filtrate was rotovaped. Column chromatography was performed to yield 3, a white solid (79% yield). ^{1}H NMR (400MHz, $CDCl_3$) 6.51 (s, 2H), 5.27 (s, 2H), 3.45 (t, 2H), 3.41 (t, 2H), 2.83 (s, 2H), 1.85 (q, 2H), 1.55 (q, 2H), 1.41 (q, 2H), 1.29 (m, 12H).

Oxanorbornene Polymer Synthesis. Synthesis of 4. To a 10 ml pear-shaped air-free flask equipped with a stir bar was added 3 (800mg, 2.0mmol, 1.0eq) and 4ml of DCM. In a separate 10ml pear-shaped air-free flask was added Grubbs 3rd generation catalyst[51] (35.4mg, 0.04mmol, 0.02eq) and 1ml DCM. Both flasks were sealed with septa and attached to a schlenk nitrogen/vaccum line. Both flasks were freeze-pump-thawed three times. After thawing, Grubbs 3rd generation catalyst was syringed out and quickly added to the flask containing 3 and allowed to react for 10 min. After the allotted time, ethyl vinyl ether (200 µL) was added and allowed to stir for 15 minutes. Afterwards, the reaction was diluted to two times the volume and precipitated into a heavily stirred solution of hexane (300 ml). The precipitated polymer was filtered and dissolved into tetrahydrofuran (THF). The polymer was precipitated again into hexane and filtered to yield 4. MW = 25,698, PDI = 1.04 (determined by THF-GPC using a Polystyrene calibration curve) ^{1}H NMR (400MHz, $CDCl_3$) 6.0 (br, 1H), 5.7 (br, 1H), 4.95 (br, 1H), 4.4 (br, 1H), 3.4 (br, 2H), 3.25 (br, 2H), 1.79 (q, 2H), 1.5 (br, 2H), 1.34 (br, 2H), 1.2 (br, 14H).

Synthesis of 5 Quaternary Ammonium Polymers. To generate the library of quaternary ammonium poly(oxanorborneneimides), 4 (50 mg) was added to 20 ml vials equipped with a stir

bar. Next, excess of the necessary tertiary amines was added (10ml of a 1M trimethylamine solution in THF, all other amines were 200mg) to the vial and purged with nitrogen. First stage of the reactions involved stirring for 30 minutes at 80 °C. The polymers precipitated during this time. Half of the THF was evaporated and replaced with methanol which re-dissolved the polymers. The reaction was allowed to proceed overnight at 50 °C. Afterwards, the solvent was completely evaporated, washed with hexane 2 times, and dissolved into a minimal amount of water. The polymers were added to 10,000 MWCO dialysis membranes and allowed to stir for 3 days, changing the water periodically. The polymers were filtered through PES syringe filters and freeze-dried to yield all the respective quaternary ammonium polymers 5. NMR indicated conversion into the desired quaternary ammonium salts.

6.4.2. FRET PNP formation

FRET PNPs were generated using the P5 polymer scaffold, labelled either with donor Rhodamine Green or acceptor TRITC (Functionalized by incorporating a boc-protected amino monomer during the polymerization, followed by purification using a 10,000 MWCO dialysis bag). Keeping P5-Rhodamine Green's concentration constant at ~ 1.6 µM in 2 ml Eppendorf tubes, increasing concentrations of P5-TRITC in MQ water was added and the tubes were sonicated for one minute and allowed to stand for one hour. The solutions were then transferred to a 96-well microplate and the total emission spectrum of both P5 derivatives were recorded on a SpectroMax M5 microplate reader (Molecular Device) using 480 nm as the excitation wavelength (480 nm was selected so that only P5-Rhodamine Green would be excited).

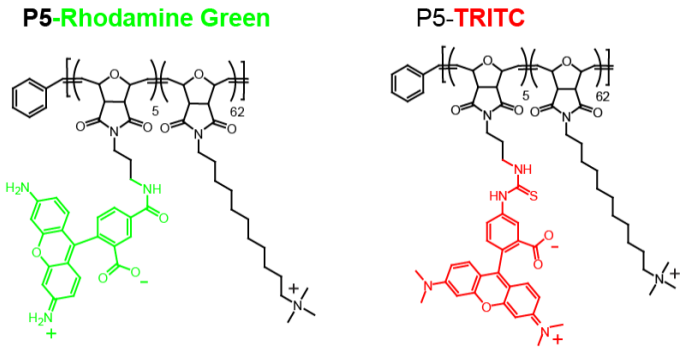

6.4.3. Determination of antimicrobial activities of cationic polymers

Bacteria were cultured in LB medium at 37 °C and 275 rpm until stationary phase. The cultures were then harvested by centrifugation and washed with 0.85% sodium chloride solution for three times.54 Concentrations of resuspended bacterial solution were determined by optical density measured at 600 nm. M9 medium was used to make dilutions of bacterial solution to a concentration of 1×10^6 cfu/mL. A volume of 50 μL of these solutions was added into a 96-well plate and mixed with 50 μL of polymer solutions in M9, giving a final bacterial concentration of 5×10^5 cfu/mL. Polymer concentration varied in half fold per a standard protocol, ranging from 1024 to 4 nM. A growth control group without polymers and a sterile control group with only growth medium were carried out at the same time. Incubation of the polymers with bacteria was performed for 16 hours. Cultures were performed in triplicates, and at least two independent experiments were repeated on different days. The MIC is defined as the lowest concentration of polymer that inhibits visible growth as observed with the unaided eye.[52]

6.4.4. Determination of hemolysis of cationic polymers

We used the previously established protocol to conduct hemolysis assays on Red Blood Cells.[36] Citrate-stabilized human whole blood (pooled, mixed gender) was purchased from Bioreclamation LLC, NY and processed as soon as received. 10 mL of phosphate buffered saline (PBS) was added to the blood and centrifuged at 5000 r.pm. for 5 minutes. The supernatant was carefully discarded and the red blood cells (RBCs) were dispersed in 10 mL of PBS. This step was repeated at least five times. The purified RBCs were diluted in 10 mL of PBS and kept on ice during the sample preparation. 0.1 mL of RBC solution was added to 0.4 mL of polymer solution in PBS in a 1.5 mL centrifuge tube (Fisher) and mixed gently by pipetting. RBCs incubated with PBS and water was used as negative and positive controls, respectively. All polymer samples as well as controls were prepared in triplicate. The mixture was incubated at 37 ˚C for 30 minutes while shaking at 150 r.p.m. After incubation period, the solution was centrifuged at 4000 r.p.m.

for 5 minutes and 100 μL of supernatant was transferred to a 96-well plate. The absorbance value of the supernatant was measured at 570 nm using a microplate reader (SpectraMax M2, Molecular devices) with absorbance at 655 nm as a reference.

6.4.5. Macrophage cell studies and TNF-alpha secretion

RAW 264.7 macrophage cell line was purchased from American Type Culture Collection (ATCC, Manassas, VA). Roswell Park Memorial Institute media (RPMI 1640) supplemented with 10% fetal bovine serum, 1% antibiotics (100 μg/ml penicillin and 100 μg/ml streptomycin) and sodium pyruvate, was used for cell culture. The cells were incubated at 37 °C under a humidified atmosphere of 5% CO_2. The cells were cultured once every four days under the above-mentioned conditions.

6.4.6. Polymer nanoparticles and LPS treatment

These studies were conducted as per the previously reported protocols.[53] Briefly, to evaluate the effect of polymer on the immune system, 1.0×10^5 of RAW 264.7 cells were cultured in a 24-well plate for 24 h. Then, cells were washed once with cold PBS and treated with different concentration of polymer for 3 h or 24h. The macrophage with 100ng/ml of lipopolysaccharide were the positive control. At the end of incubation, culture media was collected for TNF-α level measurement by ELISA (R&D Systems, MN, USA). Experiments were performed in triplicate.

6.4.7. Propidium Iodide staining assay

E. coli CD-2, *P. Aeruginosa* ATCC19660 and MRSA CD-489 (1×10^8 cfu/mL) were incubated with 1 μM P5 PNPs in M9 media at 37 ˚C and 275 rpm for 3 h. The bacteria solutions were then mixed with PI (2 μM) and incubated for 30 min in dark. Five microliters of the samples were placed on a glass slide with a glass coverslip and observed with a confocal laser scanning microscopy, Zeiss 510 (Carl Zeiss, Jena, Germany) using a 543-nm excitation wavelength.

6.4.8. Resistance development

E. coli CD-2 was inoculated in M9 medium with 85 nM (2/3 of 128 nM, MIC) of P5 PNPs at 37 ˚C and 275 rpm for 16 h (~ 64 bacterial generations for 1 serial passage). The culture was then harvested and tested for MIC as describe above. *E. coli* CD-2 was cultured without polymer as well every time as a control for comparison of MICs. In the case of P5 PNPs, 20 serial passages were performed giving ~ 1,300 generations.

6.4.9. Biofilm formation and treatment

Bacteria were inoculated in lysogeny broth (LB) medium at 37 ˚C until stationary phase. The cultures were then harvested by centrifugation and washed with 0.85% sodium chloride solution three times. Concentrations of resuspended bacterial solution were determined by optical density measured at 600 nm. Seeding solutions were then made in M9 medium to reach an OD_{600} of 0.1. A 100 μL amount of the seeding solutions was added to each well of the 96-well microplate. The plates were covered and incubated at room temperature under static conditions for 1 day. The stock solution of polymers was then diluted to the desired level and incubated with the biofilms for 3 hours at 37˚C. Biofilms were washed with phosphate buffer saline (PBS) three times and viability was determined using an Alamar Blue assay. Minimal M9 medium without bacteria was used as a negative control.54

Biofilm-3T3 Fibroblast Cell Coculture was performed using the previously reported protocol.[54]A total of 20000 NIH 3T3 (ATCC CRL-1658) cells were cultured in Dulbecco's modified Eagle medium (DMEM; ATCC 30-2002) with 10% bovine calf serum and 1% antibiotics at 37 °C in a humidified atmosphere of 5% CO_2. Cells were kept for 24 h to reach a confluent monolayer. Bacteria (*P. aeruginosa*) were inoculated and harvested as mentioned above. Afterward, seeding solutions 10^8 cells/mL were inoculated in buffered DMEM supplemented with glucose. Old medium was removed from 3T3 cells followed by addition of 100 μL of seeding solution. The cocultures were then stored in a box humidified with damp paper towels at 37 °C overnight

without shaking. Polymer NPs and other control solutions were diluted in DMEM media prior to use to obtain the desired testing concentrations. Old media was removed from coculture, replaced with freshly prepared testing solutions, and incubated for 3 h at 37 °C. Cocultures were then analyzed using LDH cytotoxicity assay to determine mammalian cell viability using manufacturer's instructions[55]. To determine the bacteria viability in biofilms, the testing solutions were removed and cocultures were washed with PBS. Fresh PBS was then added to disperse remaining bacteria from biofilms in coculture by sonication for 20 min and mixing with pipet. The solutions containing dispersed bacteria were then plated onto agar plates, and colony forming units were counted after incubation at 37 °C overnight.

6.4.10. Biofilm penetration studies using confocal microscopy

10^8 bacterial cells/ml of E2-Crimson (Red Fluorescent Protein) expressing *E. coli*, supplemented with 1 mM of IPTG ((isopropyl β-D-1-thiogalactopyranoside), were seeded (2 ml in M9 media) in a confocal dish and were allowed to grow. After 3 days media was replaced by 1000 nM of RhodGreen-P5 PNPs and biofilms were incubated for 1 hour, biofilm samples incubated with only M9 media were used as control. After 1 h, biofilms were washed with PBS three times and were incubated with 100 μM of the substrates for 1 h. The cells were then washed with PBS three times. Confocal microscopy images were obtained on a Zeiss LSM 510 Meta microscope by using a 63× objective. The settings of the confocal microscope were as follows: green channel: λ_{ex}=488 nm and λ_{em}=BP 505-530 nm; red channel: λ_{ex}=543 nm and λ_{em}=LP 650 nm. Emission filters: BP=band pass, LP=high pass.

6.4.11. Mammalian cell viability assay

A total of 20,000 NIH 3T3 (ATCC CRL-1658) cells were cultured in Dulbecco's modified Eagle medium (DMEM; ATCC 30-2002) with 10% bovine calf serum and 1% antibiotics at 37 ºC in a humidified atmosphere of 5% CO_2 for 48 h.[48] Old media was removed, and cells were washed one time with phosphate-buffered saline (PBS) before addition of PNPs in the prewarmed 10%

serum containing media. Cells were incubated for 24 h at 37 ºC under a humidified atmosphere of 5% CO_2. Cell viability was determined using Alamar blue assay according to the manufacturer's protocol (Invitrogen Biosource). After a wash step with PBS three times, cells were treated with 220 μL of 10% alamar blue in serum containing media and incubated at 37 ºC under a humidified atmosphere of 5% CO_2 for 3 h. After incubation, 200 μL of solution from each well was transferred in a 96-well black microplate. Red fluorescence, resulting from the reduction of Alamar blue solution, was quantified (excitation/emission: 560 nm/590 nm) on a SpectroMax M5 microplate reader (Molecular Device) to determine the cellular viability. Cells without any PNPs were considered as 100% viable. Each experiment was performed in triplicate.

6.4.12. Therapeutic Indices Against Biofilms

Bacteria were inoculated in lysogeny broth (LB) medium at 37 ˚C until stationary phase. The cultures were then harvested by centrifugation and washed with 0.85% sodium chloride solution three times. Concentrations of resuspended bacterial solution were determined by optical density measured at 600 nm. Seeding solutions were then made in M9 medium to reach an OD_{600} of 0.1. A 100 μL amount of the seeding solutions was added to each well of the 96-well microplate. The plates were covered and incubated at room temperature under static conditions for 1 day. The stock solution of P5 PNPs was then diluted to the desired level and incubated with the biofilms for 3 hours at 37˚C. Biofilms were washed with phosphate buffer saline (PBS) three times and viability was determined using an Alamar Blue assay. Minimal M9 medium without bacteria was used as a negative control. Concentrations were converted to Log, plotted with bacteria viability, and fitted to a curve to determine the minimum biofilm eradication concentration at 90% ($MBEC_{90}$).[56,57] The therapeutic index with respect to red blood cells was calculated by the concentration of P5 PNPs at $MBEC_{90}$ divided by the hemolysis at 50%.

6.4.13. Critical micelle concentration study

Critical Micelle Concentration of P5 PNP was determined through dilution of Nile Red encapsulated PNPs. Briefly, 16.0 mg of Polymer P5 and 2.0 mg of Nile Red was dissolved in 2 ml of dimethylsulfoxide in a 7ml scintillation vial. While under vigorous stirring, 3 ml of water was slowly added over the course of 1 hour and allowed to stir overnight. Afterwards, the vial was centrifuged, and the solution decanted to remove precipitated Nile Red that was not encapsulated. Followed by filtration through a PES syringe filter, the solution was transferred to a 3,500 MWCO dialysis bag and allowed to stir in 5L of water for two days, changing the water twice each day. Afterwards, the solution was filtered again through a PES syringe filter yielding Nile Red encapsulated P5 PNPs. Nile Red's fluorescence spectrum was monitored (Excitation = 550nm) as a function of decreasing polymer concentration. it was observed that at 2.5 μM, fluorescence decrease became non-linear. Further dilution was not possible due to limitations in the amount of Nile Red encapsulated. Therefore, the critical micelle concentration was determined to be ~ 2.5 μM and is well within the range of previously reported diblock polymer carriers.

6.5 Supplementary information

6.5.1. Critical micelle concentration study

Critical Micelle Concentration of P5 PNP was determined through dilution of Nile Red encapsulated PNPs. Briefly, 16.0 mg of Polymer P5 and 2.0 mg of Nile Red was dissolved in 2 ml of dimethylsulfoxide in a 7ml scintillation vial. While under vigorous stirring, 3 ml of water was slowly added over the course of 1 hour and allowed to stir overnight. Afterwards, the vial was centrifuged, and the solution decanted to remove precipitated Nile Red that was not encapsulated. Followed by filtration through a PES syringe filter, the solution was transferred to a 3,500 MWCO dialysis bag and allowed to stir in 5L of water for two days, changing the water

twice each day. Afterwards, the solution was filtered again through a PES syringe filter yielding Nile Red encapsulated P5 PNPs. Nile Red's fluorescence spectrum was monitored (Excitation = 550nm) as a function of decreasing polymer concentration. it was observed that at 2.5 µM, fluorescence decrease became non-linear. Further dilution was not possible due to limitations in the amount of Nile Red encapsulated. Therefore, the critical micelle concentration was determined to be ~ 2.5 µM and is well within the range of previously reported diblock polymer carriers.

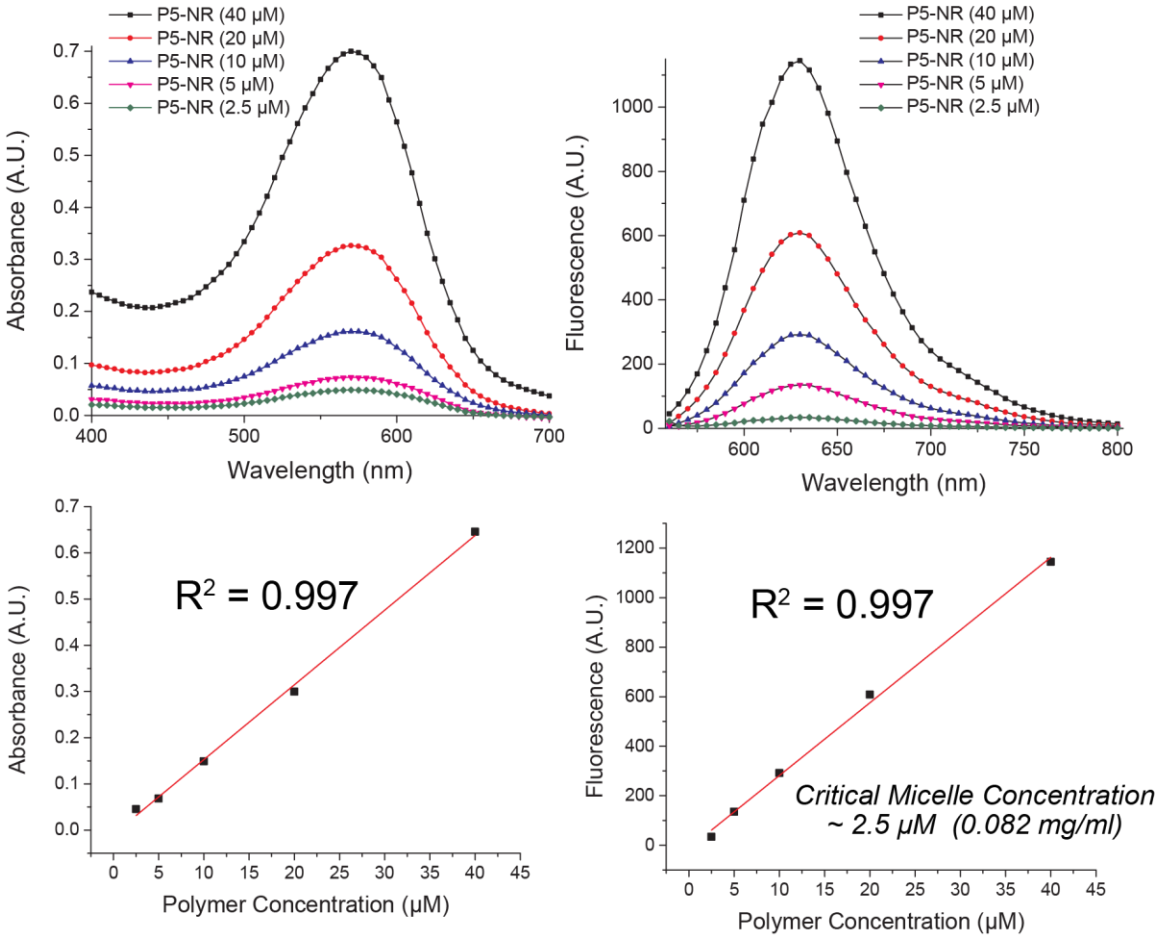

Figure 6.6. Critical micelle concentration of P5 PNPs.

6.5.2. Mammalian cell viability assay

A total of 20,000 NIH 3T3 (ATCC CRL-1658) cells were cultured in Dulbecco's modified Eagle medium (DMEM; ATCC 30-2002) with 10% bovine calf serum and 1% antibiotics at 37 ºC in a humidified atmosphere of 5% CO_2 for 48 h.[48] Old media was removed, and cells were washed one time with phosphate-buffered saline (PBS) before addition of PNPs in the prewarmed 10% serum containing media. Cells were incubated for 24 h at 37 ºC under a humidified atmosphere of 5% CO_2. Cell viability was determined using Alamar blue assay according to the manufacturer's protocol (Invitrogen Biosource). After a wash step with PBS three times, cells were treated with 220 µL of 10% alamar blue in serum containing media and incubated at 37 ºC under a humidified atmosphere of 5% CO_2 for 3 h. After incubation, 200 µL of solution from each well was transferred in a 96-well black microplate. Red fluorescence, resulting from the reduction of Alamar blue solution, was quantified (excitation/emission: 560 nm/590 nm) on a SpectroMax M5 microplate reader (Molecular Device) to determine the cellular viability. Cells without any PNPs were considered as 100% viable. Each experiment was performed in triplicate.

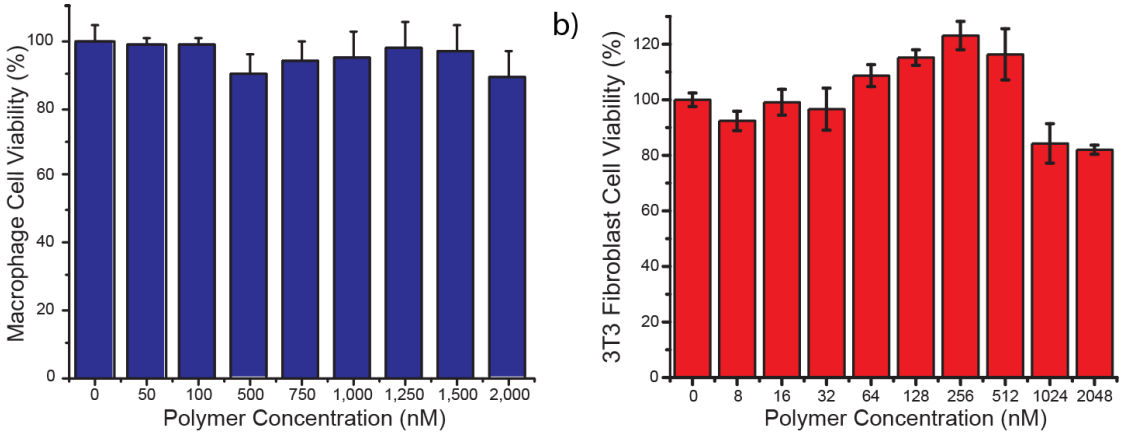

Figure 6.7. Cytotoxicity of PNPs against **a.** RAW 264.7 cells and **b.** NIH-3T3 Fibroblast cells.

6.5.3. Biofilm penetration studies using confocal microscopy

10^8 bacterial cells/ml of E2-Crimson (Red Fluorescent Protein) expressing *E. coli*, supplemented with 1 mM of IPTG ((isopropyl β-D-1-thiogalactopyranoside), were seeded (2 ml in M9 media) in a confocal dish and were allowed to grow. After 3 days media was replaced by 1000 nM of RhodGreen-P5 PNPs and biofilms were incubated for 1 hour, biofilm samples incubated with only M9 media were used as control. After 1 h, biofilms were washed with PBS three times and were incubated with 100 μM of the substrates for 1 h. The cells were then washed with PBS three times. Confocal microscopy images were obtained on a Zeiss LSM 510 Meta microscope by using a 63× objective. The settings of the confocal microscope were as follows: green channel: λ_{ex}=488 nm and λ_{em}=BP 505-530 nm; red channel: λ_{ex}=543 nm and λ_{em}=LP 650 nm. Emission filters: BP=band pass, LP=high pass.

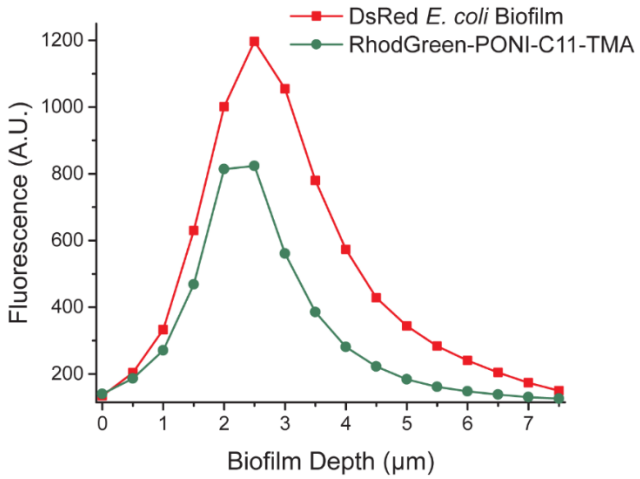

Figure 6.8. Penetration of Rhodamine Green labelled P5 PNPs (RhodGreen PONI-C11-TMA) into E2-Crimson expressing *E. coli* biofilms. The mean fluorescence of each confocal z-stack image was calculated using ImageJ software.

6.5.4. Therapeutic indices against biofilms

Bacteria were inoculated in lysogeny broth (LB) medium at 37 ˚C until stationary phase. The cultures were then harvested by centrifugation and washed with 0.85% sodium chloride solution

three times. Concentrations of resuspended bacterial solution were determined by optical density measured at 600 nm. Seeding solutions were then made in M9 medium to reach an OD_{600} of 0.1. A 100 µL amount of the seeding solutions was added to each well of the 96-well microplate. The plates were covered and incubated at room temperature under static conditions for 1 day. The stock solution of P5 PNPs was then diluted to the desired level and incubated with the biofilms for 3 hours at 37˚C. Biofilms were washed with phosphate buffer saline (PBS) three times and viability was determined using an Alamar Blue assay. Minimal M9 medium without bacteria was used as a negative control. Concentrations were converted to Log, plotted with bacteria viability, and fitted to a curve to determine the minimum biofilm eradication concentration at 90% ($MBEC_{90}$).[56,57] The therapeutic index with respect to red blood cells was calculated by the concentration of P5 PNPs at $MBEC_{90}$ divided by the hemolysis at 50%.

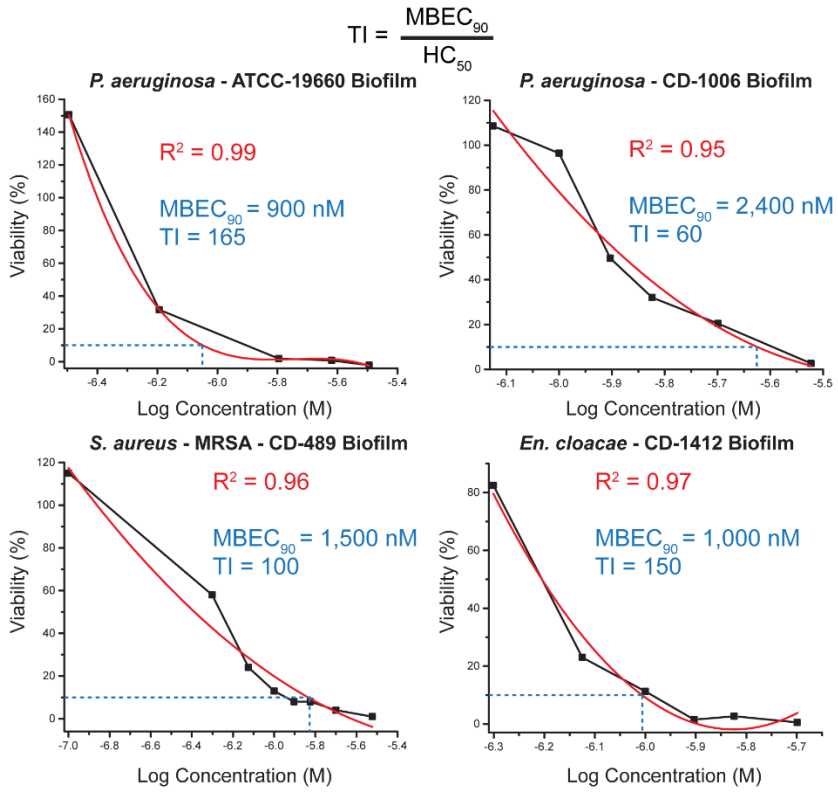

Figure 6.9. Therapeutic indices of PNPs against four bacterial biofilms.

6.6 References

1. Marshall, B. M.; Levy, S. B. *Clin. Microbiol. Rev.* **2011**, *24* (4), 718.

2. Harris, S. R.; Feil, E. J.; Holden, M. T. G.; Quail, M. A.; Nickerson, E. K.; Chantratita, N.; Gardete, S.; Tavares, A.; Day, N.; Lindsay, J. A.; Edgeworth, J. D.; De Lencastre, H.; Parkhill, J.; Peacock, S. J.; Bentley, S. D. *Science (80).* **2010**, *327* (5964), 469.

3. Van Amersfoort, E. S.; Van Berkel, T. J. C.; Kuiper, J. *Clin. Microbiol. Rev.* **2003**, *16* (3), 379.

4. Wolcott, R. D.; Ehrlich, G. D. *JAMA - J. Am. Med. Assoc.* **2008**, *299* (22), 2682.

5. Donlan, R. M. *Emerg. Infect. Dis.* **2001**, *7* (2), 277.

6. Costerton, J. W.; Stewart, P. S.; Greenberg, E. P. *Science* **1999**, *284* (5418), 1318.

7. Lewis, K. *Antimicrob. Agents Chemother.* **2001**, *45* (4), 999.

8. Fux, C. A.; Costerton, J. W.; Stewart, P. S.; Stoodley, P. *Trends Microbiol.* **2005**, *13* (1), 34.

9. Del Pozo, J. L.; Patel, R. *N. Engl. J. Med.* **2009**, *361* (8), 787.

10. Laxminarayan, R.; Duse, A.; Wattal, C.; Zaidi, A. K. M.; Wertheim, H. F. L.; Sumpradit, N.; Vlieghe, E.; Hara, G. L.; Gould, I. M.; Goossens, H.; Greko, C.; So, A. D.; Bigdeli, M.; Tomson, G.; Woodhouse, W.; Ombaka, E.; Peralta, A. Q.; Qamar, F. N.; Mir, F.; Kariuki, S.; Bhutta, Z. A.; Coates, A.; Bergstrom, R.; Wright, G. D.; Brown, E. D.; Cars, O. *Lancet Infect. Dis.* **2013**, *13* (12), 1057.

11. Baltzer, S. A.; Brown, M. H. *J. Mol. Microbiol. Biotechnol.* **2011**, *20* (4), 228.

12. Hancock, R. E. W.; Sahl, H. G. *Nat Biotech* **2006**, *24* (12), 1551.

13. Jiang, Z.; Vasil, A. I.; Gera, L.; Vasil, M. L.; Hodges, R. S. *Chem. Biol. Drug Des.* **2011**, *77* (4), 225.

14. Marr, A. K.; Gooderham, W. J.; R.E.W., H. *Curr. Opin. Pharmacol.* **2006**, *6* (5), 468.

15. Sieprawska-Lupa, M.; Mydel, P.; Krawczyk, K.; Wójcik, K.; Puklo, M.; Lupa, B.; Suder, P.; Silberring, J.; Reed, M.; Pohl, J.; Shafer, W.; McAleese, F.; Foster, T.; Travis, J.; Potempa, J. *Antimicrob. Agents Chemother.* **2004**, *48* (12), 4673.

16. Palermo, E. F.; Kuroda, K. *Appl. Microbiol. Biotechnol.* **2010**, *87* (5), 1605.

17. Mowery, B. P.; Lee, S. E.; Kissounko, D. A.; Epand, R. F.; Epand, R. M.; Weisblum, B.; Stahl, S. S.; Gellman, S. H. *J. Am. Chem. Soc.* **2007**, *129* (50), 15474.

18. Patch, J. A.; Barron, A. E. *J. Am. Chem. Soc.* **2003**, *125* (40), 12092.

19. Arnt, L.; Nüsslein, K.; Tew, G. N. *J. Polym. Sci. Part A Polym. Chem.* **2004**, *42* (15), 3860.

20. Kuroda, K.; DeGrado, W. F. *J. Am. Chem. Soc.* **2005**, *127* (12), 4128.

21. Palermo, E. F.; Vemparala, S.; Kuroda, K. *Biomacromolecules* **2012**, *13* (5), 1632.

22. Gabriel, G. J.; Madkour, A. E.; Dabkowski, J. M.; Nelson, C. F.; Nüsslein, K.; Tew, G. N. *Biomacromolecules* **2008**, *9* (11), 2980.

23. Muñoz-Bonilla, A.; Fernández-García, M. *Prog. Polym. Sci.* **2012**, *37* (2), 281.

24. Lienkamp, K.; Madkour, A. E.; Musante, A.; Nelson, C. F.; Nüsslein, K.; Tew, G. N. *J. Am. Chem. Soc.* **2008**, *130* (30), 9836.

25. Yin, L. M.; Edwards, M. A.; Li, J.; Yip, C. M.; Deber, C. M. *J. Biol. Chem.* **2012**, *287* (10), 7738.

26. Ilker, M. F.; Nüsslein, K.; Tew, G. N.; Coughlin, E. B. *J. Am. Chem. Soc.* **2004**, *126* (48), 15870.

27. Lin, C. C.; Ki, C. S.; Shih, H. *J. Appl. Polym. Sci.* **2015**, *132* (8), 41563.

28. Cole, J. P.; Lessard, J. J.; Lyon, C. K.; Tuten, B. T.; Berda, E. B. *Polym. Chem.* **2015**, *6* (31), 5555.

29. Kuroda, K.; Caputo, G. A.; DeGrado, W. F. *Chem. - A Eur. J.* **2009**, *15* (5), 1123.

30. Sambhy, V.; Peterson, B. R.; Sen, A. Angew. Chemie - Int. Ed. 2008, 47 (7), 1250.

31. Chen, C.; Liu, G.; Liu, X.; Pang, S.; Zhu, C.; Lv, L.; Ji, J. *Polym. Chem.* **2011**, *2* (6), 1389.

32. Li, X.; Robinson, S. M.; Gupta, A.; Saha, K.; Jiang, Z.; Moyano, D. F.; Sahar, A.; Riley, M. A.; Rotello, V. M. *ACS Nano* **2014**, *8* (10), 10682.

33. Dathe, M.; Wieprecht, T.; Nikolenko, H.; Handel, L.; Maloy, W. L.; MacDonald, D. L.; Beyermann, M.; Bienert, M. *FEBS Lett.* **1997**, *403* (2), 208.

34. Huang, Y.; Huang, J.; Chen, Y. *Protein Cell* **2010**, *1* (2), 143.

35. Gupta, A.; Saleh, N. M.; Das, R.; Landis, R. F.; Bigdeli, A.; Motamedchaboki, K.; Rosa Campos, A.; Pomeroy, K.; Mahmoudi, M.; Rotello, V. M. *Nano Futur.* **2017**, *1* (1), 015004.

36. Huo, S.; Jiang, Y.; Gupta, A.; Jiang, Z.; Landis, R. F.; Hou, S.; Liang, X. J.; Rotello, V. M. *ACS Nano* **2016**, *10* (9), 8732.

37. Saha, K.; Moyano, D. F.; Rotello, V. M. *Mater. Horizons* **2014**, *1* (1), 102.

38. Parameswaran, N.; Patial, S. *Crit. Rev. Eukaryot. Gene Expr.* **2010**, *20* (2), 87.

39. Nederberg, F.; Zhang, Y.; Tan, J. P. K.; Xu, K.; Wang, H.; Yang, C.; Gao, S.; Guo, X. D.; Fukushima, K.; Li, L.; Hedrick, J. L.; Yang, Y. Y. *Nat. Chem.* **2011**, *3* (5), 409.

40. Hayden, S. C.; Zhao, G.; Saha, K.; Phillips, R. L.; Li, X.; Miranda, O. R.; Rotello, V. M.; El-Sayed, M. A.; Schmidt-Krey, I.; Bunz, U. H. F. *J. Am. Chem. Soc.* **2012**, *134* (16), 6920.

41. Boulos, L.; Prévost, M.; Barbeau, B.; Coallier, J.; Desjardins, R.; Boulos, L.; Barbeau, B. *J. Microbiol. Methods* **1999**, *37* (1), 77.

42. Cox, S. D.; Mann, C. M.; Markham, J. L.; Bell, H. C.; Gustafson, J. E.; Warmington, J. R.; Wyllie, S. G. *J. Appl. Microbiol.* **2000**, *88* (1), 170.

43. Gupta, A.; Landis, R. F.; Rotello, V. M. *F1000Research* **2016**, *5* (364), 364.

44. Anderl, J. N.; Zahller, J.; Roe, F.; Stewart, P. S. *Antimicrob. Agents Chemother.* **2003**, *47* (4), 1251.

45. Landis, R. F.; Li, C. H.; Gupta, A.; Lee, Y. W.; Yazdani, M.; Ngernyuang, N.; Altinbasak, I.; Mansoor, S.; Khichi, M. A. S.; Sanyal, A.; Rotello, V. M. *J. Am. Chem. Soc.* **2018**, *140* (19), 6176.

46. Roy, S.; Elgharably, H.; Sinha, M.; Ganesh, K.; Chaney, S.; Mann, E.; Miller, C.; Khanna, S.; Bergdall, V. K.; Powell, H. M.; Cook, C. H.; Gordillo, G. M.; Wozniak, D. J.; Sen, C. K. *J. Pathol.* **2014**, *233* (4), 331.

47. Anderson, G. G.; Moreau-Marquis, S.; Stanton, B. A.; O'Toole, G. A. *Infect. Immun.* **2008**, *76* (4), 1423.

48. Gupta, A.; Das, R.; Yesilbag Tonga, G.; Mizuhara, T.; Rotello, V. M. *ACS Nano* **2018**, *12* (1), 89.

49. Lam, S. J.; O'Brien-Simpson, N. M.; Pantarat, N.; Sulistio, A.; Wong, E. H. H.; Chen, Y. Y.; Lenzo, J. C.; Holden, J. A.; Blencowe, A.; Reynolds, E. C.; Qiao, G. G. *Nat. Microbiol.* **2016**, *1*, 16162.

50. Ling, L.; Schneder, T.; Peoples, A.; Spoering, A.; Engels, I.; Conlon, B.; Mueller, A.; Schaberle, T.; Hughes, D.; Epstein, S.; Jones, M.; Lazarides, L.; Steadman, V.; Cohen, D.; Felix, C.; Fetterman, K.; Millett, W.; Nitti, A.; Zullo, A.; Chen, C.; Lewis, K. *Nature* **2015**, *517* (7535), 455.

51 Madkour, A. E.; Koch, A. H. R.; Lienkamp, K.; Tew, G. N. *Macromolecules* **2010**, *43* (10), 4557.

52. Wiegand, I.; Hilpert, K.; Hancock, R. E. W. *Nat. Protoc.* **2008**, *3* (2), 163.

53. Moyano, D. F.; Liu, Y.; Ayaz, F.; Hou, S.; Puangploy, P.; Duncan, B.; Osborne, B. A.; Rotello, V. M. *Chem* **2016**, *1* (2), 320.

54. Duncan, B.; Li, X.; Landis, R. F.; Kim, S. T.; Gupta, A.; Wang, L. S.; Ramanathan, R.; Tang, R.; Boerth, J. A.; Rotello, V. M. *ACS Nano* **2015**, *9* (8), 7775.

55. Decker, T.; Lohmann-Matthes, M. L. *J. Immunol. Methods* **1988**, *115* (1), 61.

56 Cafiso, V.; Bertuccio, T.; Spina, D.; Purrello, S.; Stefani, S. *FEMS Immunol. Med. Microbiol.* **2010**, *59* (3), 466.

57 CLSI. *Methods for Dilution Antimicrobial Susceptibility Tests for Bacteria That Grow Aerobically; Approved Standard—Tenth Edition.* CLSI document M07-A10. Wayne, PA: Clinical and Laboratory Standards Insitute; **2015**.

CHAPTER 7

FUNCTIONALIZED POLYMERS ENHANCE PERMEABILITY OF ANTIBIOITCS IN GRAM-NEGATIVE MDR BACTERIA BIOFILMS FOR SYNERGISTIC ANTIMICROBIAL THERAPY

7.1 Introduction

Antibiotic-resistant bacteria causes more than 2 million cases of infections and 23,000 deaths each year in US alone.[1] Worldwide annual death toll due to multi-drug resistant (MDR) bacteria increases to 700,000 and is expected to reach 10 million by the year 2050.[2] The 'ESKAPE' (*Enterococcus faecium, Staphylococcus aureus, Klebsiella pneumoniae, Acinetobacter baumannii, Pseudomonas aeruginosa* and *Enterobacter* species) pathogens pose the biggest threat to global health due to their multi-drug resistance.[3,4] In particular, infections caused by Gram-negative species of 'ESKAPE' pathogens show increased resistance due to an additional highly impermeable outer membrane barrier.[5,6] Threat posed by MDR bacteria is further aggravated by their ability to form bacterial biofilms, rendering infections refractory to both traditional antimicrobial therapies and host immune response.[7] Biofilm-associated infections can frequently occur on medical implants, indwelling devices and wounds.[8] Conventional strategies to treat these intractable infections involve high dosage treatment with last resort antibiotics such as colistin and carbapenems, increasing the risk of neurotoxicity and nephrotoxicity.[9] Rigorous antibiotic therapy is often followed by surgical debridement of infected tissue, resulting in low-patient compliance and excessive healthcare costs.[10,11] A significant decline in the number of approved antibiotics against MDR bacteria, with no new antibiotic developed against Gram-negative bacteria in the last fifty years, has contributed to the urgency for developing novel antimicrobial therapies.[12]

Antibiotic cocktails targeting multiple pathways in pathogens have demonstrated increased antimicrobial efficacy.[13,14] However, this strategy is associated with increased risk of antibiotic-resistance development. Moreover, antibiotic combination therapies often fail to treat

MDR Gram-negative pathogens due to limited penetration of antibiotics inside the cells.[15,16] Combination therapies utilizing antibiotics with membrane-sensitizing adjuvants have shown high efficacy in treating planktonic Gram-negative infections.[17] However, these small-molecule based therapies fail to treat biofilm-associated infections due to their inability to penetrate Extracellular Polymeric Substance (EPS) matrix of biofilms.[18,19,20]

Synthetic macromolecules such as nanoparticles and polymers have demonstrated ability to strongly bind and destabilize the bacterial outer membrane.[21,22,23,24] In addition, amphiphilic polymers exhibited excellent potential in penetrating biofilm matrix.[25,26] We hypothesized that combining the membrane-sensitizing and penetration-ability of polymers with the selective activity of antibiotics could offer enhanced efficacy in combating MDR bacterial and biofilm infections. Here, we report a combination therapy using engineered polymeric nanoparticles (PNPs) with colistin against resistant bacterial species. We observed 16- to 32-fold decrease in the colistin dosage required to combat planktonic and biofilm bacteria in combination therapy as compared to colistin alone. The observed synergy can be attributed to enhanced bacterial membrane permeability when the antibiotic was used in combination with PNPs. We further determined that antibiotic accumulation increases about 4-fold inside the biofilms in presence of PNPs, contributing to the enhanced efficacy. Overall, this combination therapy illustrates the ability of functionalized polymers to enhance the potency of antibiotics against resistant bacterial infections, while minimizing the side-effects associated with high dosages of therapeutics.

7.2 Results and discussion

We have recently reported that distribution of cationic and hydrophobic moieties on a polymer plays a critical role in determining the antimicrobial efficacy of membrane-disrupting polymers.[25] We have designed a library of polymers by varying the hydrophobicity of the cationic headgroups and changing the alkyl chain length bridging the headgroup with polymer backbone, to systematically probe the bacterial membrane permeability of the polymers (Figure 7.1 a). We

observed that the polymers with an 11-carbon alkyl chain bridge self-assembled to form cationic polymeric nanoparticles (PNPs) with a size ~15 nm, as shown by transmission electron microscopy (TEM) in Figure 7.1 c. On the other hand, polymers with smaller alkyl chain (2 and 6) bridge do not self-assemble into PNPs.

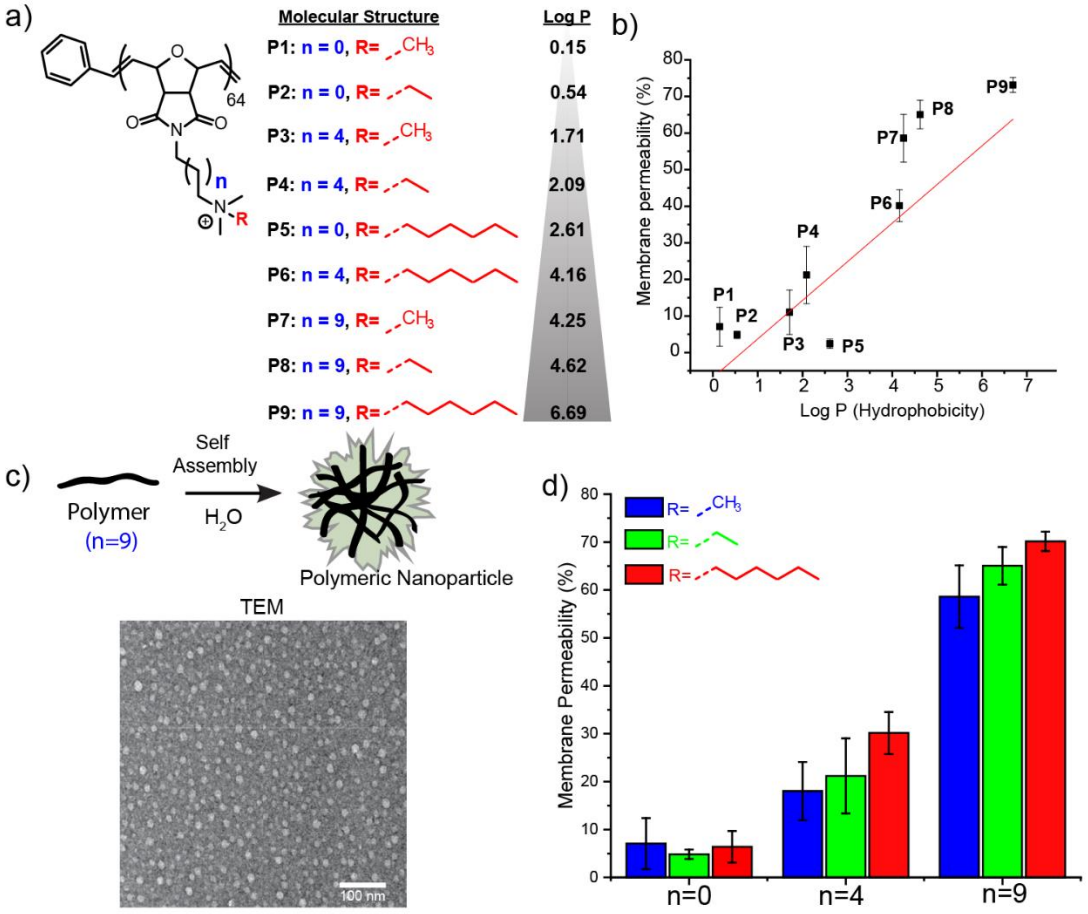

Figure 7.1. a. Molecular structures of oxanorbornene polymer derivatives. Log P represents the calculated hydrophobic values of each monomer. **b.** Membrane permeability induced by different polymer derivatives measured as (%) uptake of N-phenyl-1-napthylamine (NPN) plotted vs overall hydrophobicity of the polymer derivatives. **c.** Schematic representation showing self-assembly of polymer derivatives (n=9) into polymeric nanoparticles. Characterization of polymer nanoparticles (P7) using TEM. **d.** Bar graphs demonstrating membrane disruption as a function of polymer nanoparticles with different alkyl chain length bridging polymer backbone and cationic headgroup.

Next, we screened the membrane perturbation ability of polymers (P1-P9) against Uropathogenic clinical isolate of *E. coli* using N-phenyl-1-napthylamine (NPN) uptake assays.[27,28] We observed that membrane permeation ability of the polymers increases with the

increase in the overall hydrophobicity of the structure. However, increasing the length of alkyl chain bridging the polymer backbone to cationic headgroup has a stronger effect in membrane-sensitizing ability of polymers, as compared to increasing the hydrophobicity of the cationic headgroup alone (Figure 7.1 d). A strong structure-activity relationship was observed with the most hydrophobic polymers (P6-P9) demonstrating highest membrane perturbation activity against bacteria (Figure 7.1 b).

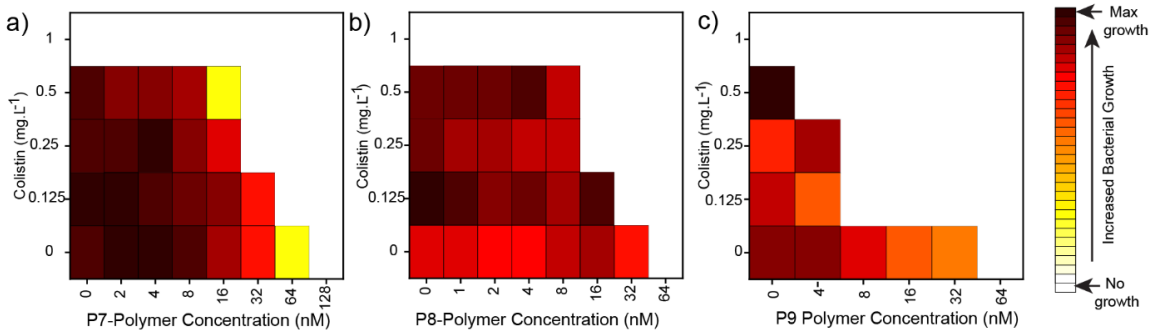

d)

Polymer	MIC_C (mg. L^{-1})	FIC_C	MIC_P (nM)	FIC_P	FIC Index	Effect
P4	1	0.5	32000	1	1.5	Additive
P5	1	0.5	32000	1	1.5	Additive
P6	1	0.0625	256	0.5	0.5625	Additive
P7	1	0.25	64	0.25	0.5	**Synergy**
P8	1	0.25	128	0.25	0.5	**Synergy**
P9	1	0.125	64	0.125	0.25	**Synergy**

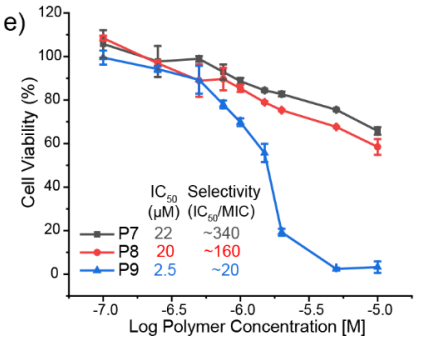

Figure 7.2. Checkerboard broth microdilution assays between colistin and polymer derivatives **a.** P7, **b.** P8 and **c.** P9 against uropathogenic *E. coli* (CD-2). Dark cells represent higher bacterial cell density. **d.** Table showing Minimum inhibitory concentrations (MICs) of colistin and different polymer derivatives. FIC indices were calculated using checkerboard broth microdilution assays as described in the methods section. **e.** Cell viability of 3T3 fibroblast cells after treatment with PNPs.

After establishing the membrane perturbing ability of the polymers, we tested these polymers (P4-P9) for synergistic therapy in combination with colistin antibiotics against bacteria. We evaluated the minimal inhibitory concentrations (MIC) for polymers and colistin using broth dilution methods as reported in Figure 7.2 d.[29,30] Next, we performed checkerboard titrations for varied combinations of polymers and colistin and evaluated their FICI (Fractional Inhibitory

Concentration Index) scores. A FICI score of ≤ 0.5 is defined as a synergistic interaction, whereas an additive interaction has FICI score between 0.5 and 4.[31,32] Polymers (P7–P9) with higher membrane-sensitizing ability exhibited synergistic response in combination with colistin antibiotic (FICI scores ranging from 0.375 – 0.5) as shown in Figure 7.2. Moreover, an 8- to 16-fold reduction in colistin dosage was observed when used in combination with P7-P9 (Table 7.1). While polymers (P4-P6) with lesser membrane permeation ability showed additive response (0.5 < FICI < 1). We further investigated the cytotoxicity of the most potent polymers (P7-P9) by performing cytotoxicity assays on human fibroblast cell line.[25] We determined the IC_{50} (half-maximal inhibitory concentration) of the cells to calculate therapeutic selectivity of polymers (ability to kill bacteria while causing minimal toxicity to mammalian cells). Least hydrophobic polymer P7 demonstrated an IC_{50} of ~22 μM, providing a therapeutic selectivity (IC_{50}/MIC) of ~360. While polymer P8 and P9 demonstrated an IC_{50} ~ 20 and 2.5 μM, generating a therapeutic selectivity of ~160 and ~20, respectively.

Table 7.1. Fold-increase in antibiotic efficacy obtained for the combination of PNPs and antibiotics tested against multiple strains.

Species (Strain)	Polymer	Fold-increase in antibiotic efficacy
E. coli (CD-2)	P4	0
E. coli (CD-2)	P5	0
E. coli (CD-2)	P6	2
E. coli (CD-2)	P7	8
E. coli (CD-2)	P8	8
E. coli (CD-2)	P9	8
P. aeruginosa (CD-1006)	P7	16
En. Cloacae (CD-1412)	P7	16
E. coli (CD-549)	P7	8
Acinetobacter species (CD-575)	P7	8

P. aeruginosa (CD-1006)	P8	8	

After establishing synergistic interaction between PNPs and colistin antibiotic against *E. coli*, we tested PNP-colistin combination against multiple uropathogenic clinical isolates to determine their broad-spectrum applicability. P7 PNPs showed synergistic effect against Gram-negative clinical isolates of *P. aeruginosa*, *E. cloacae* complex, MDR *E. coli* and *Acinetobacter* species (Figure 7.3), yielding up to 16-fold reduction in colistin dosage to combat the resistant bacteria. Similarly, other analogues of PNPs (P8) also demonstrated synergistic response with colistin against Gram-negative strains of *P. aeruginosa* (SI Figure 7.5). On the other hand, PNP-colistin combination tested against Gram-positive strains (methicillin-resistant *S. aureus, B. subtilis* and *S. epidermidis*) exhibited additive interactions (Figure 7.6). These results indicate that using membrane-sensitizing polymeric nanoparticles can be used as a general strategy to generate synergistic antimicrobial therapy against Gram-negative MDR bacteria.

We hypothesized that PNP-colistin combination disrupted Gram-negative bacterial membranes at sub-inhibitory dosages, owing to the strong cationic and hydrophobic nature of the PNPs.[25] Our claims were supported by staining assays using membrane impermeable crystal violet (CV) dye where PNP-colistin combination showed increased CV accumulation inside cells as compared to PNPs and colistin alone (Figure 7.3 f).[33,34] Additionally, bacterial membrane disruption was further monitored by measuring the zeta potential of bacterial surface. Bacteria treated with PNP-colistin combination (at sub-lethal dosages) showed sharp shift towards neutral charge as compared to the controls, indicating increased membrane disruption and decreased bacterial viability (Figure 7.3 g).[33,35]

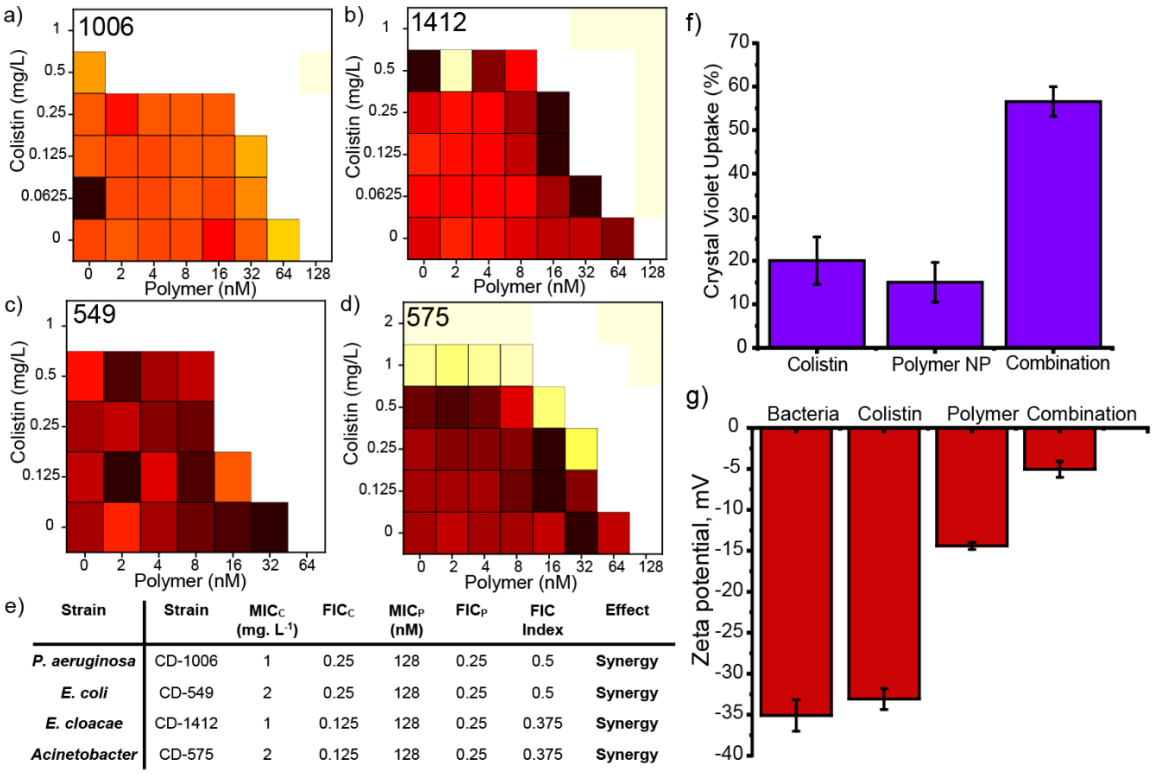

e)

Strain	Strain	MIC_C (mg. L^{-1})	FIC_C	MIC_P (nM)	FIC_P	FIC Index	Effect
P. aeruginosa	CD-1006	1	0.25	128	0.25	0.5	Synergy
E. coli	CD-549	2	0.25	128	0.25	0.5	Synergy
E. cloacae	CD-1412	1	0.125	128	0.25	0.375	Synergy
Acinetobacter	CD-575	2	0.125	128	0.25	0.375	Synergy

Figure 7.3. Checkerboard broth microdilution assays between colistin and P7 PNPs against uropathogenic **a.** *P. aeruginosa* (CD-1006), **b.** *En. cloacae* complex (CD-1412), **c.** MDR *E. coli* (CD-549), **d.** *Acinetobacter* species (CD-575). **e.** Table showing MICs (Minimum Inhibitory Concentration) and FICI (Fractional Inhibitory Concentration) scores obtained for PNP-colistin combination against different strains of bacteria. Change in bacteria membrane permeability assayed by **f.** crystal violet uptake and **g.** zeta potential in presence of PNP, colistin and PNP-colistin combination.

After establishing the ability of PNP-colistin combination against planktonic "superbugs", we investigated the combination against resistant biofilms. Biofilms are three-dimensional micro-colonies of bacteria embedded inside an extra polymeric substance (EPS) matrix that prevents the penetration of antibiotics inside the biofilms.[7,8,9] Limited biofilm penetration plays a major role in rendering antibiotics ineffective against biofilm-associated infections. On the other hand, amphiphilic PNPs have shown excellent ability to penetrate biofilms. We hypothesized that using colistin in combination with PNPs would be able to enhance the penetration and accumulation of colistin inside the biofilms, thereby increasing the overall therapeutic effect of the combination

therapy.[36,37] We treated DsRed-expressing *E. coli* biofilm with Rhodamine Green-tagged colistin in presence and absence of PNPs and examined using confocal microscopy. As shown in Figure 7.4, antibiotic accumulation inside biofilms increased by ~4-fold in presence of polymers as compared to the controls. Furthermore, fluorescent-tagged colistin was homogenously distributed throughout the biofilms when used in combination with PNPs, whereas in absence of PNPs colistin was confined to the top layer of the biofilm. These results demonstrate that cationic PNPs can increase the accumulation of antibiotics inside the biofilms.

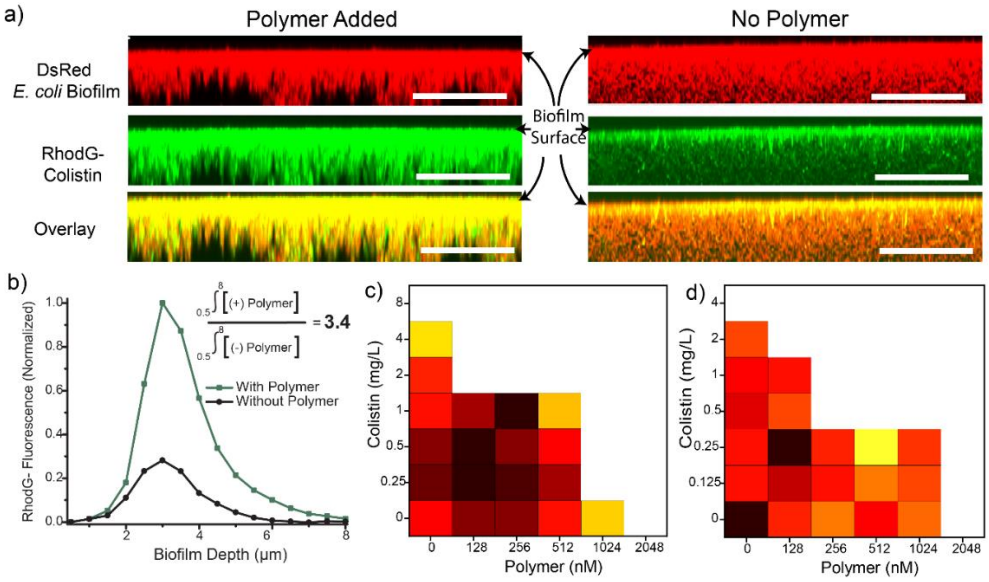

e)

Strain	Strain	$MBEC_C$ (mg. L^{-1})	FIC_C	$MBEC_P$ (nM)	FIC_P	FIC Index	Effect
P. aeruginosa	CD-1006	4	0.25	2048	0.0625	0.3125	**Synergy**
E. cloacae	CD-1412	8	0.25	2048	0.0625	0.3125	**Synergy**

Figure. 7.4. a. Representative 3D projection of confocal images stacks of DsRed (Red Fluorescent Protein) expressing *E. coli* DH5α biofilm after 1-hour treatment with Rhodamine Green-tagged colistin (1 mg. L^{-1}) in presence and absence of PNP. The panels are projection at 90° angle turning along X axis. Scale bars are 30 μm. **b.** Integrated intensity of Rhodamine Green and DsRed biofilm where 0 μm represents the top layer and ~8 um the bottom layer. Checkerboard broth microdilution assays between colistin and P7 PNPs against uropathogenic biofilm **c.** *P. aeruginosa* (CD-1006), **d.** *E. coli* (CD-2). **e.** Table showing MBECs (Minimum Biofilm Eradication Concentration) and FICI (Fractional Inhibitory Concentration) scores obtained for PNP-colistin combination against biofilms.

Next, we investigated the therapeutic efficacy of the PNP-colistin combination against biofilms. We evaluated minimum biofilm inhibition concentration (MBIC) and minimum biofilm

eradication concentration (MBEC) for PNPs and colistin using broth dilution methods as reported in Figure 4.[38,39,40] We then performed checkerboard titrations using PNP-colistin combination against biofilms and evaluated the FICI (Fractional Inhibitory Concentration Index) scores to evaluate the efficacy of combinations. FICI scores for PNP-colistin combinations demonstrated synergistic effect as compared to the FICI scores for the individual components, with ~32-fold decrease in colistin dosage. Similar checkerboard studies performed using colistin with other PNP analogues (P8) also showed synergistic effect against biofilms (Figure 7.7). These results further indicate that using cationic and hydrophobic PNPs can be used a general strategy to increase the accumulation of antibiotics inside the biofilms, thereby increasing their potency.

7.3. Conclusions

We have designed bacterial membrane-sensitizing and biofilm penetrating polymeric nanoparticles that exhibit synergistic interaction with last-resort antibiotic colistin. The bacterial membrane permeability of these polymeric nanoparticles can be regulated by incorporating hydrophobic moieties in the polymer structure. PNPs can enhance the potency of colistin up to 16-fold, owing to the increased susceptibility of bacterial membrane to the polymers. Moreover, polymeric nanoparticles enhance the accumulation of antibiotics inside the biofilms, resulting in synergistic effect of PNP-colistin combination in eradicating biofilms. PNPs render biofilms susceptible to colistin and reduce the antibiotic dosage by 32-fold as compared to antibiotic alone. Taken together, strong membrane permeability and biofilm penetration ability of PNPs make them promising candidates to enhance the efficacy of standard antibiotic therapies while circumventing the concerns associated with high antibiotic dosage. Moreover, combination therapies using PNPs have the potential to rejuvenate antibiotics that are rendered ineffective due to antibiotic-resistance.

7.4 Experimental methods

7.4.1. Oxanorbornene polymer synthesis

Oxanorbornene monomers featuring 2,6 and 11 bridging carbon chains were synthesized using our own previously reported protocol.[41] The oxanorbornene monomers were then polymerized through Ring Opening Metathesis Polymerization using Grubbs 3rd generation catalyst as reported previously.[42] Next, the oxanorbornene polymers were post-functionalized with necessary tertiary amines to generate a library of quaternary ammonium poly(oxanorbornene) derivatives using the methodology reported previously.41,[37,43] Finally, the polymers were added to 10,000 MWCO dialysis membranes and allowed to stir for 3 days, changing the water periodically. The polymers were filtered through PES syringe filters and freeze-dried to yield all the respective quaternary ammonium polymers and characterized using ^{1}H NMR.41

7.4.2. Synthesis of RhodamineGreen-Colistin

To a 7ml scintillation vial equipped with a stirbar was added Colistin (0.005 g, 0.004 mmol, 1 eq), triethylamine (1.2 µL, 0.0089 mmol, 2.05 eq) and DMF (0.5ml) and allowed to stir. Meanwhile, Rhodamine Green™ Carboxylic Acid, Succinimidyl Ester, Hydrochloride (5(6)-CR 110, SE) (0.0022 g, 0.004 mmol, 1 eq) was dissolved in 4 ml of DMF. At room temperature, the solution of Rhodamine Green was added slowly over the course of 2 hours. Once the addition was complete, the reaction mixture was covered with aluminum foil and allowed to stir overnight. Afterwards, the reaction mixture was transferred to the appropriately sized round bottom flask and rotovaped in the presence of toluene until all DMF was removed. Next, the residue was sonicated using THF and DCM and carefully decanted away. With all solvent removed, minimal amount of water was added and sonicated to dissolve the residue, filtered through a PES syringe filter and lyophilized to yield the RhodamineGreen-Colistin conjugate (red powder). MALDI analysis confirmed the M+1 species, 1512 g/mol.

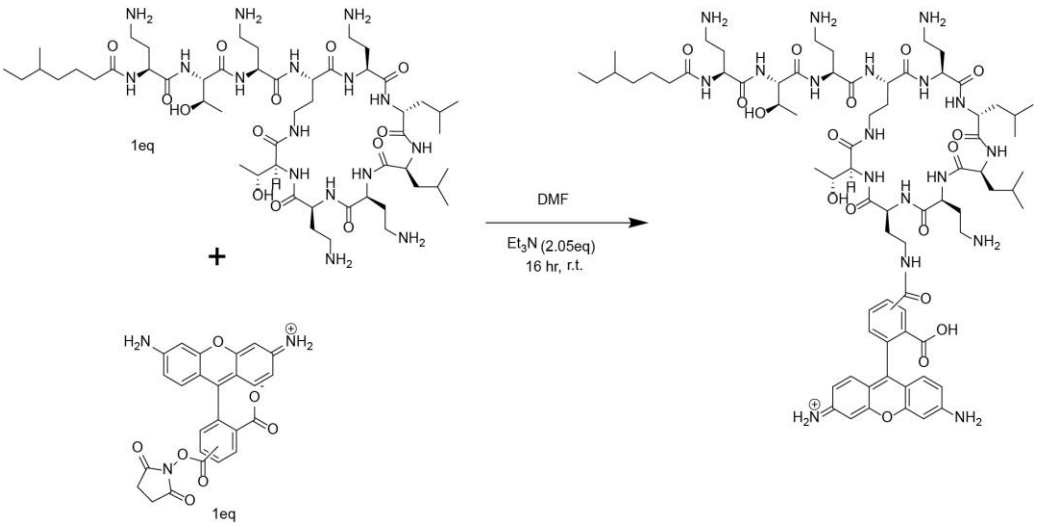

7.4.3. Determination of Minimum Inhibitory Concentrations (MICs)

MIC is defined as the lowest concentration of an antimicrobial agent required to inhibit the growth of bacteria overnight as observed from the naked eye.29 Bacteria cell were grown using the protocol described above. Next, bacterial solutions with concentrations of 1×10^6 cells/mL were prepared in M9 media. 50 µL of prepared bacteria solution were mixed with 50 µL of polymer/antibiotic prepared in M9 media in a 96-well clear plate resulting in final bacterial concentration of 5×10^5 cells/mL. Polymers were tested with half-fold variations in concentrations as per the standard protocols in concentration ranging from 64,000 nM – 4 nM. A sterile control group with no bacterial cells present and growth control group without addition of any polymers were carried out at the same time. The prepared 96-well plates were incubated for 16 hours. The experiments were performed in triplicates with two individual runs performed on different days.

7..4.4. Checkerboard titrations for combination therapy

We performed two-dimensional checkerboard titrations using micro-dilution method to determine the synergy between antibiotics and polymers.31 The concentration of Polymers and colistin were varied using 2-fold serial dilutions. The wells without any visual growth were considered as a combination that inhibits bacterial growth. For the colistin-polymer combinations, concentrations

of the components were varied according to their MIC against the respective bacterial strains. The checkerboard titrations were performed in a set of three independent plates and repeated on different days.

Fractional Inhibitory Concentration Index (FICI) for Colistin-polymer combination was calculated using FICs of colistin and polymer independently using the following equation:

$FIC_C = (MIC\ of\ colistin\ and\ polymer\ combination) \div (MIC\ of\ colistin\ alone)$

$FIC_P = (MIC\ of\ colistin\ and\ polymer\ combination) \div (MIC\ of\ polymer\ alone)$

$FICI = FIC_C + FIC_P$

FICI values $\leq$ 0.5 corresponds to synergistic combination, whereas FICI values between >0.5 and 4.0 indicates additive effect. FICI values > 4.0 respond to antagonistic effect.31

7.4.5. Mammalian cell viability assay

Cell viability studies performed using the previously established protocols.18 Briefly, 20,000 NIH 3T3 Fibroblast cells (ATCC CRL-1658) were cultured in Dulbecco's modified Eagle medium (DMEM, ATCC 30-2002) with 1% antibiotics and 10% bovine calf serum in a humidified atmosphere of 5% CO_2 at 37 °C for 48 hours. Media was replaced after 24 hours and the cells were washed (one-time) with phosphate-buffered saline (PBS) before incubation with polymers. Polymer solution were prepared in 10%serum containing media (pre-warmed) and incubated with cells in a 96-well plate for 24 hours in a humidified atmosphere at 37 °C. Alamar Blue assays were performed to assess the cell viability as per the established protocol of Invitrogen Biosource (manufacturer). Red fluorescence resulting upon the reduction of alamar blue agent was quantified using a Spectromax M5 microplate reader (Ex: 560 nm, Em: 590 nm) and used to determine cell viability. Cells incubated with no polymers were considered as 100% viable. Each experiment was performed in triplicates and repeated on two different days.

7.4.6. Membrane penetration using crystal violet assay

Bacteria cells were cultured, and their concentrations were measured using the methodology reported above. Crystal violet assay were performed using the previously reported protocols.33 Briefly, 0.1 OD bacterial solution was prepared in phosphate-buffered saline (PBS) solution then, incubated with the test material for 30 minutes at 37 °C. Untreated cell which served as the negative control was prepared similarly without treatment. The cells were harvested by centrifugation at 9300×g for 5 minutes at 4 °C followed by redispersion in PBS with 5 μg/mL crystal violet. After incubation at 37 °C for 10 minutes, the bacterial cell solution was centrifuged at 13,400×g for 15 min. The resulting pellet was resuspended in 80:20 ethanol: acetone and the OD of the solution was measured at 590 nm using a Molecular Devices SpectraMax M2. OD value from the normal untreated cell was used as blank while the OD value of crystal violet solution was considered as 100%. The percentage of crystal violet uptake was expressed as follows:

$$\%CV\ uptake = \frac{OD\ sample - OD\ blank}{OD\ CV\ only - OD\ blank}\ x\ 100$$

7.4.7. Monitoring zeta potential of bacterial membrane

Zeta potential for bacteria membrane was monitored using previously reported protocol.35 Briefly, bacteria were cultured and harvested as per the above-mentioned protocols. Next, 0.01 OD of bacteria cells in phosphate buffer (PB) solution (5 mM, pH=7.4) was incubated with the test materials (colistin only, polymer only and their combinations) at 37 °C for 15 minutes. The cells were harvested by centrifugation (7000×g for 5 minutes, 4 °C), then the resulting pellets were resuspended in PB. Solutions were then subjected to zeta potential measurements using Zetasizer Nano ZS. Untreated bacteria were used as the negative control.

7.4.8. Biofilm formation and penetration studies using confocal microscopy

DsRed-expressing bacteria were inoculated in lysogeny broth (LB) medium at 37 ˚C until stationary phase. The cultures were then harvested by centrifugation and washed with 0.85%

sodium chloride solution three times. Concentrations of resuspended bacterial solution were determined by optical density measured at 600 nm. 10^8 bacterial cells/mL of DsRed (fluorescent protein) expressing *E. coli,* supplemented with 1 mM of IPTG ((isopropyl β-D-1-thiogalactopyranoside), were seeded (2 mL in M9 media) in a confocal dish and were allowed to grow.18[c] After 3 days media was replaced by a combination of 1 mg. L^{-1} of Rhodamine Green-Colistin and P7 PNPs (150 nM) and incubated for 1 hour. Biofilm samples incubated with only Rhodamine Green-Colistin (1 mg. L^{-1}) were used as control. The cells were then washed with PBS three times. Confocal microscopy images were obtained on a Zeiss LSM 510 Meta microscope by using a 63× objective. The settings of the confocal microscope were as follows: green channel: λ_{ex}=488 nm and λ_{em}=BP 505-530 nm; red channel: λ_{ex}=543 nm and λ_{em}=LP 650 nm. Emission filters: BP=band pass, LP=high pass.

7.4.9. Determination of minimum biofilm eradication concentration (MBEC)

MBEC is defined as the minimum concentration of an antimicrobial agent at which there is no bacteria (biofilm) growth. We used previously established protocols to determine the MBECs for the polymers and antibiotics.38 Briefly, bacterial cells from an overnight culture were diluted to $1/5^{th}$ using tryptic soy broth (TSB) and incubated at 275 rpm, 37 °C until they reach mid-log phase. 150 μL of bacteria solution was added to each row of a 96-well microtiter plate with pegged lid. Biofilms were cultured by incubating the plate for 6 hours in an incubator-shaker at 37 °C at 50 rpm. Then, the pegged lid was washed with 200 μL PBS for 30 seconds and transferred to a plate containing the test material prepared in a separate 96-well plate using M9 minimal media. The plate was incubated at 37 °C for 24 hours. Then, the biofilms on the peg-lid were washed with PBS and transferred to a new plate containing only M9 minimal media. The plate was further incubated at 37 °C to determine the Minimum Biofilm Eradication Concentration (MBEC).

Checkerboard titration for synergy testing for eradication of biofilms: Two-dimensional checkerboard titrations similar as described above were used testing synergy against biofilms. The concentration of Polymers and colistin were varied using 2-fold serial dilutions and MBEC was determined using the above-mentioned protocol.31 The wells without any visual growth were considered as a combination that eliminates biofilm formation. For colistin-polymer combinations, concentrations of the components were varied according to their MBEC against the respective bacterial strains.

7.5 Supplementary Information

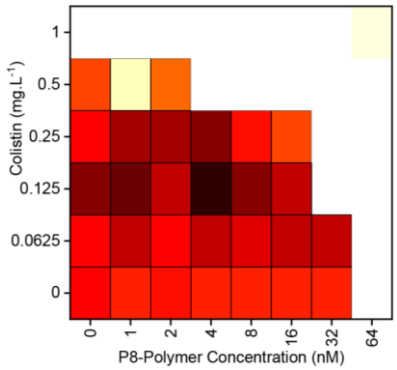

Figure 7.5. Checkerboard titration between colistin and P8 polymer against *P. aeruginosa* (CD-1006). Dark cells represent higher cell density.

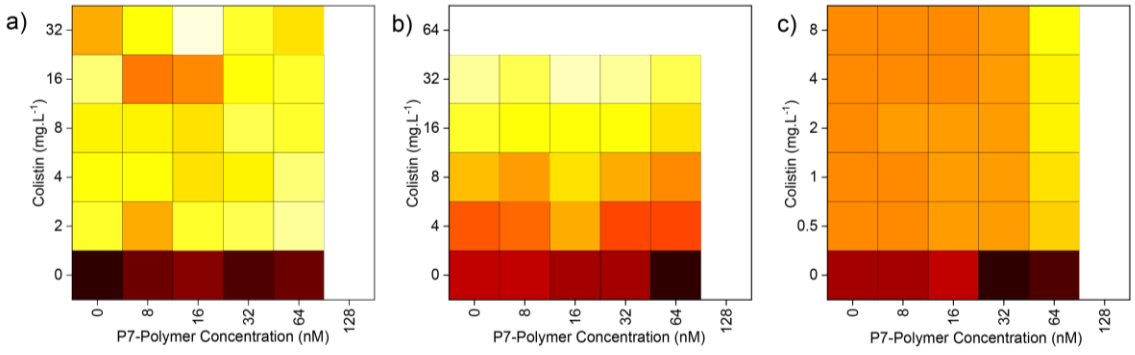

Figure 7.6. Checkerboard titration between colistin and P7 polymer against a. *Bacillus subtills* b. *S. epidermidis* and c. methicillin-resistant *S. aureus* (CD-489). Dark cells represent higher cell density. The combinations did not show any significant increase in the efficacy of the antibiotics.

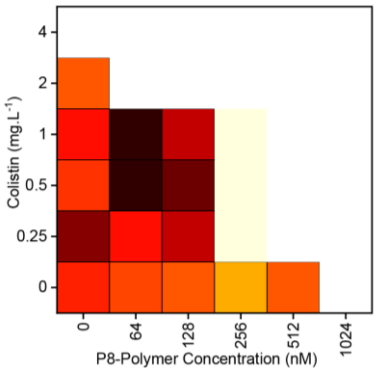

Figure 7.7. Checkerboard broth microdilution assays between colistin and P8 PNPs against uropathogenic biofilm *E. Coli* (CD-2). The combination shows upto 16-fold increase in the efficacy of colistin at sub-MBEC dosage of P8 PNPs.

7.6 References

1. B. Li, T. J. Webster, *J. Orthop. Res.* **2018**, *36*, 22.

2. C. Willyard, *Nature* **2017**, *543*, 15.

3. H. Kunishima, *Nihon Naika Gakkai Zasshi* **2014**, *102*, 2839.

4. L. B. Rice, *Infect. Control Hosp. Epidemiol.* **2010**, *31*, S7.

5. P. D. Leeson, B. Springthorpe, *Nat. Rev. Drug Discov.* **2007**, *6*, 881.

6. H. I. Zgurskaya, C. A. López, S. Gnanakaran, *ACS Infect. Dis.* **2016**, *1*, 512.

7. C. A. Fux, J. W. Costerton, P. S. Stewart, P. Stoodley, *Trends Microbiol.* **2005**, *13*, 34.

8. R. M. Donlan, *Emerg. Infect. Dis.* **2001**, *7*, 277.

9. H. Spapen, R. Jacobs, V. Van Gorp, J. Troubleyn, P. M. Honoré, *Ann. Intensive Care* **2011**, *1*, 14.

10. P. G. Bowler, B. I. Duerden, D. G. Armstrong, *Clin. Microbiol. Rev.* **2001**, *14*, 244.

11. B. Parsons, E. Strauss, *Am. J. Surg.* **2004**, *188*, 57.

12. B. Spellberg, J. H. Powers, E. P. Brass, L. G. Miller, J. E. Edwards, *Clin. Infect. Dis.* **2004**, *38*, 1279.

13. T. Tängdén, *Ups. J. Med. Sci.* **2014**, *119*, 149.

14. P. D. Tamma, S. E. Cosgrove, L. L. Maragakis, *Clin. Microbiol. Rev.* **2012**, *25*, 450.

15. E. D. Brown, G. D. Wright, *Nature* **2016**, *529*, 336.

16. A. H. Delcour, *Biochim. Biophys. Acta* **2009**, *1794*, 808.

17. J. M. Stokes, C. R. Macnair, B. Ilyas, S. French, J. P. Côté, C. Bouwman, M. A. Farha, A. O. Sieron, C. Whitfield, B. K. Coombes, E. D. Brown, *Nat. Microbiol.* **2017**, *2*, 17028.

18. P. S. Stewart, J. W. Costerton, *Lancet (London, England)* **2001**, *358*, 135.

19. J. N. Anderl, M. J. Franklin, P. S. Stewart, *Antimicrob. Agents Chemother.* **2000**, *44*, 1818.

20. A. Gupta, R. Das, G. Yesilbag Tonga, T. Mizuhara, V. M. Rotello, *ACS Nano* **2018**, *12*, 89.

21. A. Gupta, S. Mumtaz, C. H. Li, I. Hussain, V. M. Rotello, *Chem. Soc. Rev.* **2019**, *48*, 415.

22. G. N. Tew, R. W. Scott, M. L. Klein, W. F. Degrado, *Acc. Chem. Res.* **2010**, *43*, 30.

23. A. Jain, L. S. Duvvuri, S. Farah, N. Beyth, A. J. Domb, W. Khan, *Adv. Healthc. Mater.* **2014**, *3*, 1969.

24. M. J. Hajipour, K. M. Fromm, A. Akbar Ashkarran, D. Jimenez de Aberasturi, I. R. de Larramendi, T. Rojo, V. Serpooshan, W. J. Parak, M. Mahmoudi, *Trends Biotechnol.* **2012**, *30*, 499.

25. H. Takahashi, E. T. Nadres, K. Kuroda, *Biomacromolecules* **2017**, *18*, 257.

26. A. Gupta, R. F. Landis, C. H. Li, M. Schnurr, R. Das, Y. W. Lee, M. Yazdani, Y. Liu, A. Kozlova, V. M. Rotello, *J. Am. Chem. Soc.* **2018**, *140*, 12137.

27. C. R. MacNair, J. M. Stokes, L. A. Carfrae, A. A. Fiebig-Comyn, B. K. Coombes, M. R. Mulvey, E. D. Brown, *Nat. Commun.* **2018**, *9*, 458.

28. I. M. Helander, T. Mattila-Sandholm, *J. Appl. Microbiol.* **2000**, *88*, 213.

29. I. Wiegand, K. Hilpert, R. E. W. Hancock, *Nat. Protoc.* **2008**, *3*, 163.

30. X. Li, S. M. Robinson, A. Gupta, K. Saha, Z. Jiang, D. F. Moyano, A. Sahar, M. A. Riley, V. M. Rotello, *ACS Nano* **2014**, *8*, 10682.

31. F. C. Odds, *J. Antimicrob. Chemother.* **2003**, *52*, 1.

32. A. Gupta, N. M. Saleh, R. Das, R. F. Landis, A. Bigdeli, K. Motamedchaboki, A. R. Campos, K. Pomeroy, M. Mahmoudi, V. M. Rotello, *Nano Futur.* **2017**, *1*, 015004.

33. S. Halder, K. K. Yadav, R. Sarkar, S. Mukherjee, P. Saha, S. Haldar, S. Karmakar, T. Sen, *Springerplus* **2015**, *4*, 672.

34. P. Plesiat, H. Nikaido, *Mol. Microbiol.* **1992**, *6*, 1323.

35. H. Bai, H. Yuan, C. Nie, B. Wang, F. Lv, L. Liu, S. Wang, *Angew. Chemie - Int. Ed.* **2015**, *54*, 13208.

36. A. Gupta, R. F. Landis, V. M. Rotello, *F1000Research* **2016**, *5*, 364.

37. R. F. Landis, C. H. Li, A. Gupta, Y. W. Lee, M. Yazdani, N. Ngernyuang, I. Altinbasak, S. Mansoor, M. A. S. Khichi, A. Sanyal, V. M. Rotello, *J. Am. Chem. Soc.* **2018**, *140*, 6176.

38. H. Ceri, M. E. Olson, C. Stremick, R. R. Read, D. Morck, A. Buret, *J. Clin. Microbiol.* **1999**, *37*, 1771.

39. J. J. Harrison, C. A. Stremick, R. J. Turner, N. D. Allan, M. E. Olson, H. Ceri, Nat. Protoc. 2010, 5, 1236.

40. J. Li, K. Zhang, L. Ruan, S. F. Chin, N. Wickramasinghe, H. Liu, V. Ravikumar, J. Ren, H. Duan, L. Yang, M. B. Chan-Park, *Nano Lett.* **2018**, *18*, 4180.

41. A. Gupta, R. F. Landis, C. H. Li, M. Schnurr, R. Das, Y. W. Lee, M. Yazdani, Y. Liu, A. Kozlova and V. M. Rotello, *J. Am. Chem. Soc.*, 2018, **140**, 12137–12143.

42. Madkour, A. E.; Koch, A. H. R.; Lienkamp, K.; Tew, G. N. *Macromolecules* **2010**, *43* (10), 4557.

43. W. J. Peveler, R. F. Landis, M. Yazdani, J. W. Day, R. Modi, C. J. Carmalt, W. M. Rosenberg, V. M. Rotello, *Adv. Mater.* **2018**, *30*, 1800634.

CHAPTER 8

CROSSLINKED POLMER-STABILIZED NANOCOMPOSITES FOR THE TREATMENT OF BACTERIAL BIOFILMS

8.1 Introduction

MDR bacterial infections are an emerging threat to human health.[1] According to a recent report, MDR bacterial infections are responsible for 700,000 deaths each year all over the world and by 2050 this number is expected to increase to more than 10 million.[2] In particular, wounds and indwelling systems such as catheters,[3] joint prosthesis,[4] and other medical implants[5] are often infected by biofilms, micro-colonization of bacteria.[6] Biofilms secrete extracellular polymeric substances[7] (EPS) which acts as a protective barrier against antibiotics, limiting the efficacy of drugs including vancomycin,[8] teicoplanin,[9] and colistin[10] deemed as, "drugs of last resort". Excising infected tissues/implants[11] and long-term antibiotic therapy[12] is currently the best treatment for combatting biofilm-based infections. This "gold standard" treatment however has obvious limitations, including incurring extensive health care costs[13] and leaving patients bedridden with concomitant suffering.

Phytochemicals,[14,15] extracts from plants inherently responsible for their self-defense,[16] have emerged as promising tools to combat MDR bacteria.[17] These essential oils are of particular interest as "green" antimicrobial agents[18] due to their low cost,[19] biocompatibility,[20,21] and potential anti-biofilm properties.[22] Previous studies have demonstrated that numerous essential oils are severely cytotoxic towards pathogenic bacteria,[23,24] however, poor solubility[25] and stability[26] in aqueous media has substantially limited their therapeutic application. Essential oils can be encapsulated into surfactant-stabilized colloidal delivery vehicles to enhance their aqueous stability and antimicrobial activity against bacteria.[27] However, these carriers have not been shown to be stable in serum, restricting their use in relevant biological conditions. Furthermore, surfactant stabilized emulsions are susceptible to Ostwald ripening,[28] significantly impairing

long-term shelf life and practical use. It is critical to develop essential oil delivery vehicles that provide good shelf life, maintain stability in complex biofluids, and effectively treat MDR biofilms.

Previously, we have designed a self-assembled micron-sized essential oil-in-water Pickering emulsion with the use of silica nanoparticles which could effectively eradicate bacterial biofilms.[29] We hypothesized that using a polymer-stabilized essential oil platform would enable us to generate nano-sized emulsions to improve the delivery of the payload[30] and increase its stability[31] by incorporating crosslinking strategies. Herein, we report an essential oil-in-water crosslinked polymer nanocomposite (X-NC). The nanocomposite exhibits long-term shelf life high stability in serum media, and could readily penetrate throughout biofilms as evidenced by confocal experiments. X-NCs showed efficient killing of multiple pathogenic biofilms including methicillin-resistant *Staphylococcus aureus* (MRSA). Furthermore, their ability to treat wound biofilms was tested in a fibroblast-biofilm co-culture model, which showed effective eradication of biofilms while maintaining high fibroblast cell viability. Taken together, our X-NC is shown to be an excellent candidate to treat wounds and indwelling systems contaminated with pathogenic bacteria/biofilms.

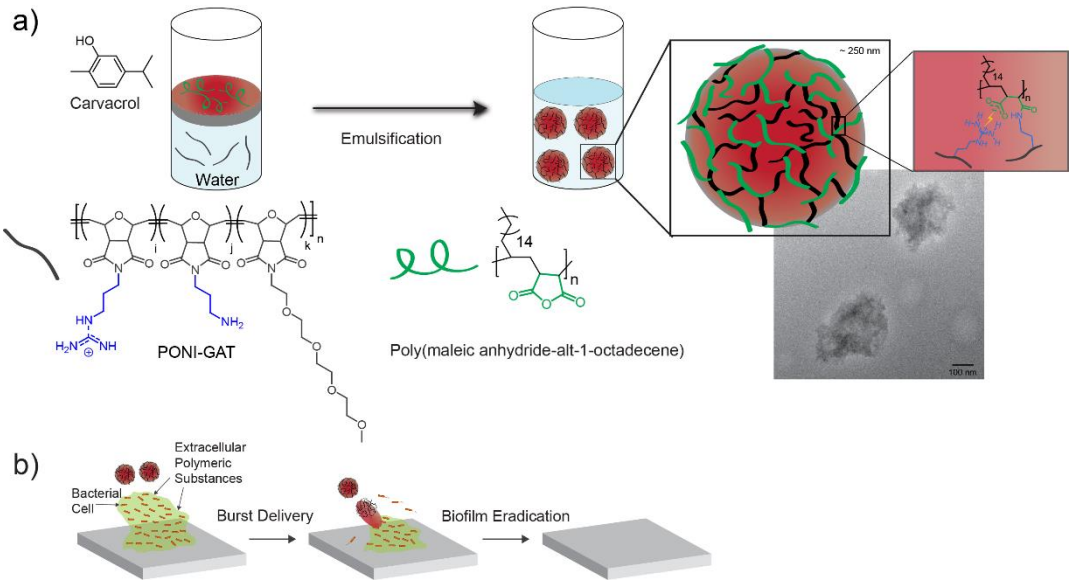

Figure 8.1. Schematic depiction of the strategy used to generate antimicrobial composites **a.** Carvacrol oil with dissolved p-MA-alt-OD is emulsified with an aqueous solution containing the PONI-GAT polymer. The anhydride units on p-MA-alt-OD react with the amines on PONI-GAT. This crosslinking reaction simultaneously pulls the polymer into the oil phase as the polymer becomes more hydrophobic, generating an oil-containing nanocomposite structure. **b.** Composites release their payload disrupting the biofilm, eliminating the bacteria.

8.2 Results and discussion

Poly(oxanorbornene imide) polymers (PONIs) were chosen to stabilize the essential oil nanocomposites as they are well-controlled,[32] easily modulated,[33] and scalable.[34] To ensure effective crosslinking to stabilize the oil, we dissolved the commercially available poly(maleic anhydride-*alt*-1-octadecene) (p-MA-alt-OD) at different weight percentages within the oil. Incorporating amine functionalities within PONI would enable fast crosslinking with the maleic anhydride units.[35] Guanidine functionality was added onto PONIs for charge neutralization with the released carboxylates from the anhydride,[36] enabling PONIs to partition further into the oil phase for further amidation reactions. In addition, tetraethylene glycol monomethyl ether (TEG-ME) functionality can impart extra amphiphilicity so that PONIs are water-soluble yet can partition into the oil. Therefore, we synthesized copolymer PONIs bearing guanidine, amino, and TEG-ME units (PONI-GAT) at a 35-35-30 monomer ratio respectively (Supporting Information – Synthesis of PONI-GAT).

Antimicrobial nanocomposites were generated using an oil emulsion template as shown in Figure 8.1. Nanocomposites were created by emulsifying carvacrol oil loaded with p-MA-alt-OD or carvacrol only (non-crosslinked control) into Milli-Q H_2O adjusted to a pH of 10 containing PONI-GAT (The pH was adjusted to ensure nucleophilicity of the amines on PONI-GAT). Upon emulsification, PONI-GAT partitions to the oil-water interface to initially stabilize the carvacrol oil droplets and with p-MA-alt-OD present, crosslinking further stabilizes the oil. Optimization, such as varying the amount of PONI-GAT and p-MA-alt-OD was performed to determine the smallest, yet most stable formulation. With a final PONI-GAT concentration of 6 μM and 10 wt% of p-MA-alt-OD, nanocomposites with a size of ~250 nm were generated.

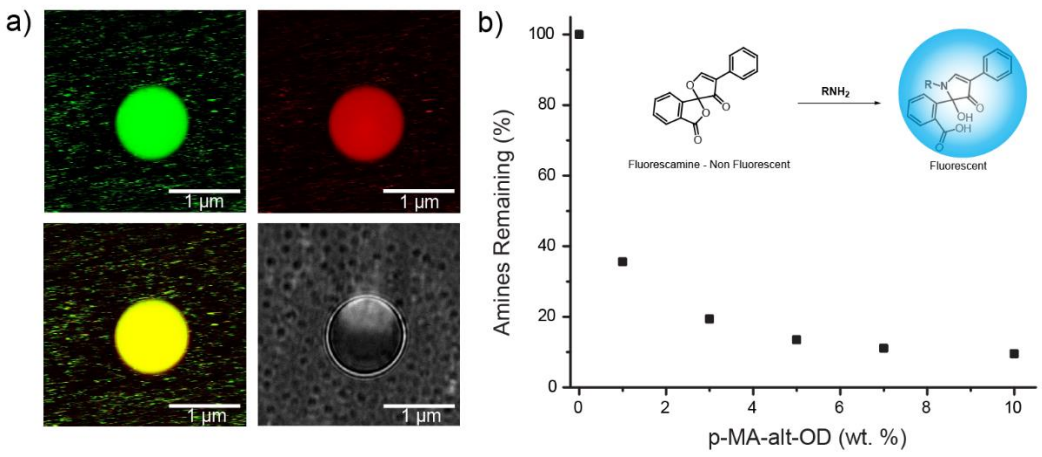

Figure 8.2. Confocal micrograph of **a.** X-NCs. PONI-GAT was partially labeled with TRITC (red fluorescence) and the oil core is loaded with DiO (green fluorescence). Scale bars are 1 µm. **b.** Percentage of amines remaining on PONI-GAT after X-NCs formation.

We hypothesize that reacting PONI-GAT with p-MA-alt-OD would change its inherent hydrophobicity and enhance partitioning within the oil. To test this hypothesis, tetramethylrhodamine-5-isothiocyanate (TRITC, red fluorescence) was conjugated to PONI-GAT while 3,3-Dioctadecyloxacarbocyanine (DiO, green fluorescence) was loaded within the oil. In addition, the formulation was modulated to generate micron-sized emulsions so that confocal experiments could be performed. As shown in Figure 8.2 a, both green and red fluorescence was co-localized within the oil, indicating a composite morphology.

Theoretically, a crosslinking reaction between amines and anhydrides at the oil-water interface would yield carboxylates, imparting negative charge. We examined the surface charge of the nanocomposite and found the surface to be negatively charged regardless of the amount of p-MA-alt-OD added. Furthermore, attenuated total reflectance Fourier transform infrared spectroscopy (ATR-FTIR) indicated complete loss of anhydrides and formation of amides/carboxylates after formation of the nanocomposite. To further explore the crosslinking, a fluorescamine assay[37] (Figure 8.2 b) was performed to identify the progression of the reaction between amines on PONI-GAT and the anhydrides on p-MA-alt-OD. PONI-GAT was used to generate a calibration curve relating to the polymer concentration and the respective fluorescence

generated from the assay. The fluorescamine assay is a valuable tool to monitor primary amines by generating fluorescence.[38] We expected that as the p-MA-alt-OD wt% increases within the oil, more amines will react, and the overall fluorescence generated from fluorescamine will decrease. The results show that a substantial reduction in remaining amines on PONI-GAT occurs as p-MA-alt-OD increases, showing almost complete reaction at 10 wt%. Taken together, the experiments described above support the stabilization of the oil via crosslinking between the amines on PONI-GAT and the anhydrides on p-MA-alt-OD, possessing a composite morphology.

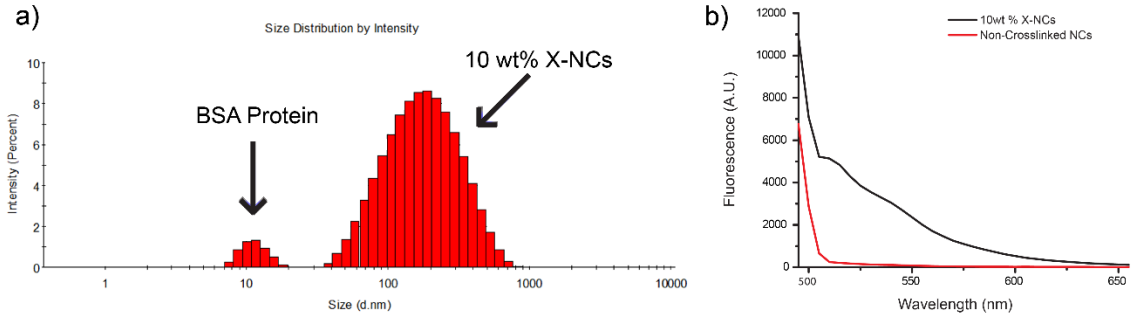

Figure 8.3. a. Stability of 10 wt% X-NCs after two days. **b.** Fluorescence spectra of loaded DiO in 10 wt% X-NCs and non-crosslinked analog. Excitation of DiO = 490nm.

Nanoemulsion stability in biological media is a challenge as biological stresses (protein adsorption/corona formation)[39] may induce destabilization and aggregation.[40] In particular, serum stability is critical when considering bacteria/biofilm treatment both topically [41] and systemically.[42] Negatively charged serum proteins can bind onto delivery vehicles, forming a corona. This corona can significantly alter the delivery vehicles size, interfacial composition, and ultimately its biological identity. [43] Our crosslinked nanocomposite vehicle which bears a negatively charged surface should be resistant to serum protein adsorption. To determine the compatibility of our X-NCs in serum conditions, we incubated X-NCs with 10% serum media for two days and analyzed the stability of the composites using dynamic light scattering (DLS). As shown in Figure 8.3 a, 10 wt% X-NCs showed complete stability with no evidence of destabilization/aggregation. As a control, non-crosslinked analogs using the same formulation minus p-MA-alt-OD showed no stability in serum. In addition, DiO was loaded into both

crosslinked nanocomposites and non-crosslinked analogs and incubated in serum for one hour. Destabilization of the non-crosslinked analog would result in leakage and quenched fluorescence of the loaded dye.[44] Figure 8.3 b shows that DiO maintains its fluorescence within the X-NCs while its non-crosslinked analog shows no fluorescence, further supporting the stability of X-NCs in serum conditions. Taken together, our crosslinking strategy provides stability in serum containing media.

Having established a composite morphology with successful crosslinking to impart stability, we probed the ability of X-NCs to penetrate into biofilms. X-NCs loaded with DiO within the oil were used to track the delivery of nanocomposites in the biofilms formed by Red Fluorescent Protein (RFP) expressing *Escherichia coli*. As shown in Figure 8.4, the X-NCs diffuse into the biofilm matrix and efficiently disperse throughout the biofilm, co-localizing with the bacteria. This data supports X-NCs deliver their payload and that the oil core and nanocomposite fabrication strategy are operative for effective delivery.

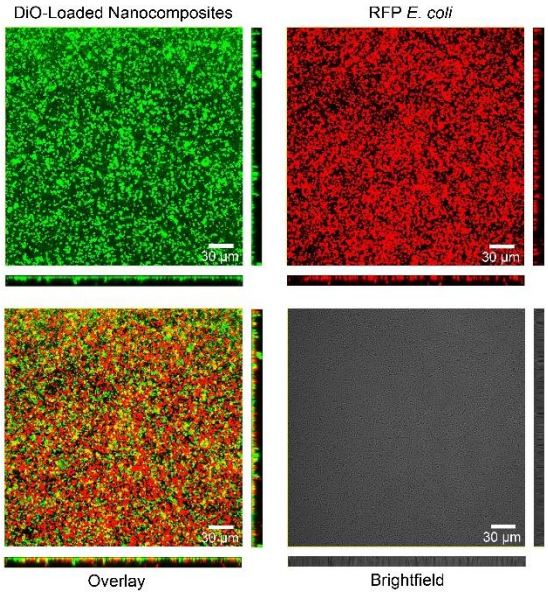

Figure 8.4. Confocal image stacks of 1 day-old *E. coli DH5α* biofilm after 3 h treatment with 10 wt% X-NCs. Scale bars are 30 µm.

Next, we investigated the therapeutic efficacy of the X-NCs against multiple pathogenic biofilms. Four pathogenic bacterial strains of clinical isolates, *Pseudomonas aeruginosa* (CD-

1006), *Staphylococcus aureus* (CD-489, a methicillin-resistant strain), *Escherichia coli* (CD-2), and *Enterobacter cloacae* (*E. cloacae*, CD-1412) complex were chosen to test our system. As shown in Figure 8.5, X-NCs were able to effectively kill bacterial cells in all four biofilms within three hours. The isolated components used to generate the nanocomposites, carvacrol oil and PONI-GAT, were ineffective at eradicating the biofilms, indicating that the combination of all the components to generate X-NCs is critical for maximum therapeutic efficiency. Notably, X-NCs are able to effectively treat both Gram negative (*E. coli*, *P. aeruginosa*, and *E. cloacae* complex) and Gram positive (*S. aureus*) bacteria, supporting the broad spectrum activity of X-NCs as a viable platform treatment complementary to traditional antibiotics.

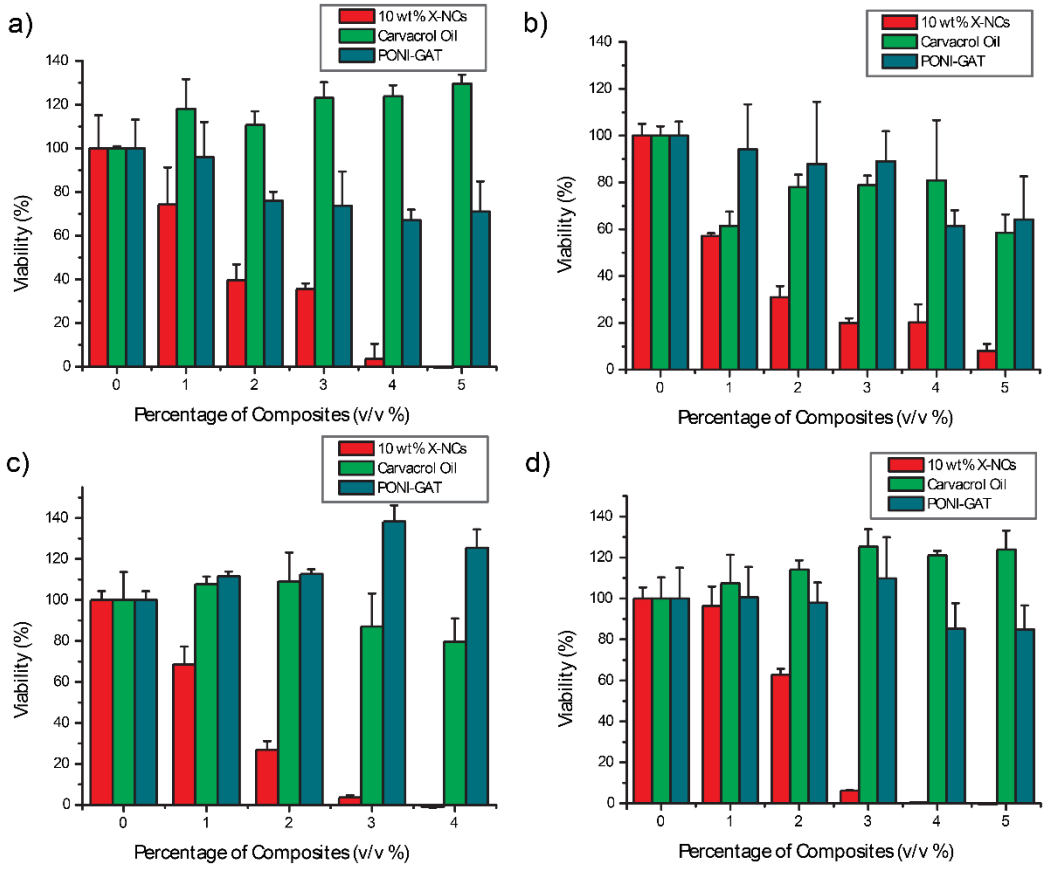

Figure 8.5. Viability of 1 day-old **a.** *E. coli* (CD-2), **b.** *S. aureus* (CD-489), **c.** *P. aeruginosa* (CD-1006), and **d.** *E. cloacae* complex (CD-1412) biofilms after 3 h treatment with 10 wt% X-NCs, carvacrol oil, and PONI-GAT at different emulsion concentrations (v/v % of emulsion). The data are average of triplicates, and the error bars indicate the standard deviations.

Biofilm infections associated with wounds and indwelling implants interfere with the host's ability to regenerate damaged tissue.[45] In particular, fibroblasts play a key role during wound healing processes by aiding to close the area and redevelop necessary extracellular matrix within the skin.[46] We used an *in vitro* co-culture model comprised of mammalian fibroblasts cells with bacterial biofilm grown over them. *P. aeruginosa* bacteria were seeded with a confluent NIH 3T3 fibroblast cell monolayer overnight to generate biofilms prior to X-NCs treatment. The cocultures were treated with X-NCs for three hours, washed, and the viabilities of both bacteria and fibroblasts were determined. As shown in Figure 8.6, X-NCs effectively treated the biofilm infection while 3T3 fibroblast viability was largely unaffected. It was observed that 15 v/v % of generated emulsion solution was sufficient to eradicate 99.5% of the bacteria within the biofilm.

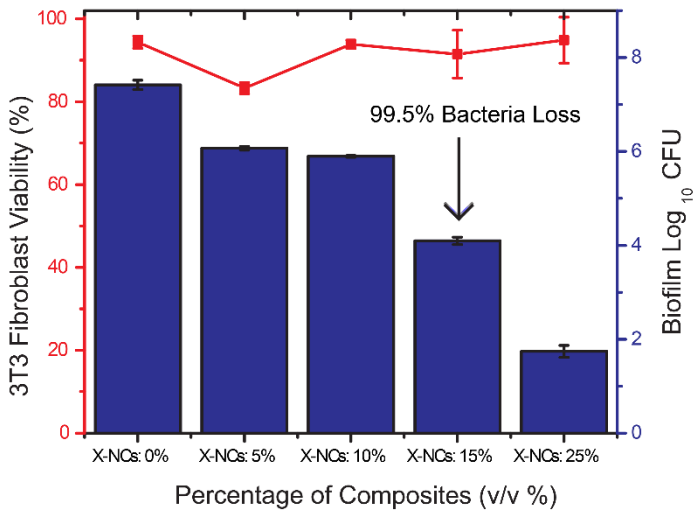

Figure 8.6. Viability of 3T3 fibroblast cells and *P. aeruginosa* biofilms in the coculture model after 3 h treatment with 10 wt% X-NCs at different emulsion concentrations (v/v % of emulsion). Scatters and lines represent 3T3 fibroblast cell viability. Bars represent $\log_{10}$ of colony forming units in biofilms. The data are average of triplicates and the error bars indicate the standard deviations.

8.3 Conclusions

In summary, we report the fabrication of a polymer-stabilized oil-in-water nanocomposite which demonstrates high therapeutic activity towards pathogenic biofilms. These nanocomposites show high stability in serum and can effectively penetrate throughout biofilms. Furthermore, effective elimination of a biofilm infection while maintaining fibroblast viability in an *in vitro* coculture was observed. We envision these nanocomposites as a valuable treatment option for topical wounds by loading them onto various medical devices. Future studies will probe composite performance in combatting topical *in* vivo biofilms along with assays to determine if bacteria acquire resistance towards the essential oil payload. Furthermore, bio-degradable analogs are currently being formulated and evaluated; expanding our arsenal. The polymer-based crosslinked emulsion strategy we present provides a promising platform to create effective delivery vehicles to combat the ever-increasing danger of MDR bacterial biofilms.

8.4 Experimental methods

8.4.1. Synthesis of PONI-GAT. Synthesis of PONI-GAT

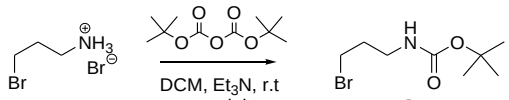

1

Synthesis of 1. To a 500ml round bottom flask equipped with a stirbar was added 150ml of dichloromethane (DCM). Next, 3-Bromopropylamine hydrobromide (10.0g, 45.7mmol, 1.0eq) was added to the DCM solution. Then, triethylamine (Et_3N) (25.5ml, 182.7mmol, 4.0eq) was added to the reaction mixture. Finally Di-*tert*-butyl dicarbonate (12.6ml, 54.8mmol, 1.2eq) was

added dropwise. After addition of di-*tert*-butyl dicarbonate, the reaction was stirred overnight at room temperature (r.t.). Afterwards, the DCM was rotovaped, diluted with 100ml of diethyl ether, and extracted with 1M HCL (1x 20ml), saturated sodium bicarbonate (2x 20ml), and brine (1x 20ml). The organic layer was dried with sodium sulfate, filtered, and rotovaped to yield 1 as a clear liquid. 1 was purified using column chromatography and silica gel as the stationary phase. ^{1}H NMR (400MHz, $CDCL_3$) 4.6 (br, 1H) 3.43 (t, 2H), 3.26 (br, 2H), 2.04 (t, 2H), 1.43 (s, 9H).

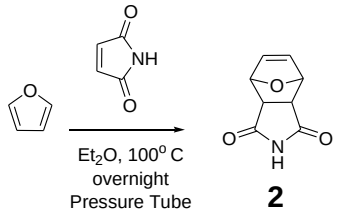

2

Synthesis of 2. In a pressure tube, furan (4.5ml, 61.7mmol, 1.5eq) and maleimide (4.0g, 41.1mmol, 1.0eq) were added in addition to 5ml of diethyl ether. The tube was sealed and heated at 100°C overnight. Afterwards, the pressure tube was cooled to r.t. and the formed solid was removed, filtered, and washed with copious amounts of diethyl ether to isolate 2 as a white solid and was used without further purification. ^{1}H NMR (400MHz, MeOD) 11.14 (s, 1H), 6.52 (s, 2H), 5.12 (s, 2H), 2.85 (s, 2H).

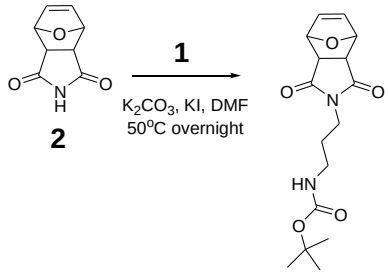

3

Synthesis of 3. To a 100ml round bottom flask equipped with a stirbar was added 30ml of dimethylformamide (DMF). Next, 2 (2.36g, 14.3mmol, 1.0eq) was added along with potassium carbonate (7.9g, 57.2mmol, 4.0eq). The reaction mixture was heated at 50oC for five minutes. Finally, potassium iodide (0.05g, 0.30mmol, 0.02eq) and 1 (3.47g, 14.6mmol, 1.02eq) were added and stirred at 50°C overnight. Afterwards, the reaction mixture was cooled to room

temperature, diluted to 150ml with ethyl acetate and washed with water (7x, 50ml) and brine (1x, 50ml). The organic layer was dried with sodium sulfate, filtered, and rotovaped to yield 3 as a white solid. 3 was purified using column chromatography and silica gel as the stationary phase. ^{1}H NMR (400MHz, CDCL3) 6.51 (s, 2H), 5.26 (s, 2H), 5.03 (br, 1H), 3.56 (t, 2H), 3.05 (q, 2H), 2.86 (s, 2H), 1.73 (quint, 2H) 1.45 (s, 9H).

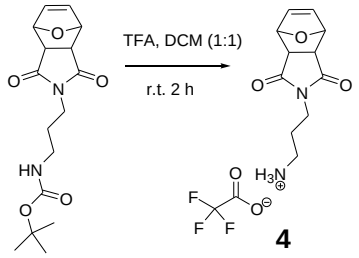

3 **4**

Synthesis of 4. To a 50ml round bottom flask equipped with a stirbar was added 3 (2.0g, 6.2mmol, 1.0eq). Nitrogen was bubbled through DCM for five minutes and 5ml was added to the flask which was purged with nitrogen. 5ml of trifluoroacetic acid (TFA, excess) was added and the reaction was stirred for two hours. Afterwards, excess TFA was removed by rotovaping with DCM (3x) yielding 4. 4 was isolated as a white solid by washing with diethyl ether (3x, 10ml) and used without further purification and directly used in the next reaction (Ninhydrin test confirms free primary amine).

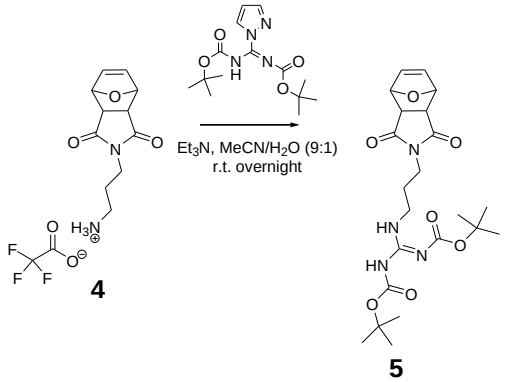

4 **5**

Synthesis of 5. To a 100ml round bottom flask equipped with a stirbar was added 4 (1.2g, 3.6mmol, 1.0eq), 45ml acetonitrile (MeCN), and 5ml of water. Triethylamine (4.7ml, 33.5mmol, 9.2eq) was added and finally *N,N′*-Di-Boc-1*H*-pyrazole-1-carboxamidine (1.7g, 5.5mmol, 1.5eq)

in portions. The reaction was allowed to stir at r.t. overnight. Afterwards, the solution was diluted with 100ml of ethyl acetate and extracted with water (2x, 50ml) and brine (2x, 50ml). The organic layer was dried with sodium sulfate, filtered, and rotovaped to yield 5. 5 was purified using column chromatography and silica gel as the stationary phase to yield a white solid. ^{1}H NMR (400MHz, $CDCL_3$) 8.49 (t, 1H), 6.49 (s, 2H), 5.25 (s, 2H), 3.53 (t, 2H), 3.47 (q, 2H), 2.83 (s, 2H), 1.82 (quint, 2H), 1.49 (s, 18H).

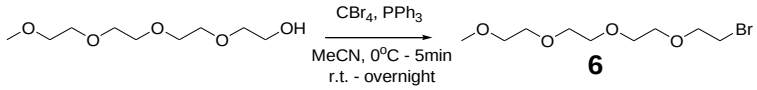

Synthesis of 6. To a 250ml round bottom flask was added Tetraethyleneglycol monomethyl ether (4.2ml, 20.9mmol, 1.0eq) and 80ml of MeCN. The reaction was cooled to 0°C and tetrabromomethane (8.4g, 25.1mmol, 1.2eq) was added. Finally, triphenylphosphine (6.6g, 25.3mmol, 1.2eq) was added in portions and allowed to stir for five minutes at 0°C. After five minutes, the reaction was warmed to room temperature and stirred overnight. Afterwards, the reaction was concentrated by rotovaping and purified using column chromatography and silica gel as the stationary phase to yield 6 as a clear oil (Potassium permanganate was used to visualize 6). ^{1}H NMR (400MHz, $CDCL_3$) 3.75 (t, 2H), 3.6 (br, 10H), 3.49 (t, 2H), 3.41 (t, 2H), 3.32 (s, 3H).

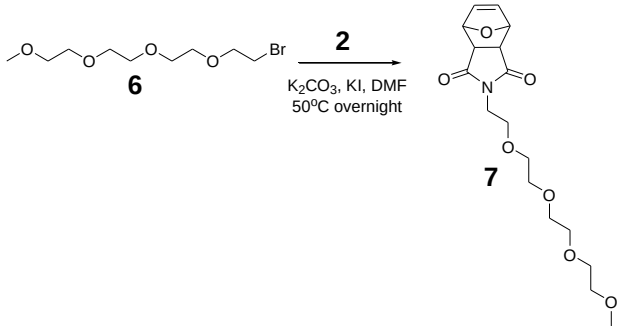

Synthesis of 7. To a 100ml round bottom flask equipped with a stirbar was added 30ml of DMF. Next, 2 (2.84g, 17.2mmol, 1.0eq) was added along with potassium carbonate (9.48g, 68.7mmol,

4.0eq). The reaction mixture was heated at 50ºC for five minutes. Finally, potassium iodide (0.05g, 0.30mmol, 0.02eq) and 6 (4.9g, 18.0mmol, 1.05eq) were added and stirred at 50ºC overnight. Afterwards, the reaction mixture was cooled to room temperature, diluted to 150ml with ethyl acetate and washed with water (7x, 50ml) and brine (1x, 50ml). The organic layer was dried with sodium sulfate, filtered, and rotovaped to yield 7. 7 was isolated as a clear oil using column chromatography and silica gel as the stationary phase. ^{1}H NMR (400MHz, $CDCL_3$) 6.49 (s, 2H), 5.23 (s, 2H), 3.66 (t, 2H), 3.6 (br, 8H), 3.58 (br, 4H), 3.51 (t, 2H), 3.35 (s, 3H), 2.83 (s, 2H).

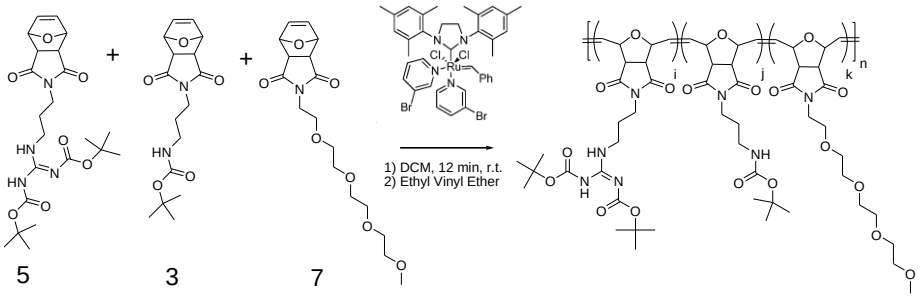

5 3 7

Synthesis of Polymer 8. To a 10ml pear-shaped flask equipped with a stirbar was added 5 (457mg, 0.98mmol, 1.0eq), 3 (317mg, 0.98mmol, 1.0eq) and 7 (300mg, 0.84mmol, 0.85eq) along with 5ml of DCM. In a separate 10ml pear-shaped flask equipped with a stirbar was added Grubbs Catalyst 3rd Generation (38.4mg, 0.043mmol, 0.04eq) along with 1ml of DCM. Both flasks underwent freeze-pump thaw three times, warmed to room temperature and the catalyst transferred to the reaction mixture. After 12 minutes, ethyl vinyl ether (200µl, excess) was quickly added and stirring continued for 15 minutes. The polymer was precipitated using 200ml of 1:1 hexane:ethyl ether. The polymer was collected by filtration, dissolved in a minimal amount of DCM and precipitated again in the same hexane:ethyl ether solution yielding 8 as a gray solid. MW = 31,736 (MW was determined through gel permeation chromatography (tetrahydrofuran) with a polystyrene calibration curve). ^{1}H NMR (400MHz, $CDCL_3$) 11.4 (s, 1H), 8.39 (br, 1H), 6.01 (s, 2H), 5.72 (br, 2H), 4.95 (br, 2H), 4.41 (br, 2H), 3.55 (br, 11H), 3.32 (br, 2H), 3.30 (s, 2H), 3.29 (br, 2H), 3.01 (br, 1H), 1.82 (br, 1H), 1.7 (br, 3H), 1.42 (s, 12H), 1.35 (s, 6H).

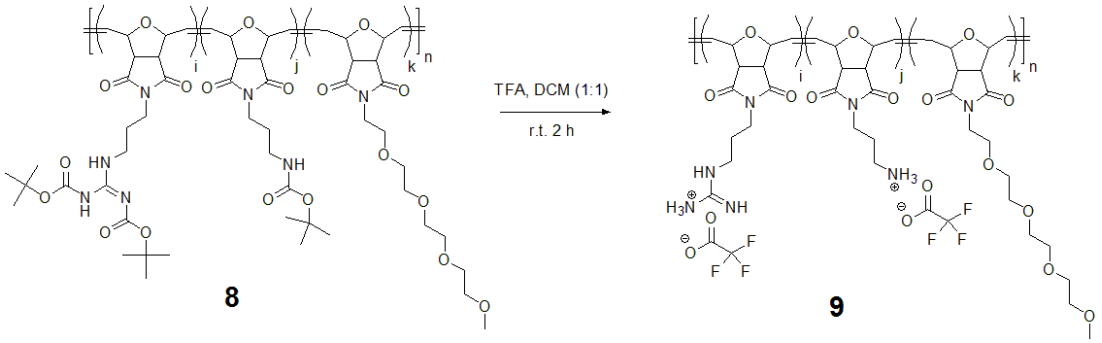

Synthesis of Polymer 9 – PONI-GAT. To a 50ml round bottom flask equipped with a stirbar was added Polymer 8 (400mg). Dichloromethane was purged with nitrogen for five minutes and 12ml was added to the flask, sealed with a septum and purged with nitrogen for five minutes. The main nitrogen line was left in the septum and the nitrogen pressure was reduced to a steady stream. 12ml of trifluoroacetic acid (excess) was added and the reaction was allowed to stir for two hours. Afterwards, excess TFA was removed by rotovaping with DCM (3x). The reaction residue was dissolved in a minimal amount of water, filtered through a polyethersulfone (PES) syringe filter and lyophilized to yield 9 as an off-white solid which readily dissolves in water. MW ~ 23,486. ^{1}H NMR (400MHz, D_2O) 6.1 (br, 2H), 5.91 (br, 2H), 5.2 (br, 2H), 4.64 (br, 2H), 3.65 (br, 19H), 3.39 (s, 2H), 3.21 (br, 2H), 3.01 (br, 2H), 1.99 (br, 2H), 1.89 (br, 2H) (^{1}H NMR confirms complete loss of all Boc protecting groups).

8.4.2. Preparation of Nanocomposites

Stock nanocomposite solutions were prepared in 0.6 ml Eppendorf tubes. To prepare the stock X-NC emulsions, 3 µL of carvacrol oil (containing 10 wt% p-MA-alt-OD) was added to 497 µL of Milli-Q H_2O (previously adjusted to a pH of 10) containing 6 µM of PONI-GAT and emulsified in an amalgamator for 50 s. The non-crosslinked analogs were done in the same fashion however without p-MA-alt-OD dissolved in carvacrol. The emulsions were allowed to rest overnight prior to use.

Fluorescamine Assay - The fluorescamine calibration curve was generated by mixing various concentrations of PONI-GAT with fluorescamine (dissolved in acetonitrile – 2.5 mg/ml, 50 µL aliquots) in phosphate buffer (PB – 5mM, pH = 7.4). The solutions were sonicated in the dark for 5 min, diluted with ethanol and their emission maxima at 470 nm analyzed. The percentage of amines remaining on PONI-GAT at different wt% of p-MA-alt-OD after emulsification was performed by diluting the stock emulsion solution by half. Afterwards, 450 µL of PB was added along with 50 µL of fluorescamine. The solutions were sonicated in the dark for 5 min, diluted with ethanol and their emission maxima at 470 nm analyzed.

8.4.3. Biofilm Formation

Bacteria were inoculated in LB broth at 37°C until stationary phase. The cultures were then harvested by centrifugation and washed with 0.85% sodium chloride solution three times. Concentrations of resuspended bacterial solution were determined by optical density measured at 600 nm. Seeding solutions were then made in M9 to reach OD_{600} of 0.1. 100 µL of the seeding solutions were added to each well of the microplate. M9 medium without bacteria was used as a negative control. The plates were covered and incubated at room temperature under static conditions for a desired period. Planktonic bacteria were removed by washing with PB saline three times. Varied v/v % of X-NCs, made in M9 medium, were incubated with the biofilms for 3 h. Biofilms were washed with phosphate buffer saline (PBS) three times and viability was determined using an Alamar Blue assay. M9 medium without bacteria was used as a negative control.

Biofilm – 3T3 Fibroblast Cell Coculture. A total of 20,000 NIH 3T3 (ATCC CRL-1658) cells were cultured in Dulbecco's modified Eagle medium (DMEM; ATCC 30-2002) with 10% bovine calf serum and 1% antibiotics at 37ºC in a humidified atmosphere of 5% CO_2. Cells were kept for 24 hours to reach a confluent monolayer. Bacteria (P. aeruginosa) were inoculated and harvested. Afterwards, seeding solutions were made in buffered DMEM supplemented with glucose to reach

an OD_{600} of 0.1. Old medium was removed from 3T3 cells followed by addition of 100 μL of seeding solution. The cocultures were then stored in a box with damp paper towels at 37°C overnight without shaking. Testing solutions at different concentrations were made by diluting nanocomposites into DMEM prior to use. Media was removed from coculture, replaced with testing solutions, and incubated for 3 hours at 37°C. Cocultures were then analyzed using a LDH cytotoxicity assay to determine mammalian cell viability. To determine the bacteria viability in biofilms, the testing solutions were removed and cocultures were washed with PBS. Fresh PBS was then added to disperse remaining bacteria from biofilms in coculture by sonication for 20 min and mixing with pipet. The solutions containing dispersed bacteria were then plated onto agar plates and colony forming units were counted after incubation at 37°C overnight.

8.5 References

1. A. Gupta, R. F. Landis, V. M. Rotello, *F1000Research* **2016**, *5*, 364.

2. F. Walsh, *BBC News* **2014**, 1.

3. B. W. Trautner, R. O. Darouiche, *Am. J. Infect. Control* **2004**, *32*, 177.

4. Z. Song, L. Borgwardt, N. Hoiby, H. Wu, T. S. Sorensen, A. Borgwardt, *Orthop. Rev. (Pavia).* **2013**, *5*, 65.

5. S. Veerachamy, T. Yarlagadda, G. Manivasagam, P. K. Yarlagadda, *Proc. Inst. Mech. Eng. H.* **2014**, *228*, 1083.

6. T. Bjarnsholt, *Apmis* **2013**, *121*, 1.

7. M. Kostakioti, M. Hadjifrangiskou, S. J. Hultgren, *Cold Spring Harb. Perspect. Med.* **2013**, *3*, a010306.

8. I. G. Boneca, G. Chiosis, *Expert Opin. Ther. Targets* **2003**, *7*, 311.

9. D. L. Boger, *Med. Res. Rev.* **2001**, *21*, 356.

10. K. Dafopoulou, B. B. Xavier, A. Hotterbeekx, L. Janssens, C. Lammens, E. De, H. Goossens, A. Tsakris, S. Malhotra-Kumar, S. Pournaras, *Antimicrob. Agents Chemother.* **2015**, *60*, 1892.

11. P. Kujath, C. Kujath, *Eur. J. Med. Res.* **2010**, *15*, 544.

12. H. Wu, C. Moser, H.-Z. Wang, N. Høiby, Z.-J. Song, *Int. J. Oral Sci.* **2015**, *7*, 1.

13. A. S. Lynch, G. T. Robertson, *Annu. Rev. Med.* **2008**, *59*, 415.

14. H. Wang, T. O. Khor, L. Shu, Z.-Y. Su, F. Fuentes, J.-H. Lee, A.-N. T. Kong, *Anticancer. Agents Med. Chem.* **2012**, *12*, 1281.

15. M. H. Farzaei, R. Bahramsoltani, Z. Abbasabadi, R. Rahimi, *J. Pharm. Pharmacol.* **2015**, *67*, 1467.

16. T. Hintz, K. K. Matthews, R. Di, *Biomed Res. Int.* **2015**, *2015*, 246264.

17. K. V. Kon, M. K. Rai, *Expert Rev. Anti. Infect. Ther.* **2012**, *10*, 775.

18. J. Vergis, P. Gokulakrishnan, R. K. Agarwal, A. Kumar, *Crit. Rev. Food Sci. Nutr.* **2015**, *55*, 1320.

19. M. F. Maia, S. J. Moore, *Malar. J.* **2011**, *10 Suppl 1*, S11.

20. G. Freire Rocha Caldas, A. V. Araujo, G. S. Albuquerque, J. da C. Silva-Neto, J. H. Costa-Silva, I. R. A. de Menezes, A. C. L. Leite, J. G. M. da Costa, A. G. Wanderley, *Evid. Based. Complement. Alternat. Med.* **2013**, *2013*, 856168.

21. R. P. Mittal, A. Rana, V. Jaitak, *Curr. Drug Targets* **2019**, *20*, 605.

22. C.-M. Saviuc, V. Drumea, L. Olariu, M.-C. Chifiriuc, E. Bezirtzoglou, V. Lazar, *Curr. Pharm. Biotechnol.* **2015**, *16*, 137.

23. J. Sharifi-Rad, M. Sharifi-Rad, S. M. Hoseini-Alfatemi, M. Iriti, M. Sharifi-Rad, M. Sharifi-Rad, *Int. J. Mol. Sci.* **2015**, *16*, 17812.

24. F. Hosseinkhani, F. Jabalameli, M. Banar, N. Abdellahi, M. Taherikalani, W. B. van Leeuwen, M. Emaneini, *Rev. Soc. Bras. Med. Trop.* **2016**, *49*, 172.

25. C. Samperio, R. Boyer, W. N. 3rd Eigel, K. W. Holland, J. S. McKinney, S. F. O'Keefe, R. Smith, J. E. Marcy, *J. Agric. Food Chem.* **2010**, *58*, 12950.

26. C. Turek, F. C. Stintzing, *Compr. Rev. Food Sci. Food Saf.* **2013**, *12*, 40.

27. Y. Chang, L. McLandsborough, D. J. McClements, *Food Chem.* **2015**, *172*, 298.

28. K. Ziani, Y. Chang, L. McLandsborough, D. J. McClements, *J. Agric. Food Chem.* **2011**, *59*, 6247.

29. B. Duncan, X. Li, R. F. Landis, S. T. Kim, A. Gupta, L.-S. Wang, R. Ramanathan, R. Tang, J. a Boerth, V. M. Rotello, *ACS Nano* **2015**, *9*, 7775.

30. J. Akhtar, H. H. Siddiqui, S. Fareed, Badruddeen, M. Khalid, M. Aqil, *Drug Deliv.* **2016**, *23*, 2026.

31. B. Zeeb, M. Gibis, L. Fischer, J. Weiss, *J. Colloid Interface Sci.* **2012**, *387*, 65.

32. Z. M. AL-Badri, G. N. Tew, *Macromolecules* **2008**, *41*, 4173.

33. C. C. Lin, C. S. Ki, H. Shih, *J. Appl. Polym. Sci.* **2015**, *132*, 41563.

34. J. P. Cole, J. J. Lessard, C. K. Lyon, B. T. Tuten, E. B. Berda, *Polym. Chem.* **2015**, *6*, 5555.

35. B. Duncan, R. F. Landis, H. A. Jerri, V. Normand, D. Benczédi, L. Ouali, V. M. Rotello, *Small* **2015**, *11*, 1302.

36. A. Pantos, I. Tsogas, C. M. Paleos, *Biochim. Biophys. Acta* **2008**, *1778*, 811.

37. E. O'Reilly, J. Lanza, *Ecology* **1995**, *76*, 2656.

38. S. Udenfriend, S. Stein, P. Bohlen, W. Dairman, W. Leimgruber, M. Weigele, *Science* **1972**, *178*, 871.

39. P. Sanchez-Moreno, P. Buzon, H. Boulaiz, J. M. Peula-Garcia, J. L. Ortega-Vinuesa, I. Luque, A. Salvati, J. A. Marchal, *Biomaterials* **2015**, *61*, 266.

40. P. Sanchez-Moreno, J. L. Ortega-Vinuesa, A. Martin-Rodriguez, H. Boulaiz, J. A. Marchal-Corrales, J. M. Peula-Garcia, *Int. J. Mol. Sci.* **2012**, *13*, 2405.

41. A. Baran, I. Flisiak, J. Jaroszewicz, M. Swiderska, *J. Dermatolog. Treat.* **2015**, *26*, 134.

42. N. Berthold, P. Czihal, S. Fritsche, U. Sauer, G. Schiffer, D. Knappe, G. Alber, R. Hoffmann, *Antimicrob. Agents Chemother.* **2013**, *57*, 402.

43. J. Wolfram, Y. Yang, J. Shen, A. Moten, C. Chen, H. Shen, M. Ferrari, Y. Zhao, *Colloids Surfaces B Biointerfaces* **2014**, *124*, 17.

44. R. P. Haugland, *Handbook of Fluorescent Probes and Research Products*, **2002**.

45. S. Roy, H. Elgharably, M. Sinha, K. Ganesh, S. Chaney, E. Mann, C. Miller, S. Khanna, V. K. Bergdall, H. M. Powell, C. H. Cook, G. M. Gordillo, D. J. Wozniak, C. K. Sen, *J. Pathol.* **2014**, *233*, 331.

46. B. K. Sun, Z. Siprashvili, P. A. Khavari, *Science* **2014**, *346*, 941.

BIBLIOGRAPHY

Ahamed, M.; AlSalhi, M. S.; Siddiqui, M. K. J. *Clin. Chim. Acta* **2010**, *411* (23–24), 1841.

Akhtar, J.; Siddiqui, H. H.; Fareed, S.; Badruddeen; Khalid, M.; Aqil, M. *Drug Deliv.* **2016**, *23* (6), 2026.

AL-Badri, Z. M.; Tew, G. N. *Macromolecules* **2008**, *41* (12), 4173.

Algar, W. R.; Prasuhn, D. E.; Stewart, M. H.; Jennings, T. L.; Blanco-Canosa, J. B.; Dawson, P. E.; Medintz, I. L. *Bioconjug. Chem.* **2011**, *22* (5), 825.

Allahverdiyev, A. M.; Kon, K. V.; Abamor, E. S.; Bagirova, M.; Rafailovich, M. *Expert Rev. Anti. Infect. Ther.* **2011**, *9* (11), 1035.

Anastas, P.; Eghbali, N. *Chem. Soc. Rev.* **2010**, *39* (1), 301.

Anderl, J. N.; Zahller, J.; Roe, F.; Stewart, P. S. *Antimicrob. Agents Chemother.* **2003**, *47* (4), 1251.

Anderl, J. N.; Franklin, M. J.; Stewart, P. S. *Antimicrob. Agents Chemother.* **2000**, *44* (7), 1818.

Anderson, G. G.; Kenney, T. F.; Macleod, D. L.; Henig, N. R.; O'Toole, G. A. *Pathog. Dis.* **2013**, *67* (1), 39.

Anderson, G. G.; Moreau-Marquis, S.; Stanton, B. A.; O'Toole, G. A. *Infect. Immun.* **2008**, *76* (4), 1423.

Arnt, L.; Nüsslein, K.; Tew, G. N. *J. Polym. Sci. Part A Polym. Chem.* **2004**, *42* (15), 3860.

Backus, K. M.; Boshoff, H. I.; Barry, C. S.; Boutureira, O.; Patel, M. K.; D'Hooge, F.; Lee, S. S.; Via, L. E.; Tahlan, K.; Barry, C. E.; Davis, B. G. *Nat. Chem. Biol.* **2011**, *7* (4), 228.

Bai, H.; Yuan, H.; Nie, C.; Wang, B.; Lv, F.; Liu, L.; Wang, S. *Angew. Chemie - Int. Ed.* **2015**, *54* (45), 13208.

Bai, Y.; Chen, J.; Zimmerman, S. C. *Chem. Soc. Rev.* **2018**, *47* (5), 1811.

Baltzer, S. A.; Brown, M. H. *J. Mol. Microbiol. Biotechnol.* **2011**, *20* (4), 228.Baran, A.; Flisiak, I.; Jaroszewicz, J.; Swiderska, M. *J. Dermatolog. Treat.* **2015**, *26* (2), 134.

Benoit, D. S. W.; Koo, H. *Nanomedicine* **2016**, *11* (9), 873.

Berry, V.; Gole, A.; Kundu, S.; Murphy, C. J.; Saraf, R. F. *J. Am. Chem. Soc.* **2005**, *127* (50), 17600.

Berthold, N.; Czihal, P.; Fritsche, S.; Sauer, U.; Schiffer, G.; Knappe, D.; Alber, G.; Hoffmann, R. *Antimicrob. Agents Chemother.* **2013**, *57* (1), 402.

Bertozzi, C. R. *Acc. Chem. Res.* **2011**, *44* (9), 651.

Bhakdi, S.; Tranum-Jensen, J. *Microbiol. Rev.* **1991**, *55* (4), 733 LP.

Bi, L.; Yang, L.; Narsimhan, G.; Bhunia, A. K.; Yao, Y. *J. Control. Release* **2011**, *150* (2), 150.

Bjarnsholt, T. *Apmis* **2013**, *121* (SUPPL.136), 1.

Blanco, E.; Shen, H.; Ferrari, M. *Nat. Biotechnol.* **2015**, *33* (9), 941.

Boger, D. L. *Med. Res. Rev.* **2001**, *21* (5), 356.

Boneca, I. G.; Chiosis, G. *Expert Opin. Ther. Targets* **2003**, *7* (3), 311.

Boucher, H. W.; Talbot, G. H.; Bradley, J. S.; Edwards, J. E.; Gilbert, D.; Rice, L. B.; Scheld, M.; Spellberg, B.; Bartlett, J. *Clin. Infect. Dis.* **2009**, *48* (1), 1.

Bowler, P. G.; Duerden, B. I.; Armstrong, D. G. *Clin. Microbiol. Rev.* **2001**, *14* (2), 244.

Brenner, J. S.; Pan, D. C.; Myerson, J. W.; Marcos-Contreras, O. A.; Villa, C. H.; Patel, P.; Hekierski, H.; Chatterjee, S.; Tao, J.-Q.; Parhiz, H.; Bhamidipati, K.; Uhler, T. G.; Hood, E. D.; Kiseleva, R. Y.; Shuvaev, V. S.; Shuvaeva, T.; Khoshnejad, M.; Johnston, I.; Gregory, J. V; Lahann, J.; Wang, T.; Cantu, E.; Armstead, W. M.; Mitragotri, S.; Muzykantov, V. *Nat. Commun.* **2018**, *9* (1), 2684.

Bresee, J.; Bond, C. M.; Worthington, R. J.; Smith, C. A.; Gifford, J. C.; Simpson, C. A.; Carter, C. J.; Wang, G.; Hartman, J.; Osbaugh, N. A.; Shoemaker, R. K.; Melander, C.; Feldheim, D. L. *J. Am. Chem. Soc.* **2014**, *136* (14), 5295.

Bresee, J.; Maier, K. E.; Boncella, A. E.; Melander, C.; Feldheim, D. L. *Small* **2011**, *7* (14), 2027.

Brooks, B. D.; Brooks, A. E. *Adv. Drug Deliv. Rev.* **2014**, *78*, 14.

Brown, E. D.; Wright, G. D. *Nature* **2016**, *529*, 336.

Brust, M.; Walker, M.; Bethell, D.; Schiffrin, D. J.; Whyman, R. *J. Chem. Soc. Chem. Commun.* **1994**, No. 7, 801.

Bryers, J. D. *Biotechnol. Bioeng.* **2008**, *100* (1), 1.

Bush, K.; Courvalin, P.; Dantas, G.; Davies, J.; Eisenstein, B.; Huovinen, P.; Jacoby, G. A.; Kishony, R.; Kreiswirth, B. N.; Kutter, E.; Lerner, S. A.; Levy, S.; Lewis, K.; Lomovskaya, O.; Miller, J. H.; Mobashery, S.; Piddock, L. J. V.; Projan, S.; Thomas, C. M.; Tomasz, A.; Tulkens, P. M.; Walsh, T. R.; Watson, J. D.; Witkowski, J.; Witte, W.; Wright, G.; Yeh, P.; Zgurskaya, H. I. *Nature Reviews Microbiology*. England November 2011, pp 894–896.

Cafiso, V.; Bertuccio, T.; Spina, D.; Purrello, S.; Stefani, S. *FEMS Immunol. Med. Microbiol.* **2010**, *59* (3), 466.

Capeletti, L. B.; De Oliveira, L. F.; Gonçalves, K. D. A.; De Oliveira, J. F. A.; Saito, Â.; Kobarg, J.; Santos, J. H. Z. Dos; Cardoso, M. B. *Langmuir* **2014**, *30* (25), 7456.

Center for Disease Dynamics Economics & Policy. *Cent. Dis. Dyn. Econ. Policy, CDDEP Washington, D.C* **2015**, *8* (2), 1.

Center for Disease Dynamics Economics & Policy. *Cent. Dis. Dyn. Econ. Policy, CDDEP Washington, D.C* **2015**, *8* (2), 1.

Centers for Disease Control and Prevention. **2003**.

Ceri, H.; Olson, M. E.; Stremick, C.; Read, R. R.; Morck, D.; Buret, A. *J. Clin. Microbiol.* **1999**, *37* (6), 1771.

Chambers, E.; Mitragotri, S. *Exp. Biol. Med. (Maywood).* **2007**, *232* (7), 958.

Chang, Y.; McLandsborough, L.; McClements, D. J. *Food Chem.* **2015**, *172*, 298.

Chen, C.; Liu, G.; Liu, X.; Pang, S.; Zhu, C.; Lv, L.; Ji, J. *Polym. Chem.* **2011**, *2* (6), 1389.

Choi, S.; Isaacs, A.; Clements, D.; Liu, D.; Kim, H.; Scott, R. W.; Winkler, J. D.; DeGrado, W. F. *Proc. Natl. Acad. Sci.* **2009**, *106* (17), 6968.

Christena, L. R.; Mangalagowri, V.; Pradheeba, P.; Ahmed, K. B. A.; Shalini, B. I. S.; Vidyalakshmi, M.; Anbazhagan, V.; Subramanian, N. S. *RSC Adv.* **2015**, *5* (17), 12899.

Chu, L.; Gao, H.; Cheng, T.; Zhang, Y.; Liu, J.; Huang, F.; Yang, C.; Shi, L.; Liu, J. *Chem. Commun.* **2016**, *52* (37), 6265.

Costerton, J. W. *Int J Antimicrob Agents* **1999**, *11*.

Costerton, J. W.; Post, J. C.; Ehrlich, G. D.; Hu, F. Z.; Kreft, R.; Nistico, L.; Kathju, S.; Stoodley, P.; Hall-Stoodley, L.; Maale, G.; James, G.; Sotereanos, N.; DeMeo, P. *FEMS Immunol. Med. Microbiol.* **2011**, *61* (2), 133.

Costerton, W.; Veeh, R.; Shirtliff, M.; Pasmore, M.; Post, C.; Ehrlich, G. *J. Clin. Invest.* **2003**, *112* (10), 1466.

Courvalin, P. *Clin. Infect. Dis.* **2006**, *42 Suppl 1*, S25.

Cox, S. D.; Mann, C. M.; Markham, J. L.; Bell, H. C.; Gustafson, J. E.; Warmington, J. R.; Wyllie, S. G. *J. Appl. Microbiol.* **2000**, *88* (1), 170.

Cui, L.; Iwamoto, A.; Lian, J.-Q.; Neoh, H.; Maruyama, T.; Horikawa, Y.; Hiramatsu, K. *Antimicrob. Agents Chemother.* **2006**, *50* (2), 428.

Daddi Oubekka, S.; Briandet, R.; Fontaine-Aupart, M.-P.; Steenkeste, K. *Antimicrob. Agents Chemother.* **2012**, *56* (6), 3349.

Dafopoulou, K.; Xavier, B. B.; Hotterbeekx, A.; Janssens, L.; Lammens, C.; De, E.; Goossens, H.; Tsakris, A.; Malhotra-Kumar, S.; Pournaras, S. *Antimicrob. Agents Chemother.* **2015**, *60* (3), 1892.

Daniel, M.-C.; Astruc, D. *Chem. Rev.* **2004**, *104* (1), 293.

Das, R.; Landis, R. F.; Tonga, G. Y.; Cao-Milán, R.; Luther, D. C.; Rotello, V. M. *ACS Nano* **2019**, *13* (1), 229.

Dathe, M.; Wieprecht, T.; Nikolenko, H.; Handel, L.; Maloy, W. L.; MacDonald, D. L.; Beyermann, M.; Bienert, M. *FEBS Lett.* **1997**, *403* (2), 208.Davies, J.; Wright, G. D. *Trends Microbiol.* **1997**, *5* (6), 234.

Davis, M. E.; Chen, Z.; Shin, D. M. *Nat. Rev. Drug Discov.* **2008**, *7* (9), 771.

De, M.; Ghosh, P. S.; Rotello, V. M. *Adv. Mater.* **2008**, *20* (22), 4225.

Death, A.; Notley, L.; Ferenci, T. *J. Bacteriol.* **1993**, *175* (5), 1475.

Decker, T.; Lohmann-Matthes, M. L. *J. Immunol. Methods* **1988**, *115* (1), 61.

Delcour, A. H. *Biochim. Biophys. Acta* **2009**, *1794* (5), 808.

Dizaj, S. M.; Lotfipour, F.; Barzegar-Jalali, M.; Zarrintan, M. H.; Adibkia, K. *Mater. Sci. Eng. C* **2014**, *44*, 278.

Dong, H.; Huang, J.; Koepsel, R. R.; Ye, P.; Russell, A. J.; Matyjaszewski, K. *Biomacromolecules* **2011**, *12* (4), 1305.

Donlan, R. M. *Emerg. Infect. Dis.* **2001**, *7* (2), 277.

Du, L.; Qin, H.; Ma, T.; Zhang, T.; Xing, D. *ACS Nano* **2017**, *11* (9), 8930.

Duncan, B.; Kim, C.; Rotello, V. M. *J. Control. Release* **2010**, *148* (1), 122.

Duncan, B.; Landis, R. F.; Jerri, H. A.; Normand, V.; Benczédi, D.; Ouali, L.; Rotello, V. M. *Small* **2015**, *11* (11), 1302.

Duncan, B.; Li, X.; Landis, R. F.; Kim, S. T.; Gupta, A.; Wang, L. S.; Ramanathan, R.; Tang, R.; Boerth, J. A.; Rotello, V. M. *ACS Nano* **2015**, *9* (8), 7775.

Fabrega, J.; Luoma, S. N.; Tyler, C. R.; Galloway, T. S.; Lead, J. R. *Environ. Int.* **2011**, *37* (2), 517.

Fabrega, J.; Renshaw, J. C.; Lead, J. R. *Environ. Sci. Technol.* **2009**, *43* (23), 9004.

Falagas, M. E.; Kasiakou, S. K. *Clin. Infect. Dis.* **2005**, *40* (9), 1333.

Farzaei, M. H.; Bahramsoltani, R.; Abbasabadi, Z.; Rahimi, R. *J. Pharm. Pharmacol.* **2015**, *67* (11), 1467.

Fayaz AM Girilal M, Yadav R, Kalaichelvan PT, Venketesan R, B. K. *Nanomedicine* **2010**, *6(1)* (1), 103.

Feng, Z. V.; Gunsolus, I. L.; Qiu, T. A.; Hurley, K. R.; Nyberg, L. H.; Frew, H.; Johnson, K. P.; Vartanian, A. M.; Jacob, L. M.; Lohse, S. E.; Torelli, M. D.; Hamers, R. J.; Murphy, C. J.; Haynes, C. L. *Chem. Sci.* **2015**, *6* (9), 5186.

Forier, K.; Raemdonck, K.; De Smedt, S. C.; Demeester, J.; Coenye, T.; Braeckmans, K. *J. Control. Release* **2014**, *190*, 607.

Freire Rocha Caldas, G.; Araujo, A. V.; Albuquerque, G. S.; Silva-Neto, J. da C.; Costa-Silva, J. H.; de Menezes, I. R. A.; Leite, A. C. L.; da Costa, J. G. M.; Wanderley, A. G. *Evid. Based. Complement. Alternat. Med.* **2013**, *2013*, 856168.

Fröhlich, E. *Int. J. Nanomedicine* **2012**, *7*, 5577.

Fux, C. A.; Costerton, J. W.; Stewart, P. S.; Stoodley, P. *Trends Microbiol.* **2005**, *13* (1), 34.

Fux, C. A.; Stoodley, P.; Hall-Stoodley, L.; Costerton, J. W. *Expert Rev. Anti. Infect. Ther.* **2003**, *1* (4), 667.

Gabriel, G. J.; Madkour, A. E.; Dabkowski, J. M.; Nelson, C. F.; Nüsslein, K.; Tew, G. N. *Biomacromolecules* **2008**, *9* (11), 2980.

Gao, W.; Chen, Y.; Zhang, Y.; Zhang, Q.; Zhang, L. *Adv. Drug Deliv. Rev.* **2018**, *127*, 46.

Gauthier, A.; Puente, J. L.; Finlay, B. B. *Infect. Immun.* **2003**, *71* (6), 3310.

Ghosh, P.; Han, G.; De, M.; Kim, C. K.; Rotello, V. M. *Adv. Drug Deliv. Rev.* **2008**, *60* (11), 1307.

Ghuysen, J.-M. *Trends Microbiol.* **1994**, *2* (10), 372.

Giri, K.; Rivas Yepes, L.; Duncan, B.; Kolumam Parameswaran, P.; Yan, B.; Jiang, Y.; Bilska, M.; Moyano, D.; Thompson, M. A.; Rotello, V. M.; Prakash, Y. S. *RSC Adv.* **2015**.

Goodman, C. M.; McCusker, C. D.; Yilmaz, T.; Rotello, V. M. *Bioconjug. Chem.* **2004**, *15* (4), 897.

Gu, H.; Ho, P. L.; Tong, E.; Wang, L.; Xu, B. *Nano Lett.* **2003**, *3* (9), 1261.

Gupta, A.; Das, R.; Yesilbag Tonga, G.; Mizuhara, T.; Rotello, V. M. *ACS Nano* **2018**, *12* (1), 89.

Gupta, A.; Landis, R. F.; Li, C. H.; Schnurr, M.; Das, R.; Lee, Y. W.; Yazdani, M.; Liu, Y.; Kozlova, A.; Rotello, V. M. *J. Am. Chem. Soc.* **2018**, *140* (38), 12137.

Gupta, A.; Landis, R. F.; Rotello, V. M. *F1000Research* **2016**, *5* (0), 364.

Gupta, A.; Landis, R. F.; Rotello, V. M. *F1000Research* **2016**, *5* (364), 364.

Gupta, A.; Mumtaz, S.; Li, C.-H.; Hussain, I.; Rotello, V. M. *Chem. Soc. Rev.* **2018**, *48* (2), 415.

Gupta, A.; Saleh, N. M.; Das, R.; Landis, R. F.; Bigdeli, A.; Motamedchaboki, K.; Campos, A. R.; Pomeroy, K.; Mahmoudi, M.; Rotello, V. M. *Nano Futur.* **2017**, *1* (1), 015004.

Gustafson, H. H.; Holt-Casper, D.; Grainger, D. W.; Ghandehari, H. *Nano Today* **2015**, *10* (4), 487.

Habimana, O.; Steenkeste, K.; Fontaine-Aupart, M.-P.; Bellon-Fontaine, M.-N.; Kulakauskas, S.; Briandet, R. *Appl. Environ. Microbiol.* **2011**, *77* (1), 367.

Halder, S.; Yadav, K. K.; Sarkar, R.; Mukherjee, S.; Saha, P.; Haldar, S.; Karmakar, S.; Sen, T. *Springerplus* **2015**, *4*, 672.

Hall-Stoodley, L.; Hu, F. Z.; Gieseke, A.; Nistico, L.; Nguyen, D.; Hayes, J.; Forbes, M.; Greenberg, D. P.; Dice, B.; Burrows, A.; Wackym, P. A.; Stoodley, P.; Post, J. C.; Ehrlich, G. D.; Kerschner, J. E. *J. Am. Med. Assoc.* **2006**, *296* (2), 202.

Hall-Stoodley, L.; Stoodley, P.; Kathju, S.; Høiby, N.; Moser, C.; William Costerton, J.; Moter, A.; Bjarnsholt, T. *FEMS Immunol. Med. Microbiol.* **2012**, *65* (2), 127.

Han, H. K.; Amidon, G. L. *AAPS PharmSci* **2000**, *2* (1), E6.

Han, X.; Wang, C.; Liu, Z. *Bioconjug. Chem.* **2018**, *29* (4), 852.

Hancock, R. E. W.; Sahl, H. G. *Nat Biotech* **2006**, *24* (12), 1551.

Harris, S. R.; Feil, E. J.; Holden, M. T. G.; Quail, M. A.; Nickerson, E. K.; Chantratita, N.; Gardete, S.; Tavares, A.; Day, N.; Lindsay, J. A.; Edgeworth, J. D.; de Lencastre, H.; Parkhill, J.; Peacock, S. J.; Bentley, S. D. *Science (80-.).* **2010**, *327* (5964), 469.

Harrison, J. J.; Stremick, C. A.; Turner, R. J.; Allan, N. D.; Olson, M. E.; Ceri, H. *Nat. Protoc.* **2010**, *5* (7), 1236.

Hayden, S. C.; Zhao, G.; Saha, K.; Phillips, R. L.; Li, X.; Miranda, O. R.; Rotello, V. M.; El-Sayed, M. A.; Schmidt-Krey, I.; Bunz, U. H. F. *J. Am. Chem. Soc.* **2012**, *134* (16), 6920.

Helander, I. M.; Mattila-Sandholm, T. *J. Appl. Microbiol.* **2000**, *88* (2), 213.

Hentzer, M.; Wu, H.; Andersen, J. B.; Riedel, K.; Rasmussen, T. B.; Bagge, N.; Kumar, N.; Schembri, M. A.; Song, Z.; Kristoffersen, P.; Manefield, M.; Costerton, J. W.; Molin, S.; Eberl, L.; Steinberg, P.; Kjelleberg, S.; Hoiby, N.; Givskov, M. *EMBO J.* **2003**, *22* (15), 3803.

Hetrick, E. M.; Shin, J. H.; Paul, H. S.; Schoenfisch, M. H. *Biomaterials* **2009**, *30* (14), 2782.

Higgins, M. K.; Bokma, E.; Koronakis, E.; Hughes, C.; Koronakis, V. *Proc. Natl. Acad. Sci. United States Am.* **2004**, *101* (27), 9994.

Hintz, T.; Matthews, K. K.; Di, R. *Biomed Res. Int.* **2015**, *2015*, 246264.

Hiramatsu, K.; Cui, L.; Kuroda, M.; Ito, T. *Trends Microbiol.* **2001**, *9* (10), 486.

Høiby, N.; Bjarnsholt, T.; Givskov, M.; Molin, S.; Ciofu, O. *Int. J. Antimicrob. Agents* **2010**, *35* (4), 322.

Hong, T.; Smith Moland, E.; Abdalhamid, B.; Hanson, N. D.; Wang, J.; Sloan, C.; Fabian, D.; Farajallah, A.; Levine, J.; Thomson, K. S. *Clin. Infect. Dis.* **2005**, *40* (10), e84.

Hosseinkhani, F.; Jabalameli, F.; Banar, M.; Abdellahi, N.; Taherikalani, M.; Leeuwen, W. B. van; Emaneini, M. *Rev. Soc. Bras. Med. Trop.* **2016**, *49* (2), 172.

Hostetler, M. J.; Templeton, A. C.; Murray, R. W. *Langmuir* **1999**, *15* (11), 3782.

Hu, C.-M. J.; Fang, R. H.; Copp, J.; Luk, B. T.; Zhang, L. *Nat. Nanotechnol.* **2013**, *8*, 336.

Hua, L.; Cohen, T. S.; Shi, Y.; Datta, V.; Hilliard, J. J.; Tkaczyk, C.; Suzich, J.; Stover, C. K.; Sellman, B. R. *Antimicrob. Agents Chemother.* **2015**, *59* (8), 4526.

Huang, D. W.; Sherman, B. T.; Lempicki, R. A. *Nucleic Acids Res.* **2009**, *37* (1), 1.

Huma, Z.; Gupta, A.; Javed, I.; Das, R.; Hussain, S. Z.; Mumtaz, S.; Hussain, I.; Rotello, V. M. *ACS Omega* **2018**, *3* (12), 16721.

Huo, S.; Jiang, Y.; Gupta, A.; Jiang, Z.; Landis, R. F.; Hou, S.; Liang, X. J.; Rotello, V. M. *ACS Nano* **2016**, *10* (9), 8732.

Hussain, S. M.; Hess, K. L.; Gearhart, J. M.; Geiss, K. T.; Schlager, J. J. *Toxicol. In Vitro* **2005**, *19* (7), 975.

Ikuma, K.; Madden, A. S.; Decho, A. W.; Lau, B. L. T. *Environ. Sci. Nano* **2014**, *1* (2), 117.

Ilker, M. F.; Nüsslein, K.; Tew, G. N.; Coughlin, E. B. *J. Am. Chem. Soc.* **2004**, *126* (48), 15870.

Jacobson, K. H.; Gunsolus, I. L.; Kuech, T. R.; Troiano, J. M.; Melby, E. S.; Lohse, S. E.; Hu, D.; Chrisler, W. B.; Murphy, C. J.; Orr, G.; Geiger, F. M.; Haynes, C. L.; Pedersen, J. A. *Environ. Sci. Technol.* **2015**, *49* (17), 10642.

Jain, A.; Duvvuri, L. S.; Farah, S.; Beyth, N.; Domb, A. J.; Khan, W. *Adv. Healthc. Mater.* **2014**, *3* (12), 1969.

James, G. A.; Swogger, E.; Wolcott, R.; Pulcini, E. D.; Secor, P.; Sestrich, J.; Costerton, J. W.; Stewart, P. S. *Wound Repair Regen.* **2008**, *16* (1), 37.

Javani, S.; Lorca, R.; Latorre, A.; Flors, C.; Cortajarena, A. L.; Somoza, Á. *ACS Appl. Mater. Interfaces* **2016**, *8* (16), 10147.

Jayawardana, K. W.; Jayawardena, H. S. N.; Wijesundera, S. A.; De Zoysa, T.; Sundhoro, M.; Yan, M. *Chem. Commun.* **2015**, *51* (60), 12028.

Jernberg, C.; Lofmark, S.; Edlund, C.; Jansson, J. K. *Microbiology* **2010**, *156* (Pt 11), 3216.

Jiang, Z.; Vasil, A. I.; Gera, L.; Vasil, M. L.; Hodges, R. S. *Chem. Biol. Drug Des.* **2011**, *77* (4), 225.

Jones, N.; Ray, B.; Ranjit, K. T.; Manna, A. C. *FEMS Microbiol. Lett.* **2008**, *279* (1), 71.

K., B.; P., C.; G., D.; J., D.; B., E.; P., H.; G.A., J.; R., K.; B.N., K.; E., K.; S.A., L.; S., L.; K., L.; O., L.; J.H., M.; S., M.; L.J.V., P.; S., P.; C.M., T.; A., T.; P.M., T.; T.R., W.; J.D., W.; J., W.; W., W.; G., W.; P., Y.; H.I., Z. *Nat. Rev. Microbiol.* **2011**, *9* (12), 894.

Katz, E.; Willner, I. *Angew. Chemie - Int. Ed.* **2004**, *43* (45), 6042.

Kell, A. J.; Stewart, G.; Ryan, S.; Peytavi, R.; Boissinot, M.; Huletsky, A.; Bergeron, M. G.; Simard, B. *ACS Nano* **2008**, *2* (9), 1777.

Kim Lewis. *Nat. Rev. Microbiol.* **2007**, *5* (1), 48.

Kim, C. S.; Duncan, B.; Creran, B.; Rotello, V. M. *Nano Today* **2013**, *8* (4), 439.

Kim, J.-W.; Shashkov, E. V; Galanzha, E. I.; Kotagiri, N.; Zharov, V. P. *Lasers Surg. Med.* **2007**, *39* (7), 622.

Kim, J. S.; Kuk, E.; Yu, K. N.; Kim, J.-H.; Park, S. J.; Lee, H. J.; Kim, S. H.; Park, Y. K.; Park, Y. H.; Hwang, C.-Y.; Kim, Y.-K.; Lee, Y.-S.; Jeong, D. H.; Cho, M.-H. *Nanomedicine Nanotechnology, Biol. Med.* **2007**, *3* (1), 95.

Knetsch, M. L. W.; Koole, L. H. *Polymers*. 2011, pp 340–366.

Knoll, B. M.; Mylonakis, E. *Clin. Infect. Dis.* **2014**, *58* (4), 528.

Koebnik, R.; Locher, K. P.; Van Gelder, P. *Mol. Microbiol.* **2000**, *37* (2), 239.

Kohanski, M. A.; DePristo, M. A.; Collins, J. J. *Mol. Cell* **2010**, *37* (3), 311.

Kon, K. V.; Rai, M. K. *Expert Rev. Anti. Infect. Ther.* **2012**, *10* (7), 775.

Kostakioti, M.; Hadjifrangiskou, M.; Hultgren, S. J. *Cold Spring Harb. Perspect. Med.* **2013**, *3* (4), a010306.

Kresge, C. T.; Leonowicz, M. E.; Roth, W. J.; Vartuli, J. C.; Beck, J. S. *Nature* **1992**, *359* (6397), 710.

Kubacka, A.; Diez, M. S.; Rojo, D.; Bargiela, R.; Ciordia, S.; Zapico, I.; Albar, J. P.; Barbas, C.; Martins dos Santos, V. A. P.; Fernández-García, M.; Ferrer, M. *Sci. Rep.* **2014**, *4*, 4134.

Kujath, P.; Kujath, C. *Eur. J. Med. Res.* **2010**, *15* (12), 544.

Kunishima, H. *Nihon Naika Gakkai Zasshi* **2014**, *102* (11), 2839.

Kuroda, K.; Caputo, G. A. *Wiley Interdiscip. Rev. Nanomedicine Nanobiotechnology* **2013**, *5* (1), 49.

Kuroda, K.; Caputo, G. A.; DeGrado, W. F. *Chem. - A Eur. J.* **2009**, *15* (5), 1123.

Kuroda, K.; DeGrado, W. F. *J. Am. Chem. Soc.* **2005**, *127* (12), 4128.

Lam, S. J.; O'Brien-Simpson, N. M.; Pantarat, N.; Sulistio, A.; Wong, E. H. H.; Chen, Y. Y.; Lenzo, J. C.; Holden, J. A.; Blencowe, A.; Reynolds, E. C.; Qiao, G. G. *Nat. Microbiol.* **2016**, *1*, 16162.

Lambert, P. A. *Adv. Drug Deliv. Rev.* **2005**, *57* (10), 1471.

Landis, R. F.; Gupta, A.; Lee, Y. W.; Wang, L. S.; Golba, B.; Couillaud, B.; Ridolfo, R.; Das, R.; Rotello, V. M. *ACS Nano* **2017**, *11* (1), 946.

Landis, R. F.; Li, C. H.; Gupta, A.; Lee, Y. W.; Yazdani, M.; Ngernyuang, N.; Altinbasak, I.; Mansoor, S.; Khichi, M. A. S.; Sanyal, A.; Rotello, V. M. *J. Am. Chem. Soc.* **2018**, *140* (19), 6176.

Langdon, A.; Crook, N.; Dantas, G. *Genome Med.* **2016**, *8* (1), 39.

Laxminarayan, R.; Duse, A.; Wattal, C.; Zaidi, A. K. M.; Wertheim, H. F. L.; Sumpradit, N.; Vlieghe, E.; Hara, G. L.; Gould, I. M.; Goossens, H.; Greko, C.; So, A. D.; Bigdeli, M.; Tomson, G.; Woodhouse, W.; Ombaka, E.; Peralta, A. Q.; Qamar, F. N.; Mir, F.; Kariuki, S.; Bhutta, Z. A.; Coates, A.; Bergstrom, R.; Wright, G. D.; Brown, E. D.; Cars, O. *Lancet Infect. Dis.* **2017**, *13* (12), 1057.

Lee, J. H.; Jeong, S. H.; Cha, S.-S.; Lee, S. H. *Nat. Rev. Drug Discov.* **2007**, *6*, 938.

Leeson, P. D.; Springthorpe, B. *Nature reviews. Drug discovery*. England November 2007, pp 881–890.

Levy, S. B.; Bonnie, M. *Nat. Med.* **2004**, *10* (12S), S122.

Lewis, K. *Antimicrob. Agents Chemother.* **2001**, *45* (4), 999.

Li, B.; Webster, T. J. *J. Orthop. Res.* **2018**, *36* (1), 22.

Li, J.; Zhang, K.; Ruan, L.; Chin, S. F.; Wickramasinghe, N.; Liu, H.; Ravikumar, V.; Ren, J.; Duan, H.; Yang, L.; Chan-Park, M. B. *Nano Lett.* **2018**, *18* (7), 4180.

Li, L. L.; Xu, J. H.; Qi, G. Bin; Zhao, X.; Yu, F.; Wang, H. *ACS Nano* **2014**, *8* (5), 4975.

Li, L.; Xu, B. *Curr. Pharm. Des.* **2005**, *11* (24), 3111.

Li, X.-Z.; Nikaido, H. *Drugs* **2004**, *64* (2), 159.

Li, X.; Yeh, Y.-C.; Giri, K.; Mout, R.; Landis, R. F.; Prakash, Y. S.; Rotello, V. M. *Chem. Commun.* **2015**, *51* (2), 282.

Lienkamp, K.; Madkour, A. E.; Musante, A.; Nelson, C. F.; Nüsslein, K.; Tew, G. N. *J. Am. Chem. Soc.* **2008**, *130* (30), 9836.

Lin, C. C.; Yeh, Y. C.; Yang, C. Y.; Chen, C. L.; Chen, G. F.; Chen, C. C.; Wu, Y. C. *J. Am. Chem. Soc.* **2002**, *124* (14), 3508.

Ling, L.; Schneder, T.; Peoples, A.; Spoering, A.; Engels, I.; Conlon, B.; Mueller, A.; Schaberle, T.; Hughes, D.; Epstein, S.; Jones, M.; Lazarides, L.; Steadman, V.; Cohen, D.; Felix, C.; Fetterman, K.; Millett, W.; Nitti, A.; Zullo, A.; Chen, C.; Lewis, K. *Nature* **2015**, *517* (7535), 455.

Livermore, D. M. *Clin. Microbiol. Rev.* **1995**, *8* (4), 557.

Los, F. C. O.; Randis, T. M.; Aroian, R. V; Ratner, A. J. *Microbiol. Mol. Biol. Rev.* **2013**, *77* (2), 173.

Love, C.; Tomas, M. B.; Tronco, G. G.; Palestro, C. J. *RadioGraphics* **2005**, *25* (5), 1357.

Lynch, A. S.; Robertson, G. T. *Annu. Rev. Med.* **2008**, *59*, 415.

MacNair, C. R.; Stokes, J. M.; Carfrae, L. A.; Fiebig-Comyn, A. A.; Coombes, B. K.; Mulvey, M. R.; Brown, E. D. *Nat. Commun.* **2018**, *9* (1), 458.

Madkour, A. E.; Koch, A. H. R.; Lienkamp, K.; Tew, G. N. *Macromolecules* **2010**, *43* (10), 4557.

Mah, T. *Future Microbiol.* **2012**, *7* (9), 1061.

Mahmoudi, M.; Serpooshan, V. *ACS Nano* **2012**, *6* (3), 2656.

Maia, M. F.; Moore, S. J. *Malar. J.* **2011**, *10 Suppl 1* (Suppl 1), S11.

Malléa, M.; Chevalier, J.; Eyraud, A.; Pagès, J.-M. *Biochem. Biophys. Res. Commun.* **2002**, *293* (5), 1370.

Marr, A. K.; Gooderham, W. J.; R.E.W., H. *Curr. Opin. Pharmacol.* **2006**, *6* (5), 468.

Matsuzaki, K.; Sugishita, K. I.; Fujii, N.; Miyajima, K. *Biochemistry* **1995**, *34* (10), 3423.

McNulty, C.; Thompson, J.; Barrett, B.; Lord, L.; Andersen, C.; Roberts, I. S. *Mol. Microbiol.* **2006**, *59* (3), 907.

Meers, P.; Neville, M.; Malinin, V.; Scotto, A. W.; Sardaryan, G.; Kurumunda, R.; Mackinson, C.; James, G.; Fisher, S.; Perkins, W. R. *J. Antimicrob. Chemother.* **2008**, *61* (4), 859.

Mei, L.; Lu, Z.; Zhang, X.; Li, C.; Jia, Y. *ACS Appl. Mater. Interfaces* **2014**, *6* (18), 15813.

Meletis, G. *Ther. Adv. Infect. Dis.* **2016**, *3* (1), 15.

Miller, K. P.; Wang, L.; Benicewicz, B. C.; Decho, A. W. *Chem. Soc. Rev.* **2015**, *44* (21), 7787.

Mittal, R. P.; Rana, A.; Jaitak, V. *Curr. Drug Targets* **2019**, *20* (6), 605.

Moriarty, T. F.; Elborn, J. S.; Tunney, M. M. *Br. J. Biomed. Sci.* **2007**, *64* (3), 101.

Mowery, B. P.; Lee, S. E.; Kissounko, D. A.; Epand, R. F.; Epand, R. M.; Weisblum, B.; Stahl, S. S.; Gellman, S. H. *J. Am. Chem. Soc.* **2007**, *129* (50), 15474.

Moyano, D. F.; Rotello, V. M. *Langmuir* **2011**, *27* (17), 10376.

Moyano, D. F.; Liu, Y.; Ayaz, F.; Duncan, B.; Osborne, B. A.; Rotello, V. M. *Chem* **2016**, *1* (2), 320.

Muñoz-Bonilla, A.; Fernández-García, M. *Prog. Polym. Sci.* **2012**, *37* (2), 281.

Muzykantov, V. R. *Expert Opin. Drug Deliv.* **2010**, *7* (4), 403.

Natan, M.; Gutman, O.; Lavi, R.; Margel, S.; Banin, E. *ACS Nano* **2015**, *9* (2), 1175.

Nederberg, F.; Zhang, Y.; Tan, J. P. K.; Xu, K.; Wang, H.; Yang, C.; Gao, S.; Guo, X. D.; Fukushima, K.; Li, L.; Hedrick, J. L.; Yang, Y. Y. *Nat. Chem.* **2011**, *3* (5), 409.

Ng, V. W. L.; Ke, X.; Lee, A. L. Z.; Hedrick, J. L.; Yang, Y. Y. *Adv. Mater.* **2013**, *25* (46), 6730.

Ngo, J. T.; Adams, S. R.; Deerinck, T. J.; Boassa, D.; Rodriguez-Rivera, F.; Palida, S. F.; Bertozzi, C. R.; Ellisman, M. H.; Tsien, R. Y. *Nat. Chem. Biol.* **2016**, *12* (6), 459.

Nickel, J. C.; Ruseska, I.; Wright, J. B.; Costerton, J. W. *Antimicrob. Agents Chemother.* **1985**, *27* (4), 619.

Nikaido, H. *Clin. Infect. Dis.* **1998**, *27 Suppl 1*, S32.

Nikaido, H. *Science (80-.).* **1994**, *264* (5157), 382.

Ning, X.; Lee, S.; Wang, Z.; Kim, D.; Stubblefield, B.; Gilbert, E.; Murthy, N. *Nat Mater* **2011**, *10* (8), 602.

Nirmala Grace, A.; Pandian, K. *Colloids Surfaces A Physicochem. Eng. Asp.* **2007**, *297* (1–3), 63.

Nordmann, P.; Naas, T.; Fortineau, N.; Poirel, L. *Curr. Opin. Microbiol.* **2007**, *10* (5), 436.

Norrby, S. R. *J. Antimicrob. Chemother.* **2002**, *45* (1), 5.

Ochman, H.; Lawrence, J. G.; Groisman, E. A. *Nature* **2000**, *405* (6784), 299.

O'Connell, K. M. G.; Hodgkinson, J. T.; Sore, H. F.; Welch, M.; Salmond, G. P. C.; Spring, D. R. *Angew. Chemie Int. Ed.* **2013**, *52* (41), 10706.

Odds, F. C. *J. Antimicrob. Chemother.* **2003**, *52* (1), 1.

Okamoto, Y.; Kojima, R.; Schwizer, F.; Bartolami, E.; Heinisch, T.; Matile, S.; Fussenegger, M.; Ward, T. R. *Nat. Commun.* **2018**, *9* (1), 1943.

Oliver, A.; Cantón, R.; Campo, P.; Baquero, F.; Blázquez, J. *Science (80-.).* **2000**, *288* (5469), 1251.

O'Reilly, E.; Lanza, J. *Ecology* **1995**, *76* (8), 2656.

Orf, K.; Cunnington, A. J. *Front. Microbiol.* **2015**, *6*, 666.

Owens, D. E.; Peppas, N. A. *Int. J. Pharm.* **2006**, *307* (1), 93.

Paixão, L.; Rodrigues, L.; Couto, I.; Martins, M.; Fernandes, P.; de Carvalho, C. C. C. R.; Monteiro, G. A.; Sansonetty, F.; Amaral, L.; Viveiros, M. *J. Biol. Eng.* **2009**, *3*, 18.

Palermo, E. F.; Kuroda, K. *Appl. Microbiol. Biotechnol.* **2010**, *87* (5), 1605.

Palermo, E. F.; Vemparala, S.; Kuroda, K. *ACS Symp. Ser.* **2013**, *1135* (1), 319.

Pantos, A.; Tsogas, I.; Paleos, C. M. *Biochim. Biophys. Acta* **2008**, *1778* (4), 811.

Park, S. K.; Venable, J. D.; Xu, T.; Yates, J. R. *Nat. Methods* **2008**, *5* (4), 319.

Parker, C. T.; Pradel, E.; Schnaitman, C. A. *J. Bacteriol.* **1992**, *174* (3), 930.

Parsons, B.; Strauss, E. *Am. J. Surg.* **2004**, *188* (1 SUPPL. 1), 57.

Patch, J. A.; Barron, A. E. *J. Am. Chem. Soc.* **2003**, *125* (40), 12092.

Peer, D.; Karp, J. M.; Hong, S.; Farokhzad, O. C.; Margalit, R.; Langer, R. *Nat. Nanotechnol.* **2007**, *2* (12), 751.

Peulen, T. O.; Wilkinson, K. J. *Environ. Sci. Technol.* **2011**, *45* (8), 3367.

Pierson, E.; Hung, D. T.; Clatworthy, A. E. *Nat. Chem. Biol.* **2007**, *3* (9), 541.

Pillai, P. P.; Kowalczyk, B.; Kandere-Grzybowska, K.; Borkowska, M.; Grzybowski, B. A. *Angew. Chemie - Int. Ed.* **2016**, *55* (30), 8610.

Pires, D. P.; Vilas Boas, D.; Sillankorva, S.; Azeredo, J. *J. Virol.* **2015**, *89* (15), 7449.

Pirofski, L.; Casadevall, A. *Infect. Immun.* **1999**, *67* (8), 3703.

Plesiat, P.; Nikaido, H. *Mol. Microbiol.* **1992**, *6* (10), 1323.

Pornpattananangkul, D.; Zhang, L.; Olson, S.; Aryal, S.; Obonyo, M.; Vecchio, K.; Huang, C.-M.; Zhang, L. *J. Am. Chem. Soc.* **2011**, *133* (11), 4132.

Pozo, J. L. Del; Patel, R. *N Engl J Med* **2009**, *361* (8), 787.

Prabhu, S.; Poulose, E. K. *Int. Nano Lett.* **2012**, *2* (1), 32.

Primožič, M.; Knez, Ž.; Pandey, J. K.; Leitgeb, M. *SCIREA J. Clin. Med.* **2018**, *3* (1), 1.

Radovic-Moreno, A. F.; Lu, T. K.; Puscasu, V. A.; Yoon, C. J.; Langer, R.; Farokhzad, O. C. *ACS Nano* **2012**, *6* (5), 4279.

Raghupathi, K. R.; Koodali, R. T.; Manna, A. C. *Langmuir* **2011**, *27* (7), 4020.

Rahme, L. G.; Stevens, E. J.; Wolfort, S. F.; Shao, J.; Tompkins, R. G.; Ausubel, F. M. *Science (80-.).* **1995**, *268* (5219), 1899.

Rai, A.; Pinto, S.; Velho, T. R.; Ferreira, A. F.; Moita, C.; Trivedi, U.; Evangelista, M.; Comune, M.; Rumbaugh, K. P.; Simões, P. N.; Moita, L.; Ferreira, L. *Biomaterials* **2016**, *85* (June), 99.

Rajalingam, K.; Al-Younes, H.; Müller, A.; Meyer, T. F.; Szczepek, A. J.; Rudel, T. *Infect. Immun.* **2001**, *69* (12), 7880.

Rampioni, G.; Leoni, L.; Williams, P. *Bioorg. Chem.* **2014**, *55*, 60.

Rasko, D. A.; Sperandio, V. *Nat. Rev. Drug Discov.* **2010**, *9* (2), 117.

Rauwerda, J. A. *Diabetes. Metab. Res. Rev.* **2004**, *20* (SUPPL. 1), S123.

RD, W.; GD, E. *JAMA* **2008**, *299* (22), 2682.

Regiel-Futyra, A.; Kus-Liškiewicz, M.; Sebastian, V.; Irusta, S.; Arruebo, M.; Stochel, G.; Kyzioł, A. *ACS Appl. Mater. Interfaces* **2015**, *7* (2), 1087.

Ren, G.; Hu, D.; Cheng, E. W. C.; Vargas-Reus, M. A.; Reip, P.; Allaker, R. P. *Int. J. Antimicrob. Agents* **2009**, *33* (6), 587.

Rice, L. B. *Infect. Control Hosp. Epidemiol.* **2010**, *31* (S1), S7.

Rice, L. B. *The Journal of Infectious Diseases*. United States April 2008, pp 1079–1081.

Richter, A. P.; Brown, J. S.; Bharti, B.; Wang, A.; Gangwal, S.; Houck, K.; Cohen Hubal, E. A.; Paunov, V. N.; Stoyanov, S. D.; Velev, O. D. *Nat Nano* **2015**, *10* (9), 817.

Römling, U.; Balsalobre, C. *J. Intern. Med.* **2012**, *272* (6), 541.

Roy, S.; Elgharably, H.; Sinha, M.; Ganesh, K.; Chaney, S.; Mann, E.; Miller, C.; Khanna, S.; Bergdall, V. K.; Powell, H. M.; Cook, C. H.; Gordillo, G. M.; Wozniak, D. J.; Sen, C. K. *J. Pathol.* **2014**, *233* (4), 331.

Saha, K.; Moyano, D. F.; Rotello, V. M. *Mater. Horizons* **2014**, *1* (1), 102.

Sambhy, V.; MacBride, M. M.; Peterson, B. R.; Sen, A. *J. Am. Chem. Soc.* **2006**, *128* (30), 9798.

Samperio, C.; Boyer, R.; Eigel, W. N. 3rd; Holland, K. W.; McKinney, J. S.; O'Keefe, S. F.; Smith, R.; Marcy, J. E. *J. Agric. Food Chem.* **2010**, *58* (24), 12950.

Sanchez-Moreno, P.; Buzon, P.; Boulaiz, H.; Peula-Garcia, J. M.; Ortega-Vinuesa, J. L.; Luque, I.; Salvati, A.; Marchal, J. A. *Biomaterials* **2015**, *61*, 266.

Sanchez-Moreno, P.; Ortega-Vinuesa, J. L.; Martin-Rodriguez, A.; Boulaiz, H.; Marchal-Corrales, J. A.; Peula-Garcia, J. M. *Int. J. Mol. Sci.* **2012**, *13* (2), 2405.

Sasser, T. A.; Van Avermaete, A. E.; White, A.; Chapman, S.; Johnson, J. R.; Avermaete, T. Van; Gammon, S. T.; Leevy, W. M. *Curr. Top. Med. Chem.* **2013**, *13* (4), 479.

Sauer, K.; Camper, A. K.; Ehrlich, G. D.; Costerton, J. W.; Davies, D. G. *J. Bacteriol.* **2002**, *184* (4), 1140.

Saviuc, C.-M.; Drumea, V.; Olariu, L.; Chifiriuc, M.-C.; Bezirtzoglou, E.; Lazar, V. *Curr. Pharm. Biotechnol.* **2015**, *16* (2), 137.

Scott, R. W.; DeGrado, W. F.; Tew, G. N. *Curr. Opin. Biotechnol.* **2008**, *19* (6), 620.

Seijo, B.; Fattal, E.; Roblot-Treupel, L.; Couvreur, P. *Int. J. Pharm.* **1990**, *62* (1), 1.

Seil, J. T.; Webster, T. J. *Int. J. Nanomedicine* **2012**, *7*, 2767.

Shah, M.; Su, D.; Scheliga, J. S.; Pluskal, T.; Boronat, S.; Motamedchaboki, K.; Campos, A. R.; Qi, F.; Hidalgo, E.; Yanagida, M.; Wolf, D. A. *Cell Rep.* **2016**, *16* (7), 1891.

Sharifi-Rad, J.; Sharifi-Rad, M.; Hoseini-Alfatemi, S. M.; Iriti, M.; Sharifi-Rad, M.; Sharifi-Rad, M. *Int. J. Mol. Sci.* **2015**, *16* (8), 17812.

Sharma, V. K.; Yngard, R. A.; Lin, Y. *Adv. Colloid Interface Sci.* **2009**, *145* (1–2), 83.

Sherlock, S. P.; Tabakman, S. M.; Xie, L.; Dai, H. *ACS Nano* **2011**, *5* (2), 1505.

Sieprawska-Lupa, M.; Mydel, P.; Krawczyk, K.; Wójcik, K.; Puklo, M.; Lupa, B.; Suder, P.; Silberring, J.; Reed, M.; Pohl, J.; Shafer, W.; McAleese, F.; Foster, T.; Travis, J.; Potempa, J. *Antimicrob. Agents Chemother.* **2004**, *48* (12), 4673.

Silhavy, T. J.; Kahne, D.; Walker, S. *Cold Spring Harb. Perspect. Biol.* **2010**, *2* (5), a000414.

Simon-Deckers, A.; Loo, S.; Mayne-L'hermite, M.; Herlin-Boime, N.; Menguy, N.; Reynaud, C.; Gouget, B.; Carrière, M. *Environ. Sci. Technol.* **2009**, *43* (21), 8423.

Singh, P. K.; Tack, B. F.; McCray, P. B.; Welsh, M. J. *Am. J. Physiol. Lung Cell. Mol. Physiol.* **2000**, *279* (5), L799.

Sondi, I.; Salopek-Sondi, B. *J. Colloid Interface Sci.* **2004**, *275* (1), 177.

Song, J.; Kim, H.; Jang, Y.; Jang, J. *ACS Appl. Mater. Interfaces* **2013**, *5* (22), 11563.

Song, J.; Kong, H.; Jang, J. *Chem. Commun.* **2009**, No. 36, 5418.

Song, Z.; Borgwardt, L.; Hoiby, N.; Wu, H.; Sorensen, T. S.; Borgwardt, A. *Orthop. Rev. (Pavia).* **2013**, *5* (2), 65.

Spapen, H.; Jacobs, R.; Van Gorp, V.; Troubleyn, J.; Honoré, P. M. *Ann. Intensive Care* **2011**, *1* (1), 14.

Spellberg, B.; Powers, J. H.; Brass, E. P.; Miller, L. G.; Edwards, J. E. *Clin. Infect. Dis.* **2004**, *38* (9), 1279.

Stein, G. E.; Johnson, L. B. *Clin. Infect. Dis.* **2011**, *52* (9), 1156.

Stewart, P. S.; Costerton, J. W. *Lancet (London, England)* **2001**, *358* (9276), 135.

Stokes, J. M.; French, S.; Ovchinnikova, O. G.; Bouwman, C.; Whitfield, C.; Brown, E. D. *Cell Chem. Biol.* **2016**, *23* (2), 267.

Stokes, J. M.; Macnair, C. R.; Ilyas, B.; French, S.; Côté, J. P.; Bouwman, C.; Farha, M. A.; Sieron, A. O.; Whitfield, C.; Coombes, B. K.; Brown, E. D. *Nat. Microbiol.* **2017**, *2*, 17028.

Sun, B. K.; Siprashvili, Z.; Khavari, P. A. *Science* **2014**, *346* (6212), 941.

Tabb, D. L.; McDonald, W. H.; Yates, J. R. *J. Proteome Res.* **2002**, *1* (1), 21.

Takahashi, H.; Nadres, E. T.; Kuroda, K. *Biomacromolecules* **2017**, *18* (1), 257.

Tamma, P. D.; Cosgrove, S. E.; Maragakis, L. L. *Clin. Microbiol. Rev.* **2012**, *25* (3), 450.

Tängdén, T. *Ups. J. Med. Sci.* **2014**, *119* (2), 149.

Tew, G. N.; Scott, R. W.; Klein, M. L.; Degrado, W. F. *Acc. Chem. Res.* **2010**, *43* (1), 30.

Tian, J.; Zhang, J.; Yang, J.; Du, L.; Geng, H.; Cheng, Y. *ACS Appl. Mater. Interfaces* **2017**, *9* (22), 18512.

Tian, Y.; Qi, J.; Zhang, W.; Cai, Q.; Jiang, X. *ACS Appl. Mater. Interfaces* **2014**, *6* (15), 12038.

Torchilin, V. P. *Nat. Rev. Drug Discov.* **2014**, *13* (11), 813.

Trautner, B. W.; Darouiche, R. O. *Am. J. Infect. Control* **2004**, *32* (3), 177.

Tripathy, N.; Ahmad, R.; Bang, S. H.; Min, J.; Hahn, Y. B. *Chem. Commun.* **2014**, *50* (66), 9298.

Tulkens, P. M.; Arvis, P.; Kruesmann, F. *Drugs R. D.* **2012**, *12* (2), 71.

Turek, C.; Stintzing, F. C. *Compr. Rev. Food Sci. Food Saf.* **2013**, *12* (1), 40.

Udenfriend, S.; Stein, S.; Bohlen, P.; Dairman, W.; Leimgruber, W.; Weigele, M. *Science* **1972**, *178* (4063), 871.

Van Oosten, M.; Schäfer, T.; Gazendam, J. A. C.; Ohlsen, K.; Tsompanidou, E.; De Goffau, M. C.; Harmsen, H. J. M.; Crane, L. M. A.; Lim, E.; Francis, K. P.; Cheung, L.; Olive, M.; Ntziachristos, V.; Van Dijl, J. M.; Van Dam, G. M. *Nat. Commun.* **2013**, *4*, 2584.

Veerachamy, S.; Yarlagadda, T.; Manivasagam, G.; Yarlagadda, P. K. *Proc. Inst. Mech. Eng. H.* **2014**, *228* (10), 1083.

Ventola, C. L. *P T A peer-reviewed J. Formul. Manag.* **2015**, *40* (4), 277.

Vergis, J.; Gokulakrishnan, P.; Agarwal, R. K.; Kumar, A. *Crit. Rev. Food Sci. Nutr.* **2015**, *55* (10), 1320.

Villa, C. H.; Anselmo, A. C.; Mitragotri, S.; Muzykantov, V. *Adv. Drug Deliv. Rev.* **2016**, *106* (Pt A), 88.

Walsh, F. *BBC News* **2014**, No. December 2014, 1.

Wang, C.; Sun, X.; Cheng, L.; Yin, S.; Yang, G.; Li, Y.; Liu, Z. *Adv. Mater.* **2014**, *26* (28), 4794.

Wang, H.; Khor, T. O.; Shu, L.; Su, Z.-Y.; Fuentes, F.; Lee, J.-H.; Kong, A.-N. T. *Anticancer. Agents Med. Chem.* **2012**, *12* (10), 1281.

Wang, L.; Hu, C.; Shao, L. *Int. J. Nanomedicine* **2017**, *12*, 1227.

Wang, L.-S.; Gupta, A.; Rotello, V. M. *ACS Infect. Dis.* **2016**, *2* (1), 3.

Wang, Y. *Biochem. Biophys. Res. Commun.* **2002**, *292* (2), 396.

Weerakoon, W.; Atukorala, S.; Gamage, D.; Wijeratne, M. *Ceylon Med. J.* **2011**, *48* (2), 58.

White, R. L.; Burgess, D. S.; Manduru, M.; Bosso, J. A. *Antimicrob. Agents Chemother.* **1996**, *40* (8), 1914.

Wiegand, I.; Hilpert, K.; Hancock, R. E. W. *Nat. Protoc.* **2008**, *3* (2), 163.

Wilcox, M. H.; Gerding, D. N.; Poxton, I. R.; Kelly, C.; Nathan, R.; Birch, T.; Cornely, O. A.; Rahav, G.; Bouza, E.; Lee, C.; Jenkin, G.; Jensen, W.; Kim, Y.-S.; Yoshida, J.; Gabryelski, L.; Pedley, A.; Eves, K.; Tipping, R.; Guris, D.; Kartsonis, N.; Dorr, M.-B. *N. Engl. J. Med.* **2017**, *376* (4), 305.

Willyard, C. *Nature*. England February 2017, p 15.

Wolfram, J.; Yang, Y.; Shen, J.; Moten, A.; Chen, C.; Shen, H.; Ferrari, M.; Zhao, Y. *Colloids Surfaces B Biointerfaces* **2014**, *124*, 17.

Wright, G. D. *Adv. Drug Deliv. Rev.* **2005**, *57* (10), 1451.

Wu, H.; Moser, C.; Wang, H.-Z.; Høiby, N.; Song, Z.-J. *Int. J. Oral Sci.* **2014**, *7*, 1.

Wu, M.-C.; Deokar, A. R.; Liao, J.-H.; Shih, P.-Y.; Ling, Y.-C. *ACS Nano* **2013**, *7* (2), 1281.

Xu, C.; Lin, X.; Ren, H.; Zhang, Y.; Wang, S.; Peng, X. *Proteomics* **2006**, *6* (2), 462.

Xu, H.; Qu, F.; Xu, H.; Lai, W.; Wang, Y. A.; Aguilar, Z. P.; Wei, H. *BioMetals* **2012**, *25*, 45.

Yang, X.-C.; Samanta, B.; Agasti, S. S.; Jeong, Y.; Zhu, Z.-J.; Rana, S.; Miranda, O. R.; Rotello, V. M. *Angew. Chemie Int. Ed.* **2011**, *50* (2), 477.

Yin, L. M.; Edwards, M. A.; Li, J.; Yip, C. M.; Deber, C. M. *J. Biol. Chem.* **2012**, *287* (10), 7738.

Yoo, J.-W.; Chambers, E.; Mitragotri, S. *Curr. Pharm. Des.* **2010**, *16* (21), 2298.

Zeeb, B.; Gibis, M.; Fischer, L.; Weiss, J. *J. Colloid Interface Sci.* **2012**, *387* (1), 65.

Zelepukin, I. V; Yaremenko, A. V; Shipunova, V. O.; Babenyshev, A. V; Balalaeva, I. V; Nikitin, P. I.; Deyev, S. M.; Nikitin, M. P. *Nanoscale* **2019**, *11* (4), 1636.

Zgurskaya, H. I.; Krishnamoorthy, G.; Ntreh, A.; Lu, S. *Front. Microbiol.* **2011**, *2* (SEP), 189.

Zgurskaya, H. I.; López, C. A.; Gnanakaran, S. *ACS Infect. Dis.* **2016**, *1* (11), 512.

Zhang, L.; Pornpattananangku, D.; Hu, C.-M. J.; Huang, C.-M. *Curr. Med. Chem.* **2010**, *17* (6), 585.

Zhang, X.; Huang, R.; Gopalakrishnan, S.; Cao-Milán, R.; Rotello, V. M. *Trends Chem.* **2019**, *1* (1), 90.

Zhao, Y.; Chen, Z.; Chen, Y.; Xu, J.; Li, J.; Jiang, X. *J. Am. Chem. Soc.* **2013**, *135* (35), 12940.

Zhao, Y.; Tian, Y.; Cui, Y.; Liu, W.; Ma, W.; Jiang, X. *J. Am. Chem. Soc.* **2010**, *132* (35), 12349.

Zharov, V. P.; Mercer, K. E.; Galitovskaya, E. N.; Smeltzer, M. S. *Biophys. J.* **2006**, *90* (2), 619.

Zhou, Y.; Liu, B.; Yang, R.; Liu, J. *Bioconjug. Chem.* **2017**, *28* (12), 2903.

Zhu, D. Y.; Landis, R. F.; Li, C. H.; Gupta, A.; Wang, L. S.; Geng, Y.; Gopalakrishnan, S.; Guo, J. W.; Rotello, V. M. *Nanoscale* **2018**, *10* (39), 18651.

Ziani, K.; Chang, Y.; McLandsborough, L.; McClements, D. J. *J. Agric. Food Chem.* **2011**, *59* (11), 6247.